# Multi-Scale Mass Transfer Processes Controlling Natural Attenuation and Engineered Remediation: An IFRC Focused on Hanford's 300 Area Uranium Plume

*January 2009 to January 2010*

Annual Report to the
DOE Office of Science, Climate and Environmental Sciences Division

**Principal Investigator:**
John Zachara, PNNL

**Co-Principal Investigators:**
Bruce Bjornstad, PNNL
John Christensen, LBNL
Mark Conrad, LBNL
Jim Fredrickson, PNNL
Mark Freshley, PNNL
Roy Haggerty, OSU
Glenn Hammond, PNNL
Doug Kent, USGS
Allan Konopka, PNNL
Peter Lichtner, LANL

Chongxuan Liu, PNNL
Jim McKinley, PNNL
Chris Murray, PNNL
Mark Rockhold, PNNL
Yoram Rubin, U of CA, Berkeley
Vince Vermeul, PNNL
Roelof Versteeg, INL
Andy Ward, PNNL
Chunmiao Zheng, U of AL

**Pacific Northwest**
NATIONAL LABORATORY

**DISCLAIMER**

This report was prepared as an account of work sponsored by an agency of the United States Government. Neither the United States Government nor any agency thereof, nor Battelle Memorial Institute, nor any of their employees, makes **any warranty, express or implied, or assumes any legal liability or responsibility for the accuracy, completeness, or usefulness of any information, apparatus, product, or process disclosed, or represents that its use would not infringe privately owned rights**. Reference herein to any specific commercial product, process, or service by trade name, trademark, manufacturer, or otherwise does not necessarily constitute or imply its endorsement, recommendation, or favoring by the United States Government or any agency thereof, or Battelle Memorial Institute. The views and opinions of authors expressed herein do not necessarily state or reflect those of the United States Government or any agency thereof.

PACIFIC NORTHWEST NATIONAL LABORATORY
*operated by*
BATTELLE
*for the*
UNITED STATES DEPARTMENT OF ENERGY
*under Contract DE-AC05-76RL01830*

**Printed in the United States of America**

**Available to DOE and DOE contractors from the
Office of Scientific and Technical Information,
P.O. Box 62, Oak Ridge, TN 37831-0062;
ph: (865) 576-8401
fax: (865) 576-5728
email: reports@adonis.osti.gov**

**Available to the public from the National Technical Information Service,
U.S. Department of Commerce, 5285 Port Royal Rd., Springfield, VA 22161
ph: (800) 553-6847
fax: (703) 605-6900
email: orders@ntis.fedworld.gov
online ordering: http://www.ntis.gov/ordering.htm**

This document was printed on recycled paper.
(9/2003)

# Multi-Scale Mass Transfer Processes Controlling Natural Attenuation and Engineered Remediation: An IFRC Focused on Hanford's 300 Area Uranium Plume

## January 2009 to January 2010

Annual Report to the
DOE Office of Science, Climate and Environmental Sciences Division

J.M. Zachara, Principal Investigator

February 2010

**Multi-Scale Mass Transfer Processes Controlling Natural Attenuation and Engineered Remediation: An IFRC Focused on Hanford's 300 Area Uranium Plume**

**Table of Contents**

# Multi-Scale Mass Transfer Processes Controlling Natural Attenuation and Engineered Remediation: An IFRC Focused on Hanford's 300 Area Uranium Plume

### *Annual Report: January 2009 – January 2010*

**Principal Investigator:**
John Zachara, Pacific Northwest National Laboratory (PNNL) is IFRC Principal Investigator and primary contact with ERSD.

**Field Site Manager:**
Mark Freshley, PNNL, is field site manager and primary EM contact.

**PNNL Co-Principal Investigators and Major Task (FY-09 Funding):**
Here we provide a financial synopsis for the Hanford IFRC for FY 09. The synopsis is organized according to reporting categories in the quarterly and annual reports.

## FY09 IFRC FINANCIAL SUMMARY

| | | |
|---|---|---|
| FY09 Project Funding: | $ | 3,031,000 |
| Carryover from FY08: | $ | 855,327 |
| Total FY09 Funding: | $ | 3,886,327 |
| | | |
| FY09 Spent: | $ | 3,512,110 |
| Carryover to FY10: | $ | 374,217  * |

\* inlcudes 119K in commitments

| |
|---|
| **Project Management -  $319,820[1,3]** |
| **John Zachara – ($237,538)[2] -** IFRC project manager and lead scientist. Responsible for project success, reporting, financial management, productivity, and scientific accomplishment. Lead on all geochemical issues. |
| **Mark Freshley – ($76,733) -** Responsible for well and tracer permitting, development of field test plans, site operations including ES&H, sample dispersement, QA/QC planning and review, and EM interactions. |
| **Site Design and Installation -  $201,164[1,3,4]** |
| **Bruce Bjornstad – ($115,536)[6] -** Hanford IFRC site geologist responsible for the design and installation of well-field up-grades in response to experimental and measurement needs. Interface between the Hanford IFRC and the Flour-Hanford well drilling team. |
| **Data Management -  $133,145[,5]** |
| **Field Site Characterization -  $797,149[1,3]** |

| |
|---|
| **Bruce Bjornstad – ($126,284)[6]** - Interpreted all well logs and developed a site geologic facies model based on measurements and data collected during the well installation campaign. |
| **Andy Ward – ($210,987)[3,6]** - Lead for field geophysical characterization of the site, geophysical monitoring of experiments, and interpretation of resulting data. |
| **Jim McKinley – ($392,853)[3,6]** - Oversight of sediment and groundwater sampling, and geochemical characterization measurements and analyses of all type. |
| **Chris Murray – ($46,491)[6]** - Geostatistical analysis of laboratory physical, geochemical, and hydrologic measurements, and results of field hydrologic characterization. |
| **Saturated Zone Injection Experiments - $746,107[1,3]** |
| **Vince Vermeul – ($379,917)[7]** - Oversight and management of field hydrologic activities and monitoring systems, infrastructure, and injection experiments. Has determined the magnitude of intra-well vertical flows by direct measurement and is testing mitigation strategies. |
| **Mark Rockhold – ($208,840)[6]** - Responsible for hydrologic data integration and transfer to others, and for modeling the results of hydrologic characterization and non-reactive tracer experiments. |
| **Modeling and Interpretation Programs - $1,053,948[1,8]** |
| **Chongxuan Liu – ($92,233)[6]** - Responsible for the development of mass transfer models of U adsorption and desorption at both the laboratory and field scales based on collaborations with Y. Fang (PNNL), C. Zheng (UA), D. Kent (USGS), and R. Haggerty (OSU). |
| **Passive Experimentation – $260,777[3]** |
| **Jim McKinley – ($131,746)[6]** - Design and oversight of all groundwater geochemical measurements, including the comprehensive monitoring experiments to evaluate seasonal U releases from the lower vadose zone. |
| **Jim Fredrickson – ($77,227)[6]** – Design, oversight, and performance of down-hole microbiology and biogeochemistry studies. Important liaison with PNNL SFA research. |

| |
|---|
| **External Principal Investigators** |
| **John Christensen/Mark Conrad, LBNL – ($124,000)** – Tracking uranium sources and process through isotope geochemistry. |
| **Roy Haggerty, OSU – ($157,000)** – Laboratory quantification of IFRC mass transfer processes and design of field-scale mass transfer experiments. |
| **Doug Kent, USGS – ($180,000)** - Experimental determination and validation of a uranium surface complexation model for the IFRC field site. |
| **Peter Lichtner, LANL – ($100,000)** – Use of PFLOTRAN in multiple realization simulations of IFRC non-reactive and reactive tracer experiments. |
| **Yoram Rubin, U of CA, Berkeley – ($200,000)** – Development of geostatistical models for site hydrologic and geochemical properties. |
| **Roelof Versteeg/Tim Johnson, INL – ($132,800)** – Development and maintenance of IFRC site data base. Lead in modeling of geophysical data. |

**Chunmiao Zheng, U of Alabama – ($129,300) –** Hydrologic, transport, and well-flow modeling. Field experiment simulation.

1. total dollars spent
2. dollars spent by individual and the administrative team
3. includes misc procurements, travel or supplies
4. includes site support (see below)
5. includes subcontract to INL - R. Versteeg
6. includes junior scientist labor
7. includes injection team members
8. includes external subcontracts to UCB, USGS, OSU, UA, LANL and LBNL

**FY09 IFRC Procurements**

| Vendor | Description | TRANS_AMT | BRDN_AMT |
|---|---|---|---|
| Geotomo Software | Res3DINVx64 (plus 32 bit RES3DINV/RES3DINV) software | 4,900 | 5,907 |
| Central Hose & Fittings, Inc. | Water Discharge Versiflow | 17,158 | 20,685 |
| All World Scientific | Misc Lab Supplies | 527 | 635 |
| Central Hose & Fittings, Inc. | 1000 Ft of 6" Versiflo Hoses | 11,870 | 14,107 |
| Quantum Engineering Corporation | Large inflatable packer for testing 8 to 10 inch wells | 1,050 | 1,247 |
| Multi-Phase Technologies, LLC | Down-hole ERT Cables | 1,827 | 2,171 |
| Instrumentation Northwest, Inc. | Aquistar Plus Software upgrade for network-batch communication | 4,550 | 5,485 |
| Envirochem Technology Services | 200 Lb Drums of Sodium Bromide | 5,890 | 7,000 |
| Hertz Equipment Rental Corporation | Rental of Generators | 1,730 | 2,056 |
| Pape' Material Handling, Inc. | Forklift Rental/Receiving | 1,000 | 1,188 |
| Miscellaneous Payments | Misc Payments | 2,230 | 2,501 |
| Fisher Scientific Company, LLC | Misc Supplies | 36,002 | 41,885 |
| Other Misc B2B | Gov Scientific Source, Guy Brown Products, Tri-Cities Valve & Fitting | 922 | 1,143 |
| Pacific Supply & Safety, LLC | Misc Supplies | 4,145 | 4,808 |
| Technology Integration Group | Misc Supplies | 1,179 | 1,373 |
| Pcard | Commodities/Services | 133,530 | 155,106 |
| | **Total** | **228,511** | **267,298** |

**FY09 IFRC Subcontracts**

| Vendor | Description | TRANS_AMT | BRDN_AMT |
|---|---|---|---|
| University of California Berkeley | Yoram Rubin | 200,000 | 219,137 |
| US Geological Survey - LA | Doug Kent | 180,000 | 197,223 |
| Oregon State University | Roy Haggerty | 156,900 | 171,913 |
| University of Alabama | Chunmiao Zheng | 129,300 | 141,672 |
| Battelle Energy Alliance, LLC (INL) | Roelof Versteeg | 132,781 | 132,781 |
| Lawrence Berkeley National Laboratory | Mark Conrad and John Christensen | 123,999 | 123,999 |
| Los Alamos National Laboratory | Peter Lichtner | 100,155 | 100,155 |
| Donald C. Girvin | Groundwater sampling and analysis | 36,093 | 43,513 |
| Southwest Research Institute | Chemical analysis of sediment samples | 30,000 | 35,960 |
| University of Texas at Austin | CT-scanning and Image Processing Services | 11,200 | 13,502 |
| Washington Closure Hanford, LLC | Power Drop | 11,683 | 11,683 |
| Temp-Air, Inc. | Rental 40 Ton Temporary Air cooled Chiller | 5,524 | 6,589 |
| Fluor Hanford | Well Drilling/ Sample Collection | 6,129 | 6,129 |
| Central Hanford Plateau Remediation Co | Field personnel and services support | 5,457 | 5,457 |
| Williams Scotsman, Inc. | Office Trailer & Conex Boxes | 3,886 | 4,650 |
| Hertz Equipment Rental Corporation | Generator 55-59KW/DSL 5490500 Rental | 1,600 | 1,902 |
| Broadmoor RV & Truck Center, Inc. | Repair AC in Field Lab Trailer. | 1,500 | 1,808 |
| Instrumentation Northwest, Inc. | Maintenance & repair of INW TempHion Sensors | 1,500 | 1,785 |
| Pape' Material Handling, Inc. | Forklift Rental | 468 | 556 |
| Multi-Phase Technologies, LLC | Perform Field Tests of the ERT system | 360 | 427 |
| | **Total** | **1,138,534** | **1,220,842** |

**Key Collaborations:**

Harvey Bolton, John Zachara, Jim Fredrickson, Tim Scheibe, Chongxuan Liu, Alan Konopka, Andy Ward, and other PNNL, national laboratory (Scott Brooks, ORNL), Agency (Jim Davis, USGS), and university principle investigators collaborate through the PNNL SFA focused on Hanford-inspired subsurface science issues. Using IFRC site sediments, SFA investigators are: quantifying and modeling key microscopic reaction and transport processes (adsorption/desorption, precipitation/dissolution, mass transfer), measuring sediment properties for geophysical interpretation (K-U-T isotopic content of different size fraction, and electrical and thermal properties), and characterizing microbiological distributions and function. The SFA team is also developing pore-scale biogeochemical reaction models of IFRC site sediments, and collaborating on in-situ microcosm experiments in IFRC site wells. SFA research is consequently providing essential information on IFRC site microbial ecology, microscopic reactive transport models, and geophysical characterization approaches.

Peter Lichtner (LANL) and Glenn Hammond (PNNL) collaborate through a SciDAC-2 project focused on high performance modeling of the 300 A plume.

Henning Prommer (CSIRO) collaborates with the IFRC through university principle investigator Chunmiao Zheng (University of Alabama). Dr. Prommer has developed a multi-component reactive transport model for saturated porous media called PHT3D. His team has assisted in pre-modeling U injection experiments, and in evaluating the sensitivity of multi-rate, surface complexation model parameters under dynamic hydrologic conditions.

Jon Fruchter, Dawn Wellman, and Vince Vermeul (PNNL) collaborate through the EM-20 Polyphosphate Demonstration Project, which performed one injection experiment in the saturated zone. The results of the injection test indicated that remediation of the uranium plume via autunite precipitation was unlikely to be feasible at the necessary scale. The EM-20 project is now conducting laboratory experiments to evaluate an alternative strategy to remediate uranium in the capillary fringe involving polyphosphate infiltration through the vadose zone.

Jon Fruchter, Dawn Wellman, and Vince Vermeul (PNNL) and Jane Borghese [CH2M Hill Plateau Remediation Contract (CHPRC)] collaborate through the DOE-Richland Operations Office-funded 300-FF-5 CERCLA project. This project has assumed responsibility for the field-scale infiltration test of the polyphosphate remediation technology near the North Process Pond. Well monitoring technology developed for the IFRC site has been transferred to the EM project.

Haluk Beyenal (Washington State University) and Jim Fredrickson (PNNL) collaborate on an ERSP study of redox-controlling microorganisms in the 300 A unconfined aquifer. During CY09 this team inoculated flow cells and microcosms with IFRC site groundwater to initiate biofilm formation. The resulting biofilms were characterized by various microscopic methods and their influence on mineral/water biogeochemistry investigated.

Lee Slater (Rutgers University), Roelof Versteeg (INL), Andy Ward (PNNL), Fred Day-Lewis and John Lane (USGS), and Andrew Binley (Lancaster University, UK) collaborate on geophysical characterization and monitoring strategies for quantifying hydrologic transport processes in the hyporheic zone at the 300 Area with ERSP funding. This team has established a temperature monitoring network along the Columbia River shoreline immediately east and down-gradient of the IFRC site. The network

will allow flux measurements of groundwater to the river useful to the calibration of IFRC transport models.

Fred Day-Lewis (USGS), Andrew Binley (Lancaster University, UK), Kamini Singha (Penn State University), and Andy Ward (PNNL) will utilize IFRC site infrastructure and sediments to investigate multi-scale mass transfer using geo-electrical methods. The ERSP project was initiated in FY10, and the IFRC has provided the team with intact IFRC core samples in January 2010 to begin their research.

William Burgos (Penn State University), Hailang Dong (University of Miami, OH), and Ken Kemner (ANL) will be investigating biogeochemical redox reactions of uranium and oxygen with Fe-containing layer silicates from the IFRC site in newly funded ERSP research. Bulk samples of Fe(II)-containing smectites from the IFRC Ringold Formation have been provided to the research team.

# ABSTRACT

The Integrated Field-Scale Subsurface Research Challenge (IFRC) at the Hanford Site 300 Area uranium (U) plume addresses multi-scale mass transfer processes in a complex hydrogeologic setting where groundwater and riverwater interact. A series of forefront science questions on mass transfer are posed for research which relate to the effect of spatial heterogeneities; the importance of scale; coupled interactions between biogeochemical, hydrologic, and mass transfer processes; and measurements and approaches needed to characterize and model a mass-transfer dominated system. The project was initiated in February 2007, with CY 2007 and CY 2008 progress summarized in preceding reports.

The site has 35 instrumented wells, and an extensive monitoring system. It includes a deep borehole for microbiologic and biogeochemical research that sampled the entire thickness of the unconfined 300 A aquifer. Significant, impactful progress has been made in CY 2009 with completion of extensive laboratory measurements on field sediments, field hydrologic and geophysical characterization, four field experiments, and modeling. The laboratory characterization results are being subjected to geostatistical analyses to develop spatial heterogeneity models of U concentration and chemical, physical, and hydrologic properties needed for reactive transport modeling. The field experiments focused on: 1) physical characterization of the groundwater flow field during a period of stable hydrologic conditions in early spring, 2) comprehensive groundwater monitoring during spring to characterize the release of U(VI) from the lower vadose zone to the aquifer during water table rise and fall, 3) dynamic geophysical monitoring of salt-plume migration during summer, and 4) a U reactive tracer experiment (desorption) during the fall. Geophysical characterization of the well field was completed using the down-well Electrical Resistance Tomography (ERT) array, with results subjected to robust, geostatistically constrained inversion analyses. These measurements along with hydrologic characterization have yielded 3D distributions of hydraulic properties that have been incorporated into an updated and increasingly robust hydrologic model. Based on significant findings from the microbiologic characterization of deep borehole sediments in CY 2008, down-hole biogeochemistry studies were initiated where colonization substrates and spatially discrete water and gas samplers were deployed to select wells. The increasingly comprehensive field experimental results, along with the field and laboratory characterization, are leading to a new conceptual model of U(VI) flow and transport in the IFRC footprint and the 300 Area in general, and insights on the microbiological community and associated biogeochemical processes.

A significant issue related to vertical flow in the IFRC wells was identified and evaluated during the spring and fall field experimental campaigns. Both upward and downward flows were observed in response to dynamic Columbia River stage. The vertical flows are caused by the interaction of pressure gradients with our heterogeneous hydraulic conductivity field. These impacts are being evaluated with additional modeling and field activities to facilitate interpretation and mitigation. The project moves into CY 2010 with ambitious plans for a drilling additional wells for the IFRC well field, additional experiments, and modeling. This research is part of the ERSP Hanford IFRC at Pacific Northwest National Laboratory.

# INTRODUCTION

**Scientific Theme, Goal and Objectives, and Approach**

The overall scientific theme of the Hanford IFRC is multi-scale mass transfer and its role in controlling contaminant behavior in a groundwater system with complex process coupling. The project is being conducted within Hanford's 300 A uranium (U) plume that discharges to the Columbia River. The groundwater plume has persisted far longer than predicted, and seasonally variable groundwater U concentrations have not been successfully modeled by any approach yet applied. Contaminated sediments from the site are coarse-textured, but display remarkably slow, kinetically controlled U desorption in the laboratory setting. The aquifer hosting the plume is in intimate hydrologic communication with the Columbia River which exhibits large stage oscillations on daily and seasonal frequency. Our primary project goal is to characterize, understand, and model a complex field scale biogeochemical system displaying kinetic processes and dynamic hydrology driven by groundwater-river coupling. While our primary motivation is scientific impact, we also seek knowledge about the complex workings of this contaminated system that may be transferred to the site steward for effective and sustainable remediation.

Given the varied knowledge base that exists for the site, our objectives are multiple and diverse:

- Develop and implement a comprehensive, scientifically-based characterization strategy for the field site to establish geostatistical relationships for properties controlling water transport, chemical migration, mass transfer, and microbiologic activity.

- Characterize the microbial ecology of the site in collaboration with the PNNL SFA, and devise field experiments to probe factors controlling in-situ microbiologic activities including the role of mass transfer.

- Perform field injection experiments to evaluate hypotheses on mass transfer influencing uranium adsorption and desorption within the saturated zone, and the overall influence of these processes on uranium concentrations and plume behavior.

- Utilize unique river-stage induced changes in water table elevation, groundwater flow direction and velocity, and water composition to evaluate mechanisms for continued uranium supply to and mixing within the groundwater plume.

- Develop a field scale reactive transport simulator for uranium based on mass-transfer limited surface complexation that incorporates spatial heterogeneities in physical, hydrologic, and chemical properties. Understand scale relationships of key parameters and update to incorporate microbiological processes when known.

The project is primarily a field investigation. A 35-well, triangular field site ($\sim$1600 m$^2$) has been established within one of three contaminated source term regions of the U(VI) groundwater plume. The well field contains 26 monitoring wells that are fully screened through the U(VI) plume in the saturated zone, and 9 depth discrete monitoring wells. The wells are instrumented with down-hole pressure transducers, specific conductance probes, thermistors, and electrical resistance tomography electrodes.

Sediment samples collected during well installation have been characterized for physical, chemical, and hydrologic properties in the laboratory according to a Characterization Plan (PNNL-SA-62816, http://ifchanford.pnl.gov/).  Extensive field hydrologic and geophysical characterization has been performed, which when integrated with laboratory characterization measurements, will yield a comprehensive 3-D hydrogeochemical model of the field site that will be used for knowledge integration, learning, and experiment simulation.  Field injection experiments using 300 A site groundwaters that vary in uranium concentration and that have been spiked with non-reactive tracers or temperature-modified, are used in combination with passive monitoring experiments to understand coupled processes occurring in the lower vadose zone and saturated zone.

The Hanford IFRC is an integrated project effort, with each P.I. contributing expertise necessary for project success.   There are no separate projects or activities.  There are highly coordinated activities of different type whose results sum to yield a comprehensive understanding of our complex field system.  PNNL participants are primarily responsible for project management, characterization and conceptual model development, and field experiment performance.  External participants emphasize data integration, field experiment design and interpretation, process model calibration, and modeling.

The IFRC collaborates with the PNNL-SFA on several key activities that are beyond the scope of the original IFRC proposal. The microbiology of core samples from the IFRC well field has been studied by PNNL-SFA collaborators (Dr. Alan Konopka and colleagues), providing the first information on the nature, function, and biogeochemistry of the microbial community in Hanford's river corridor unconfined aquifer. This information is now providing the basis for IFRC field studies.  The SFA is also developing linked surface complexation-mass transfer models of IFRC site sediments based on laboratory measurements (e.g., intact core experiments and deconstruction studies; Dr. Chongxuan Liu).  The up-scaling of derived thermodynamic and kinetic parameters to the field is being investigated as a joint IFRC/SFA activity.  The IFRC also collaborates with a high performance computing project (Dr. P. Lichtner, P.I.) focused on the 300 Area and supported by the SciDAC-2 program.

**Project History**

Project funding was received in February 2007 for field research in Hanford's 300 A focused on multi-scale mass transfer influencing the persistent U(VI) plume at this location and attempts to remediate it.  Efforts during CY 07 involved assembling the project team; designing the field site; planning the scientific program, creating management systems and control documents for the project; establishing a web-site, and obtaining permits for injection wells and field experiments.  The IFRC well-field was installed during CY 08, a large sample inventory was retrieved for laboratory characterization, a detailed characterization plan was developed, significant field hydrologic characterization was completed, and microbiologic studies were initiated at multiple depths in the saturated zone.

In CY 09, the current reporting period, considerable progress was made on geophysical field site characterization, laboratory characterization of field samples, testing and evaluating the field site infra-structure and monitoring capabilities, performing exploratory and hypothesis-driven experimentation of different types, and system modeling with multiple reactive transport simulators.

**CY 09 Accomplishments and Report Objective**

Year three (CY 09) was a productive year for the Hanford IFRC with the following identified as major operational accomplishments:

1.) A comprehensive report defining the geology/hydrogeology and well completion characteristics of the IFRC well-field was published (PNNL-18340) for use by project participants, SESP collaborators, and Hanford site remediation contractors and regulators.
2.) The hydraulic conductivity structure of the site has been characterized by a combination of electromagnetic borehole flow meter surveys, constant rate injection tests, and non-reactive tracer experiments. Geostatistical analysis of these observations is providing multiple realizations for refinement of the hydraulic conductivity field by comparisons of hydrologic model calculations (PFLOTRAN) to non-reactive tracer results.
3.) Phase I of the sediment characterization plan has been completed with physical and chemical measurements performed on 200 sediment samples from the IFRC site. Geostatistical analysis of the results is underway to yield physical/geochemical heterogeneity models of the site.
4.) A pedo-facies transfer model is nearing completion that will allow estimation of in-situ grain size distributions from down-hole spectral gamma logs that were recorded before well completion.
5.) A preliminary U surface complexation model has been developed for IFRC saturated zone sediments. This model and an associated mass-transfer model has been incorporated into our IFRC site simulators and their parameters evaluated through sensitivity calculations.
6.) Laboratory experiments that evaluated U(VI) desorption and adsorption within intact and repacked sediment columns have provided insights on probable in-situ rates and magnitude of surface complexation in the saturated zone.
7.) Field geophysical characterization of the site has been completed through a combination of down-hole and surface electrical measurements. Results have been interpreted through inversion modeling to yield a 3D electro-facies map of the IFRC experimental domain. Laboratory measurements are underway on intact sediment cores to allow extrapolation of electrical properties to sediment physical/hydraulic properties.
8.) Three major field injection experiments were performed in the saturated zone: a non-reactive tracer experiment (with dilute solutes and chilled water) to refine the site hydrologic model, a non-reactive tracer experiment with salinity contrast to evaluate the sensitivity of the down-hole ERT arrays for dynamic plume monitoring, and a preliminary desorption experiment where waters of low U(VI) concentration were injected.
9.) A comprehensive monitoring experiment was performed from April-June to monitor U(VI) release from the lower vadose zone and it's mixing with the plume as the water table rose and fell in response to seasonal river stage changes.
10.) Colonization substrates and biogeochemical microcosms of varied type were installed in select wells to monitor in-situ microbiologic activities and function.
11.) Two reactive transport simulators are being iteratively parameterized with physical, hydrologic, and geochemical measurements, parameters, and information from the IFRC site as it becomes available. The models are being used to simulate field experimental results for publication.

Most of the above accomplishments have been described in three FY 09 Hanford IFRC Quarterly Reports (July 2009, October 2009, and January 2010). An additional report that describes how physical

heterogeneity is being characterized at the IFRC site was developed as an ERSP interim measure in December 2009.  It is posted on the ERSP web-site.   In this CY 09 Annual Report we provide a relatively comprehensive summary of this year's research activities. There are intentional omissions that will be described in poster session at the annual ERSP meeting in March 2010.  The report addresses the following topics:  **I. Project Status and Important Issues, II. Observed Behaviors of the IFRC Site, III. Site Infrastructure, IV. Characterization, V. Saturated Zone Experimental Program, VI. Modeling and Interpretation, VII. Project Data Base, VIII. Placing the IFRC Site in Perspective: Multiple Realizations and Plume Scale Modeling, IX. Challenges and Concerns, X. Future Research Plans, and XI. Outreach Activities**.

# I. PROJECT STATUS AND IMPORTANT ISSUES

There have been no significant changes to the project scope or objectives during CY 09.
All laboratory and field measurements performed to date support the validity and importance of our original scientific theme of multi-scale mass transfer, albeit with qualifications requiring additional research. Consequently the project is moving forward with previously stated experimental objectives and plans (e.g., Figure I-1).The development of the vadose zone infiltration site has been postponed until after the Hanford IFRC mid-term peer review in April, 2010, as described in the CY 08 Annual Report.  This delay will allow our project to be responsive to the results of a nearby EM field demonstration project on U immobilization in the lower vadose zone through poly-phosphate surface infiltration. The EM project installed an infiltration well gallery in the summer of 2009, and a demonstration experiment of this potentially far-fetched concept is planed during spring 2010.  The IFRC passive field monitoring experiment performed in spring 2009 and described in the July 2009 Quarterly has provided the only definitive direct measurements of U flux from the lower vadose zone during periods of high water table available for the 300 A.

Several important issues have arisen over the past year. The first of these is that the hydrologic boundary conditions of the IFRC well field are not sufficiently constrained by distant wells that existed previously as part of the 300 A surveillance array. The gradient across the IFRC site is on the order of a centimeter. Accurate modeling of IFRC flow directions and plume migration require very accurate head and gradient measurements with high temporal resolution.  A second issue is that our shallow monitoring wells are not adequately screened to monitor the full range of water table fluctuation and hence, U solubilization from, the lower vadose zone.  Both of these issues can be remedied by the installation of a series of new wells as described in the January 2010 Quarterly report.  We have recently received estimated costs that will allow us to install 8-10 new wells.  Their locations have been staked in the field and we are working toward their installation in mid-March 2010 to allow monitoring of the spring water table excursion into the contaminated lower vadose zone.  This new, unplanned phase of well installation is described in **Section III**.

The observance of vertical well bore flows in our 26 fully screened wells has arisen as a significant issue in the last quarter of FY 09 that was described in the January 2010 Quarterly.  Two new activities have been initiated to further characterize and understand this problem, and to identify a mitigation strategy if needed (Figure I-1; vertical flow characterization/mitigation and well bore flow modeling).  Vertical flows complicate interpretation of our field experiments, and must be taken seriously.  An update on this issue and a discussion of potential mitigation strategies is provided in this report.

The Hanford IFRC has established strong collaborations with PNNL's Scientific Focus Area (SFA) research team beginning in CY 08.  A summary of SFA research can be found at www.pnl.gov/biology/sfa.  The SFA is investigating biogeochemical processes controlling contaminant dynamics in subsurface microenvironments and transition zones, and has a strong emphasis on microscopic reaction and transport processes, their modeling, and parameter up-scaling to the field. The following SFA activities are being performed in collaboration with the Hanford IFRC:  i.) uranium reactive transport laboratory experiments and modeling using intact sediment cores from the IFRC saturated and lower vadose zones (October 2009 Quarterly); ii.) installation of down-well microcosms, coupons, and flux meters to investigate in-situ biogeochemical processes in the IFRC well-field (January

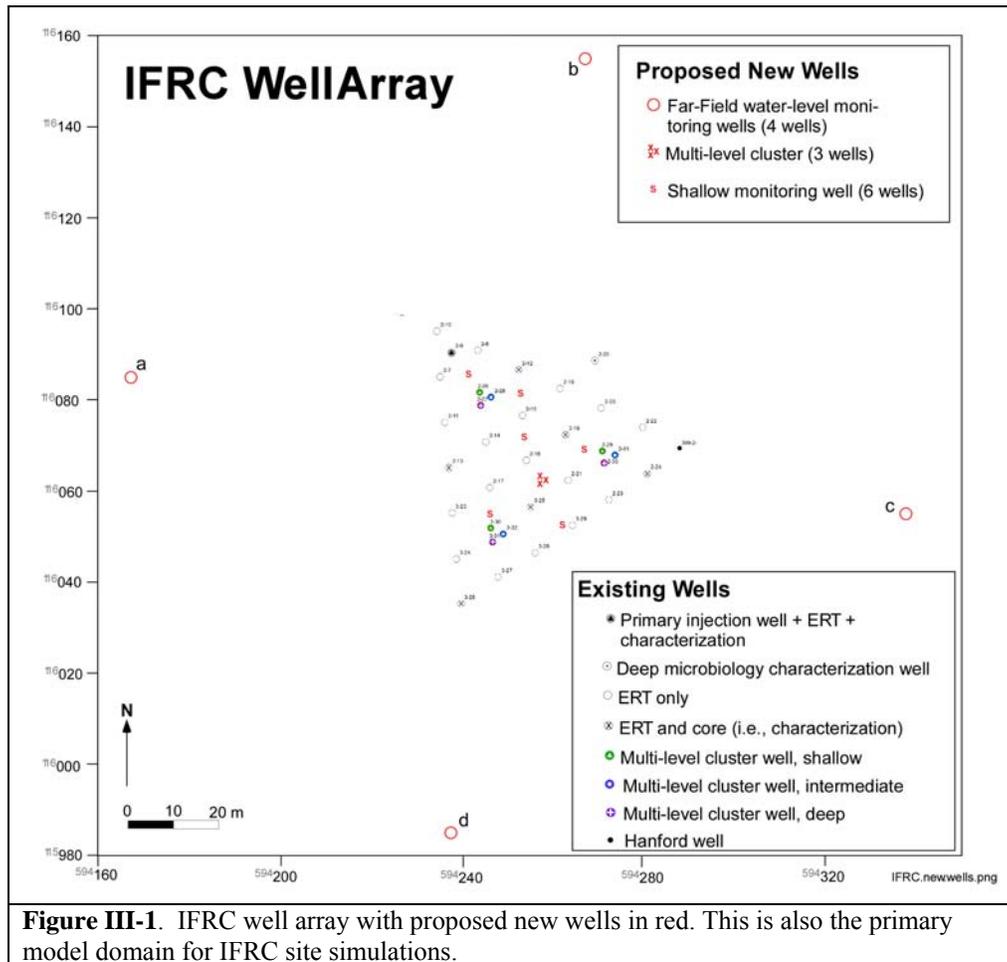2010 Quarterly and this report), and iii.) development of pore scale reactive transport models including surface complexation and mass transfer for microscopic to megascopic scaling studies at the IFRC.

Legend: ■ = Completed (blue), ▨ = In progress (yellow), ▦ = Not started (red)

| Hypothesis/Experiment Year | FY 2007 Year 1 | | | | FY 2008 Year 2 | | | | FY 2009 Year 3 | | | | FY 2010 Year 4 | | | | FY2011 Year 5 | | | |
|---|---|---|---|---|---|---|---|---|---|---|---|---|---|---|---|---|---|---|---|---|
| Quarter | 1 | 2 | 3 | 4 | 1 | 2 | 3 | 4 | 1 | 2 | 3 | 4 | 1 | 2 | 3 | 4 | 1 | 2 | 3 | 4 |
| **Site Infrastructure** | | | | | | | | | | | | | | | | | | | | |
| Site design and set-up | | | ■ | ■ | ■ | ■ | | | | | | | | | | | | | | |
| Well installation | | | | | | | ■ | ■ | ■ | | | ■ | ■ | ▨ | ▨ | | | | | |
| Plan for vadose zone site | | | | | | | | | | | | | | ▦ | ▦ | | | | | |
| Vadose zone site installation | | | | | | | | | | | | | | | | ▦ | ▦ | | | |
| **Characterization** | | | | | | | | | | | | | | | | | | | | |
| Characterization plan | | | | | | | | | ■ | ■ | | | | | | | | | | |
| Field hydrology | | | | | | | | | | ■ | ■ | | ■ | ▨ | ▨ | ▨ | | | | |
| Groundwater composition | | | | | | | | | | ■ | ■ | ■ | ■ | ▦ | ▦ | ▦ | ▦ | ▦ | ▦ | ▦ |
| Field geophysics | | | | | | | | | | ■ | ■ | ■ | | | | | | | | |
| Laboratory phys./chem. measurements | | | | | | | | | | ■ | ■ | | | ▨ | ▨ | ▨ | | | | |
| **Saturated Zone Experiments** | | | | | | | | | | | | | | | | | | | | |
| Experimental plan | | | | | | | | | ■ | ■ | | | ▨ | ▨ | | | | | | |
| Multitracer/cold water | | | | | | | | | | ■ | ■ | | | ▨ | ▨ | ▨ | | | | |
| Desorption injection | | | | | | | | | | | | ■ | | ▨ | ▨ | ▨ | | | | |
| Adsorption injection | | | | | | | | | | | | | | | ▦ | ▦ | | | ▦ | ▦ |
| Passive rising/falling WT | | | | | | | | | | | ■ | ■ | ▨ | ▨ | ▨ | | | ▦ | ▦ | |
| Vertical flow characterization/mitigation | | | | | | | | | | | ■ | | ▨ | ▨ | | | | | | |
| Isotopic exchange | | | | | | | | | | | | | | ▨ | | | ▦ | ▦ | ▦ | |
| In-situ microbiologic activity | | | | | | | | | | | | ■ | | ▨ | ▦ | ▦ | ▦ | ▦ | ▦ | ▦ |
| **Vadose Zone Experiments** | | | | | | | | | | | | | | | | | | | | |
| Experimental plan | | | | | | | | | | | | | | ▦ | ▦ | | | | | |
| **Modeling and Interpretation** | | | | | | | | | | | | | | | | | | | | |
| Updated hydrogeologic model | | | ■ | ■ | ■ | ■ | ■ | ■ | ■ | ■ | ■ | ■ | ■ | ▨ | ▨ | ▨ | | | | |
| Site geostatistical model | | | | | | | | | | ■ | ■ | ■ | ■ | ▨ | ▨ | ▨ | ▨ | | | |
| Geochemical model | | | | | | | | | | ■ | ■ | ■ | ▨ | ▨ | ▨ | ▨ | | | | |
| Multi-scale mass transfer | | | | | | | | | | ■ | ■ | ■ | ▨ | ▨ | ▨ | ▨ | | | | |
| Well bore flow modeling | | | | | | | | | | ■ | ■ | ■ | ▨ | ▨ | ▨ | | | | | |
| Conditional simulations | | | | | | | | | | | ■ | ■ | ▨ | ▨ | ▦ | ▦ | | | | |
| Integrated process model | | | | | | | | | | | ■ | ■ | ▨ | ▨ | ▦ | ▦ | ▦ | ▦ | ▦ | |
| **Data Management** | | ■ | ■ | ■ | ■ | ■ | ■ | ■ | ■ | ■ | ■ | ■ | ■ | ▦ | ▦ | ▦ | ▦ | ▦ | ▦ | ▦ |
| **Management Activities** | | | | | | | | | | | | | | | | | | | | |
| NEPA documentation & permitting | | ■ | ■ | | | | | ■ | ■ | ■ | | | | | | | | | | |
| Project documents | | ■ | ■ | ■ | | | | | | | | | | | | | | | | |
| Project management | | ■ | ■ | ■ | ■ | ■ | ■ | ■ | ■ | ■ | ■ | ■ | ■ | ▨ | ▨ | ▨ | ▨ | ▨ | ▨ | ▨ |
| Reporting | | ■ | ■ | ■ | ■ | ■ | ■ | ■ | ■ | ■ | ■ | ■ | ■ | ▨ | ▨ | ▨ | ▨ | ▨ | ▨ | ▨ |

■ Completed    ▨ In progress    ▦ Not started

**Figure I-1.** 5-Year schedule (updated, 2/15/2010).

## II.    OBSERVED BEHAVIORS OF THE IFRC SITE

The 60 m triangular IFRC well field has now been functional for 16 months after an installation investment of approximately $2000 K. Much has been learned over this time period through research performed by both IFRC and PNNL-SFA investigators. Many physical, chemical, and microbiologic analyses have been performed on collected sediments and groundwaters, and extensive field hydrologic and geophysical characterization measurements have been completed. A series of exploratory and hypothesis-driven injection experiments have been performed, as well as a comprehensive passive monitoring experiment. State-of-art reactive transport models are now being parameterized and used to simulate results.  Overall, the site displays complex behavior that has puzzled investigators in multiple disciplines. Key generalized observations and findings of these activities are summarized below.

1.)    There are three hydraulic conductivity (K) zones in the saturated zone: top, middle, and bottom. The upper and lower zones are high K (averaging 8640 and 6886 m/d, respectively) and the middle zone is lower K (average of 3446 m/d).  There are significant x-y and x-z variations in the thickness of these zones. In situ geophysical measurements show promise to map these zones.

2.)    A paleo-erosional channel runs through the center of the well field that is manifest as a topographic low in the Hanford-Ringold contact at the base of the U-contaminated aquifer zone. Tracer behavior indicates that fast flow paths exist in the upper and lower high K zones associated with this geologic feature.

3.)    There is evidence for field-scale, mass transfer limited physical domains in spite of high average hydraulic conductivities. Non-reactive tracer is slow to enter and to be released by these zones that are associated with the lower K middle zone. Significant tailing is consequently observed in the field breakthrough curves of non-reactive tracers monitored by the fully screened wells.

4.)    The IFRC site groundwater is in intimate hydrologic communication with the Columbia River. Each and every river stage oscillation causes head change in the IFRC wells.  This highly dynamic behavior is well-described by IFRC site hydrologic models.

5.)    Vertical well-bore flows occur in the fully screened wells. Vectors are both up and down and vary between wells.  Magnitudes and timing correlate with river stage and associated pressure gradients. The vertical well flows can reverse multiple times during field experiment performance and complicate results interpretation.

6.)    The non-reactive tracer results have been difficult to simulate with site hydrologic models, in part because observed behaviors are not fully consistent with measured hydraulic conductivity values. Improvements, however, occur with the incorporation of new characterization results from ongoing measurements, and inversion modeling of tracer experiments. Vertical well-bore flows were an unrecognized complication that influenced well-specific breakthrough curves, and these are now being dealt with explicitly.

7.)    Geochemical characterization of the sediments is difficult because contaminant U(VI) is very slow to desorb and difficult to remove from the sediments.  Intact cores of sediments from the lower vadose and saturated zone exhibit mass transfer limited adsorption-desorption.

8.)    Labile, adsorbed contaminant U(VI) concentrations are low but quantifiable in the saturated zone (<1 µg/g) because of groundwater removal, but increase in the lower vadose zone (2-6 µg/g).

9.) Surface complexation strength decreases in moving from the seasonally saturated lower vadose zone to the continually saturated aquifer region.  This may result from the advective removal of fines.

10.) Significant concentrations of dissolved U(VI) are released from the lower vadose zone to groundwater in the SE quadrant of the site during spring high water. Dissolved U(VI) concentrations are high at the rising water-table interface as it advances into the vadose zone.

11.) Natural mixing of groundwaters in the different hydraulic conductivity zones appears to be limited, as high U(VI) that is solubilized from the vadose zone remains elevated in the upper aquifer zone for months after high water and displays distinct isotopic signature.

12.) A relatively abundant, active, and phylogenetically diverse subsurface microbial community has been observed and characterized in the IFRC aquifer sediments by PNNL-SFA collaborators.

# III.    SITE INFRASTRUCTURE

Up to 13 new wells, located on Figure III-1, are planned to support ongoing activities with the IFRC project.  The proposed wells fall into three functional categories: 1) four, far-field, groundwater – monitoring wells, 2) another three-well cluster, and 3) up to six shallow groundwater-monitoring wells within the footprint of the IFRC Site.



**Figure III-1**.  IFRC well array with proposed new wells in red. This is also the primary model domain for IFRC site simulations.

A subcontract is being prepared with the Hanford contractor (CHPRC) to drill, sample, and complete these wells in time for the spring 2010 experiments.  As with the original set of wells, all new wells will be completed with 4-inch PVC.  Screens for the far-field wells will be 25 ft long and installed to monitor changes in unconfined hydraulic gradient beyond the perimeter of the IFRC site.   New shallow wells within the footprint will be completed with 15-20 ft screens that will monitor the top of the uppermost aquifer, which includes the shallowest of the wells within the three-well cluster.  The other two cluster wells will be completed with 2-ft screens at the middle and bottom of the unconfined (Hanford formation) aquifer, respectively.  The far-field monitoring and three-well cluster wells have first and second priority.  Lastly, as many of the six shallow, monitoring wells will be completed with the remaining funds in the time available before the spring experiments.

# IV.    CHARACTERIZATION

## IV.1.  Hydrologic Characterization

Modeling of flow and transport experiments performed at the 300 Area IFRC site requires estimates of physical, hydraulic, and transport parameters, and initial and boundary conditions. Field hydraulic characterization that has been performed to date includes short-duration constant rate injection tests in fourteen of the IFRC wells to estimate bulk Hanford Fm hydraulic conductivity (K). Electromagnetic borehole flow-meter (EBF) testing was also performed in twenty-six of the wells, with 30- to 60-cm (1-2 ft) spacing between measurements. The EBF data for six of the tested wells exhibited non-representative results caused by strong ambient flow conditions and/or flow bypass through the sand-pack.  Therefore reliable EBF data are available for twenty (of 26 tested) wells.

The short-duration constant rate injection and electromagnetic borehole flowmeter (EBF) data have been combined to estimate absolute values of hydraulic conductivity at the measurement locations. Variography has been performed to estimate the spatial autocorrelation structure and anisotropy of hydraulic conductivity at the site. Various methods for spatial interpolation and stochastic simulation (e.g. kriging, co-kriging, inverse-distance interpolation, and sequential Gaussian simulation) have been employed for generating spatially-distributed K values representing the IFRC well field and its surroundings (Rockhold et al. 2010; Zheng et al. 2009; Chen et al. 2009). Figure IV.1-1 shows cutaway views of estimated 3D hydraulic conductivity distributions at the IFRC site. The constant rate injection test and EBF data have also been reanalyzed and alternative representations of the 3D K distribution have been generated using a Bayesian method as discussed in **Section VI.3** (Murakami et al. 2009).
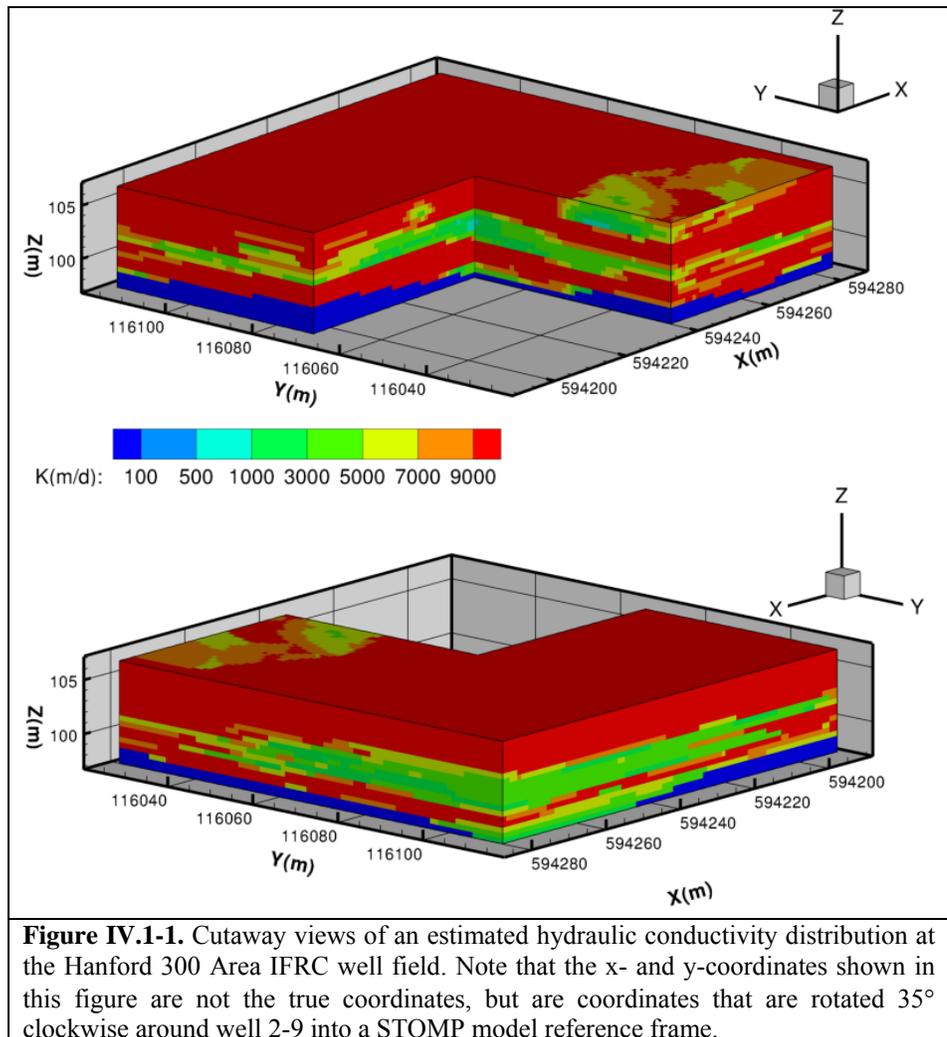


**Figure IV.1-1.** Cutaway views of an estimated hydraulic conductivity distribution at the Hanford 300 Area IFRC well field. Note that the x- and y-coordinates shown in this figure are not the true coordinates, but are coordinates that are rotated 35° clockwise around well 2-9 into a STOMP model reference frame.

Relatively few intact core samples from the IFRC site have been analyzed to determine porosities. Accurate measurement of porosity from intact core samples can be problematic for this site owing to the very coarse nature of the (gravel- and cobble-dominated) Hanford Fm relative to the typical size (4- or 5-in diam.) of core barrels used for sampling. Analyses of data from a previous 300 Area limited field investigation (LFI) have shown relatively strong correlations between core porosities and gamma log readings (Figure IV.1-2). Correlations have also been developed for different grain size distribution metrics and spectral gamma log data (Williams et al. 2008; Draper et al. 2009).

Borehole gamma and spectral gamma log data are currently being evaluated for use in conjunction with core data to estimate porosity and other properties at the site using different methods (e.g. co-kriging and petrophysical relationships). In addition, measurements of relative permeability-saturation-capillary pressure relations are being made on intact cores in preparation for vadose zone flow and transport experiments that are planned for FY 11. Transport experiments have also been performed on intact IFRC cores, in collaboration with a PNNL SFA project (John Zachara, PI). Densities, porosities, and grain-size distributions are being measured on all intact cores that have been used for these other experiments to maximize the data obtained from the intact core samples.
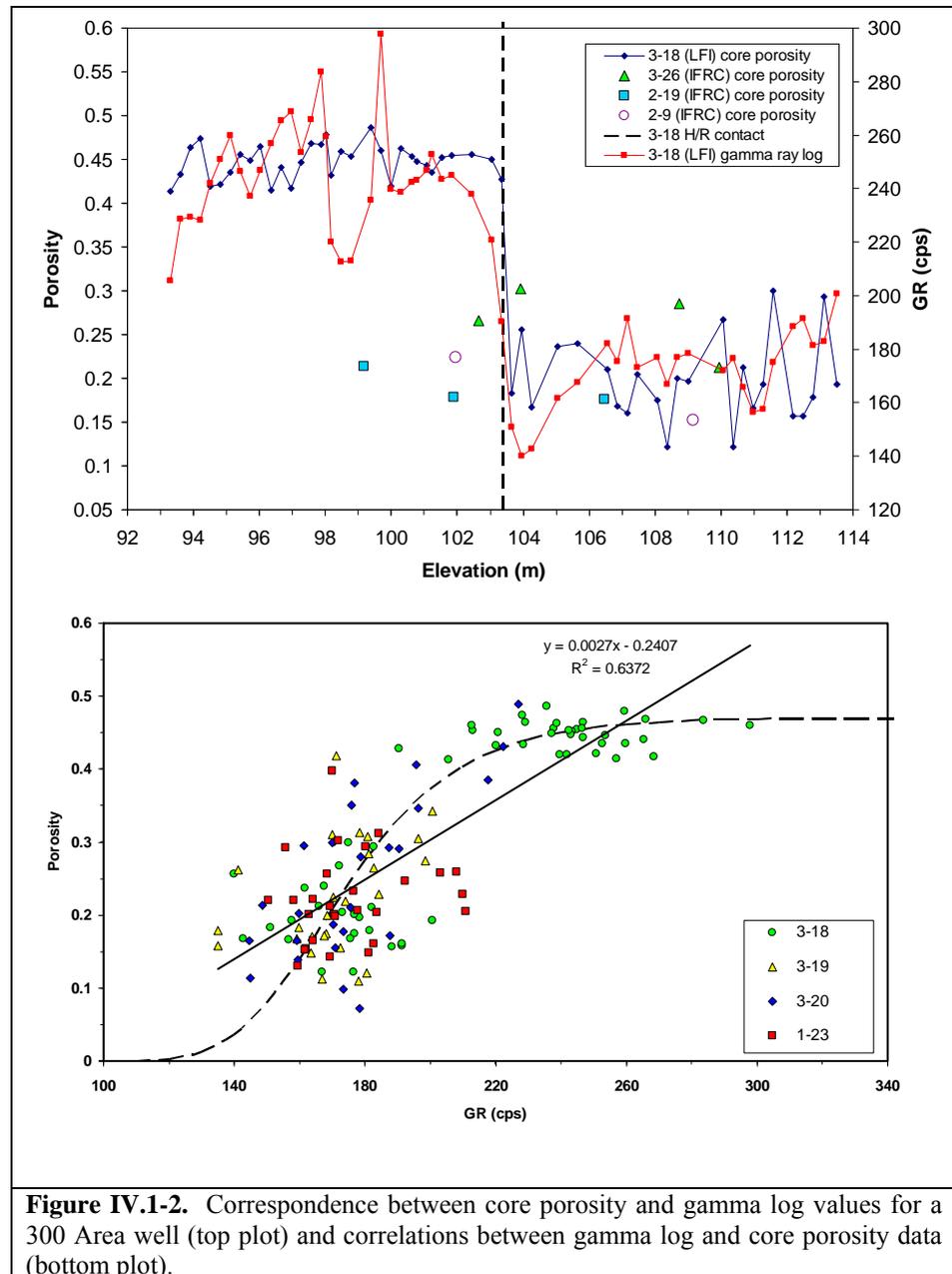


**Figure IV.1-2.** Correspondence between core porosity and gamma log values for a 300 Area well (top plot) and correlations between gamma log and core porosity data (bottom plot).

**IV.2.  Geophysical Characterization**

The objective of the field geophysical characterization task is to support the flow and transport modeling efforts by providing detailed 3D information on hydrologic and reactive properties both within the IFRC wellfield and in the larger Hanford 300 Area.  IFRC field geophysical research has three primary elements.

1.) Determination of macroscopic 3D and 4D distributions of physical properties from borehole logs and electrical geophysical measurements.
2.) Development of transform functions between physical properties and hydrological and geochemical properties of interest. This effort is performed in collaboration with the PNNL SFA, which supports broadband spectral measurements on IFRC cores.
3.) Estimation of hydrologic properties through the use of coupled electrical geophysical/hydrogeological codes.

In the first years the focus has been on elements (1), and the groundwork has been laid for components (2) and (3).  In subsequent years we anticipate shifting the focusing work to elements (2) and (3).  In this section we first describe the geophysical instrumentation and data, and then give a brief overview of the efforts and results for each effort, as well as on the proposed work for subsequent years.

Approach and Instrumentation

The Hanford 300 Area IFRC is equipped with an extensive downhole electrical resistivity and induced polarization (ERT/IP) array. This array consists of electrodes placed either adjacent to the wells (in the vadose zone) or in the wells (in the saturated zone). A total of 28 wells are instrumented with 30 electrodes each. Data from these wells is collected by an 8 channel, 256 electrode resistivity/IP system.  Each well is connected to a central trailer to facilitate switching between acquisition



**Figure IV.2-1**. Superimposed 2D resistivity sections covering the larger Hanford 300 area.  The sections show the general extent and depth of the Hanford Ringold contact.
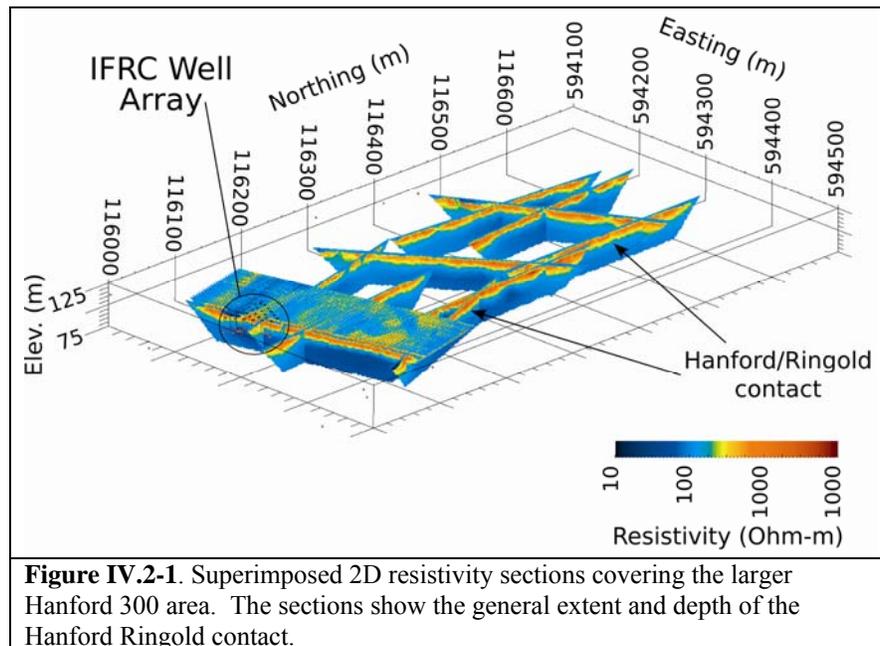
configurations.  In addition to data collected by this array, a number of geophysical borehole data were collected during and after the well installations (Table IV.2-1).  Surface geophysical data were collected prior to and subsequent to the IFRC well field installation. These include larger scale 2D surface ERT lines used to map the Hanford Ringold contact depth and also to identify the location of paleochannels within the Hanford formation (Figure IV.2-1).

The well electrode array is also being used for passive monitoring efforts in which timelapse data are collected to track natural variations in resistivity due to river stage fluctuations. 3D electrical characterization data were collected both in December 2008/January 2009 (using a single channel resistivity system) and again in August 2009 using a multichannel system purchased and installed in the summer of 2009.

**Table IV.2-1** Geophysical borehole data collected at the 300 Area IFRC site. Data collection prior to well completion was collection was done by Stoller. Data collection subsequent to well completion was done by Golder.

| Type of log | When collected | Note |
|---|---|---|
| Spectral Gamma | Prior to well completion | |
| Neutron Moisture | Prior to well completion | |
| Acoustic Televiewer | Subsequent to well completion | |
| Crosshole radar | Subsequent to well completion | Zero offset data |
| EM induction | Subsequent to well completion | Data is noisy in most wells due to instrumentation |
| Gamma | Subsequent to well completion | |
| Magnetic Susceptibility | Subsequent to well completion | |

Results

*Borehole Logs and Electrical Geophysical Measurements.* A primary objective of the geophysical characterization effort is to determine macroscopic 3D and 4D distributions of physical properties primarily from resistivity and IP measurements but also from borehole logs. Borehole logs can be interpolated (i.e., kriged) to give estimates of property distributions (Figure IV.2-2) but these distributions are highly uncertain away from the boreholes.

The primary dataset for the bulk conductivity characterization of the IFRC well field includes several hundred thousand resistivity measurements distributed
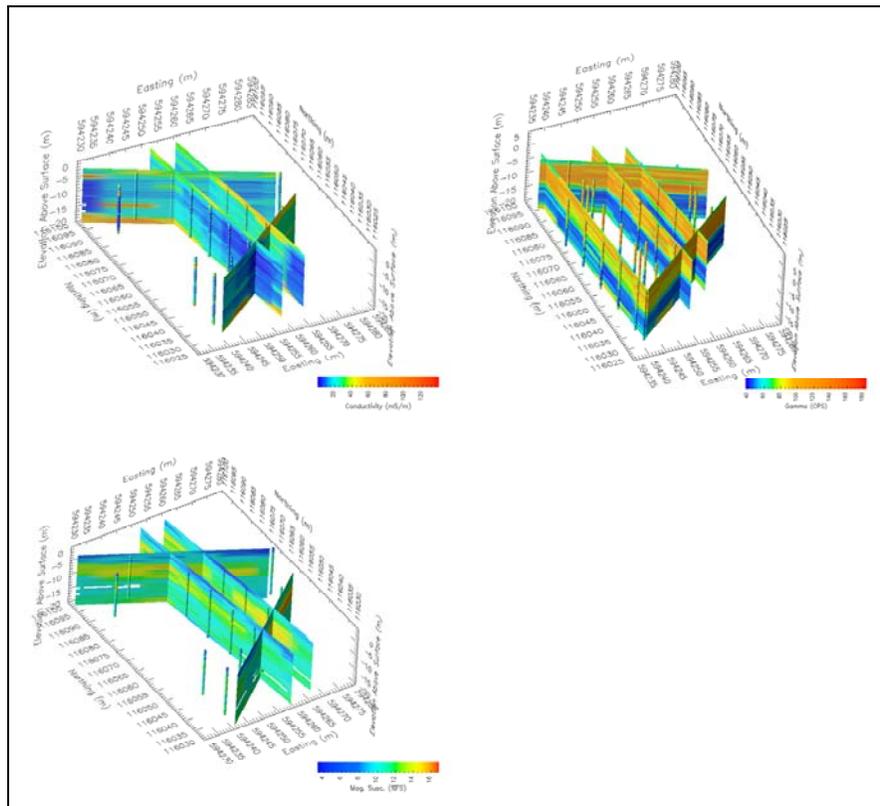


**Figure IV.2-2.** Electrical conductivity (left), Gamma count (middle), and magnetic susceptibility (right) based on kriged interpolations of borehole logs.

over the 840 electrodes. These measurements were collected with the multichannel ERT/IP system in overlapping groupings of wells over a period of six days.

Commercially available ERT/IP inversion codes are not capable of simultaneously inverting data sets of the size and scale of the IFRC characterization data set described above.  To invert these data, we used a parallel high performance ERT/IP inversion code developed at the Idaho National Laboratory, an effort supported in part by IFRC funding. This code and the application of this code to perform a regularized inversion of the data for the IFRC array are described in Johnson et al., 2010 and Versteeg et al., 2010.

Standard regularized inversion suffers from two primary limitations in terms of providing quantitative estimates of the distribution of subsurface electrical properties. Such quantitative estimates are necessary for flow and transport properties to be reliably inferred by combining bulk conductivity estimates, chargeability estimates, and petrophysical transforms. The first limitation is the smoothing effect of regularized inversion, which arises do to the inability of resistivity and IP data to resolve electrical properties at sufficiently small scales. That is, regularized inversions, while qualitatively useful, are not geostatistically accurate and are therefore of limited utility when used to infer regions of continuous flow and transport properties



**Figure IV.2-3**.  Left column: (A) Regularized Inversion (B). Ensemble mean of 100 realizations (C) Ensemble standard deviation of 100 realizations. Right column: Three equally probably realizations (subset of the 100 realizations).

with relatively sharp boundaries. The second limitation is that uncertainty estimates are difficult to produce using regularized inversion, particularly for large data sets such as the IFRC characterization data set. Without uncertainty estimates it is not possible to determine how much weight should be placed on geophysically derived estimates of flow and transport properties in comparison to those derived with other data types in a multiple data-type integration scheme. Such a scheme (the MAD scheme, **Section VI.3**) is being employed by Co-PI Rubin in an effort to reduce uncertainty in flow and transport property
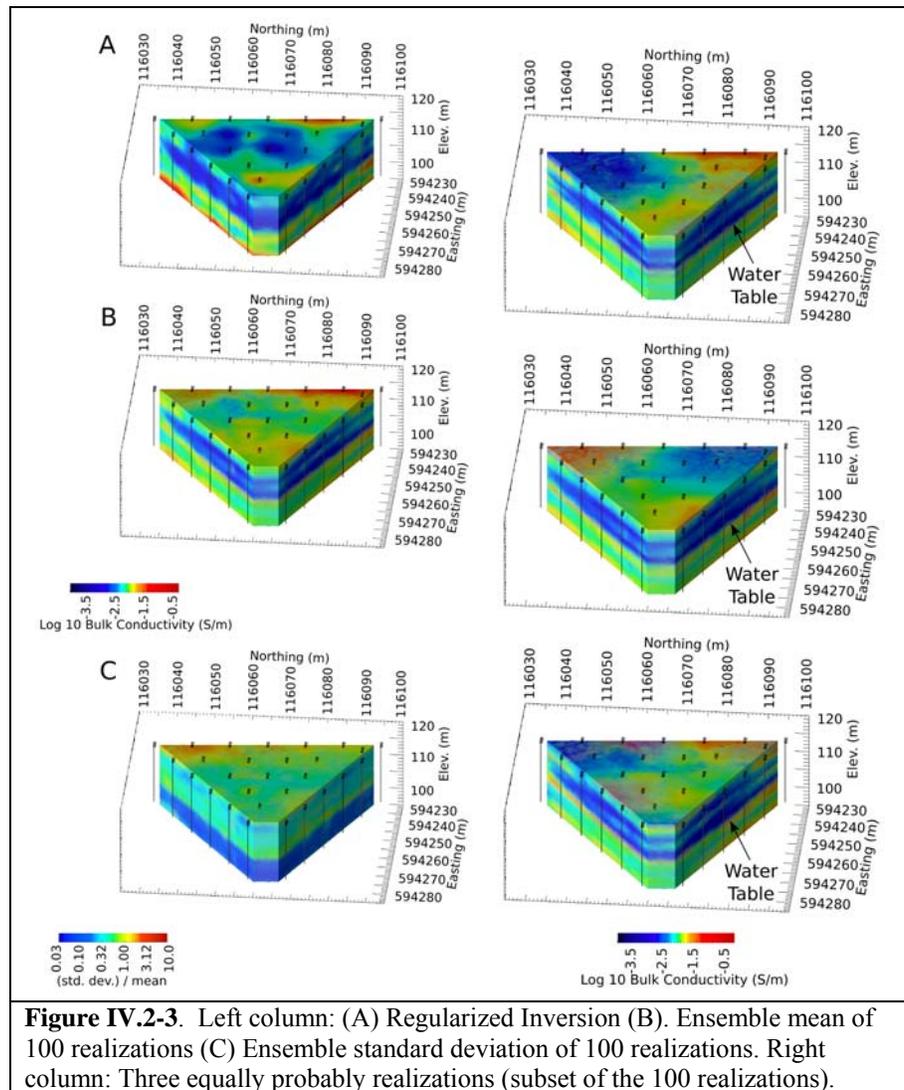
estimates. In order to utilize geophysically derived estimates of flow and transport properties in the MAD scheme, these estimates must be accompanied by corresponding measures of uncertainty.

In order to optimize the utility of bulk conductivity characterization results to IFRC flow and transport modelers, we have addressed each of the limitations discussed above by developing a method of ERT inversion that utilizes spatial covariance information to constrain the ERT inversions instead of regularization (or smoothness) constraints. In this approach, a gradient based optimization technique is used to generate an ensemble of bulk conductivity realizations which both honor what is known about the spatial covariance structure of bulk conductivity, while simultaneously honoring the resistivity measurements. The spatial covariance structure is estimated through geostatistical analysis of borehole electromagnetic induction logs, resulting in a probability distribution of semivariograms that are used to constrain realizations in the ensemble. Each realization is geostatistically accurate, thereby addressing the smoothness limitation of regularized inversion. In addition, statistical measures of the bulk conductivity distribution, including the probability distribution functions for each estimated parameter, may be developed through ensemble statistical analyses, thereby addressing the uncertainty issue.

A manuscript describing and demonstrating this approach for the IFRC data set was submitted to Water Resources Research in January of 2010 (Johnson et al., 2010; Versteeg et al., 2010). Results of this effort are shown in Figure IV.2-3. This figure shows (on the right) 3 equally probable realizations of the bulk conductivity structure of the IFRC well field. On the left we show the regularized solution for comparison, the ensemble mean, and the ensemble standard deviation of 100 realizations. Comparing the realizations gives a visual indication of the variability and uncertainty in the bulk conductivity distribution, which are summarized by the mean and standard deviation. Notable features include the strong contrast in conductivity at the water table, and the continuity of layered structures at the site. A well defined higher conductivity unit at the surface of the site is likely associated with backfill materials used to replace contaminated surface materials removed during prior remediation efforts. Of particular note in each realization is the layered structure of the saturated zone, consisting of a lower bulk conductivity unit in the center bounded by higher bulk conductivity sections at the top and bottom. These units correlate well with hydraulic conductivity estimated along several using electromagnetic borehole flowmeter (EBF) data, as discussed in detail in the January 2010 Quarterly Report, and herein.

*Transform Functions Between Physical Properties and Others.* Once estimates of electrical properties have been generated, the challenge is to translate these estimates into hydrogeological and geochemical properties of interest. This requires the development and application of a petrophysics transform which relates electrical properties to hydraulic properties

There are two approaches for developing IFRC specific petrophysical relationships between electrical and hydrogeological properties.

1.) In the correlation-based approach we use field-based measurements of hydrogeologic and/or geochemical properties of interest and we correlate these measurements with ERT/IP-based estimates of electrical conductivity and chargeability. Any resulting correlation provides an estimated petrophysical transform, including uncertainty. This approach relies heavily on the assumption that contiguous regions of electrical properties correspond to contiguous regions of hydrologic properties. As shown below this assumption seems to hold in the saturated zone, where bulk conductivity and hydraulic conductivity appear to be well correlated.
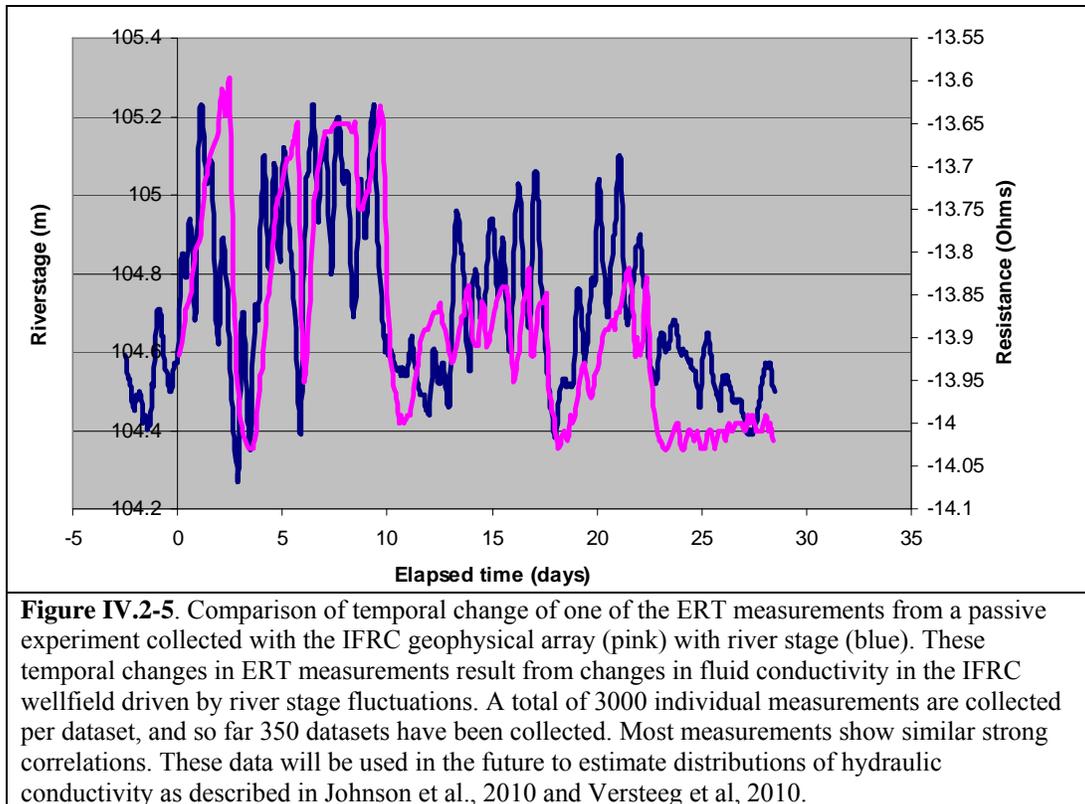
2.) An alternative approach is through direct column-scale measurements of electrical properties and corresponding hydrogeological properties of sediments. This effort is currently ongoing under sponsorship of the PNNL SFA, and results of these will be presented at the SESP 2010 meeting.

Recent results of the first approach are shown in Figure IV.2-4, in which correlations between the EBF derived estimates of hydraulic conductivity and the estimates of bulk conductivity extracted from the ensemble mean distribution (Figure IV.2-3) are shown for the saturated zone for two representative wells (other wells show similar results). Work on translating these results into a petrophysical transform is under way (it looks like there is a shift between the two datasets which need to be accounted for and corrected). These transform results and the results from the geostatistical ERT inversion together will constitute a method of estimating the 3D structure of hydraulic conductivity in high resolution, including uncertainty in those estimates.



**Figure IV.2-4** Scaled EBF derived hydraulic conductivity estimates (**blue**) and ERT derived estimates of bulk electrical conductivity (**red**) extracted from the ensemble mean distribution. Note that the EBF logs only start at the saturated part, but the conductivity estimates extend across the saturated and unsaturated zones. Data are normalized for easy comparison. Note that the spatial shift between these data sets needs to be resolved to define a correct petrophysical transform.

The apparent strong positive correlation between bulk electrical conductivity and hydraulic conductivity in the saturated zone seen in Figure IV.2-4 can be explained when (as is plausible) current flow is primarily ionic. In this case the fluid conductivity is much greater than the matrix conductivity, and current flow in the electrical double layer (i.e. surface conduction) is negligible. Like fluid flow, current flows primarily through connected pore space, and is sensitive to the same mechanical properties that govern fluid flow such as effective porosity and tortuosity. Correlations between mechanical and electrical properties in the unsaturated zone may also be significant, but will follow different physical models because current flow is not likely to be dominated by ionic currents.

*Coupled Electrical Geophysical and Hydrologic Code*. In contrast to inferring hydrogeologic properties from electrical properties using petrophysical estimates as described above, a second (complimentary) inversion-based approach was recently developed and discussed in Johnson et al., 2010; Versteeg et al., 2010. In this approach we perform a joint inversion of time-lapse head, concentration, and electrical resistivity data to estimate hydraulic conductivity. This approach requires an electrically conductive tracer experiment where tracer transport modifies bulk conductivity and can be monitored through time-lapse resistivity measurements. Although electrical geophysical data were collected during the tracer experiments conducted at the IFRC (and this data did show qualitative changes associated with these

**Figure IV.2-5**. Comparison of temporal change of one of the ERT measurements from a passive experiment collected with the IFRC geophysical array (pink) with river stage (blue). These temporal changes in ERT measurements result from changes in fluid conductivity in the IFRC wellfield driven by river stage fluctuations. A total of 3000 individual measurements are collected per dataset, and so far 350 datasets have been collected. Most measurements show similar strong correlations. These data will be used in the future to estimate distributions of hydraulic conductivity as described in Johnson et al., 2010 and Versteeg et al, 2010.

tracers) the data did not provide sufficient spatial and temporal resolution to be of use in our joint inversion approach. This is primarily due to the constraints on ERT/IP data acquisition imposed by other data acquisition efforts. However, we can also use passive tracers such as the changes in bulk conductivity resulting from natural changes in groundwater conductivity driven by fluctuations in river stage). Figure IV.2-5 shows changes in resistance measurements collected from December 2009 through February 2010 and corresponding changes in river stage over the same interval in a passive experiment in which time-lapse electrical geophysical data are collected at 200 minute intervals. These resistance measurements are few samples of approximately 3000 measurements collected during each interval.

Summary and Future Directions

While we anticipate that we will continue to enhance and refine the imaging component of the geophysical monitoring effort (specifically by the use of spectral IP data in the imaging), the future geophysical efforts at the Hanford 300 Area IFRC will primarily focus on two tasks.

1.) Imaging of active and passive experiments. Issues concerning data acquisition (both in terms of interference between different sensors and in terms of spatial and temporal acquisition configurations) have been resolved. Hardware, processing tools and framework are in place for future active experiments to be imaged successfully such that results can be provided to the modeling team. This aligns with element (3) above, and will leverage coupling between the electrical geophysical and reactive transport models.

2.) Further development of the petrophysical transform component. This will be done both through physical measurements of cores and samples, and the development and validation of conceptual

and numerical models linking electrical geophysical properties to hydrological and geochemical properties and processes.

## IV.3.  Uranium Isotopic Systematics

Ongoing uranium isotopic research is being carried out on the 300 Area groundwater plume and sediments in general, and with a specific focus on the IFRC experimental plot.  The research has several different aims, including understanding the sources of U in the plume, the temporal dynamics of the plume in its interaction with the Columbia River, the discharge rate of U to the river, the interaction between groundwater U and U held in vadose zone/aquifer sediments, and providing guidance in the selection of particular 300 Area wells for sources of groundwater for use in various experiments conducted within the IFRC plot.  Many of the analyses described herein were performed by a separate ERSP project to LBNL.  The IFRC is supporting ongoing analyses of sediments and water samples from the experimental site as well as other locations to develop a rigorous conceptual model of U source terms in different hydrologic compartments of the IFRC site: upper vadose zone, lower vadose zone, upper high K zone, middle low K zone, and deep high K zone.

Approach

Uranium isotopic analyses ($^{234}$U/$^{238}$U, $^{235}$U/$^{238}$U, $^{236}$U/$^{238}$U) have been conducted on groundwater samples collected by the IFRC team and by the Hanford groundwater monitoring program.  In addition, U isotopic analyses were conducted on sediment leachates provided by James McKinley and Doug Kent on core samples from the IFRC plot, as well as on leachates from sediments samples from trenches excavated at sites below the former NP and SP Ponds provided by John Zachara.  U isotopic analyses were conducted on chemically separated U using a multi-collector ICP source magnetic sector mass spectrometer (MC-ICPMS) at LBNL.
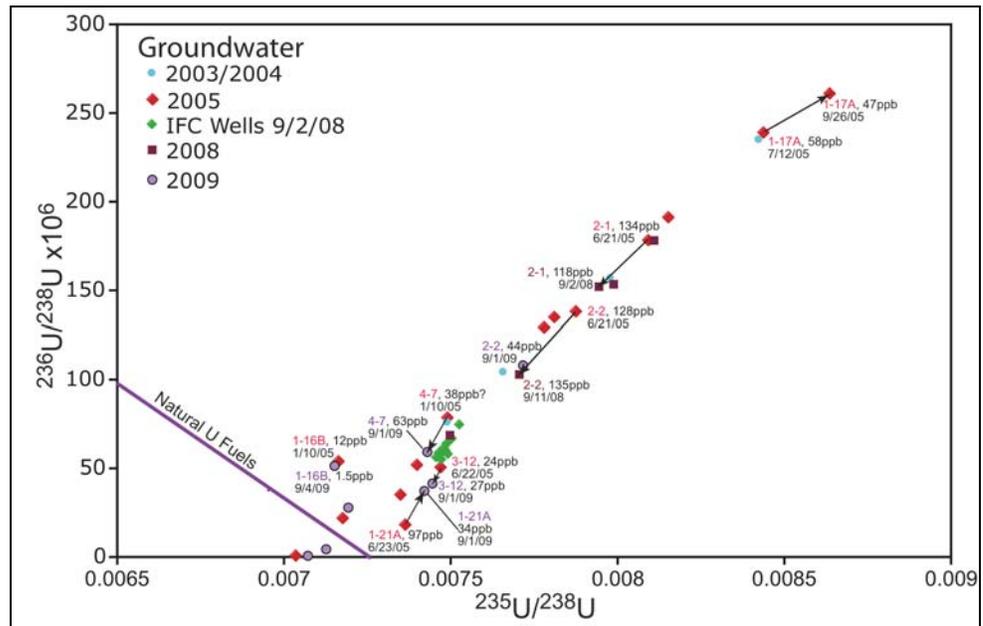


**Figure IV.3-1.** Plot of $^{236}$U/$^{238}$U vs. $^{235}$U/$^{238}$U for 300 Area groundwater samples for 2003-to 2009.  Numbers by particular data points give well number, U concentration (ppb), and sample date.  Samples from well 1-17A show significant U isotopic change between July 2005 and September 2005.  An earlier sample (blue) of 1-17A from August 2003 is nearly identical to the July 2005 sample. Samples from wells 2-1 and 2-2 also show significant changes over 3 yrs. Shorter term changes have now been documented through samples from the Spring 2009 Passive U Mobilization Experiment (see below and Figure IV.3-5).

28

<u>Results</u>

*Groundwater Spatial and Temporal Isotopic Variation.* In Figure IV.3-1, the measured $^{236}U/^{238}U$ of groundwater samples are plotted against their measured $^{235}U/^{238}U$. On such a figure, natural U fuels with variable burn-up in a nuclear reactor would plot along the solid purple line that runs from the composition of natural U ($^{236}U/^{238}U = 0$, and $^{235}U/^{238}U = 0.007253$) upward to the left. Any sample with a U isotopic composition that plots to the left of this line includes a component of depleted U. Hanford enriched U fuels with various degrees of burn-up plot off Figure IV.3-1 far to the upper right, and form arrays sub-parallel to the natural U fuel line. Taken as a group, 300 Area groundwater samples form an array that extends from the left side of the natural U fuel line (no sample has been measured so far that actually falls on the natural U fuel line) upwards to the right towards enriched U fuels. This indicates that the U isotopic variation within the plume is due to variable mixing between processed enriched U fuel of fairly restricted composition, and depleted U (and perhaps low burn-up natural U fuel). Near the lower end of the array, a smaller array splays off, suggesting a significant component of natural U in some groundwater samples (e.g. 399-3-12 and 399-1-21A).

So far, a limited set of groundwater samples (wells 399-1-17A, 399-2-1, 399-2-2, 399-3-12, 399-1-21A, 399-4-7, 399-1-16B) has been analyzed for U isotopic composition that addresses the temporal evolution of the 300 Area Plume (Figure IV.3-1). Groundwater samples taken from 399-1-17A in August 2003 and July 2005 are very similar in U isotopic composition, while the Sept. 2005 sample is shifted further toward higher $^{236}U/^{238}U$ and $^{235}U/^{238}U$ (i.e. toward enriched U fuels). Samples from other wells (e.g. 399-2-2, and 399-2-1) also show large shifts between 2005 and 2008 but in the opposite direction, followed, in the case of 399-2-2 by little change between Sept. 2008 and Sept. 2009. Though these shifts (and smaller shifts seen in serial samples from 399-4-7, 3-12, 1-21A) may be due in part to migration of the U plume, in the light of the U isotopic results from IFRC Passive U Mobilization experiment described below, it may be more an effect of mobilization of U from the vadose zone local to those wells.

Groundwater from wells 399-1-6, 399-1-14A, 399-1-15, 399-1-18A are relatively low in U concentration (5-8 µg/L) and show evidence on mixing diagrams (1/[U] vs. $^{234}U/^{238}U$ and vs. $^{236}U/^{238}U$) of dilution by natural U, either from groundwater or Columbia River water. In contrast, groundwater from a deep well 399-1-16B decreased in U concentration between 2005 and 2008 by a factor of 8 with little shift in U isotopic composition, and no shift towards natural U on mixing diagrams. This is suggestive of adsorption of U to the aquifer sediments, rather than simple dilution, as the main cause of the observed decrease in U concentration in that well.

*Multiple Uranium Isotopic Signatures of 300 Area and IFRC Sediments.* To investigate sources of U in the 300 Area, sediment samples from four pits excavated beneath the former North and South process ponds (Zachara et al. 2005), and samples from borings produced from IFRC well construction were analyzed for U isotopic composition. Bicarbonate extractions were performed on the "Pit" samples, while extractions with both bicarbonate and model groundwater solutions were conducted on the boring samples from IFRC wells. The extracted U was quantified and measured for isotopic composition. Comparing the U isotopic compositions of model groundwater leachates and bicarbonate leachates of IFRC sediments little or no difference can be seen. Because bicarbonate leachates of sediments from 399-2-5 were analyzed, for consistency the discussion below refers to the IFRC bicarbonate leachates.

The results of the U isotopic analyses are presented in Figure IV.3-2 with the groundwater samples from Figure IV.3-1 shown in grey for comparison. There are significant U isotopic differences between the NP and SP ponds, along with U isotopic variation with depth. There are also spatial U isotopic heterogeneities at the scale of the IFRC plot. Sediment samples from 399-2-5 and the SPP2 pit (both in the main portion of the SPP) are similar (cf. Figure IV.3-3), while samples from 399-3-31 and 399-2-26 (from a sub-pond of the SPP originally episodically connected to the main SPP by a conduit/canal) are very different.
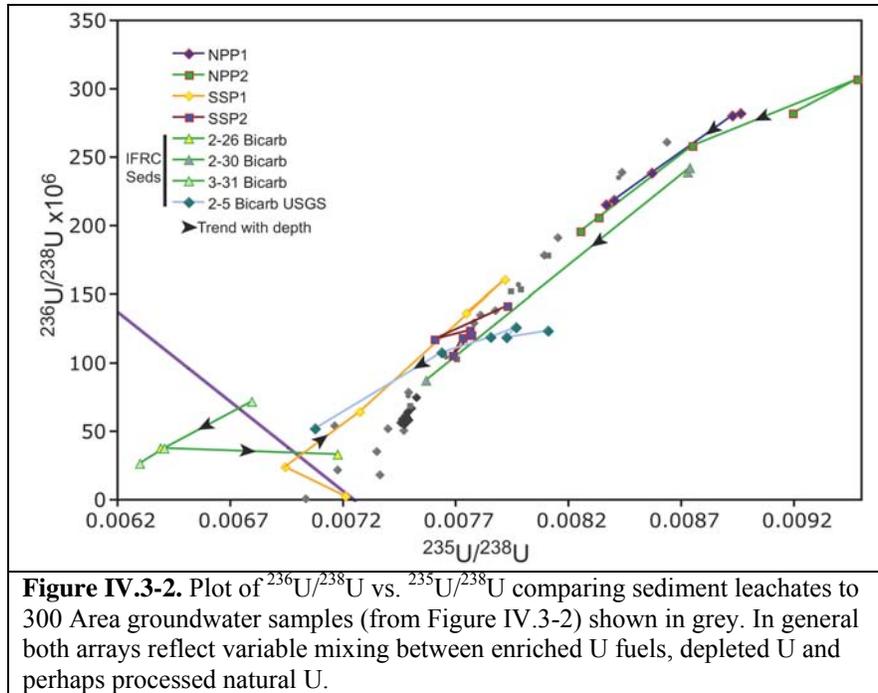


**Figure IV.3-2.** Plot of $^{236}U/^{238}U$ vs. $^{235}U/^{238}U$ comparing sediment leachates to 300 Area groundwater samples (from Figure IV.3-2) shown in grey. In general both arrays reflect variable mixing between enriched U fuels, depleted U and perhaps processed natural U.

In fact some sediment samples from 399-3-31 and 399-2-26 fall the farthest to the left of the natural U fuels line of any 300 Area sample. Overall the U isotopic compositions of the sediment leachates cover the entire range observed in the 300 Area groundwater U plume, and extend that range both toward even higher $^{235}U/^{238}U$ (further toward enriched U fuels) and to lower $^{235}U/^{238}U$ (depleted U). Therefore the U isotopic variation seen in the groundwater plume may then be attributable in large part to contributions from spatially (horizontally and vertically) and isotopically heterogeneous vadose/aquifer sediment sources beneath the former sites
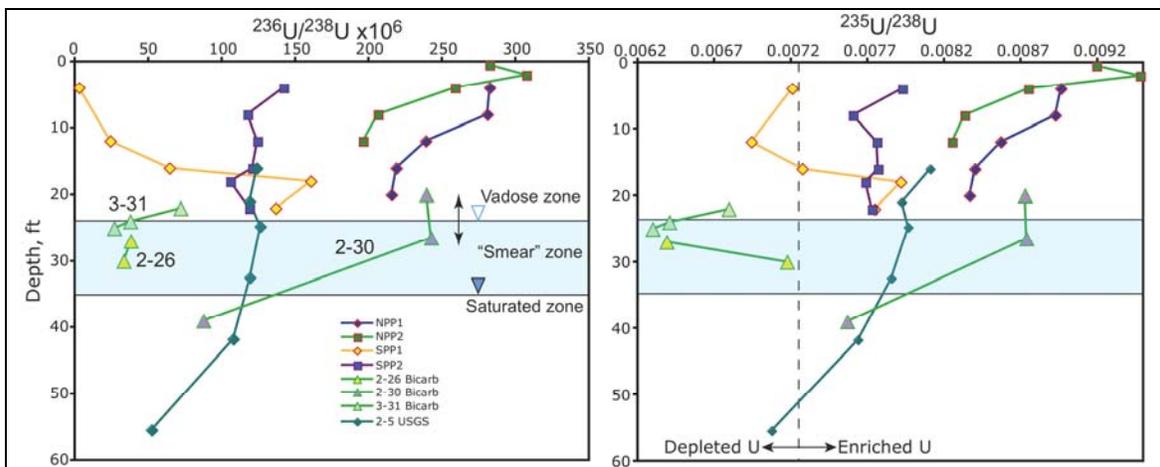


**Figure IV.3-3.** Plots of sampling depth against sediment leachate $^{236}U/^{238}U$ (left) and $^{235}U/^{238}U$ (right). The vertical dashed line in the right panel represents the natural $^{235}U/^{238}U$ ratio. Plotted are results for NPP1, NPP2, SPP1, SPP2 sub-pond excavations and for samples from borings from wells 2-26, 2-30, 2-31 and 2-5 in the IFRC plot. Significant U isotopic local spatial heterogeneity (vertical & horizontal) is represented by the sampled IFRC sediments, nearly spanning that of the other sub-pond sediment profiles. This variability can be accessed by groundwater through changing water table elevation in response to river stage fluctuation.

30

of the North and South process ponds and process trenches. This would be in contrast to a simpler model where the U plume isotopic variability is only due to simple mixing within the plume itself of two distinct sources. If there were ever two distinct U sources (say an enriched U fuel and depleted U of a particular composition), the variable mixing that gave rise to the observed arrays probably occurred as a result of the U disposal histories of the ponds/trenches and sequestration of a portion of that U to sub-pond/trench sediments.

The uranium isotopic data from the sediment leachates are also presented in Figure IV.3-3 as a function of sample depth. Within the "smear" zone there is considerable U isotopic heterogeneity, even considering just the IFRC core samples from wells 3-31, 2-26 and 2-30 and 2-5. As the water table rises through the "smear" zone, there is then the potential for mobilization of U with systematically changing isotopic composition with depth and horizontal position that allows mapping back of changing groundwater composition to particular "smear" zone sediments. This will be discussed further below in the context of the Spring 2009 Passive Mobilization Experiment.

*Fitting the IFRC Experimental Plot into the 300 Area U Isotopic Context.* Samples from a single sampling campaign of the IFRC wells conducted on 9/2/08 (~ 8 hr period) have been analyzed for U isotopic composition, and reveal systematic groundwater U isotopic variation at the scale of the IFRC plot. The results are presented in Figure IV.3-1 (green diamonds), see also Figure IV.3-5, for a more detailed version. The IFRC samples for that day fall toward the lower end of the 300 Area groundwater U isotopic array, and follow the splaying trend set by other local wells towards natural U. The trend of the IFRC well samples are bracketed at the upper end by well 399-3-20 (a 2008 sample), and at the lower end by wells 3-12 (2005 and 2009 samples) and 1-21A (a 2009 sample). The U isotopic variation can be mapped onto the IFRC plot using the measured $^{236}U/^{238}U$ (Figure IV.3-4). Contours of $^{236}U/^{238}U$ suggest a
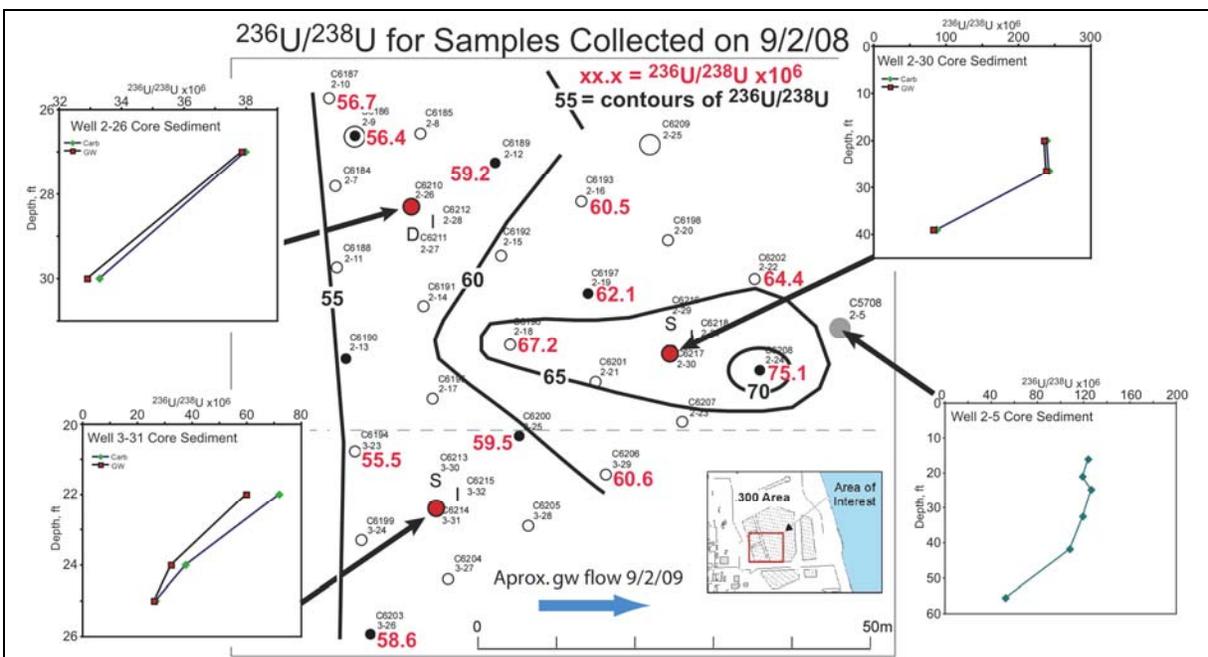


**Figure IV.3-4.** Map of the IFRC experimental plot showing locations of groundwater sampling wells and locations of sediment samplings (red circles). Red numbers are $^{236}U/^{238}U$ measured on groundwater samples collected over an 8 hour period on 9/2/08. Approximate groundwater flow at that time was toward the river at <4 (?) m/day. Black contours are for groundwater $^{236}U/^{238}U$. Small insets show depth profiles of $^{236}U/^{238}U$ for the four borings for wells 2-26, 2-30, 3-31 and 2-5 that are compared and shown in greater detail in Figures IV.3-2 and IV.3-3. The local effect of sediment hosted U at 2-30 (and 2-5) on groundwater can be seen.

local high in groundwater $^{236}U/^{238}U$ (and $^{235}U/^{238}U$), that may be to due higher $^{236}U/^{238}U$ (and $^{235}U/^{238}U$) in the local sediments represented by the borings from wells 2-30 and 2-5.

*Results from the Spring 2009 Passive U Mobilization Experiment.* An exploratory set of samples from well 399-3-30 collected during the spring 2009 Passive U Mobilization Experiment have been analyzed for U isotopic composition.  Further analyses are in progress. During this experiment, rises in the water table into the lower vadose zone (the "smear" zone) zone due to spring river stage increases were found to be associated with rapid elevations in groundwater U concentration (e.g. from 40 μg/L to 270 μg/L over two days, see further description in **Section V.3**).  This first analyzed set focused on bailed samples, picking the top four peaks in U concentration (sampling dates 4/27/09, 5/29, 6/5 and 6/10), four intermediate concentration samples (sampling dates 4/26, 4/29, 4/30 and 5/18), and a sample collected on 4/23, two days before the first rise in U concentration.  The U isotopic data for these samples is presented in Figure IV.3-5, which is at a more detailed scale than Figure IV.3-1 and Figure IV.3-2.  The sample bailed from well 3-30 on 4/23/09 has a similar U concentration (40 μg/L) to and is approximately in the range of the IFRC well samples collected 9/2/08.  With increasing U concentration, the groundwater U isotopic composition evolves nearly orthogonally away from the 9/2/08 array towards the lower left (i.e. toward lower $^{236}U/^{328}U$ and depleted $^{235}U/^{238}U$).  The four samples with the peak U concentrations all cluster near the line connecting the compositions of the sediment leachates from 22 ft and 24 ft depths in the 3-31 borings (which is very near well 3-30).  This indicates that the source of U that produced the observed peaks in concentration in 3-30 originated in the local lower vadose ("smear") zone sediments represented by 3-31.  The samples from 4/26, 4/29, 4/30 represent variable mixtures between the local groundwater U and the U from the smear zone (40%, 60% and 80% "smear" U, respectively). The sample from the small U concentration peak (~80 μg/L) on 5/18 appears to have come from a different source (with higher $^{236}U/^{238}U$ and $^{235}U/^{238}U$, perhaps like the 2-5 or 2-30 sediments) and was imported to well 3-30 by groundwater movement between the two peaks of water table elevation. The work so far demonstrates the great promise of U isotopic systematics for tracing, apportioning and pinpointing sources of U involved in transfer between the lower vadose zone and groundwater.
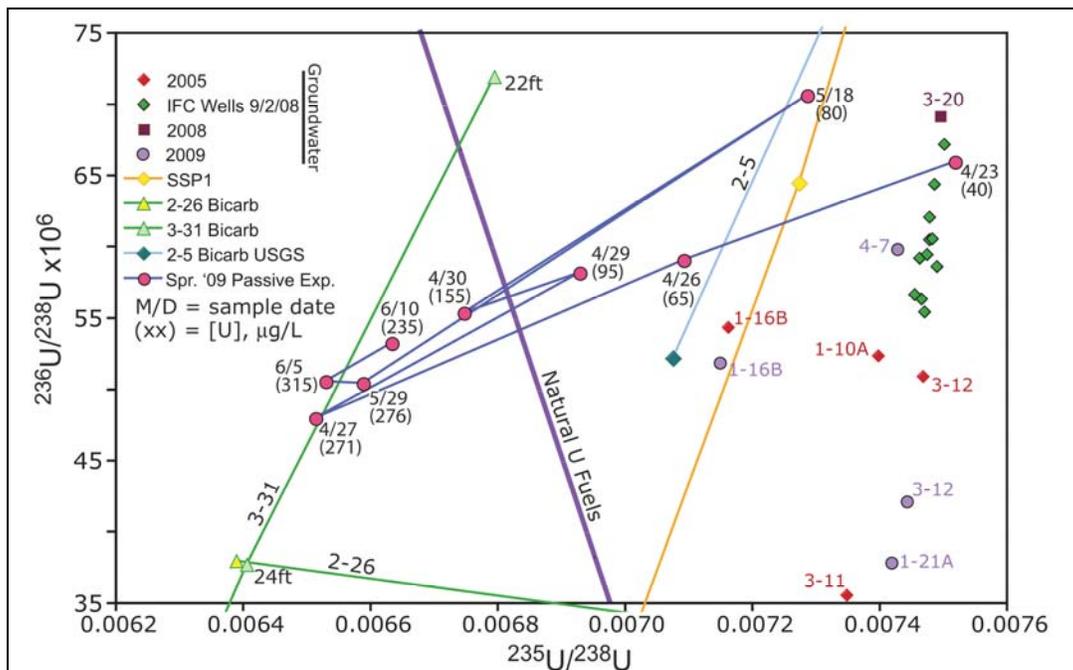


**Figure IV.3-5.** Plot of $^{236}U/^{238}U$ vs. $^{235}U/^{238}U$ for a set of samples from 399-3-30 (magenta circles) taken during the Spring 2009 Passive U Mobilization Experiment.  Numbers by the magenta data points are the date of sampling, and U concentration (μg/L).

## IV.4.  Well Bore Flows

The presence of well-bore vertical flows in our fully screened wells was documented by different measurement types in the January 2010 Quarterly.  This issue has caused considerable debate among project participants as to its causes and implications for past and future experimentation.  While vertical well bore flows are commonly acknowledged in groundwater monitoring, the highly dynamic nature of intra-well flows at the IFRC site and the presence of wells that are both in and out of phase with each other is unprecedented. For example, during the U desorption experiment in November, 2009 (**Section V.4**), a solution of 180 mg/L NaBr was injected into the aquifer, and traveled differentially in the three aquifer zones.  After long residence (>15,000 min) the specific conductivity electrodes recorded patterns of oscillating high and low values in some parts of the IFRC site (Figure IV.4-1).  The conductivities were plotted against pressure variations within the wells, defined as the instantaneous pressure minus the rolling, just-previous, ten-hour average.  The values thus calculated short-term fluctuations in river stage/water table elevation, without longer-range effects. For some wells, the variation in specific conductivity was in-phase with the pressure variation (Figure IV.4-1, Well 2-18); for others, the variation was out-of-phase (Figure IV. 4-1, Well 2-8).  These relationships could be described by a relatively simple conceptual model (Figure IV.4-2).  A flow barrier, which could be relatively permeable, within the upper high-K aquifer zone,
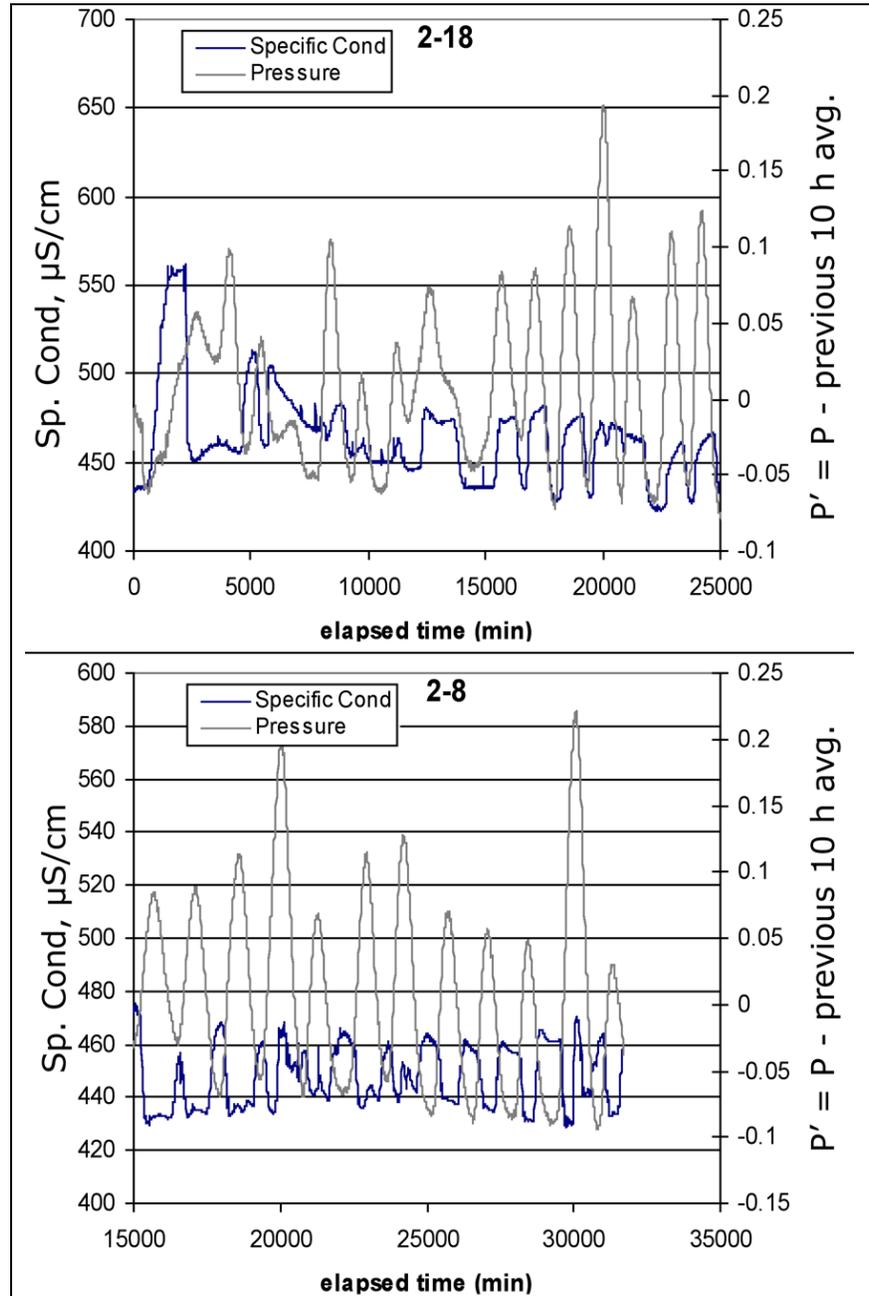


**Figure IV.4-1.** Pressure and specific conductance relationships in two wells tested during an injection experiment using relatively high-conductivity bromide solutions.

33

would impose pressure gradients on wells penetrating the low-K zone. Water would therefore flow downward within the boreholes on the impetus (river) side of the barrier, and upward on the side opposite. The magnitude of the flows would correspond to the rate of water table rise, and would be of opposite phase on either side of the boundary.

Vertical well bore flows are extremely significant to experimental results from both injection and passive monitoring experiments as displayed in the January 2010 Quarterly, and as will be discussed in **Sections V.3 and VI.5**. Normally well bore concentrations are assumed to



**Figure IV.4-2**. A simple conceptual model for induced flow, in-phase and out-of-phase with cycling Columbia River stage and the dependent water table at the IFRC.

represent a flux average of the different hydraulic conductivity units that are sampled by the well. When vertical well-bore flows occur, the well water composition is dominated by the zone that preferentially discharges into the well because of a localized higher head. At the IFRC, these discharge zones oscillate between top or bottom depending on both well location and river stage, giving rise to complicated temporal patterns in solute composition depending on concentration differences between the top and bottom high K zones. One of our project participants has developed a modeling approach to account for intra-borehole flow and solute mixing on flux-averaged well concentrations (Zheng, 2006; MT3DMS v5.2 Supplemental User's Guide). This modeling approach is based on the following relationship:

$$C_{avg}^t = \frac{\left|Q_w^t\right|C_w^t + \sum_{i=1}^{N}\left|Q_i^t\right|C_i^t}{\left|Q_w^t\right| + \sum_{i=1}^{N}\left|Q_i^t\right|}$$

$C_{avg}^t$     is the flux-averaged composite concentration inside the wellbore at time $t$;

$Q_w^t$     is the total prescribed flow **into** the multi-node well (i.e., source) at time $t$;

$C_w^t$     is the concentration of the injected source $Q_w^t$ at time $t$;

$Q_i^t$     is the flow rate at node (layer) $i$ **discharging** into the multi-node well (i.e., sink) at time $t$;

$C_i^t$     is the concentration associated with the sink outflow $Q_i^t$, i.e., the concentration in the aquifer at node (layer) $i$ at time $t$; and

$N$     is the total number of nodes (layers) that makes up the multi-node well.

The implementation of this modeling approach to IFRC tracer experiment data is described in **Section VI.5**. A mitigation study was initiated in December 2009 to determine if the well bore flows between the two high K zones could be attenuated by placing an inflatable packer in the well at the approximate depth location of the low K intermediate zone. Two wells were selected for study: 2-21 which exhibits predominantly upward well-bore flows (Figure IV.4-3a), and 2-10 (Figure IV.4-3b) which exhibits tendency for downward flows. The EBF was deployed in the upper high K zone at a depth of approximately 40'. The study of 2-21 was completed first before moving on to 2-10, which is still in progress. The packer was very effective at limiting vertical flows in both wells over a significant range in river stage and directional bias. The packer was slightly less effective in 2-10, but only because foam was not used on the packer for tight seal against the wire-wrap well screen. We conclude that the installation of inflatable packers would allow tracer experiments in the upper high K and intermediate low K zones without the complications of vertical well-bore flows. The upper high K zone is of primary importance to U(VI) resupply to the plume as demonstrated by the passive experiment described in the July 2009 Quarterly and in **Section V.3.**



**Figure IV.4-3.** Effect of packer placement at the depth of the intermediate low K zone on vertical flows in a.) well 2-21 and b.) 2-10.
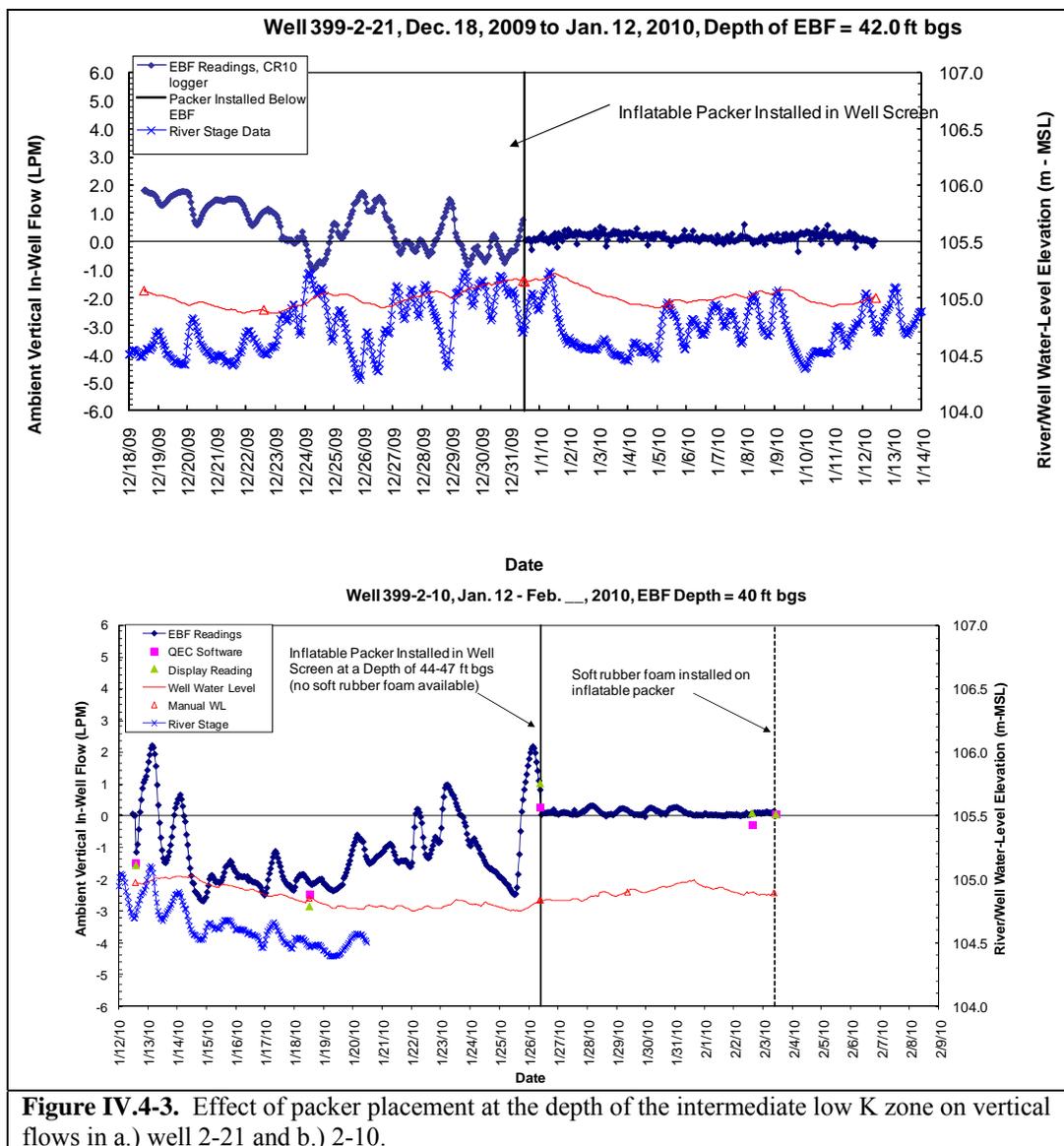
# V. SATURATED ZONE EXPERIMENTAL PROGRAM

## V.1. Non-Reactive Tracer Experiments

This section of the report focuses on the first two large-scale tracer tests that were performed at the 300 Area IFRC site in November 2008 and March 2009. The modeling of these two experiments is described in **Section VI.** Table 1 summarizes the injection volumes, rates, concentrations, and other operational parameters for the first and second tracer tests, hereafter referred to as the Nov08 and Mar09 tracer tests, respectively. The primary purpose of these two tracer tests was to augment the field hydrologic characterization data from the site (i.e. short-duration, constant rate injection and electromagnetic borehole flow-meter tests) with transport data to better define the hydraulic conductivity and effective porosity distributions. These are the primary data sets being used by PNNL and collaborators for parameterization and calibration of plot-scale flow and transport models of the IFRC site.

Tracer Experiments

The Nov08 and Mar09 tracer tests both utilized well 2-9, located near the northern apex of the triangular well field, as the injection well. This well has a 7.62-m (25-ft) –long well screen that spans the entire saturated thickness of the Hanford Fm at this location. For the Nov08 test, a relatively large injection volume was used in an attempt to achieve the maximum injectate concentration (C/Co = 1) at the closest monitoring wells (2-7, 2-8, and 2-10). River stage fluctuations were relatively large in the Nov08 tracer test, such that the tracer plume drifted to the west, out of the monitored domain, during the early stages of the experiment. The tracer plume then drifted back into the monitored domain later in the experiment. The Mar09 tracer test was performed during a period when the river stage fluctuations were less extreme. FigureV.1-1 shows observed water levels and computed gradients and flow directions for the periods of monitoring during both the Nov08 and Mar09 tracer tests.

**Table V.1-1**. Summary of operational parameters for November 2008 and March 2009 tracer tests performed at Hanford 300 Area IFRC site.

|  | **November 2008** | **March 2009** |
|---|---|---|
| Injection well | 2-9 | 2-9 |
| Screened interval (elevation, m) | 104.7 - 97.1 | 104.7 - 97.1 |
| Injection volume (gal) | 160,000 | 40,600 |
| Injection rate (gpm) | 180 | 71.7 |
| Average Br conc (mg/L) | 56 | 95 |
| Total injected Br mass (kg) | 33.87 | 14.58 |
| Temperature of injectate (°C) | ~16.7 (ambient) | ~10 (chilled) |
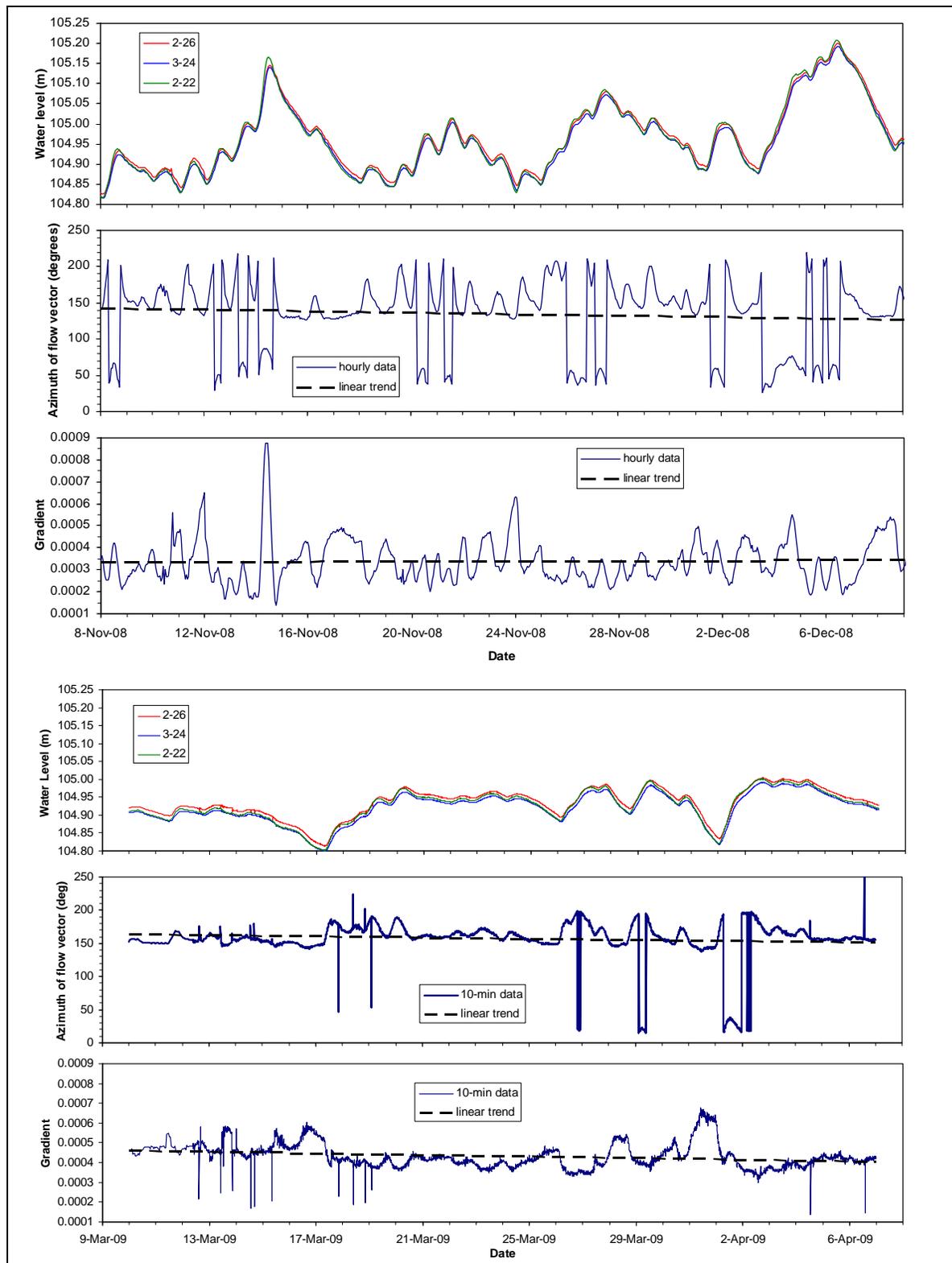
**Figure V.1-1.** Observed water levels and computed flow directions and gradients during the November 2008 (top 3 panels) and March 2009 tracer tests (bottom 3 panels) at the Hanford 300 Area IFRC site.

Characteristic Solute Tracer Behavior

A slower rate and longer duration of injection were used in the Mar09 tracer test in an attempt to get the tracer plume to stay within the monitored domain for a longer period of time. This strategy, in combination with the more stable hydrodynamic conditions that occurred during the experiment, resulted in a more successful experiment, relative to the Nov08 test. The injected tracer plume stayed within the monitored domain for a longer period of time, as anticipated. Further details of both experiments are discussed further in **Section VI**.

The solute tracer data from the two experiments displayed complex behavior that is shown more completely in **Section VI** where their modeling is discussed. Three cluster wells (399-2-26, 399-2-27, 399-2-28; 399-2-29, 399-2-30, 399-2-31; and 399-3-29, 399-3-30, 399-3-31) were screened at discrete depths that approximately represent the three hydraulic conductivity zones discussed previously. The other wells were fully-
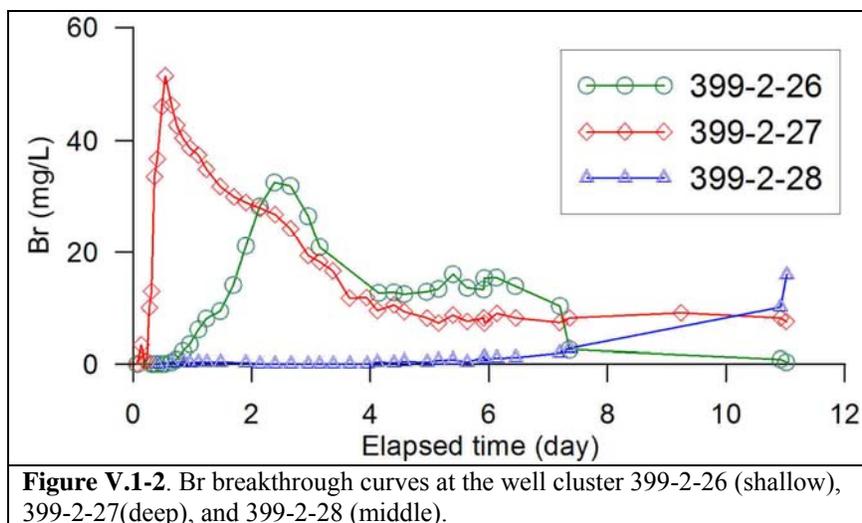


**Figure V.1-2**. Br breakthrough curves at the well cluster 399-2-26 (shallow), 399-2-27(deep), and 399-2-28 (middle).

screened over the entire Hanford formation saturated zone depth. The observed Br concentrations in the fully screened wells were depth-mixed and potentially effected by vertical borehole flows as described in **Section IV.4** and later in **Section VI**. In spite of these complications, a generalized pattern of transport behavior (Figure V.1- 2) has been observed for the site recurrently in all tracer experiments. This response is shown for the northern multi-level well cluster where the average transport velocity decreases in the following order: deep > shallow >> middle. These behaviors are generally consistent with EBF hydraulic test results. The deep high velocity zone displays considerable tailing apparently caused by finer grained heterogeneities.

Heat Tracer Behavior

As indicated by Table 1, the Mar09 experiment also involved using chilled injection water to evaluate the use of heat as a tracer. High-resolution monitoring of temperature (20 min intervals) was performed using thermistor strings in 28 wells over an 11.8-day period. The thermistor strings were deployed within the well bore. Temperature measurements were recorded from a total of 672 individual thermistors yielding a robust data set. Temperature displayed significant vertical variability in all monitored wells (Figure V.1-3), reflecting the important role of aquifer heterogeneity in the vertical direction, and also well-bore flow. It is much less expensive to obtain the 3D temperature distribution compared with a solute tracer. Also, the additional parameter, thermal conductivity, normally varies only over a small range compared with hydraulic conductivity. Thus, heat could be used as a good groundwater tracer to complement groundwater head and solute tracer data to better constrain the hydraulic conductivity estimates. The

temperature breakthrough data set for all wells in the Mar09 experiment is currently under evaluation, and additional temperature tracer experiments are planned for CY 2010.
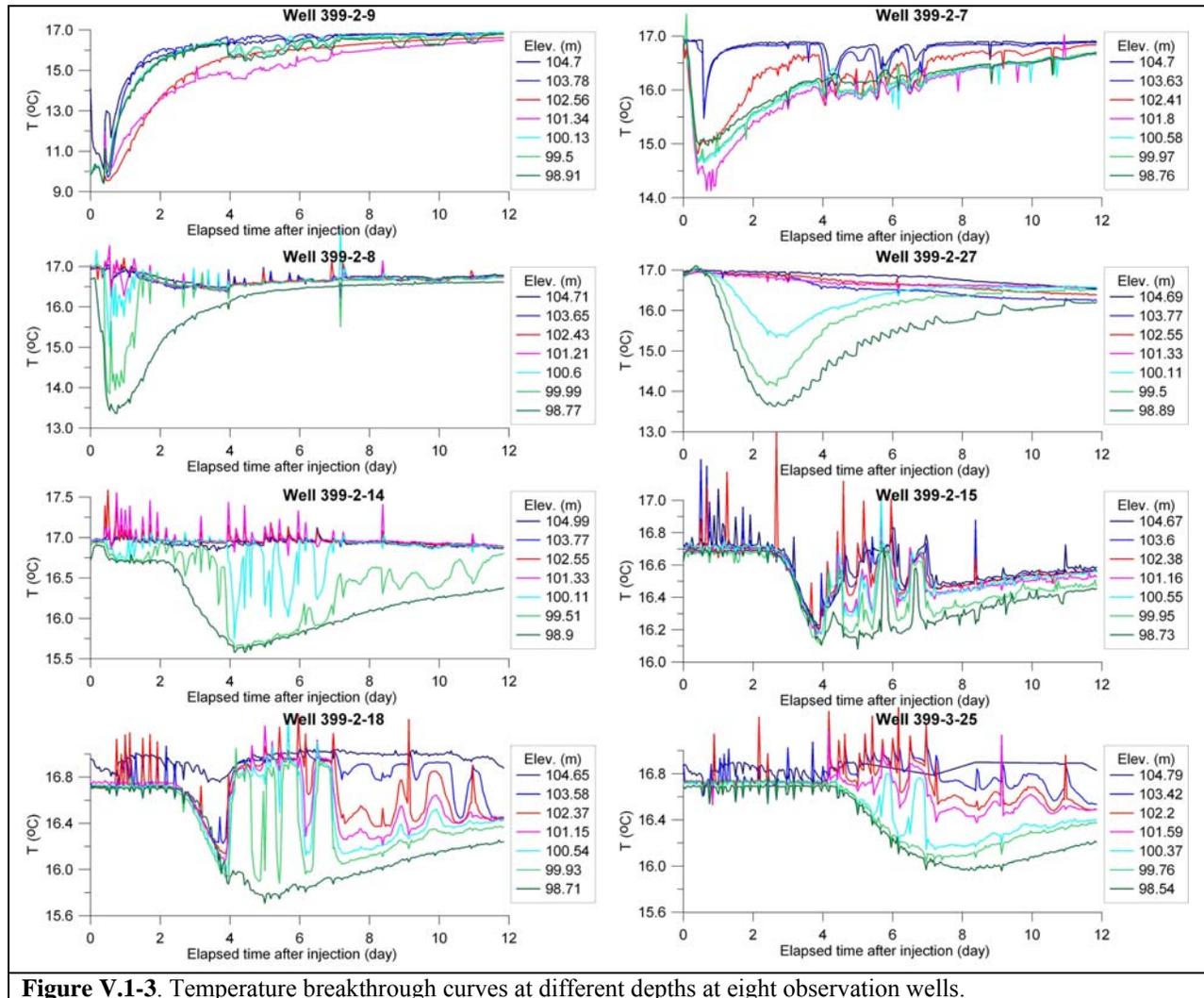


**Figure V.1-3**. Temperature breakthrough curves at different depths at eight observation wells.

## V.2.    Exploratory Geophysics Monitoring Experiment

Concept

The objectives of the electrical geophysical component of the bromide tracer experiment were to track the migration of a low-resistivity bromide tracer using indirect electrical imaging methods.  The geophysical component of this experiment had three objectives:

1.)  Test the capabilities of the new MPT-DAS1 electrical resistivity system and access the compatibility with existing tracer monitoring infrastructure at IFRC.
2.)  Develop an approach for the rapid acquisition of resistivity data to permit tracking of tracer movement.
3.)  Map the spatiotemporal distribution of tracer plume within the IFRC well field.

All three of these objectives were met with varying degrees of success. System performance and compatibility (1) were assessed by comparing baseline measurements to previously collected resistivity data using other systems deployed at IFRC. Baseline measurements were comparable and the MPT-DAS1 provided a higher switching capacity of 256 electrodes as well as 8 more measuring channels to allow for more rapid data acquisition than was previously available. A method for rapid tracking of the plume was developed (2) based on surface electrodes that utilized the MALM method for rapid surface mapping in 4 minutes. Baseline MALM measurements were valid and similar to previously published results used to track tracer movement. MALM measurements during the experiment produced an invalid response and low signal strength due to a current leak caused by incompatibility with the injection equipment deployed during this experiment. Mapping of the tracer plume (3) was achieved by using the dipole-dipole gradient electrode array on surface and subsurface electrodes. However, these data acquisition efforts required 4 hours (surface) and 5 days (subsurface) to complete a full measurement which is not rapid enough for time series measurements.

Approach

The Hanford 300 Area IFRC is equipped with 28 permanent electrical geophysical monitoring wells (ERT wells) arranged in a hexagonal lattice structure. Each of these wells contains 30 electrodes for a total of 840 electrodes. A full 3D tomography of the well field typically requires up to 5 days using the available 8-channel x 256 electrode switching resistivity/IP system. Five sets of manually switched surveys are required to complete a tomogram of all 840 electrodes. Tracking of fast-moving tracer plumes during interference testing will require optimal configuration of the electrodes and/or techniques for rapid acquisition of good-quality data.

The injection of an electrically conductive tracer (bromide) within an aquifer is a classic MALM survey method (Mitrofan et al. 2008, Pant 2004, Wood and Palmer 2000, Osiensky 1997). The MALM method utilizes a current electrode within the volume of interest and numerous surrounding potential measurement electrodes arranged in a regularized grid for rapid measurements of plume topology. The MALM method allows for the direct measurement of the electrical potential field by measuring a pole-pole geometry that focuses a current source within the volume of interest. The unknown or dynamically changing volume is best resolved when it is more electrically conductive than the surrounding material. The IFRC MALM array utilized 172 electrodes installed in an azimuthal geometry (concentric circular pattern) for anisotropy and heterogeneity
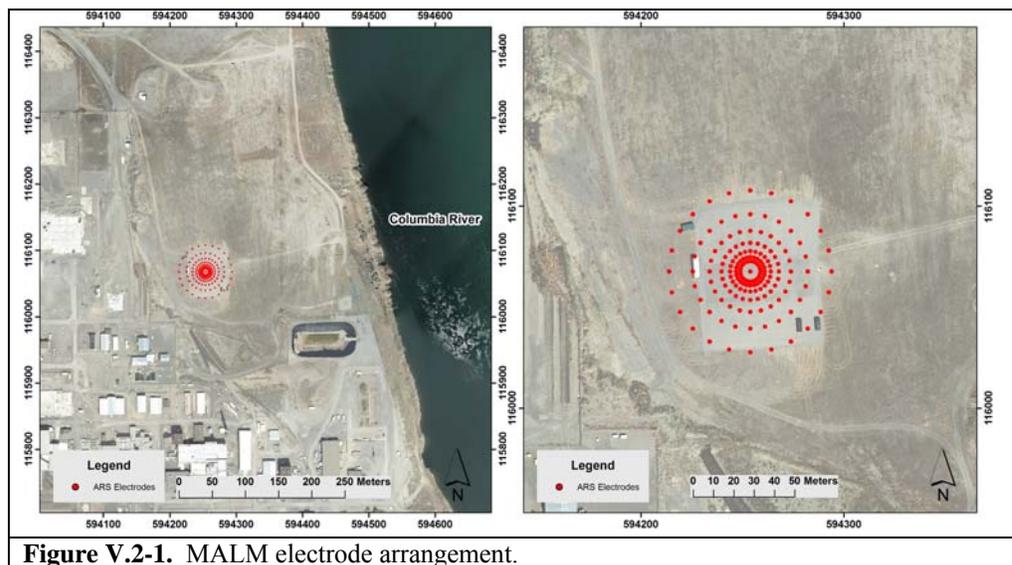


**Figure V.2-1.** MALM electrode arrangement.

studies (Figure V.2-1).  Data quality from the potential electrodes is primarily dependent on the proper installation and measurement from the one current source within the bromide injection zone.  The benefit of this centralized current electrode is realized in relatively rapid electric field measurements, on the order of 4 minutes, to delineate the tracer plume.

The groundwater on July 09 at the injection well had a specific conductance of 0.55 mS/cm or a resistivity ≈ 22 Ω-m.  The injected bromide tracer concentration stabilized at a specific conductance of 1.1 mS/cm or a resistivity ≈ 9 Ω-m.  The target (9 Ω-m) and background (22 Ω-m) resistivity values used in this tracer injection have been resolved in similar MALM experiments (Mitrofan et al. 2008, Pant 2004, Wood and Palmer 2000, Osiensky 1997).

Results

Quality control methods for MALM data involved plotting the ratio of voltage (V) to current (I) as a function of distance from the injection well. It is important to note that these plots are typically used to check for current leakage and are not processed to resolve a target at this stage.  Figure V.2-2a shows the baseline MALM raw V/I at the IFRC prior to bromide injection.  Ideally, V/I should decrease monotonically with distance from the injection point as shown in Figure V.2-2b.
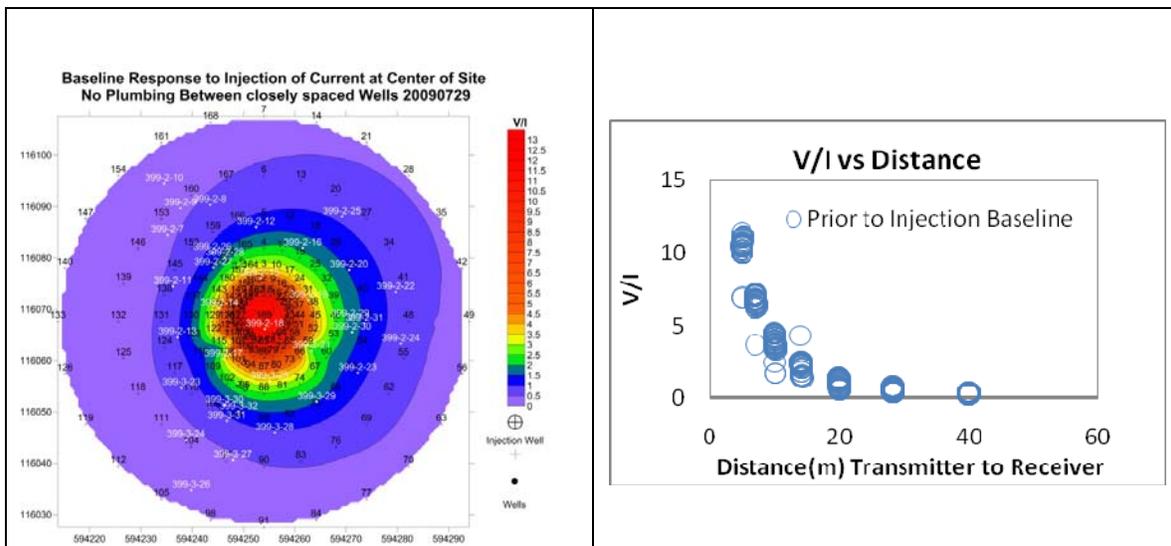


**Figure V.2- 2.**  Quality control MALM plots, a) baseline MALM raw V/I at IFRC prior to bromide injection with pipes and injection equipment not installed, b) baseline V/I versus distance from the injection point prior to bromide injection and equipment installation.

A forward model of the V/I response for the IFRC geometry is shown in Figures V.2- 3a and 3b. The baseline conditions are valid for a MALM model of current flow in which V/I decreases monotonically with distance from a central injection point.  Figure V.2-3b shows a valid MAML response in which V/I decreases monotonically with distance from the injection point.

Figure V.2-4 shows the measured MALM response at the IFRC with pipes and injection equipment installed during tracer injection. The ideal response in which V/I decreases with distance from injection point is no longer apparent. In fact, there is an increase in V/I with distance trending towards the extraction well to the east (Figure V.2-4a).  Furthermore, there is a significant decrease in signal strength with increasing distance from the transmitter (Figure V.2- 4b) compared to the baseline response (Figure

V.2-3 a, b). Signal strength decrease by a factor of over 100 from the baseline to the injection with values close to the noise floor of the MPT-DAS-1 instrument.



**Figure V.2-3.** Simulated MALM response for the IFRC site prior to installation of infrastructure and bromide injection, a) forward model of V/I with current injection response, and b) baseline MALM raw V/I versus distance from the injection point.
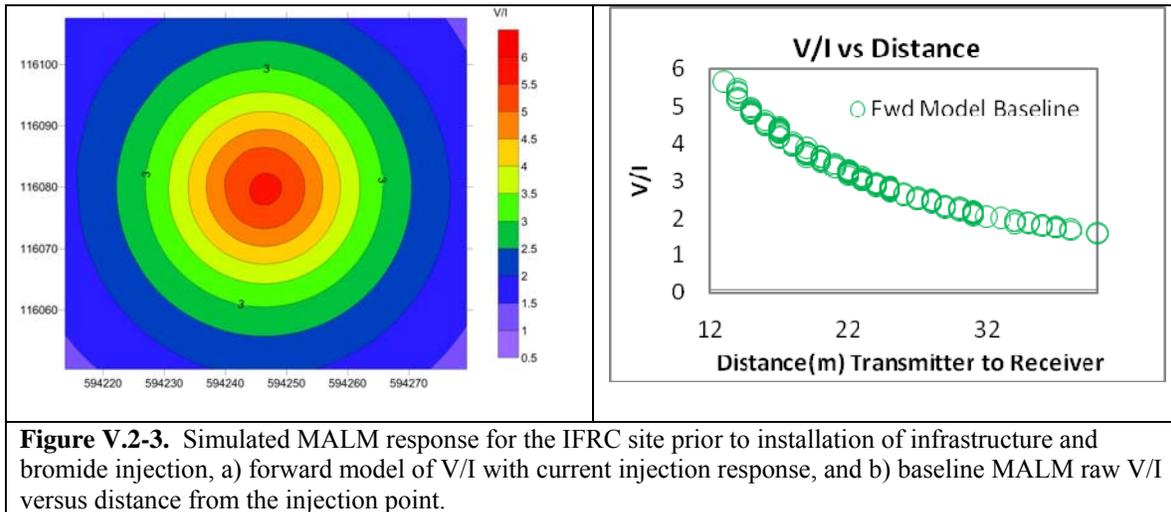
In the MALM model of current flow, an increase in V/I with distance from the central injection point is an artifact that indicates that current is travelling through pathways other than the earth. Current leakage can occur in numerous ways where pipes and wires cross a site. Very low signal strengths (V/I) are indicative of strong short circuits similar to a metallic connection. The MPT-DAS1 utilizes both current and voltage auto-ranging to maximize signal quality by preventing saturation of the receiving channels. The extremely low received voltages observed after the injection experiment started (Figure V.2-4b, Figure V.2-5) indicates that the system was unable to inject current and receive a suitably strong voltage. The system reached its maximum current but was unable to receive an appropriate voltage because the current was being conducted away by a short circuit formed by the tracer infrastructure.



**Figure V.2-4** Quality control MALM plots at IFRC with pipes and injection equipment installed duing rtracer injection, a) MALM raw V/I, b) V/I versus distance from the injection point.
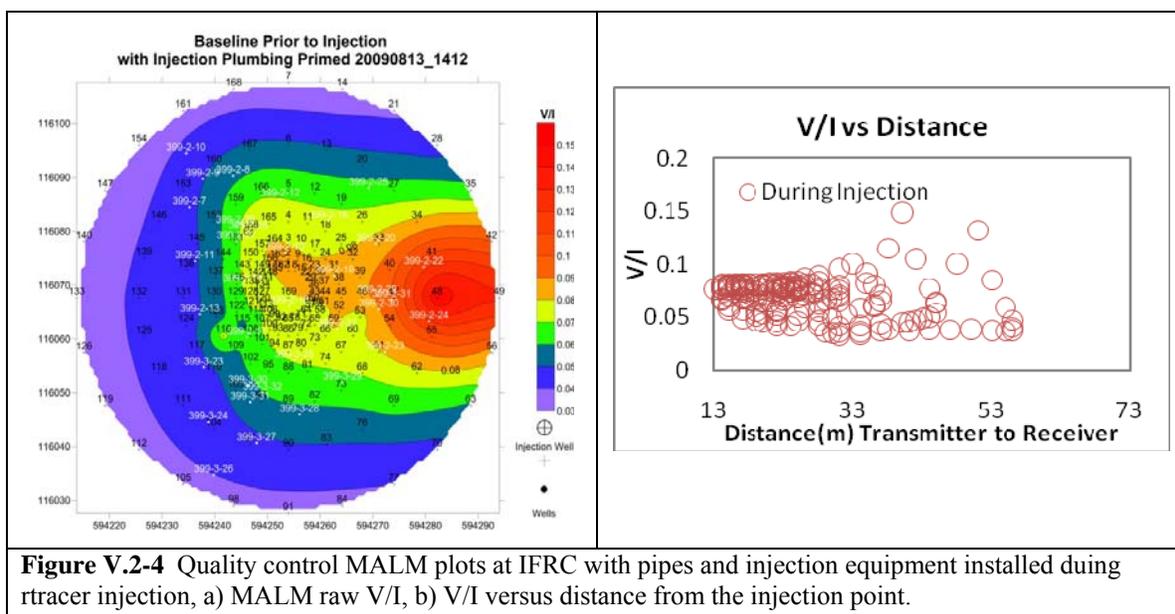
*Alternative Electrode Arrays.* Due to data quality problems with the bulk of the electrical measurements taken during the injection experiment (MALM), alternative ERT and surface electrode arrays which required more time to acquire were utilized. Post injection surface and ERT characterization were started as soon as it became apparent that the MALM and injection equipment were not compatible. Dipole-dipole gradient array resistivity data were acquired (5 hour acquisition time) from the same surface electrodes used during the MALM effort. A 3D tomography of the baseline measurements and a map of low resistivity contours from 1-25 ohm-m are shown in Figure V.2-6. The 1-25 ohm-m values were chosen in order to focus on temporal changes in resistivity related to the 9 ohm-m tracer injection. A low-resistivity plume like feature (red circle) persists around the injection well after 76 hr, 4560 min (Figure V.2-6c).



**Figure V.2-5.** Reduction in signal strength (V/I) for collocated measurements after the installation of tracer injection equipment.

This low resistivity target coincides with direct samples of tracer in the injection well after 3 days (4320 min). A second low resistivity target is located along a western trench like feature (green rectangle, Figure V.2-6c). This trench like feature was visualized during previous EM and 2D resistivity surveys.

A full 3D well electrode ERT survey required 5 days to complete. Figure V.2-7a displays the distribution of resistivity within the well field and Figure V.2-7b shows the same dataset with high resistivity values masked. These measurements include full reciprocals for error and noise analysis resulting in 90.5 hours of collection time and approximately 281,350 measurements. Both plots clearly show a low resistivity feature in the water table and vadose zone near injection well (C6205 / 399-3-28) that trends



**Figure V.2-6**. (A) Baseline 3D inversion model of dipole-dipole and gradient array resistivity data collected prior to injection experiment, (B) 0-25 ohm m resistivity area for baseline in plain view (C) 0-25 ohm-m resistivity area of post injection gradient array survey. The Red Circle indicates a new low resistivity feature around the injection well that is associated with the bromide injection. The green box indicates a low resistivity trench feature that has also been imaged with prior EM and 2D resistivity surveys.

above and to the north-east of the injection point.  This anomaly is attributed to the bromide injection and suggests that the part of the plume moved to the east of the injection well and remained long enough to be imaged with the full 3D ERT tomography method.

Summary and Future Directions

Performance of the MPT-DAS-1 ERT system is acceptable and indicates that baseline measurements are comparable with the single channel system, while allowing for more rapid data acquisition than was previously available.  The MALM method for rapid tracking of tracer plumes required only 4 minutes to delineate the plume within the IFRC well field.  However, the system was unable to resolve spatio-temporal behavior of the plume due to current leakage introduced by the injection equipment.  Alternate electrical measurements utilizing ERT and surface electrodes and the dipole-dipole gradient electrode geometry were able to resolve the bromide tracer injected into a low permeability region of the IFRC aquifer.  The surface dipole-dipole gradient was able to track the plume and required only 4 hrs for a snapshot.  However, as previously deployed, a full 3D well electrode ERT survey required at least 5 days to complete a single measurement and would have been unable to adequately track the plume.

Work is underway to test and deploy a ERT electrode geometry for rapid data acquisition that is less susceptible to electrical noise/current leakage such as the dipole-dipole gradient array.  Work is also underway to minimize sources of electrical noise such as extraction wells inside the IFRC well field. The optimized electrode configuration is being prepared for testing with an operational injection system prior to the next experiment.  In addition, a plan is being prepared to conduct 4D azimuthal surveys to characterize the effects of river stage on the manifestation of anisotropy and heterogeneity.
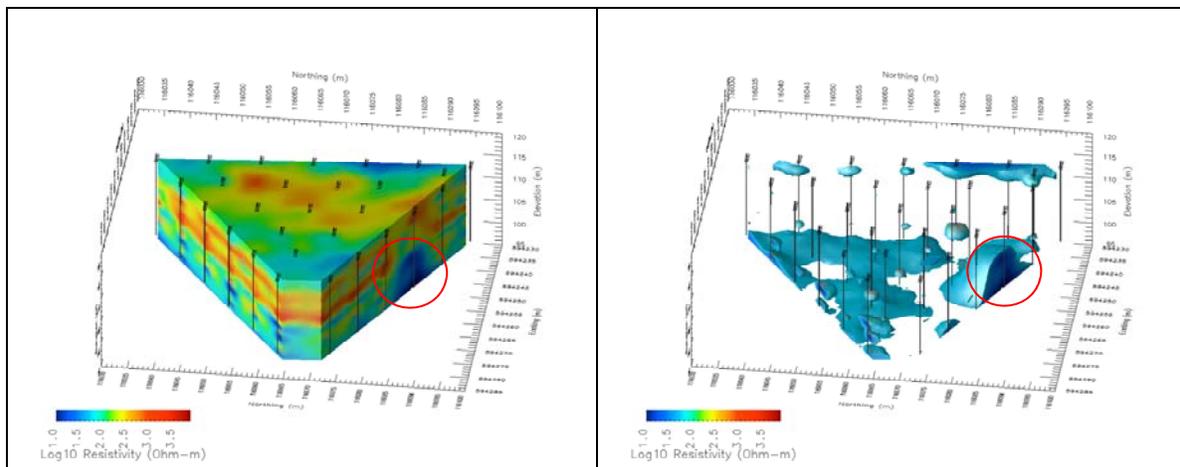


**Figure V.2-7.**  Preliminary ERT FERM3D L2-norm inversion model a) full 3-D distribution of resistivity showing evidence of bromide tracer 5 days after injection, b) same dataset with higher resistivity values masked. Note the low resistivity feature in the water table and vadose zone (red circle) near injection well (C6205) that trends above and to the north-east of the injection point.

## V.3.   Spring 2009 Passive Monitoring Experiment

Concept

It was hypothesized that the rise of the IFRC water table in response to the rise in the Columbia River stage during spring snowmelt could contribute significant contaminant uranium to the unconfined aquifer.

In addition, physical and chemical observations during forced-water injections of aqueous tracers suggested that a measurable upward or downward flow of groundwater within the fully screened boreholes could affect the concentrations of chemical tracers and contaminant U determined by pumping samples from the boreholes. Detailed measurements during the spring thaw from March 31 to June 17, 2009, showed that both phenomena occurred. The borehole flow and passive uranium experiment results, and their implications for future experimentation are described here.

Conventional long-screen groundwater monitoring wells, including those that extend over the full saturated thickness of an aquifer, have been used extensively in the environmental field to characterize site hydrogeology and geochemistry, and are generally recognized to provide a composite concentration for the interrogated depth interval. However, when interpreting aqueous monitoring data from conventional long-screen well installations, both the vertical distribution of transmissivity and vertical flow within the well bore need to be considered when long screen intervals can act as a conduit for vertical well bore flow. This may occur when they connect transmissive zones of differing hydraulic head. Vertical flows can result in temporal variability in measured aqueous concentrations that is directly related to changes in wellbore flow direction (i.e., upward vs. downward). Even where well bore flow is negligible, discrete highly transmissive zones can dominate the aqueous concentration measured in a long-screen well by providing the majority of the water sampled by pumping from the screened interval.

Measurements of differential conductivity within the IFRC boreholes showed the presence of a stratified hydrologic system at the site, consisting of a central, relatively low-K zone between upper and lower high-K zones. The boundaries of the low-K zone undulate across the site, and the magnitude and differences in conductivity are still under evaluation. Tracer injections into the lower and middle zones indicated that the movement of fluid in the zones differed, with lower zone injections traveling quickly to, and exiting, at the south-central site boundary. Electromagnetic flow meter (EBF) tests at the site during changes in river stage showed that some wells exhibited flows in-phase with the river fluctuations (i.e., the borehole flow was upward as the river stage rose, and downward as it fell), while other wells had flows that were out-of-phase. The distribution of these wells across the site (Figure V.3-1) defined distinct areas of in-phase and out-of-phase behavior.
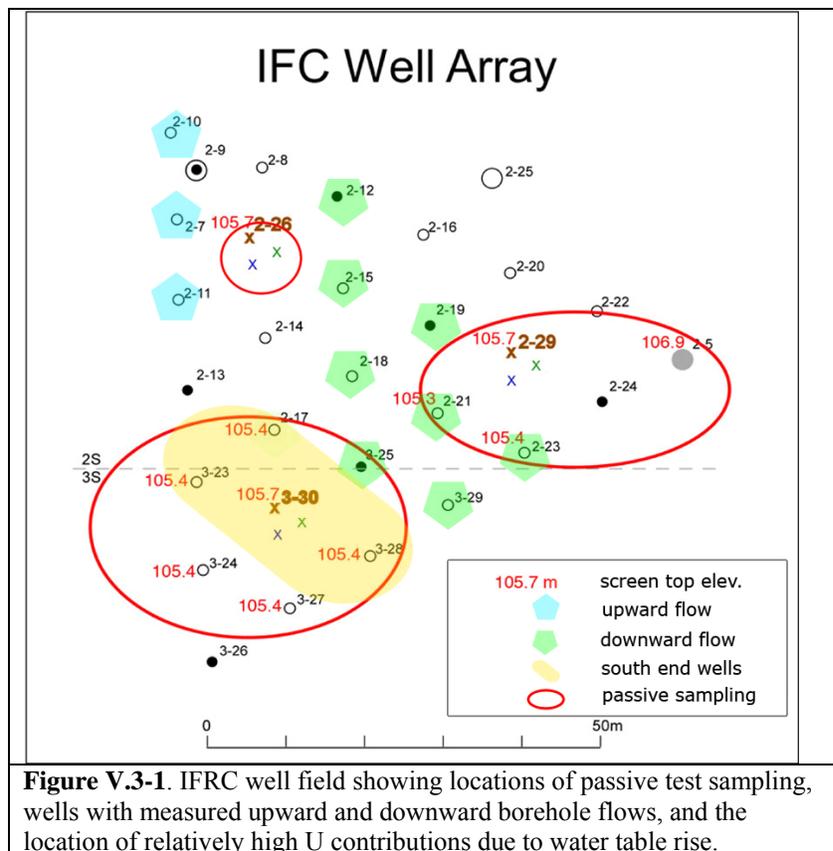


**Figure V.3-1**. IFRC well field showing locations of passive test sampling, wells with measured upward and downward borehole flows, and the location of relatively high U contributions due to water table rise.

<u>Approach</u>

For the passive experiment, wells across the site were sampled from before until just after the maximum height of the spring water table (March 31 – June 17, 2009). Twelve wells were sampled daily, by bailing water from the uppermost 15 cm of the aquifer, and by pumping using the installed, mid-screen pumps. Conductivity and depth to the water table were recorded. Samples were subsequently analyzed for U concentration using a kinetic phosphorescence analyzer (KPA). The water table rose above the well screen intervals on May 30, 2009, which was assumed to affect the U concentration in the bailed samples, since they could not sample the top of the aquifer.
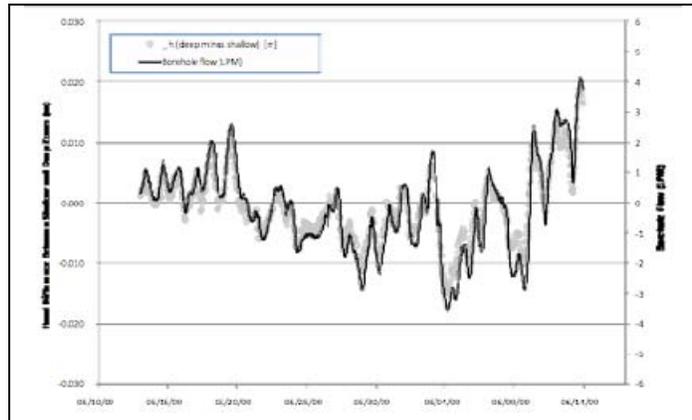


**Figure V.3-2**. The correlation of borehole flow in Well 2-21 to the difference in pressure between the upper and lower screened intervals in the South End well cluster.

In parallel with the passive experiment, a single well, 2-21, was instrumented with a borehole flow meter and continuously monitored for flow direction. Simultaneously, the pressure in the adjacent deep and shallow wells in the South End three-well cluster was monitored. The pressure difference in the two wells during periods of zero flow were used to determine the pressure conditions defining a zero-head condition, and the pressure differences after subtracting the resultant pressure offset were used to determine the change in hydraulic head during the test. The flow meter data correlated perfectly with the head-change data (Figure V.3-2). As described below in more detail, the passive experiment included bailing groundwater samples from the aquifer surface, then pumping a comparable sample using the installed, mid-screen pumps. The potential effects of borehole flow on the passive experiment results are shown in Figure V.3-3. The bailed sample, removed from the aquifer top, shows large spikes in U concentration, while the pumped sample shows similar spikes of lower magnitude. These results were expected, since the pumped sample represented a weighted average of water pumped from the screened interval, while the bailed sample represented water influenced by contaminant U in the overlying vadose zone during water table rise. The dramatic dips in U concentration during bailing, however, may result from upward flow within the well bore, introducing relatively contaminant-free
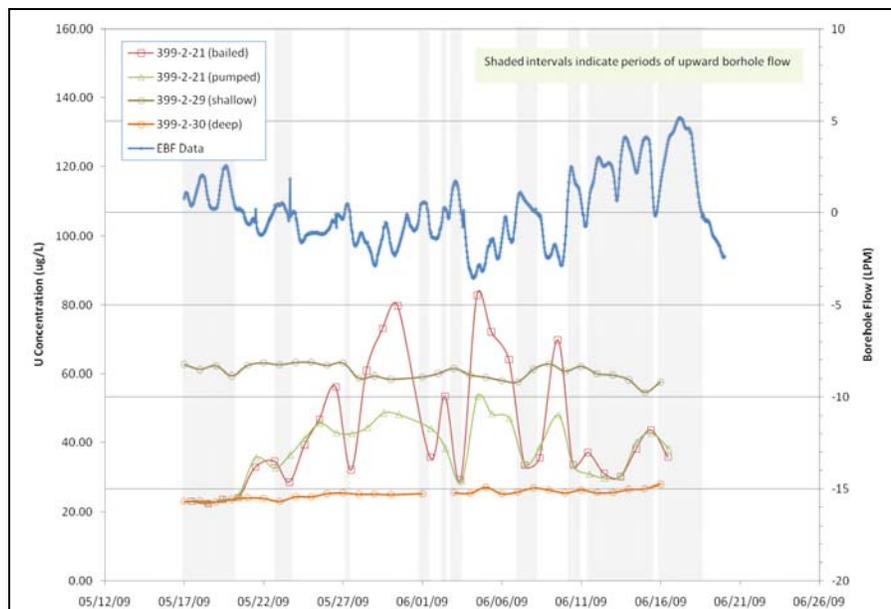


**Figure V.3-3**. Variable concentration in bailed and pumped samples within the long screen interval in Well 2-21.

groundwater to the aquifer surface. The contribution of U to the aquifer from the vadose zone may therefore be better represented as an envelope around the bailed-sample concentration spikes.

Results

The most significant U contributions to the aquifer originated from four wells near the southern three-well cluster (the South End wells), particularly the shallow well in the cluster (3-30) and the fully screened well to its north (2-17), shown in Figure V.3-4. As shown in the figure, the water table rose to a high value at the end of May, then retreated. This rise contributed U at a contribution of up to 90 μg/L in the pumped sample from Well 3-30 and up to 270 μg/L in the bailed sample. The water table rose above the screen in early June, and the pumped and bailed samples were uniform after that, reaching up to



**Figure V.3-4**. Water table depth, its relationship to the height of the well screen, and U concentrations, in South End Wells 3-30 and 2-17. These wells exhibited the highest U concentrations during the passive experiment.
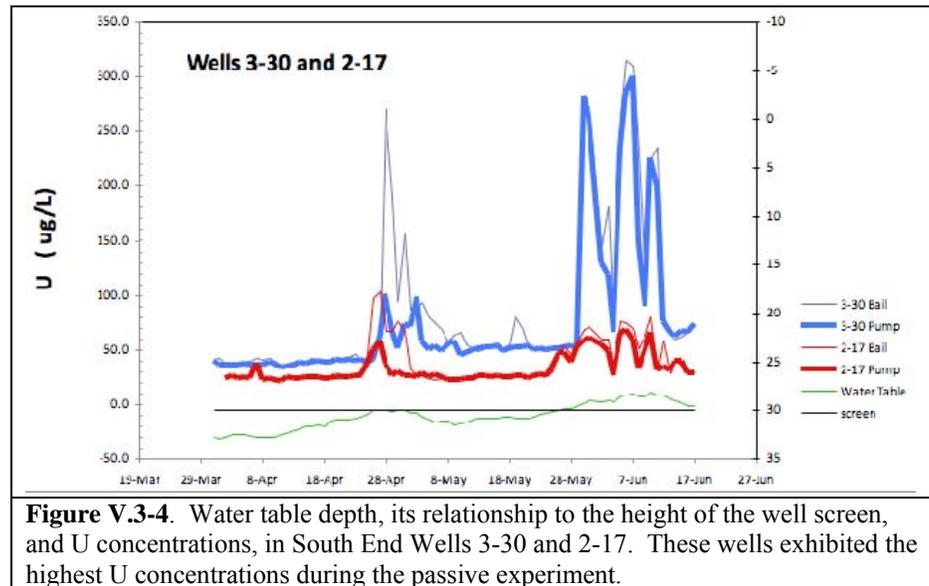
300 μg/L. Other wells in the vicinity of Well 3-30 also contributed significant U during the rise of the water table. When plotted on the same scale for comparison, Wells 3-23, 3-30, 3-28, and 2-17 (overlain in yellow on Figure V.3- 1) were shown to contribute significant U to the aquifer (Figure V.3-5), in excess of other wells at the IFRC. This associated group of wells may represent a significant pool of contaminant U available to the aquifer from the vadose zone.

Examination of all of the samples (Figure V.3-6) indicated that the minimum level of contaminant U in the IFRC wells was approximately 20 μg/L. In general, the lowest aquifer concentrations were observed prior to the spring rise in the water table. In the figure, the South End wells are color coded separately for collection dates prior to May 30; after May 30, when the water level was above the screened interval, all of the South End wells are colored yellow. Samples from other wells are represented by crosses. The plots show that the maximum concentrations for wells outside of the South End group had maximum U concentrations of approximately 75 μg/L. The South End wells had excess U concentrations in bailed samples compared to pumped samples (represented by positions within the plot that are below a line connecting like concentrations on the abscissa and ordinate), as did other wells in the plot. Well 3-30, in particular, had significant excess U in bailed vs. pumped samples, and after May 30, only South End wells reached concentrations in excess of 75 μg/L during the major water table rise in June. With respect to bore-hole flows, note that Well 3-30 was a shallow-completion member of a three-well cluster, did not extend into or through the low-K intermediate stratigraphic zone, and could not have been affected by flow from the lower high-K zone.

A comparison of shallow-completion wells over the course of the passive experiment (Figure V.3-7) indicated a rise in overall U concentrations during the course of the experiment. Groundwaters in the three corners of the IFRC showed an increase in U concentration over the period shown. The eastern part of the site (Well 2-29) showed an increase from 50 to 60 µg/L U, and in the northern part of the site (Well 2-26) the U concentration increased from 35 to 70 µg/L. The rise of the water table thus represented a significant contribution of contaminant U to the aquifer.

Summary and Future Directions

Although the mechanism for contaminant U migration to the aquifer from the vadose zone had been hypothesized, the passive experiment represented the first direct evidence for U capture from the vadose zone during seasonal fluctuations in the Columbia River stage. Two activities are planned to address the shortcomings of these results. Additional wells with screened intervals above the highest expected water table elevation will be constructed, and the influence of borehole flows will be negated by the installation of packer in the low-K zone. The passive experiment will be repeated in the Spring of 2010.
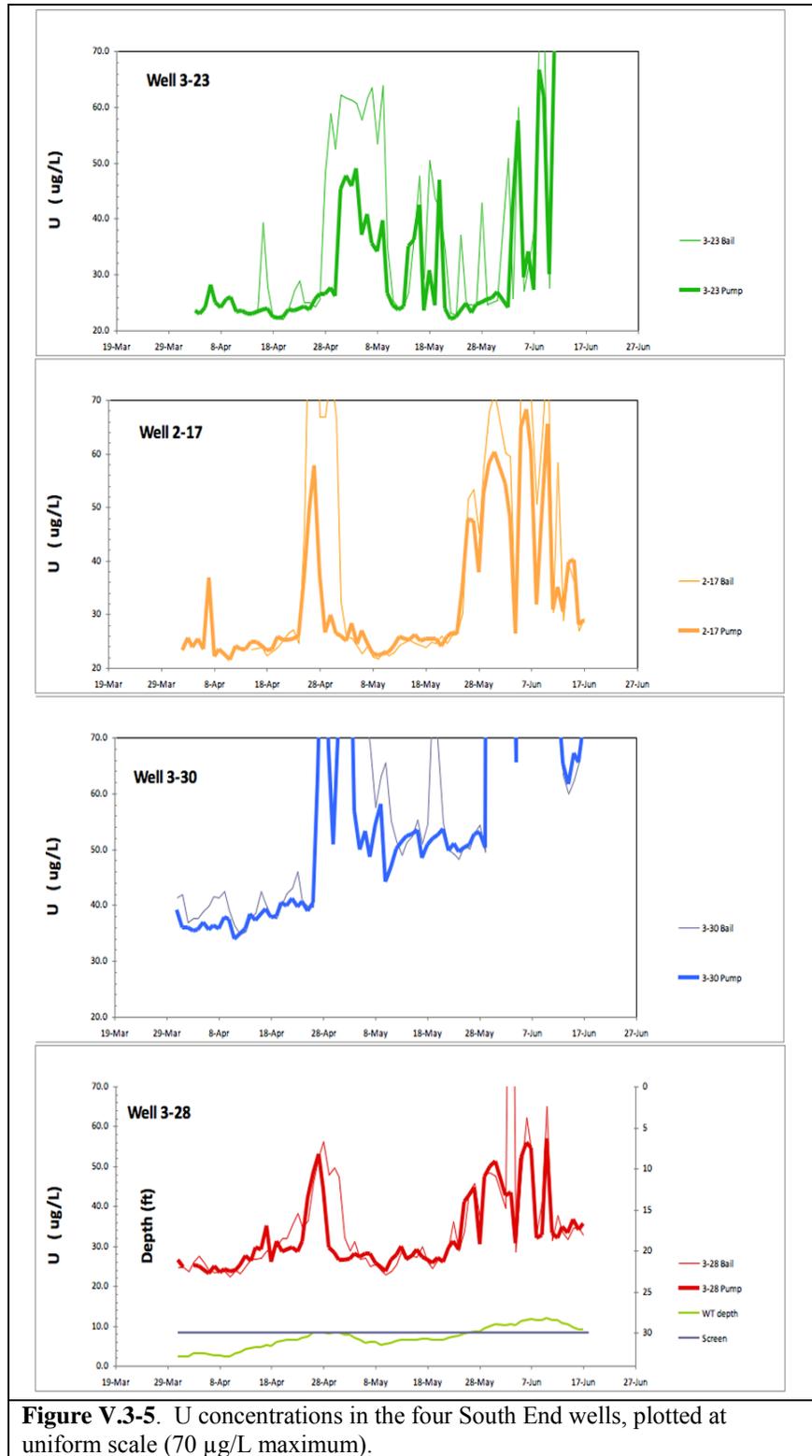


**Figure V.3-5**. U concentrations in the four South End wells, plotted at uniform scale (70 µg/L maximum).

An important goal of integrated laboratory and passive field experiments in 2010 is the development of a 3-D reactive transport model of the lower vadose zone and upper aquifer. The model will allow simulation of annual U recharge events as controlled by the specific annual hydrologic pattern, and the potential future duration that vadose zone recharge to the aquifer may continue given the U inventory. This model must integrate rate limited desorption, dynamic river-driven hydrology, and the spatial distribution of relevant properties including U concentration, surface complexation strength and rate, hydraulic conductivity, and other properties. The development of both the process and spatial heterogeneity models needed for this activity are described in **Section VI.**
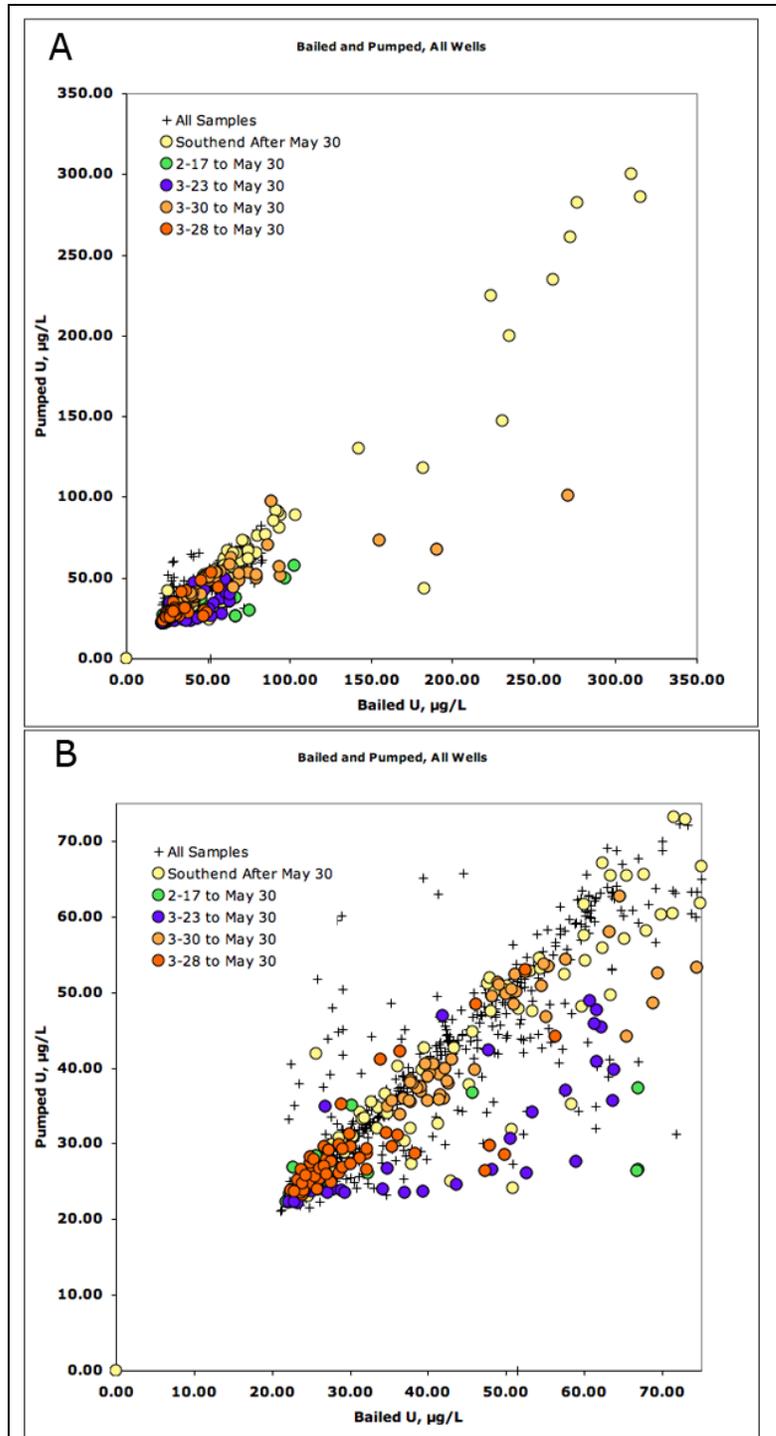


**Figure V.3-6**. All sample pairs, Bailed and Pumped, showing the predominance of South End wells in the magnitude of measured U concentrations during the passive experiment. South End well samples are uniformly colored Yellow if collected after May 30, when the water table rose above the level of the well screens. A. Concentrations up to the maximum; B. Detail of A, showing that wells other than the South End wells contributed U only up to a concentration of 70 µg/L.
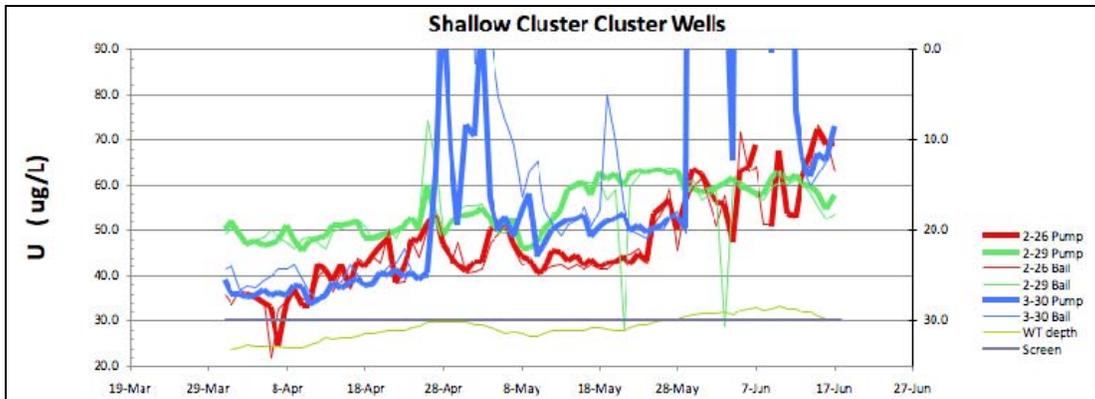
**Figure V.3-7**. U concentrations for the three shallow wells from the three well clusters, showing a general increase in U concentrations across the IFRC site during the passive experiment.

## V.4. November 2009 Desorption Experiment

Understanding the in-situ geochemical and transport behavior of U(VI) within the contaminant plume is a primary project objective to be explored through injection and passive monitoring experiments. Because of the complex transport behavior observed in the Nov. 2008 and March 2009 non-reactive tracer experiments, we felt it prudent to perform a preliminary U injection experiment to evaluate site infrastructure performance and general patterns of U(VI) behavior prior to moving on to a more comprehensive and costly field experiment.

A U(VI) tracer experiment brings the additional complication of vertical variation in U(VI) concentrations within the plume (Figure V.4-1). Dissolved U(VI) concentrations are highest at the top of the aquifer, and decrease with depth. Additionally, there are both seasonal variations that result from the high spring water table that solubilizes contaminant U(VI) from the deep vadose zone, and annual variations that result from the differences in the absolute height of high water attained in the spring. The spring high water in 4/08-7/08 was markedly higher than in 4/09-7/09, resulting in higher upper aquifer U concentrations in 9/1/08 than in 9/1/09. These concentration differences with
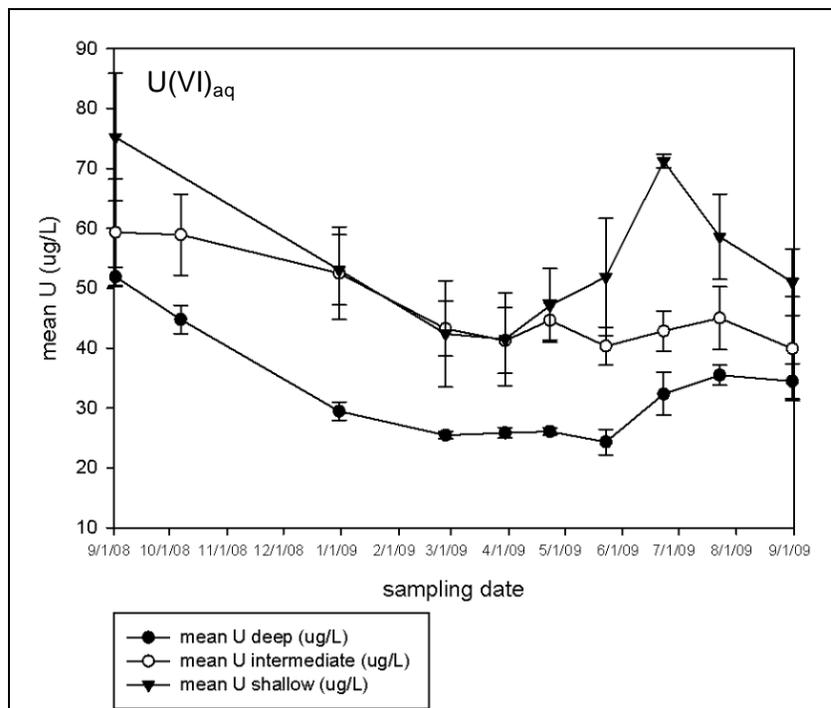


**Figure V.4-1**. U(VI) groundwater concentrations in IFRC multi-level monitoring wells.

depth are significant and require explicit consideration given previous discussions of well bore vertical flows in this report and the January 2010 Quarterly.

The Experiment

The experiment was performed in early November 2009 during a projected stable river stage period by the Corps of Engineers (COE). It was performed like the November 2008 and March 2009 experiments, with 70,000 gallon of up-gradient groundwater injected into fully screened well 2-9. The up-gradient groundwater contained 5 ug/L of dissolved U, while the upper and lower groundwater zones at the time of injection displayed stable, average concentrations of 35 and 25 ug/L, respectively. The concentration difference in the injection water was designed to induce in-situ desorption. The dynamic range of the experiment was not especially large given the relatively small concentration difference between the tracer (e.g., up-gradient) and the in-situ waters, and the average variance of in-well U measurements resulting from analytical uncertainty and natural variation (+/- 1.5 µg/L).

Results

Representative results for tracer (Br⁻) and U breakthrough in various wells are shown in Figure V.4-2 referenced to elapsed time after injection. Well 2-9 is the injection well, and concentrations at early time display characteristics of the injectate. Br and U decay toward background levels as in-situ groundwater displaces and mixes with the injected upgradient water, and U rapidly desorbs. U concentrations initially trend toward 35 ug/L, the concentration in the upper aquifer, but then oscillate between 25 and 35 ug/L indicating periods of downward and upward flows. Depth discrete Well 2-27d (screened in the deep, low K zone only) and fully screened Well 2-12 in the second well tier display nearly identical behavior, with a peak breakthrough of Br and U of C/Co=0.5 at approximately 500 min. U concentrations in both wells stabilized at ~25 ug/L, the concentration present in the deep aquifer zone. The similar breakthrough behavior of both wells indicates that fully screened Well 2-12 was dominated by upward flow during the entire period, and was monitoring breakthrough in the lower aquifer zone. Distal well 3-28 in the fifth well tier displayed attenuated breakthrough of Br (C/Co max ~ 0.2), and U concentrations representative of lower aquifer background concentrations (25 ug/L) with small deflections that paralleled those of Br. The behavior of fully screened Well 3-28 indicated that it was dominated by lower aquifer waters over the monitoring period, with possible flow oscillations at 4600 and 8250 min. Approximately 35% of the fully screened wells revealed complex U, Br, and specific conductance breakthrough patterns that were strongly impacted by vertical flow oscillations between the upper and lower hydraulic conductivity zones.

Summary and Future Directions

While the experimental results have not yet been modeled with our newly completed and parameterized reactive transport simulator, we were surprised to see little visual evidence for rate controlled U desorption in the breakthrough data. Thus these initial results were contrary to our conceptual and numeric model developed in the laboratory. The breakthrough time and relative concentration for both Br and U were similar in wells with normal breakthrough curves that were not complicated by oscillations in vertical flow. As revealed by the diagnostic post-breakthrough U concentration (e.g., 25 ug/L), this well set (including 2-12, 2-27d, and 3-28 in Figure IV.3-2) primarily monitored the lower high K zone that has exhibited fast and preferential transport in the non-reactive tracer experiments. It may thus be weakly reactive, with macro-pore dominated transport.
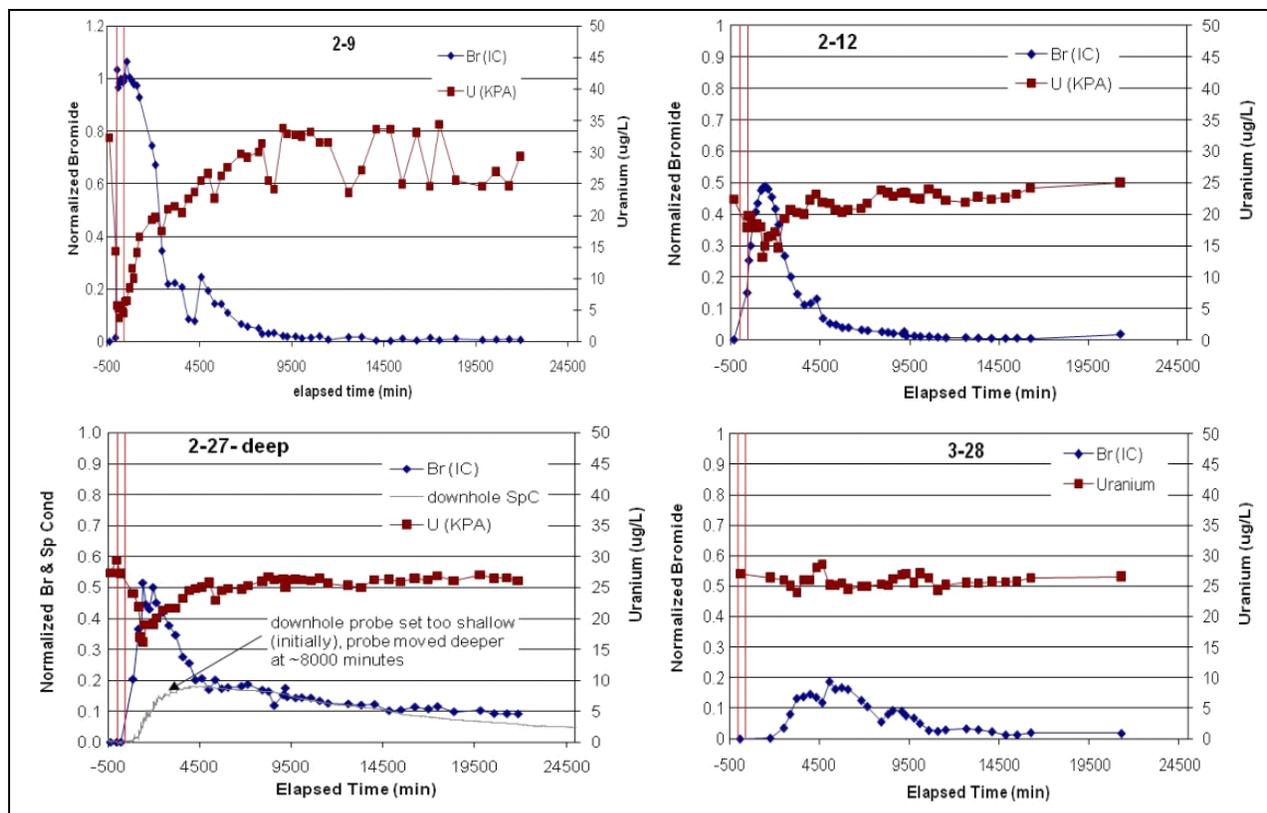
**Figure V.4-2**. U(VI) concentrations and normalized Br⁻ concentrations in select IFRC wells during the fall 2010 desorption experiment.

Given that this experiment was exploratory and preliminary, the results support the need for the following actions.

- Carefully model high quality breakthrough curves from the current experiment with the recently completed reactive transport simulator to improve parameterization of in-situ surface complexation and mass transfer models for the three hydraulic conductivity zones. The current model has been parameterized with data from intact, laboratory core experiments only.

- Perform extensive pre-modeling calculations to identify optimal strategies for injection (e.g. volume, duration, and location) to allow robust study of in-situ kinetic and thermodynamic processes given noted behaviors and time-scales. Consider multiple pulse and long slow injections to develop in-situ conditions that are sensitive to reaction kinetics.

- Localize a desorption injection experiment to the upper high K zone only. This zone has higher dissolved U concentrations and U-$K_d$ values,, and lower hydraulic conductivity than the deeper high K zone. This zone can be isolated using inflatable packers (e.g., Figure IV.4-3), and four new wells screened only in this zone are planned for spring 2010.

## V.5. Site Microbiology and Biogeochemistry

PNNL SFA Collaboration

The PNNL Scientific Focus Area (SFA) is focused on interdisciplinary research to define the role of subsurface microenvironments and transition zones on contaminant fate and transport at Hanford. PNNL SFA research results on the microbial ecology and biogeochemistry of Hanford formation subsurface sediments (see the PNNL SFA FY2009 Annual Report) obtained during the first phase of IFRC well-drilling revealed a relatively abundant, active, and phylogenetically diverse subsurface microbial community. Molecular analyses, enrichment cultures, and sediment microcosm experiments revealed that total populations declined and community structure and function shifted upon transition from the Hanford formation sand and gravels to the underlying fine-grained Ringold Formation (Unit E). Further changes in community structure and function were noted upon transition from the upper oxidized region of the fine-grained Ringold to the reduced region approximately 2-3 ft. below (Figure V.5-1). Informed by SFA microbiological investigations of IFRC core samples, a joint IFRC-SFA *in situ* microbial ecology-biogeochemistry experiment was initiated in October, 2009. The objective of this experiment was to probe, at finer spatial resolution and in greater detail, the changes in microbial community structure and function as well as Fe redox reactions with various iron-bearing mineral phases and sediments in relation to transitions in geochemical and hydrologic properties across the Hanford-Ringold textural and intra-Ringold redox boundaries.



**Figure V.5-1**. Redox boundary in fine-grained 300 A Ringold Unit E sediments about 3.5 ft below the Hanford-Ringold contact. The boundary is hypothesized to a redox transition zone where $O_2$ is consumed by microbiologic respiration facilitating reduction of sediment-associated Fe(III) and potentially sulfate. Sedimentary organic matter is believed to be the electron donor driving these biogeochemical reactions.

Down-Hole Well Experiment

Two IFRC wells (3-24 and 3-27) were selected for in-well microbial ecology-biogeochemistry studies as the screened interval for these two wells extends into the reduced region of the Ringold E unit. A well developed in the deep characterization borehole (2-25) was used to obtain additional information on aqueous geochemistry and dissolved gas composition across the redox transition zone in the fine-grained Ringold and below via a multi-level sampling (MLS) system. Down-hole microcosm MLS units containing site sediments, Fe(III) oxides, basalt coupons, synthetic magnetite, bio-sep beads for microbial capture, an *i-*
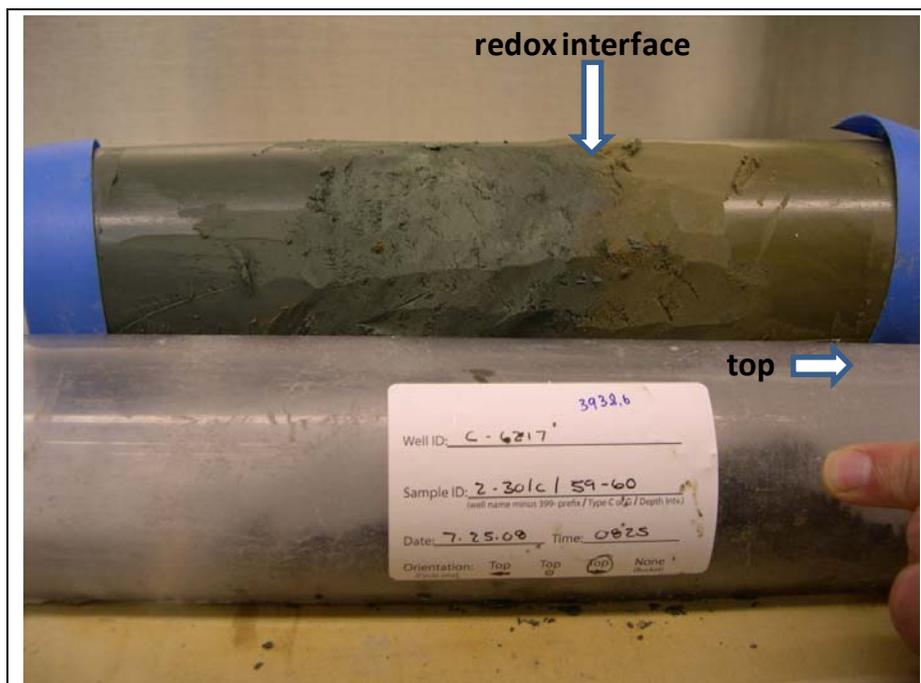
chip for *in situ* cultivation of Fe(III)-reducing and Fe(II)-oxidizing microorganisms (E. Roden), and aqueous and gas phase diffusion cell samplers (Figure V.5-2a) were deployed at three depths in wells 3-24 (Figure V.5-2b) and 3-27 on October 22, 2009. The sampling depths included: i.) within the Hanford formation, ii.) above the redox transition zone in upper Ringold formation, and iii.) below the redox transition zone in the upper Ringold formation. The in situ MLS microcosms and associated samples are being used to analyze a range of microbiologic, geochemical, and hydrologic properties that will be used to test SFA hypotheses regarding microbial community structure and biogeochemical processes across two key transition zones in the Hanford 300A subsurface. The first set of samples was retrieved from well 3-24 on December 7, 2009 and the samples are currently being analyzed. The second MLS microcosm in 3-27 will be retrieved in late February, 2010. Preliminary results from 3-24 are provided below.
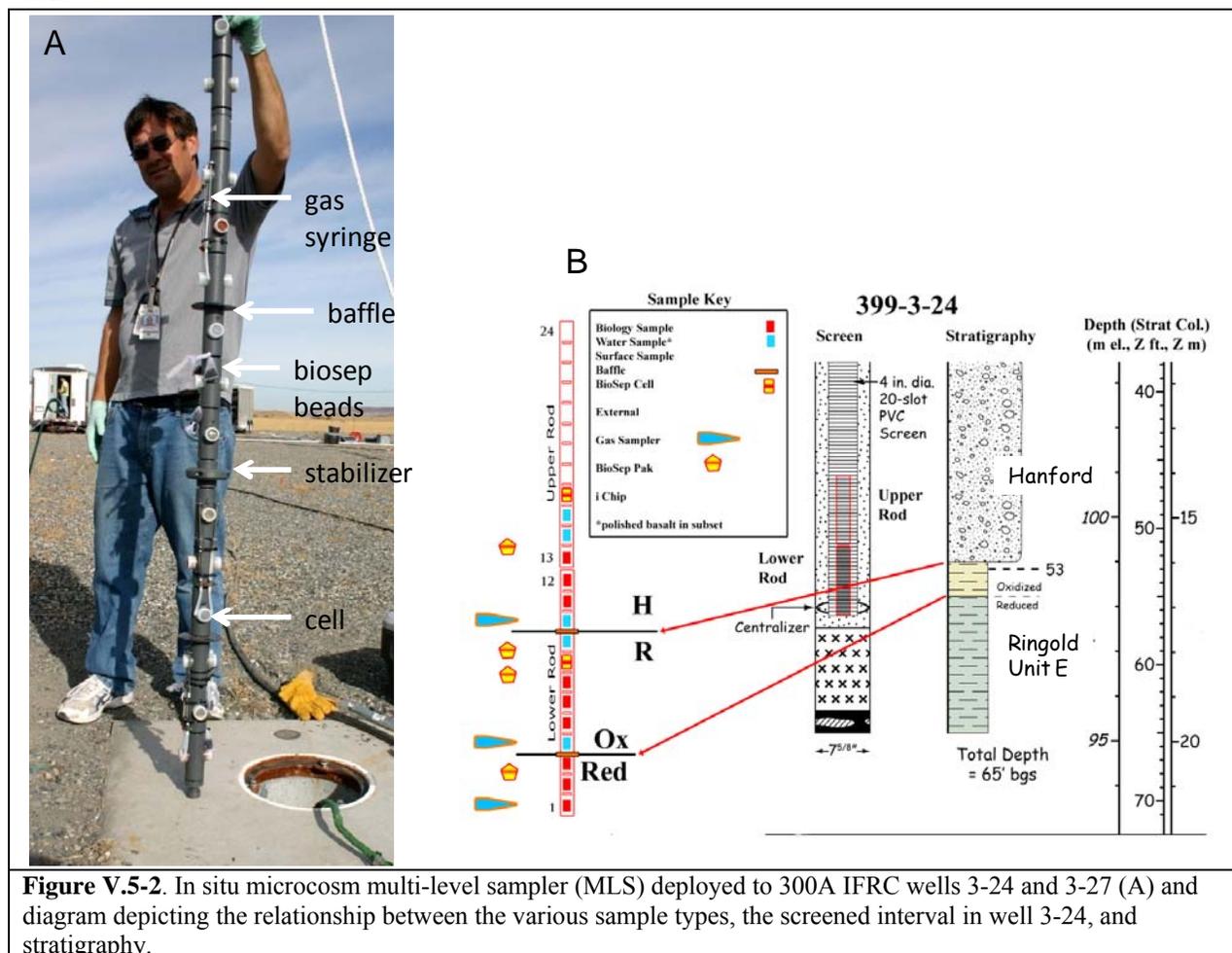


**Figure V.5-2**. In situ microcosm multi-level sampler (MLS) deployed to 300A IFRC wells 3-24 and 3-27 (A) and diagram depicting the relationship between the various sample types, the screened interval in well 3-24, and stratigraphy.

Preliminary Results

Dissolved gases samples were collected by using a gas-tight syringe connected to a section of gas-permeable tubing sealed at one end. The syringes were placed within each baffled interval (Figure V.5-2), and were shipped to Oak Ridge National Laboratory immediately upon retrieval from the well where they were analyzed for gas composition. The gas analyses (duplicate analytical samples, presented as ppm on a volume basis in the equilibrated syringe gas phase, and as dissolved concentrations, based on Henry's Law constants at aquifer temperature,) reveal a clear redox transition trending from oxic in the

54

lower Hanford formation (10A, B) to the bottom (1A, B) reduced fine-grained Ringold Unit E (Table V.5-1). These trends include a significant decrease in $O_2$ concurrent with increases in $H_2$, CO and $CH_4$ over the same interval. It is interesting to note that the $H_2$ concentration measured in the reduced Ringold is consistent with thermodynamic controls on its concentration when $CO_2$ is the terminal electron accepting process (i.e., methanogenesis) in microbial systems where organic matter fermentation is the primary energy source.

**Table V.5-1**. Gas analyses from MLS equilibrated in well 3-24.

| Gas ID | Depth bgs feet | Equilibrated Gas Phase | | | | Calculated Solution Concentration | | | |
|---|---|---|---|---|---|---|---|---|---|
| | | $H_2$ (ppmv) | $O_2$ (ppmv) | CO (ppmv) | $CH_4$ (ppmv) | $H_2$ (mol/L) nM | $O_2$ (mol/L) μM | CO (mol/L) nM | $CH_4$ (mol/L) nM |
| IFRC-MLS-3-24-10A | 52.5 | bd | 178331.2 | bd | bd | bd | 266 | bd | bd |
| IFRC-MLS-3-24-10B | | bd | 190346.4 | bd | bd | bd | 284 | bd | bd |
| IFRC-MLS-3-24-4A | 54.95 | bd | 1707.4 | bd | bd | bd | 2.5 | bd | bd |
| IFRC-MLS-3-24-4B | | 0.52 | 2077.8 | 0.39 | bd | 0.42 | 3.1 | 0.4 | bd |
| IFRC-MLS-3-24-1A | 56.07 | 6.14 | 1861 | 0.22 | 326.8 | 5.01 | 2.8 | 0.2 | 540 |
| IFRC-MLS-3-24-1B | | 7.49 | 1210.6 | 0.55 | 341.8 | 6.11 | 1.8 | 0.6 | 560 |
| detection limits | | 0.08 | 903 | 0.13 | 300 | 0.11 | 1.3 | 0.1 | 490 |

Due to the limited depth screened within the reduced region of the Ringold, we were unable to obtain a water sample for aqueous geochemistry in 3-24. However, a 25' MLS was deployed in well 2-25 (the deep microbiology characterization borehole) across the redox transition zone in the upper Ringold Formation. This zone of generally fine-textured sediments exists below the depth of intense monitoring in the IFRC well-field proper. The intent of this sampling was to obtain ground water composition data that could be compared with information on the microbiological properties that were previously determined by measurements made on fresh borehole sediments. The emerging water composition data reveals distinct changes in select ground water inorganic constituents (Figure V.5-3), including dissolved Mn and Fe, across the Ringold redox transition zone extending from approximately 58' to 67' in well 2-25. A peak in dissolved sulfide (~1.5 mg $L^{-1}$) was observed in this same region coinciding precisely with the region of the reduced Ringold Unit E as determined from the direct inspection of cores during well drilling and logging. Analyses of core material from 2-25 revealed the presence of framboidal pyrite in the reduced region of the Ringold and a pyritic sulfur concentration of 0.277 (wt. %) compared to the overlying oxidized region where pyritic sulfur was below detection and framboidal pyrite was not observed. Interestingly, there is also a peak (22-26 μg $L^{-1}$) in sulfate concentration over the 63-64' interval. All of these results are consistent with the reduced region within the fine-grained Ringold Unite E being a naturally active zone of microbial sulfate reduction. The MLS has been recently redeployed over the depth interval of 82-107' below the ground surface in 2-25 and results of water and gas samples will be available in approximately 2 months. The MLS will subsequently be re-deployed to measure dissolved gas concentrations across the upper region of the interval of this well so that we will have gas measurements, not considered during the first deployment, to compliment the aqueous geochemistry measurements.
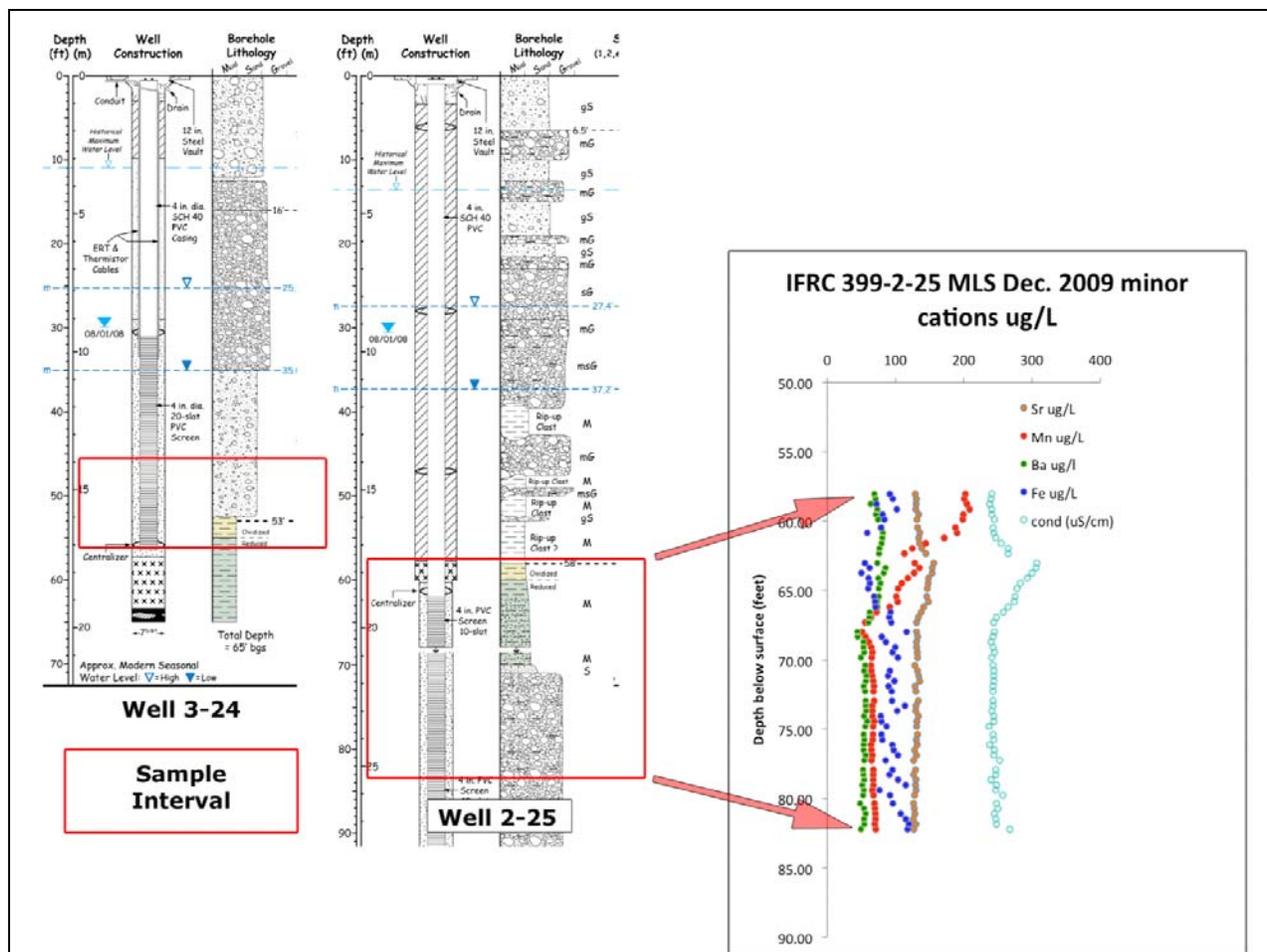
**Figure V.5-3**. The multi-level sampler retrieved water samples from well 2-25 every 6" during the course of a 1-month equilibration period. Based on visual inspection of cored sediments from this borehole, the redox interface within the fine-grained Ringold Unit E is present at 60'. Shown here are selected minor cations, including two with TEAP significance (Mn and Fe). A comprehensive suite of analytes was measured. The relationship between sample intervals in Wells 3-24 and 2-25 is indicated.

BioSep beads were used as microbial "traps" to assess community structure across the various transition zones. Scanning electron microscopy analyses of the beads clearly indicated microbial colonization of the beads over the 6-week interval (Figure V.5-4) as did various measures of microbial biomass (ATP, PicoGreen DNA quantitation, and qPCR of 16S Bacterial rDNA gene copy). Biomass concentrations were generally highest in beads baited (imbibed prior to deployment) with ferrihydrite, compared to unbaited beads or beads baited with acetate or nitrate, and were highest in the oxic regions of the Hanford and upper Ringold Unit E. Geobacteraceae 16S gene copies, as determined by DNA extracted from the untreated beads, were detected throughout the interval but were clearly highest in the reduced Ringold interval, accounting for up to 13% of the total Bacterial 16S gene copies. Cluster analysis (Sorensen similarity) of community composition as measured by terminal restriction fragment length profiling (TRFLP) of DNA extracted from the treated and untreated beads revealed that the variation in microbial community structure was larger between samples from the different MLS intervals than that between the various baiting treatments (Figure V.5-5). Most probable number (MPN) analyses of viable Fe(III)- and sulfate-reducing bacteria associated with the ferrihydrite-coated sand samples are underway and

preliminary indications are that viable populations of these functional groups are $10^2$-$10^4$-fold higher in the oxide-coated sands incubated in the MLS section that was below the Ringold redox interface.

Summary and Future Directions

In summary, there is a very well-defined redox transition zone in the Hanford 300A subsurface that extends from the base of the Hanford formation, through the upper oxidized Ringold Unit E and into underlying reduced Ringold sediments. The electron acceptors include $O_2$, nitrate, possibly Mn(III/IV), Fe(III), sulfate and $CO_2$. Concentrations of dissolved ions and gases are all in general agreement and preliminary microbial analyses indicate that active microbial populations are catalyzing the redox transformations. $H_2$ concentrations suggest the fermentation of sedimentary organic carbon as the primary energy source but it is currently unknown whether $H_2$ may be out-gassing from the underlying Columbia River basalt aquifer. While the areal extent of the reduced fine-grained Ringold sediments is unknown, its widespread presence could have important implications for the subsurface migration of redox sensitive contaminants along the Hanford Columbia River corridor.

Follow-on investigations will initially focus on defining the fine-scale redox changes across the transition zone, identifying the potential source(s) of electron donors, the in situ microbial activities and biogeochemical reaction rates, in-depth microbial community structure, and the fluxes and movement direction of water, ions and gases within the transition zone and sub-domains within.
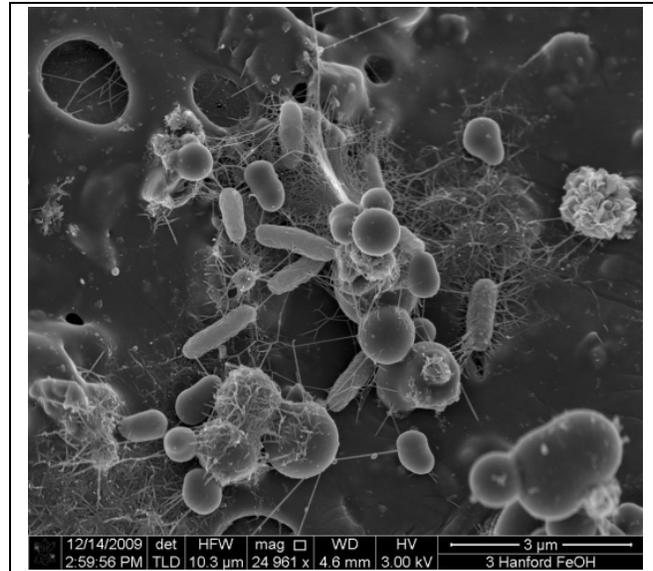


**Figure V.5-4**. Scanning electron microscopy analyses of the surface of a BioSep bead baited with ferrihydrite and incubated in well 3-24. Note the copious quantities of collapsed EPS in and between cells.
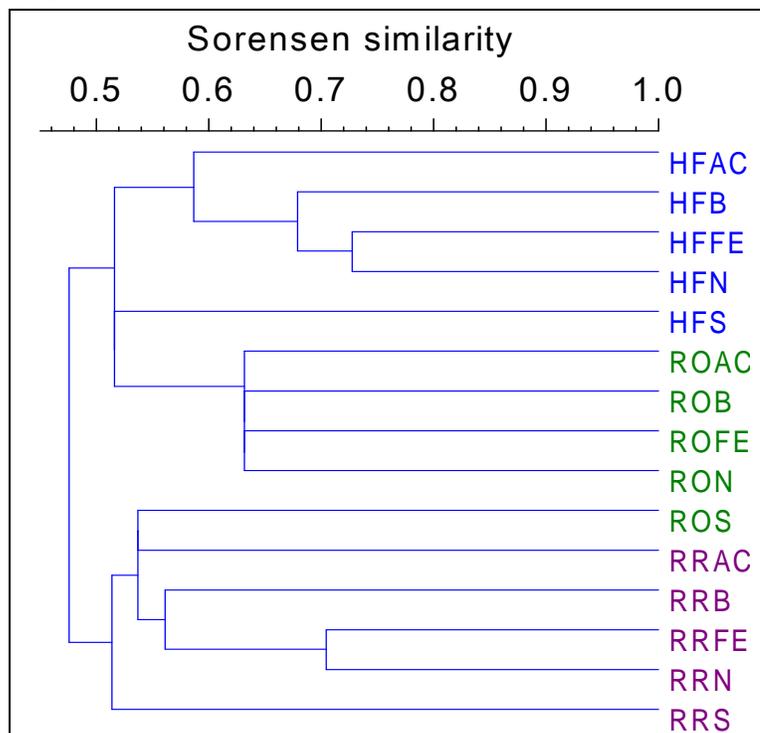


**Figure V.5-5**. Cluster analysis (Sorensen similarity) of bacterial TRFLP profiles for down-well microcosm samples from well 399-3-24. Key: HF=Hanford formation; RO=Ringold oxidized; RR=Ringold reduced; AC=acetate; B=beads only; FE=ferrihydrite; N=nitrate; S=clean, sterile Hanford sand fraction.

# VI.    MODELING AND INTERPRETATION

## VI.1.  Geochemical Heterogeneity Model

Geostatistical analysis of the bicarbonate extractable U provided information on the spatial distribution of available U in the lower vadose zone and upper aquifer within the experimental plot.  We examined the spatial distribution of both extractable U and the fraction of sediment < 2 mm, focusing on the "smear zone", the zone within which the water table fluctuates due to variation in the flow of the Columbia River. This analysis also served as the basis for an uncertainty analysis that included Monte Carlo estimates of the mass of extractable U within the smear zone.  Work to be conducted in the near future will include geostatistical analysis of the spatial distribution of U-233 and U-238 sorption distribution coefficients ($K_d$), and the surface area of the sediments.  Those results will provide input grids needed for reactive transport modeling of uranium transport in the IFRC experimental plot.

We initially examined the spatial distribution of 100 h  bicarbonate extractable U measured on the < 2 mm fraction of the sediment.  The maximum extractable U found within wells in the IFRC experimental plot is highly heterogeneous (Figure VI.1-1).  Extractable U also varies vertically, with a tendency for higher extractable U at higher elevations (Figure VI.1-2); the variability in extractable U values also increases for the upper portion of the smear zone (Table VI.1-1).  The mean concentration of extractable U is still increasing for the three highest elevation intervals (Table VI.1-1), indicating that the current data set does not bound the zone of high concentration.  However, the existing dams on the Columbia River above the Hanford Site currently restrict the maximum groundwater elevation to approximately 107 m, which sets a de facto upper bound on the portion of the smear zone that is likely to contribute to ongoing contamination of the groundwater due to fluctuation of the groundwater through the zone of high U concentrations.

**Table VI.1-1**. Summary statistics of extractable uranium data by elevation intervals.

| µg U/g soil | All Samples | <104m | 104-104.5m | 104.5-105m | 105-105.5m | 105.5-106m | 106-106.5m | 106.5-107m | 107-107.5m | 107.5-108m | 108-108.5m | >108.5m |
|---|---|---|---|---|---|---|---|---|---|---|---|---|
| N of cases | 90 | 8 | 4 | 8 | 9 | 7 | 12 | 16 | 6 | 7 | 6 | 7 |
| Minimum | 0.28 | 0.28 | 0.33 | 0.45 | 0.62 | 0.46 | 0.54 | 0.46 | 0.63 | 0.49 | 0.65 | 1.67 |
| Maximum | 16.82 | 1.34 | 1.69 | 3.97 | 3.50 | 4.67 | 4.04 | 6.87 | 4.99 | 16.82 | 14.81 | 10.84 |
| Range | 16.53 | 1.06 | 1.36 | 3.52 | 2.88 | 4.21 | 3.50 | 6.40 | 4.37 | 16.33 | 14.16 | 9.18 |
| Median | 1.34 | 0.42 | 0.51 | 0.73 | 1.25 | 0.82 | 1.03 | 2.27 | 1.74 | 2.32 | 2.40 | 3.40 |
| Mean | 2.26 | 0.53 | 0.76 | 1.52 | 1.48 | 1.38 | 1.36 | 2.61 | 1.97 | 4.06 | 4.46 | 5.13 |
| 95% CI Upper | 2.85 | 0.82 | 1.78 | 2.60 | 2.14 | 2.74 | 1.97 | 3.69 | 3.62 | 9.31 | 9.92 | 8.69 |
| 95% CI Lower | 1.67 | 0.24 | -0.27 | 0.43 | 0.81 | 0.02 | 0.74 | 1.53 | 0.32 | -1.19 | -1.00 | 1.57 |
| Std. Error | 0.30 | 0.12 | 0.32 | 0.46 | 0.29 | 0.56 | 0.28 | 0.51 | 0.64 | 2.15 | 2.12 | 1.45 |
| Standard Dev | 2.81 | 0.35 | 0.64 | 1.30 | 0.86 | 1.47 | 0.97 | 2.03 | 1.57 | 5.68 | 5.20 | 3.85 |
| Variance | 7.92 | 0.12 | 0.41 | 1.68 | 0.75 | 2.16 | 0.94 | 4.12 | 2.46 | 32.25 | 27.09 | 14.82 |
| C.V. | 1.25 | 0.65 | 0.85 | 0.86 | 0.58 | 1.07 | 0.71 | 0.78 | 0.80 | 1.40 | 1.17 | 0.75 |
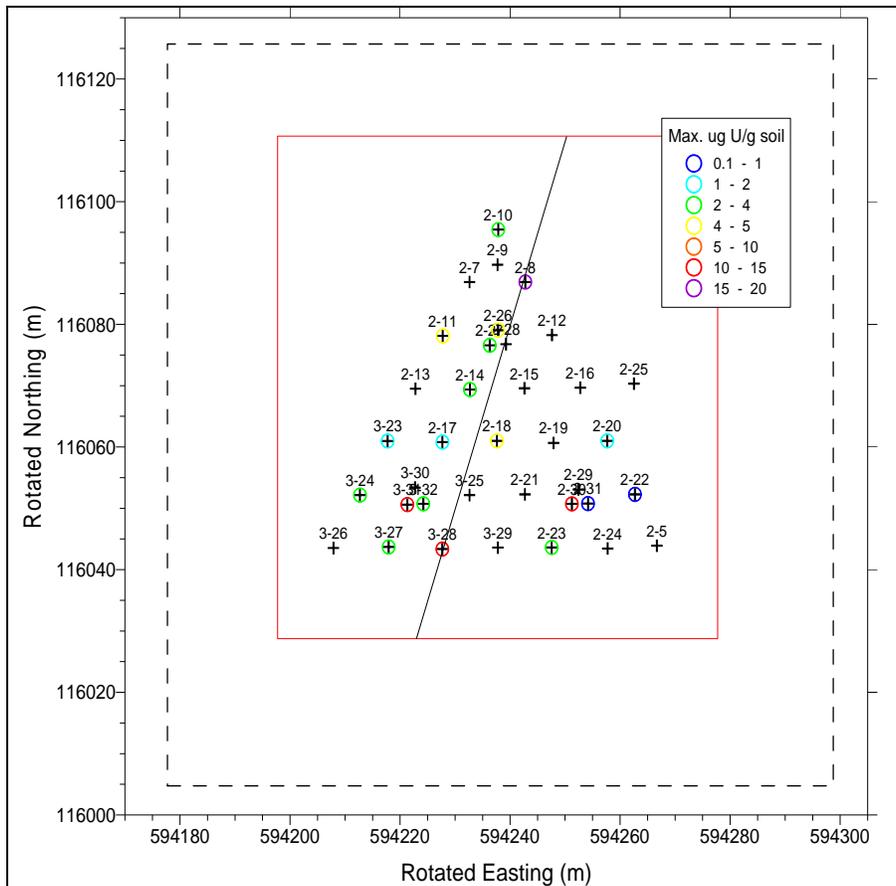
**Figure VI.1-1**. Map of the well locations in the Hanford IFRC experimental plot. Circled wells have extractable U concentration data, with colors indicating the maximum concentration levels identified in each well. The black dashed line is the expected perimeter of the reactive transport modeling grid; the red line indicates the area of the grid used for geochemical heterogeneity studies. The black line is the location of a cross-section referred to later in the report. Note that the x- and y-coordinates shown in this figure are not the true coordinates, but are coordinates that are rotated 35° clockwise around well 2-9 into a STOMP model reference frame.

The histogram of extractable U concentration data is highly skewed (Figure VI.1- 3), with many low concentration values, and a long tail of high concentrations. Because of the skewed nature of the distribution, we performed the geostatistical analysis on a normal score transform of the data. The normal score transform is an alternative to the logarithmic transform often used in the earth sciences for positively skewed data. It has the advantage that the transformed data are an exact fit to the normal distribution, while logarithmically transformed data often deviate significantly from a normal distribution.

The experimental variogram of the normal scores of the extractable U data were fit with a nested spherical model having a zero nugget, first sill of 0.4 and horizontal range of 12 m, and second sill of 0.6 and horizontal range of 70 m (Figure VI.1- 4). The vertical range is 1.6 m. Directional variograms were examined but the data were from too few locations to determine if directional anisotropy is present in the extractable U data. The variogram model and the data were used as input to a sequential Gaussian simulation program in order to generate 100 realizations of the spatial distribution of extractable U. Each 3D realization of the U distribution reproduces the variogram model as well as the conditioning data. Figure VI.1-5 is a cross-section through the 399-3-28 and the 399-2-8 based on the average value of the concentrations over the 100 realizations.
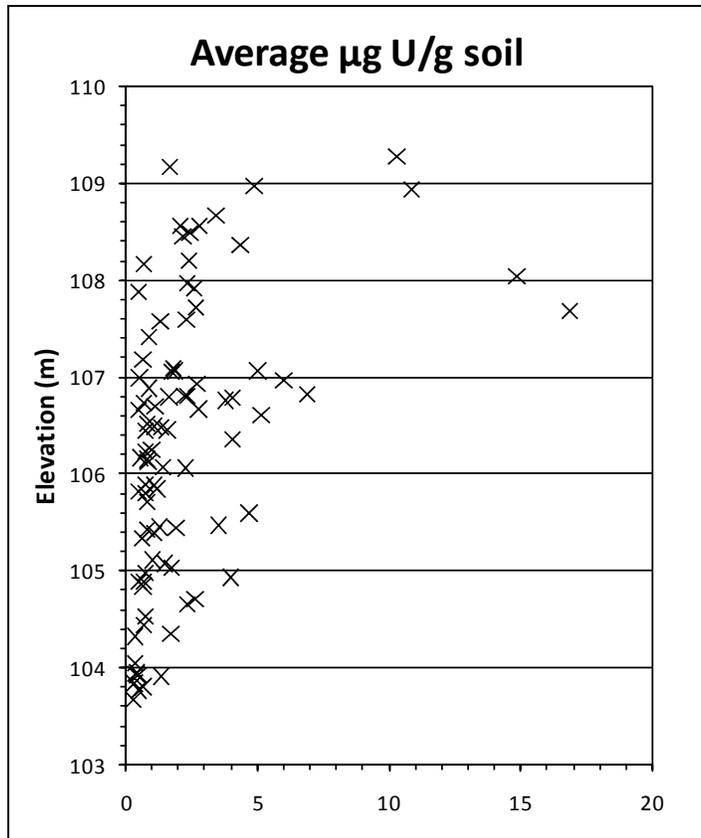


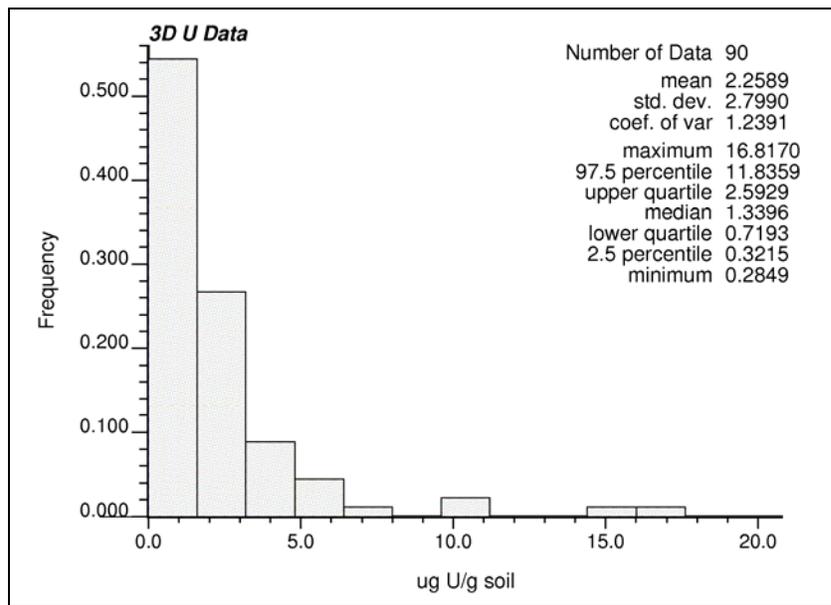**Figure VI.1-2**. Distribution of bicarbonate extractable U with depth.



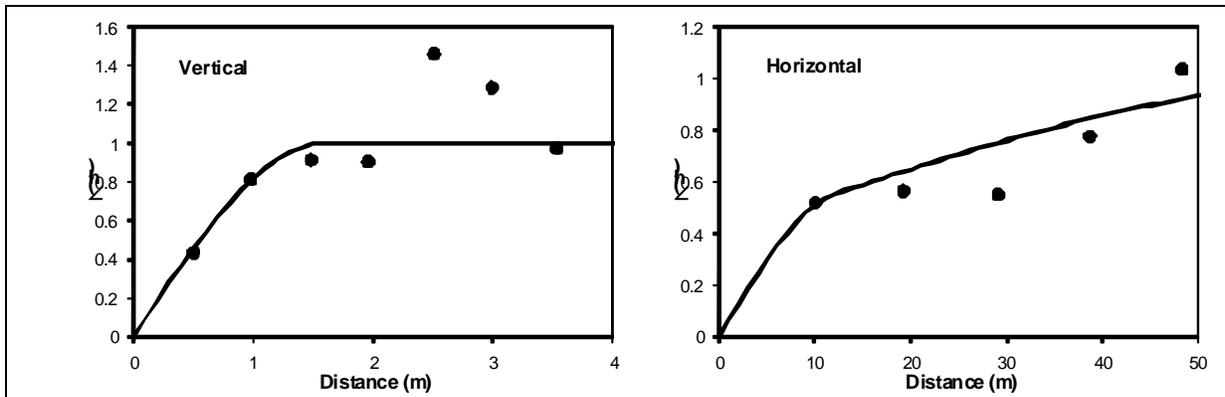**Figure VI.1-3**. Histogram of extractable U concentration data, measured on the < 2 mm fraction.

**Figure VI.1-4.** Vertical (left) and horizontal variograms of normal scores of 3D extractable uranium data. The black circles represent the experimental variogram points and the solid lines represent the models fit to the variogram. The experimental variograms were fit with a geometric nested spherical model consisting of a zero nugget, first sill of 0.4 and horizontal range of 12 m, and second sill of 0.6 and horizontal range of 70 m. The vertical range for both nested structures is 1.6 m.
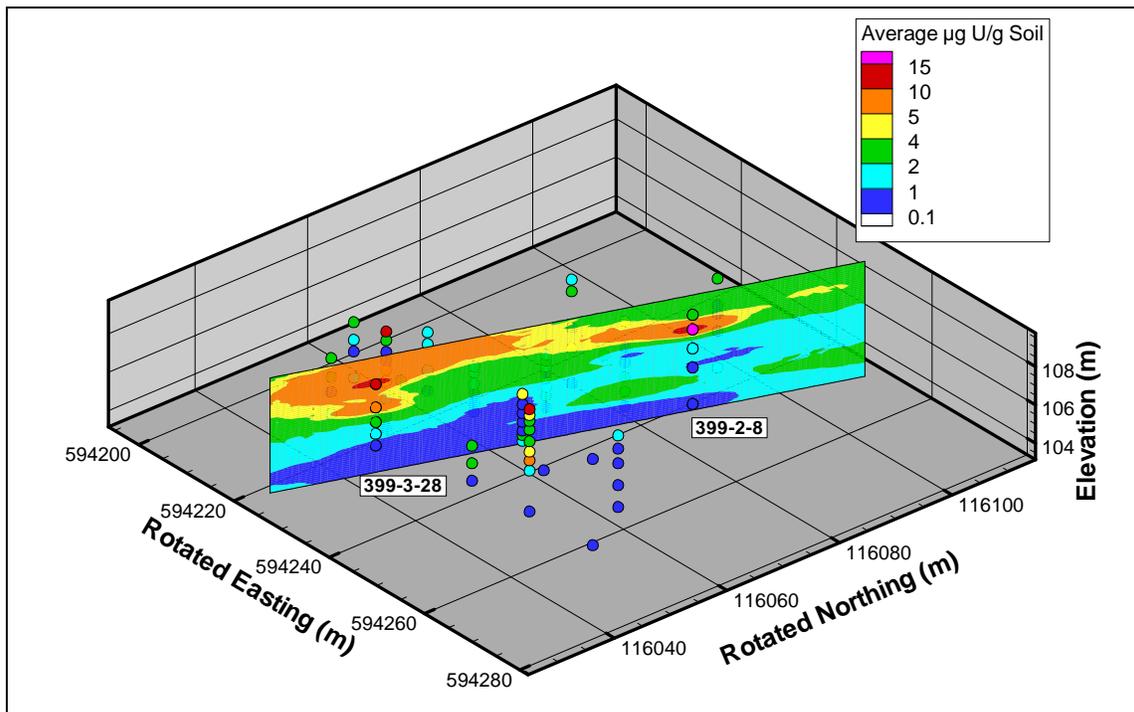


**Figure VI.1- 5**. Cross-section of the average bicarbonate extractable U in the < 2 mm sediment fraction, based on the average of 100 3D realizations of the concentrations. Cross section location shown in Figure VI.1-1.

Because the bicarbonate U extractions discussed above were performed on the < 2 mm fraction of the sediment samples, realizations of the spatial distribution of that sediment fraction were also needed, in order to calculate gravel-corrected concentrations. We examined the correlation between the concentrations of extractable U in the < 2 mm fraction and the fraction of sediment < 2 mm, and found that they were not correlated with one another (Figure VI.1-6), so that realizations of the 2 variables could be generated independently of one another. We fit a variogram model to the normal score transform of the fraction < 2 mm and generated 100 realizations of that variable. The upper zone of high extractable U

concentrations in 399-3-28 seen in Figure VI.1-5 are associated with a relatively gravel rich zone (Figure VI.1-7), while the high U concentration zone in the 399-2-8 is located in an area that has a higher proportion of sediment that is less than 2 mm.  This finding, which agrees with the lack of correlation between the extractable U concentrations and fraction < 2 mm seen in Figure VI.1-6, suggests that the distribution of high concentration material will cut across lithofacies in the Hanford formation.  We used the realizations of the extractable U concentration in the < 2 mm fraction and the realizations of the spatial distribution of the < 2 mm fraction to generate a 3D grid of gravel-corrected extractable U concentrations (Figure VI.1-8).  It is evident that the spring high water table (@106-107 m) contacts sediments with significantly higher adsorbed U then present in the saturated zone.
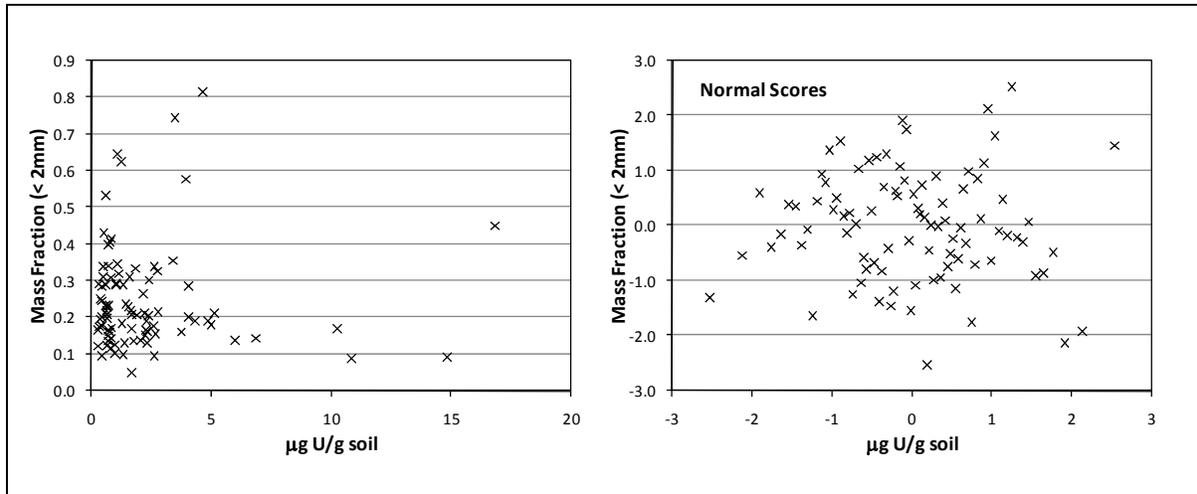


**Figure VI.1-6**.  Scatter plot of mass fraction of sediment less than 2 mm against extractable U concentrations.  Plot on the left is in the raw data units, while that on the right is on normal score transforms of both variables.
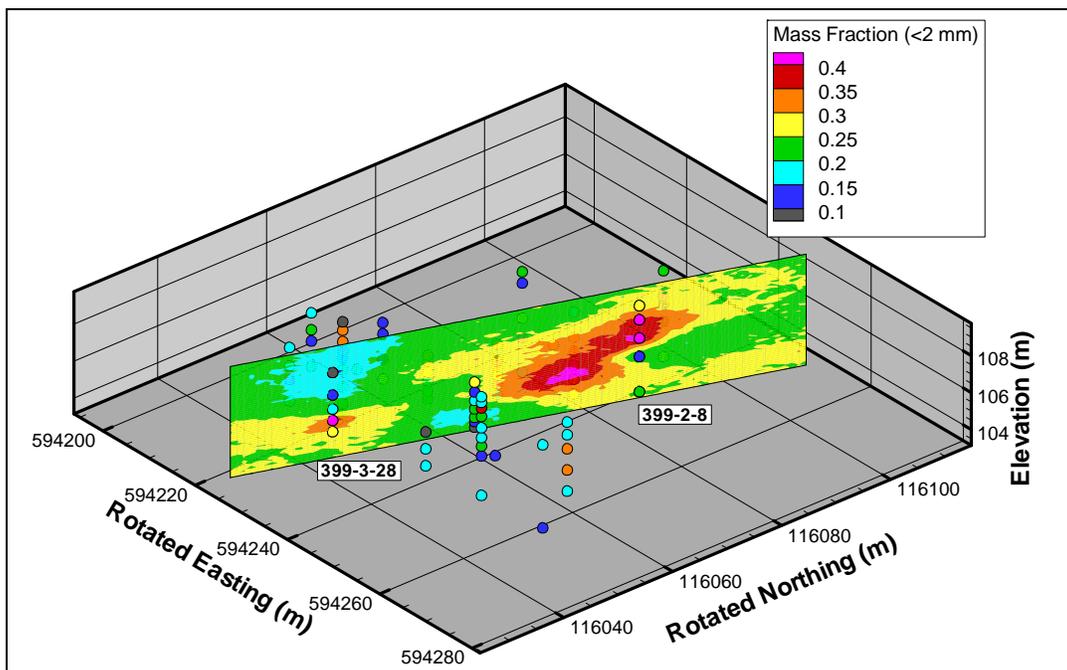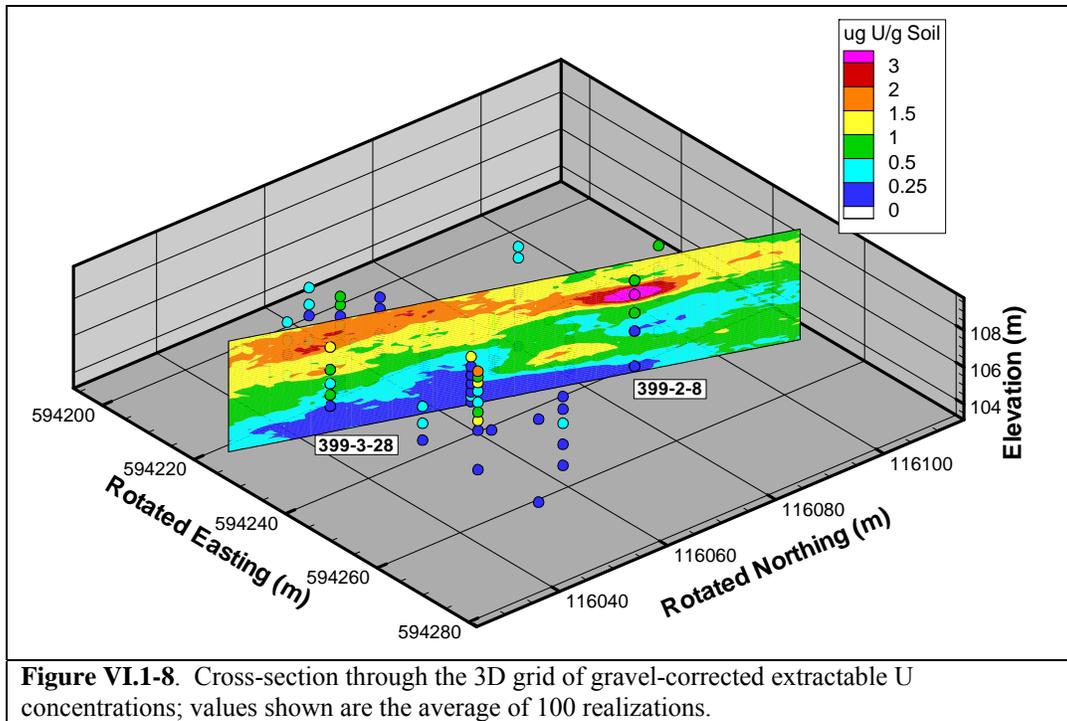


**Figure VI.1-7**.  Cross-section of the average fraction of sediment less than 2 mm.

62

**Figure VI.1-8**. Cross-section through the 3D grid of gravel-corrected extractable U concentrations; values shown are the average of 100 realizations.

The suite of 100 realizations of the gravel-corrected U concentrations can also be used to address uncertainty in the spatial distribution. For example, Figure VI.1-9 shows the probability that the gravel-corrected extractable U concentration exceeds a value of 0.8 µg U/g sediment, roughly equal to the 80th percentile of the gravel-corrected data. This approach can be used to map the probability that the concentration exceeds various levels of concentration, e.g., regulatory limits.

Several other measures of uncertainty can also be generated from the realizations. We used the suite of realizations to provide a preliminary Monte Carlo estimate of the mass of extractable U present in the smear zone in the area mapped for this study. In order to do that, we needed estimates of the bulk density of the sediment. Ongoing work by the IFRC on sediment samples and geophysical logs will include measurements of the bulk density of the sediment in the experimental plot that can be used to provide 3D grids of the bulk density. However, for purposes of illustration, we used bulk density data for the Hanford formation taken from Table 6.5 of Williams et al. (2007, PNNL-16435). The average and standard deviation of the bulk density values for the Hanford formation data in that table were 2.187 g/cm$^3$ and 0.163 g/cm$^3$, respectively. We drew 100 values from a normal distribution with those parameters and estimated the mass of extractable U in the 80 m by 82 m by 6 m (39, 360 m$^3$) study area for each realization. Statistics over the suite of realizations (Figure VI.1-10), indicate that the mean estimate is 62.2 kg, with a 95% confidence interval for the mean that ranges from 47.1 kg to 85.9 kg.

Work to be conducted in the near future will include geostatistical analysis of the spatial distribution of U-233 and U-238 sorption distribution coefficients ($K_d$), and the surface area of the sediments. Those results, together with the bicarbonate extractable U, will provide input grids needed for reactive transport modeling of uranium vadose zone release and transport in the IFRC experimental plot.
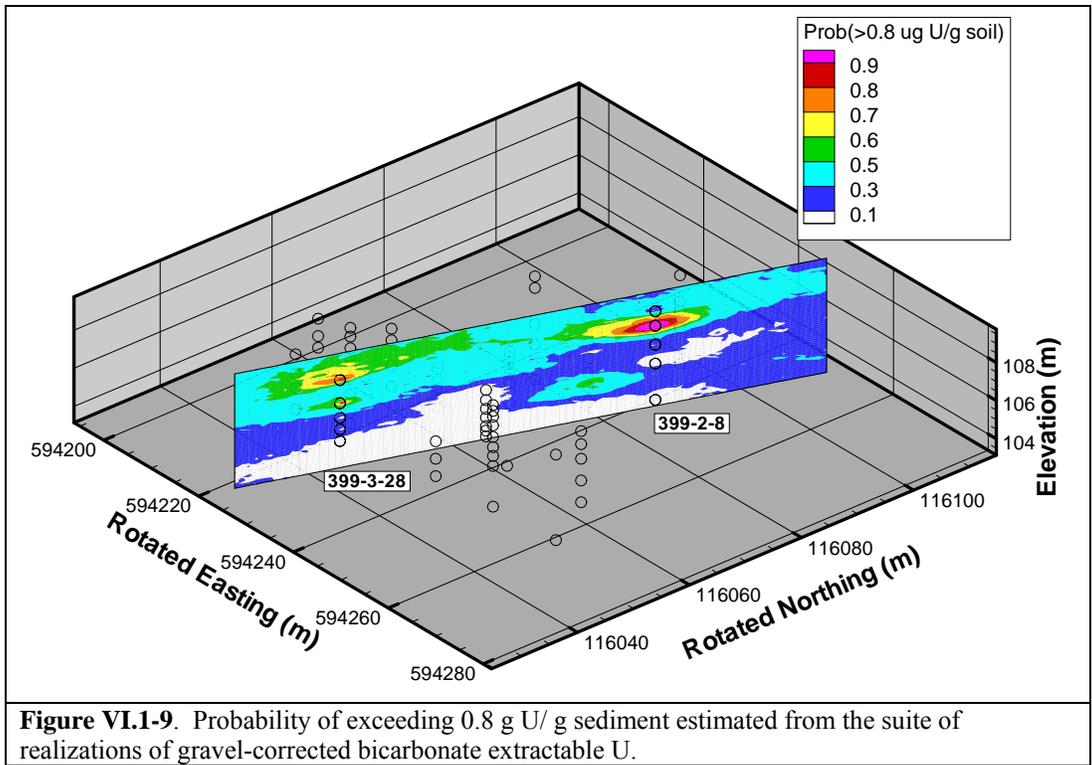
**Figure VI.1-9**. Probability of exceeding 0.8 g U/ g sediment estimated from the suite of realizations of gravel-corrected bicarbonate extractable U.
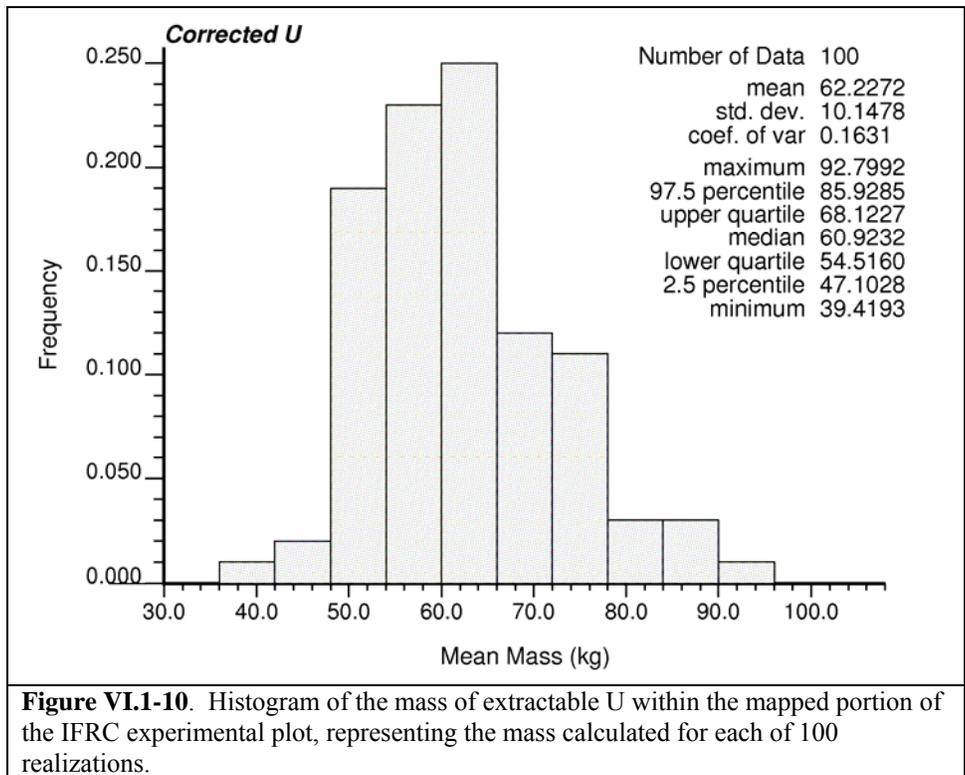


**Figure VI.1-10**. Histogram of the mass of extractable U within the mapped portion of the IFRC experimental plot, representing the mass calculated for each of 100 realizations.

**VI.2. Surface Complexation Model of U(VI) Adsorption**

The IFRC project is working to develop a field scale reactive transport simulator with kinetic, or mass transfer limited surface complexation as the dominant geochemical reaction observed in site sediments. Criteria for the model include simplicity, transparency, and a minimal number of chemical species. The geochemical reaction model will be further constrained by geostatistical spatial distributions of: i.) the mass or volume fraction < 2 mm sediment, ii.) adsorbed U, iii.) surface area, iv.) $K_d$, and v.) mass transfer rate determined by characterization measurements and geostatistical analysis as presented in **Section V1.1**.

Model Development

Experiments were conducted with the < 2 millimeter fraction of U(VI)-contaminated sediments collected from the smear- and saturated-zone at six locations within the IFRC experimental domain. These were composite sediments generated by PNNL from the three well clusters that were specifically created for surface complexation model development. The principal objective of this experimental program is to calibrate a model that describes equilibrium adsorption of U(VI) on sediments within the experimental domain over the full range of chemical conditions to which the sediments are exposed. Desorption of adsorbed contaminant uranium required at least 1000 hours to reach equilibrium. As expected, uranium adsorption generally increases with increasing uranium concentration and decreasing alkalinity (Figure VI.2-1).

Uranium adsorption data for all IFRC smear-zone composite samples were combined and fitted to various surface complexation models. The modeling approach followed that used previously for SPP vadose-zone samples (Bond et al., 2008). Highest quality fits were obtained using either reaction 1 or 2 in Table VI.2-1, with reaction 1 providing a significantly better fit as measured by the weighted sum of squares of the residuals divided by the degrees of freedom (WSOS/DF). Previous work on U(VI) adsorption on samples from the vadose zone in the South Processing Pond (SPP) showed that the best fit was obtained with a model that included both reactions in Table VI.2-1. The current dataset for the IFRC smear-zone samples could not be fitted using any two-reaction model that included reaction 1, which is to say that reaction 1 accounts for the observed compositional variability in U(VI) adsorption. However, it is possible that data collected at the higher end of the range of alkalinities applicable to the Hanford 300 area will require a two-reaction fit.

**Table VI.2-1**. Results from the best-fit surface complexation models for the IFRC smear-zone composite sediment samples.

| Number | Reaction(s) | logK | WSOS/DF |
|---|---|---|---|
| 1 | $SOH + UO_2^{2+} = UO_2OH + 2H^+$ | -4.56 | 4.8 |
| 2 | $SOH + UO_2^{2+} + H_2CO_3 = UO_2HCO_3 + 2H^+$ | -0.13 | 13.9 |

The $K_d$ values for IFRC smear-zone samples are significantly lower than those obtained previously for vadose-zone samples from the SPP (Figure VI.2-1). Fits to the U(VI) adsorption data for vadose-zone samples using only reaction 1 (Table VI.2-1) yielded a log K value of -4.43 (J. A. Davis, oral communication). This value is not significantly different than the corresponding value for the IFRC smear-zone samples, which indicates the two sets of samples have a similar intrinsic U(VI) adsorption

affinity. Specific surface areas for the SPP vadose-zone samples were 15 to 26 $m^2$/g. In contrast, specific surface areas for the IFRC smear-zone composites were 9 to 12 $m^2$/g. Thus, higher $K_d$ values for the SPP samples result from higher specific surface areas and, therefore, adsorption site concentrations, of the vadose-zone samples.

Additional experiments are underway to better constrain surface complexation model fits. Results of these experiments will span a much larger range of alkalinity values and adsorbed and dissolved U concentrations. Results of these further experiments will also allow SCM's to be obtained for each individual composite sample in order to quantify spatial variability in adsorption properties of sediments within the IFRC experimental domain. During CY 10 site-wide correlations will be developed between $K_d$, surface area, and grain size metrics to allow development of a heterogeneity model of surface complexation site concentration that parallels the chemical heterogeneity models shown for extractable U and the <2 mm fraction in **Section VI.1**.
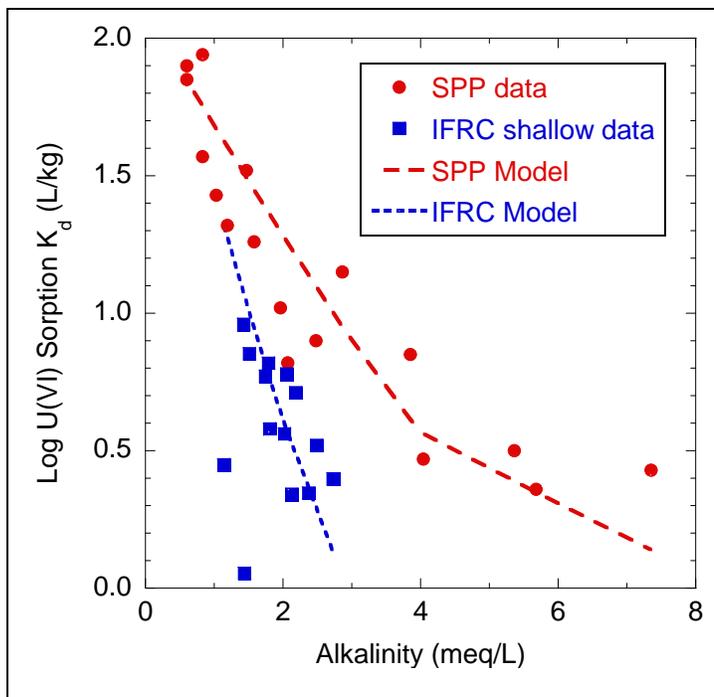


**Figure VI.2-1**. Experimentally determined and model-calculated U(VI) adsorption on smear- and saturated zone samples from six locations in the IFRC experimental domain (IFRC shallow data and Model, respectively). For comparison, experimentally determined and model-calculated U(VI) adsorption on vadose-zone sediments from previous excavations in the South Processing Pond (SPP) are also shown (Bond et al., 2008). Model lines are spline fits through model-computed adsorption points, which exhibit a degree of scatter similar to the scatter in the experimental data. This scatter originates from minor differences in chemical conditions other than alkalinity.

Experimental Application to Mass Transfer Controlled Desorption

Due to fluctuation of the Columbia River stage, the interface between Columbia River water and Hanford groundwater oscillates with an amplitude of up to 1 m/d and >2 m per season. At the Hanford 300 Area, water table oscillations (Lindberg and Peterson, 2004; Zachara et al., 2005) and water chemistry variations (Fritz and Arntzen, 2007; Ma et al., 2010) complicate the modeling, measurement and prediction efforts even in a very small area (e.g., IFRC site). Hanford groundwater and Columbia River water have distinct effects on the transport of U(VI), mainly due to their different bicarbonate concentrations. Given that the Columbia River and the Hanford 300 Area are hydraulically connected, a mixing zone exists in which water composition will be affected by river stage oscillations. Therefore understanding U(VI) desorption/adsorption under oscillating chemical conditions is essential to understand and predict the transport of U(VI) in the Hanford 300 Area.

Several studies (e.g, Liu et al., 2004; McKinley et al., 2006) have been conducted to evaluate the U(VI) adsorption/desorption and precipitation/dissolution mechanisms at the micro- and lab-scales in the 300 Area and nearby locations. Results shows that U(VI) desorption varies with aqueous chemical

compositions (Liu et. al., 2009). To fill the knowledge gap between the micro/lab-scale and field-scale, and to provide a more realistic U(VI) transport environment with well-controlled boundary conditions, experiments have been conducted by Yin et al. (2010) focusing on U(VI) adsorption/desorption under varying aqueous chemistry conditions. We briefly summarize the results of Yin et al. (2010) and discuss its implications for the Hanford 300 Area in the light of other work.

*Approach.*. Variable aqueous chemistry experiments were performed on a composite smear-zone sediment collected from the IFRC site during well installation. The sediments can be regarded as an ensemble of the lower vadose zone over the IFRC site, as the parent sample was taken from multiple boreholes, dried, homogenized and then sieved. A 50-cm by 5-cm-ID stainless steel column was packed with 1800 g <2 mm sediment. Two electrolytes were used to represent ground water (synthetic groundwater, SGW) and Columbia River water (synthetic Columbia River water, SCRW). Compositions of these two electrolytes were calculated from in-situ water chemistry and are based on a set of common "recipes" for all IFRC lab experiments. In general, SCRW has slightly lower pH (more neutral), lower bicarbonate concentration, and lower total dissolved solids. Both electrolytes are U free. During the experiment, pore-water velocity was maintained at 2.45 m/d.

*Results.* Two significant geochemical behaviors were revealed by the laboratory experiments (Figure VI.2-2). The results are typical of U(VI) leaching from Hanford 300 A vadose zone sediments and similar to those reported by Liu et al. (2008) for sediments from the North Process Pond. However these results are specific to sediments from the IFRC site, and are representative of lower vadose zone materials that are saturated during high water table and serve as a U-source to groundwater **(Section V.3).** Rate-limited desorption is indicated by a long tail and by increased U concentration after each stop flow event. The 2 mm sediment does not have a significant immobile porosity, and so a kinetic process is required to generate the results. It takes more than 35 pore volume to decrease the aqueous U(VI) concentration to less than the drinking water standard of 30 ppb. Nonetheless, other mechanisms and scales of mass transfer must be in play within the 300 A U(VI) plume because groundwater concentrations are still >30 ppb after more than a decade of flushing (much more than 35 pore volumes).

In the second experiment (Figure VI.2-2b), SGW and SCRW were alternately injected in the same direction and at the same flow rate into the column to leach adsorbed U(VI). The purpose of the "transient chemistry" desorption experiment was to understand U(VI) adsorption/desorption magnitude and rate when the aqueous composition oscillates between compositions observed in groundwater and river water. The results display changes in desorbed aqueous U(VI) concentration, driven by differences in the injected water composition. In contrast to the first experiment, aqueous U(VI) concentration first increases when clean SGW is injected into the column. This increase is caused by lowered surface complexation of U(VI) in the presence of high-bicarbonate-concentration groundwater and resulting desorption. If SGW continues to be injected, aqueous U(VI) concentrations eventually drop again (e.g., at the end of the experiment in Figure VI.2-2b). During the injection of SCRW, aqueous U(VI) concentrations rapidly decrease. This rapid decrease is caused by increased surface complexation of U(VI) in the presence of low-bicarbonate-concentration river water and resulting sorption. This sorbed U(VI) is then a source for the next cycle of groundwater flushing. The cycle can be repeated many times before the sediment becomes depleted of surface-complexed uranium.
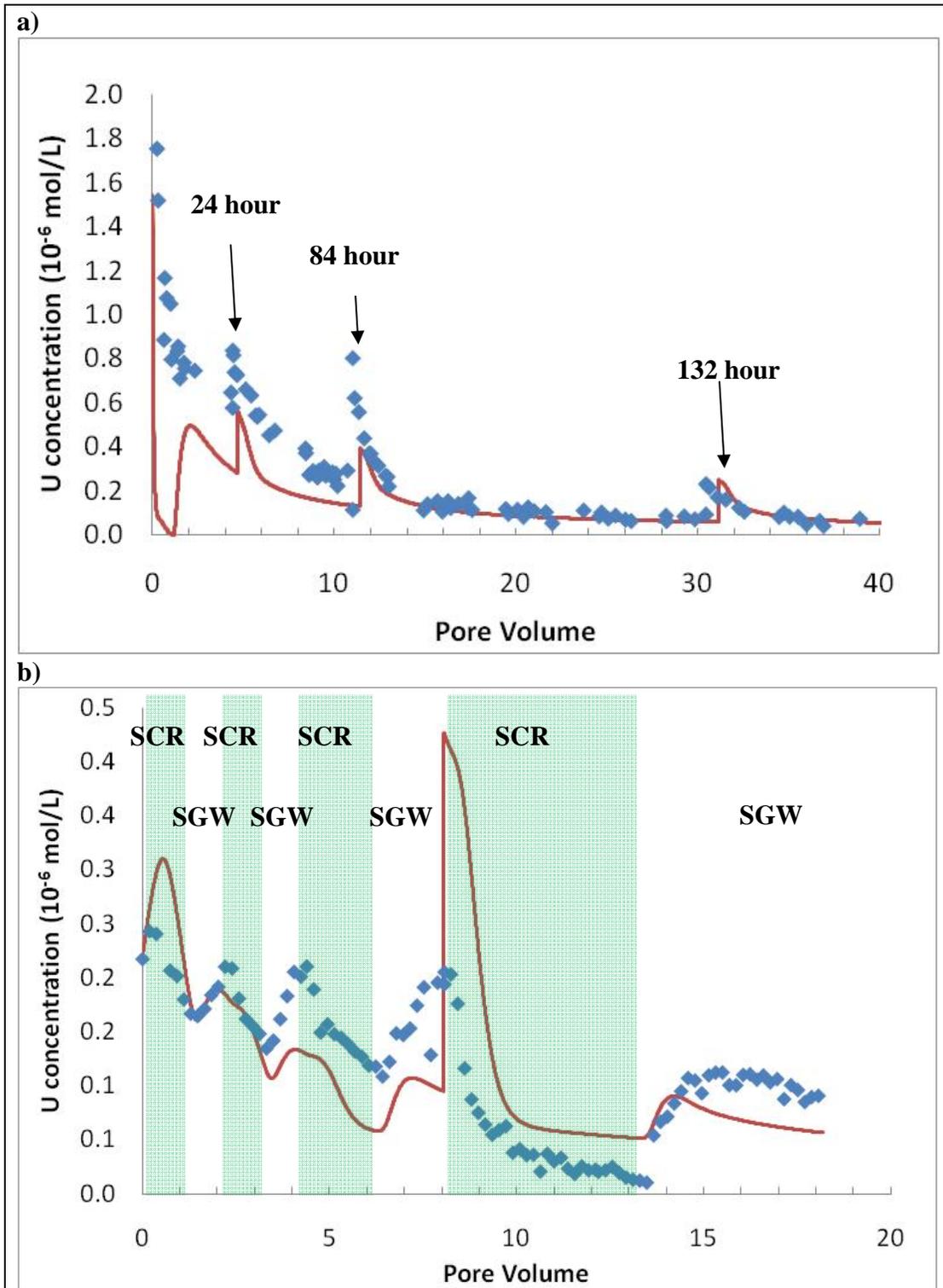
**Figure VI.2-2.** Observed (blue dots) and simulated (red line) U concentration in two leaching experiments. a) SGW was injected into the column; b) SCRW and SGW were injected into the column alternately. Shaded areas represent the SCRW injection at the upgradient end of the column. For reference, $0.126 \times 10^{-6}$ mol/L = 30 ppb (drinking water standard).

This oscillation of U(VI) concentrations is predicted by a field-scale model in Ma et al. (2010). In their results, aqueous U(VI) decreases and adsorbed U(VI) increases when Columbia River stage is high.  At the field scale, physical mass transfer and the related phenomenon of advection into low-hydraulic-conductivity zones also becomes important.  These zones serve as storage zones for both U(VI) and water of different aqueous chemistry.  Due to such field-scale mass transfer of both bicarbonate and U(VI), it is possible that large immobile domains act as "enhanced" immobile domains, capable of storing significant quantities of adsorbed U(VI).  This, in turn, has significant implications for long-term persistence of the U(VI) plume in spite of source term removal.

Conservative tracer (KBr) experiments were also performed on the columns to evaluate their physical transport properties.  Mass transfer parameters were estimated from these data using STAMMT-L (Haggerty and Reeves, 2002).  These parameters along with surface complexation parameters (site concentration and surface complexation constant) measured in the preceding section were input to a multi-rate kinetic surface complexation and dual-domain mass transfer model integrated into PHT3D (Prommer et al. 2003) by IFRC project collaborators Zheng and Prommer.  Because the initial conditions and physical/chemical properties of the sediments were measured, we only calibrated the kinetic rate constants and the ratio of immobile and mobile domain.  The resulting model captures some but not all aspects of the data (solid line in Figure IV.2-2). The U(VI) oscillations due to the water chemistry changes are in-phase with the observations. However, the magnitude of the oscillations is not accurate, which indicates that the model needs further calibration or process-level improvement.  A third column experiment (similar to the second one) has been completed that employed wet packing to reduce the uncertainties caused by preferential flow. The data will be used to further evaluate the calibrated model. Details of the parameters and model calibrations are discussed in a manuscript that will soon be submitted (Yin et al., 2010).

*Summary and Future Directions.* The experiments suggest that the sampling of the U(VI) in the field needs to be coordinated with water chemistry measurements, river stage measurements, and hydraulic modeling. The results may help to understand results of other researchers, such as those of Fritz and Arntzen (2007) who showed that the high U(VI) flux into the Columbia River is associated with low river stage. Although Fritz and Arntzen attribute the high U(VI) flux to the increased percentage of U-contaminated groundwater, our results suggest that the U(VI) flux is unlikely to be a linear function of groundwater fraction.  The exposure history of the aquifer near the river to low-bicarbonate Columbia River water is also likely to play a major role in determining U(VI) flux.

Research in CY 10 will progress to laboratory studies of U(VI) solubilization from lower vadose  zone sediments under conditions that simulate a rising and falling water table.  Operational parameters (e.g., time scales and linear velocities of water rise and fall) will closely follow those observed in the field during the Spring 2009 passive monitoring experiment (**Section V.3**).  The goal is to develop and parameterize  a reactive transport model of the lower zadose zone and upper saturated zone at the IFRC site that can adequately simulate the spring U recharge event and its mixing and impact on the saturated zone U(VI) plume.

## VI.3. Geostatistical Model of Hydraulic Conductivity

The spatial distribution of hydraulic conductivity in the saturated zone is a critical information piece needed to simulate tracer behavior at the IFRC site. During CY 09, development continued on a new approach for data inversion and assimilation called Method of Anchored Distributions (MAD, Rubin et al., 2009) and the numerical code needed for its implementation. This evolving approach was applied to the problem of robust characterization of the distribution of hydraulic conductivity at the IFRC site. The primary goal was the simultaneous inversion of the data obtained from: i.) the constant rate pump tests, ii.) the EBF data, and iii.) the March 2009 tracer test focused on the hydraulic conductivity as the target variable. In order to accomplish this goal, extensive consultations were had with the IFRC field team on a wide range of topics, including setting of priorities for well placement and interpretation of field data. Collaborations occurred between the UCB and PFLOTRAN modeling team in order to link their numerical model to MAD and use it for data assimilation and modeling of multiple realizations (**Section VIII**).

EBF Data and Pump Tests

The inversion analysis focused on the Electromagnetic Borehole Flowmeter (EBF) surveys and the drawdown data collected during the constant rate pump tests, and it was conducted in collaboration with Mark Rockhold and Vince Vermeul. The analysis objectives were to:

- Estimate of the statistical distributions of the geostatistical parameters of the conductivity, including the mean, the variance and the integral scales.
- Compute multiple realizations of the conductivity field, in 3D, conditional on the data and on the statistical distributions of the parameters.

A detailed discussion of the various aspects of this analysis is provided in Murakami et al. (2010). Only a brief summary of the results is provided here. Figure VI.3-1 shows the statistical distributions of the geostatistical parameters of the log-transmissivity field obtained using one and three pump tests. There are altogether 14 pump tests that were conducted at the site. Joint inversion of all the pump tests is computationally very demanding, and in order to avoid it, we tested inversion using a subset of the data including up to 7 tests, and found that the parameter distributions (of the type shown in Figure VI.3-1) converged to their final forms with about 3 wells. The reason for that is that the pumping wells are all located within a small area and there is a large overlap between the areas of the aquifer's domains tested by pump tests.
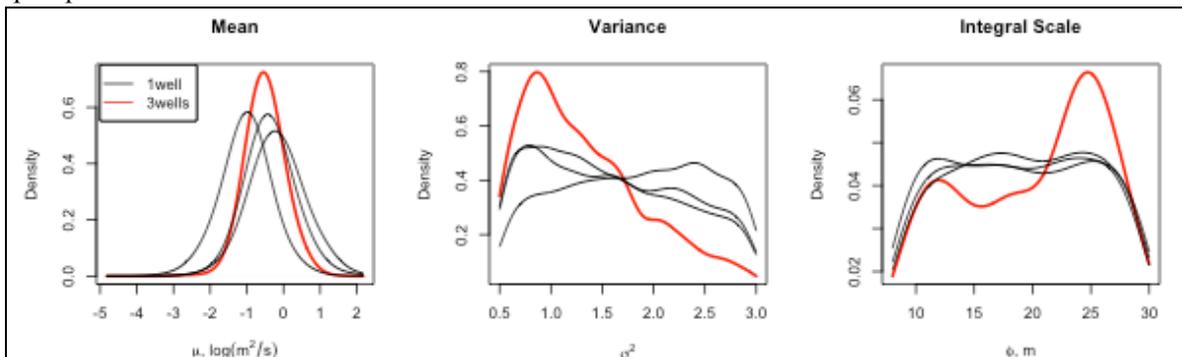


**Figure VI.3-1.** Posterior distributions of the structural parameters (mean, variance, and scale) based on the individual well test (gray lines) and based on the three well tests (red lines) for the Hanford data.

The observed zero-order moments of the drawdown curves at several observation wells with the distribution of moments predicted using parameters obtained from inversion are shown in Figure VI.3-2. This comparison is shown for observation wells with data that were not used for inversion. The comparison documents the improved predictive capability of the inferred models for various combinations of data. We note an improvement in the agreement between predictions and observations: the modes of the distributions approach the observations with the number of wells, and the distributions themselves become narrower, providing more confidence in the prediction. Figures VI.3-1 and Figure VI.3-2 show that moving from 1 to 3 observation wells improved the model's predictive capabilities. We also found that there is not much improvement by adding data from other observation wells.

Following the determination of the parameter distributions, multiple 3D realizations were generated of the conductivity fields. Figure VI.3-3 is the mean hydraulic conductivity field (an average of the realizations), intended to demonstrate the patterns of spatial variability that we were able to capture. Multiple conductivity realizations were generated that were made available to the IFRC modeling teams who used them as input for their flow and transport numerical models.
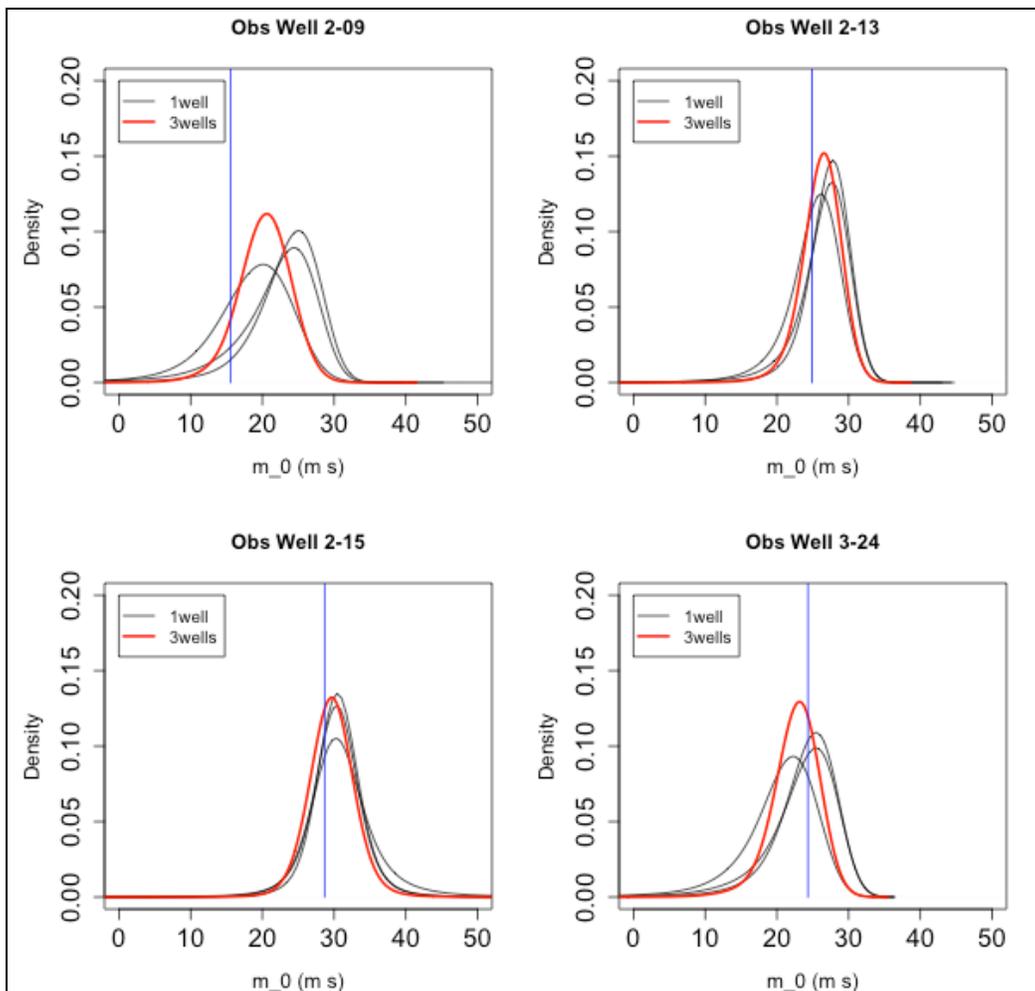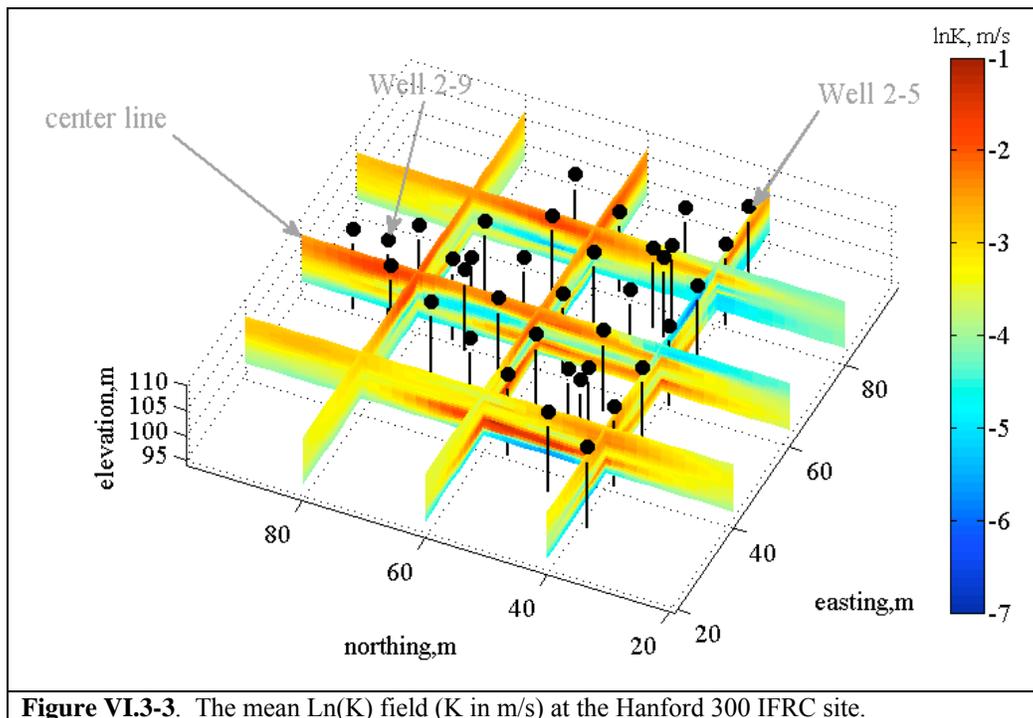


**Figure VI.3-2**. Predictive posterior distributions of the zero-order moments at the observation wells in the injection test at Well 2-18, based on the individual well test (gray lines) and based on the three well tests (red lines). The solid straight line is the value observed in the actual experiment.

**Figure VI.3-3**.  The mean Ln(K) field (K in m/s) at the Hanford 300 IFRC site.
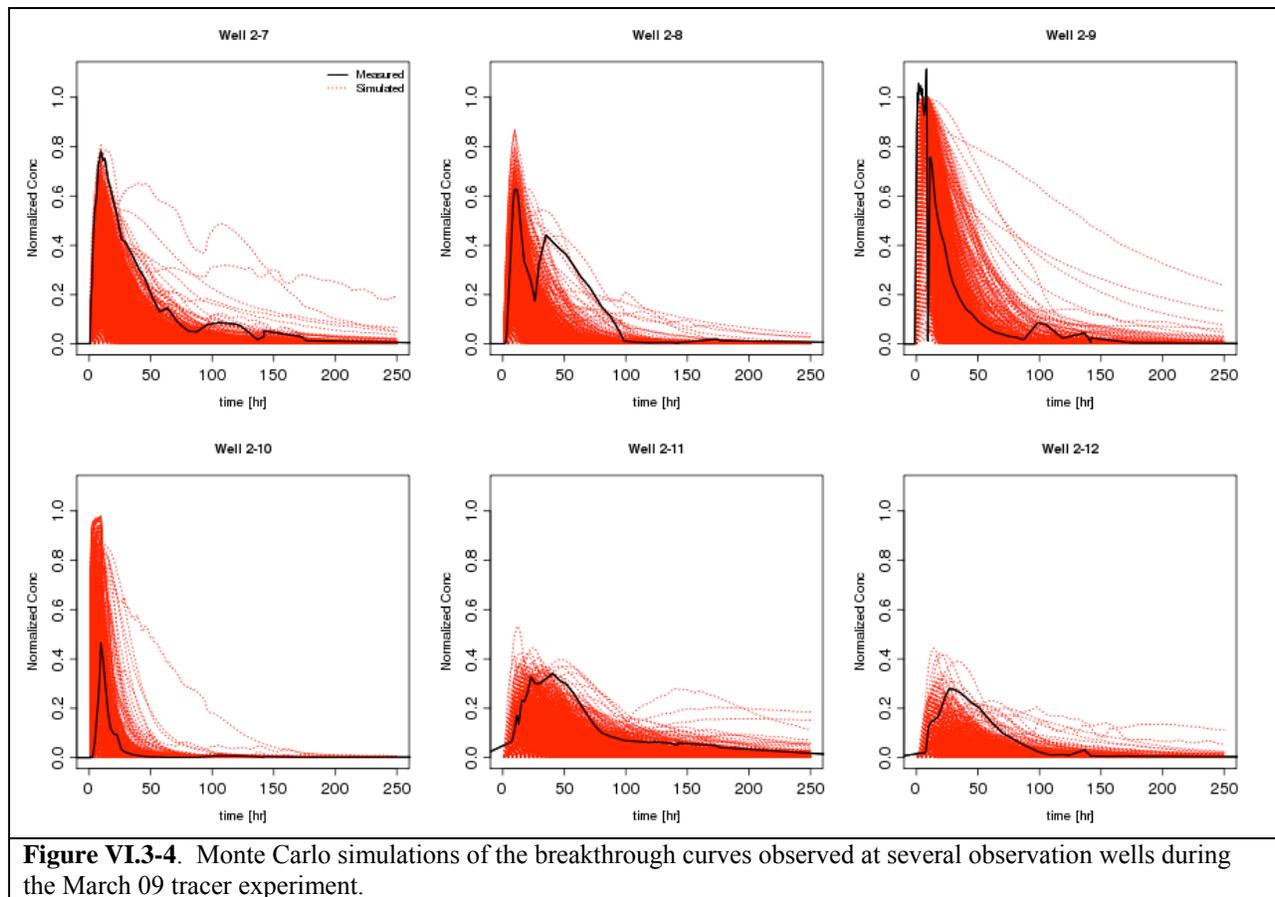
Incorporation of March 2009 Tracer Test Results

This analysis is at a preliminary stage. Its focus is on expanding the scope of data used for inversion by adding the data from the March 2009 tracer experiment to the hydrologic testing results. Multiple collaborations are involved with different members of the IFRC team including Mark Rockhold and Vince Vermeul, and with the PFLOTRAN development team including Glenn Hammond and Peter Lichtner (note discussion on multiple realizations in **Section VIII**).

A detailed 3D flow and transport model for the IFRC site was developed within the PFLOTRAN computational platform. The model covers the rectangular domain shown in Figure III-1 marked by the 4 far-field monitoring wells. Vertically it covers the saturated zone above the Hanford-Ringold interface. The model's grid block sizes in the vertical and horizontal directions are a fraction (about 30%) of the corresponding integral scale.  Boundary conditions for the flow model were obtained by interpolation, and are subject to considerable uncertainty. We expect this uncertainty to have a significant and adverse effect on the quality of the inversion.  Planned installation of the new boundary wells should solve this problem.

A large-scale Monte-Carlo simulation analysis was performed that included generating multiple realizations of the conductivity field, solving the flow and transport problems for the conditions observed during the March 2009 tracer experiment, and recording the predicted values at the locations where measurements of concentrations were taken (Figure VI.3-4). This analysis is intended to provide the basis for calculating the likelihood function that will be used to condition the conductivity fields on the March 2009 experiments. At this time (early 2010) we are analyzing the results from the Monte Carlo study.

We expect the inversion results to be negatively affected by two factors. First, the boundary conditions for the numerical model were obtained by interpolation from only a small subset of the wells. The second factor is the presence of oscillatory vertical flows that in certain wells. Vertical flows can distort the concentration data because measurements within the well may not be reflective of the concentrations

within the proximate formation. However, a large number of our simulated breakthrough curves are in statistical agreement with the observations, as shown in Figure VI.3-4. This means that many of our predictions are close to observations, and that the effects of vertical well flows were minimal.



**Figure VI.3-4**. Monte Carlo simulations of the breakthrough curves observed at several observation wells during the March 09 tracer experiment.

Future Directions

The data analysis and inversion and approach will be critically evaluated to identify where additional improvements could be made including changes in the inversion parameters, the numerical model, and various elements of the inversion algorithm. The inversion analysis will expanded to include borehole and tomographic geophysical data that has now become available in suitable format with statistical constraints (**Section IV.2**). Statistical correlations will be sought and evaluated between hydrologic attributes (e.g., hydraulic conductivity) on one hand and geophysical attributes (e.g., resistivity) on the other that could be used to constrain the inversion results by geophysical data. Preliminary findings described in **Section IV.2** are encouraging. We will employ these correlations as means for incorporating the cross-hole geophysical tomography data into our inversion, possibly through the procedure outlined in Ezzedine et al. (1999). The evolving geostatistical model of hydraulic conductivity will be iteratively supplied to the flow and transport modeling team to assess improvements in describing non-reactive and, eventually, reactive transport behavior.

## VI.4.   Modeling Non-Reactive Tracer Experiments

The aquifer in 300A is in hydrologic continuity with the Columbia River along the eastern margin of the 300A site, which experiences highly frequent stage fluctuations. The hydrologic conditions imposed by the boundary condition of the Columbia River on the east leads to highly dynamic groundwater movement in both the direction and magnitude of the flow velocity at the IFRC site. The dynamic nature of the flow field and heterogeneous hydraulic conductivity field (e.g., Figures IV.1-1 and VI..3-4) caused different tracer behaviors in the Nov08 and Mar09 tracer experiments (**Section V.1**). The calculations summarized below were performed by two different IFRC modeling teams attempting to integrate a wide range of physical and hydrologic characterization data (**Sections IV.1 and VI.3**) for the purposes of understanding transport in the IFRC well domain, and its coupling with dynamic river hydrology.  While both teams sought to reproduce tracer breakthrough behavior in the respective experiment, different approaches and intermediate objectives were pursued given overall project needs.  For example, an important objective of the Nov08 modeling was to further constrain the conceptual hydrogeologic model of the IFRC site, while that for Mar09 was to evaluate the well-bore vertical flow issue.  Varying degrees of success have been achieved in simulating the tracer experiment results and further improvements are sought.
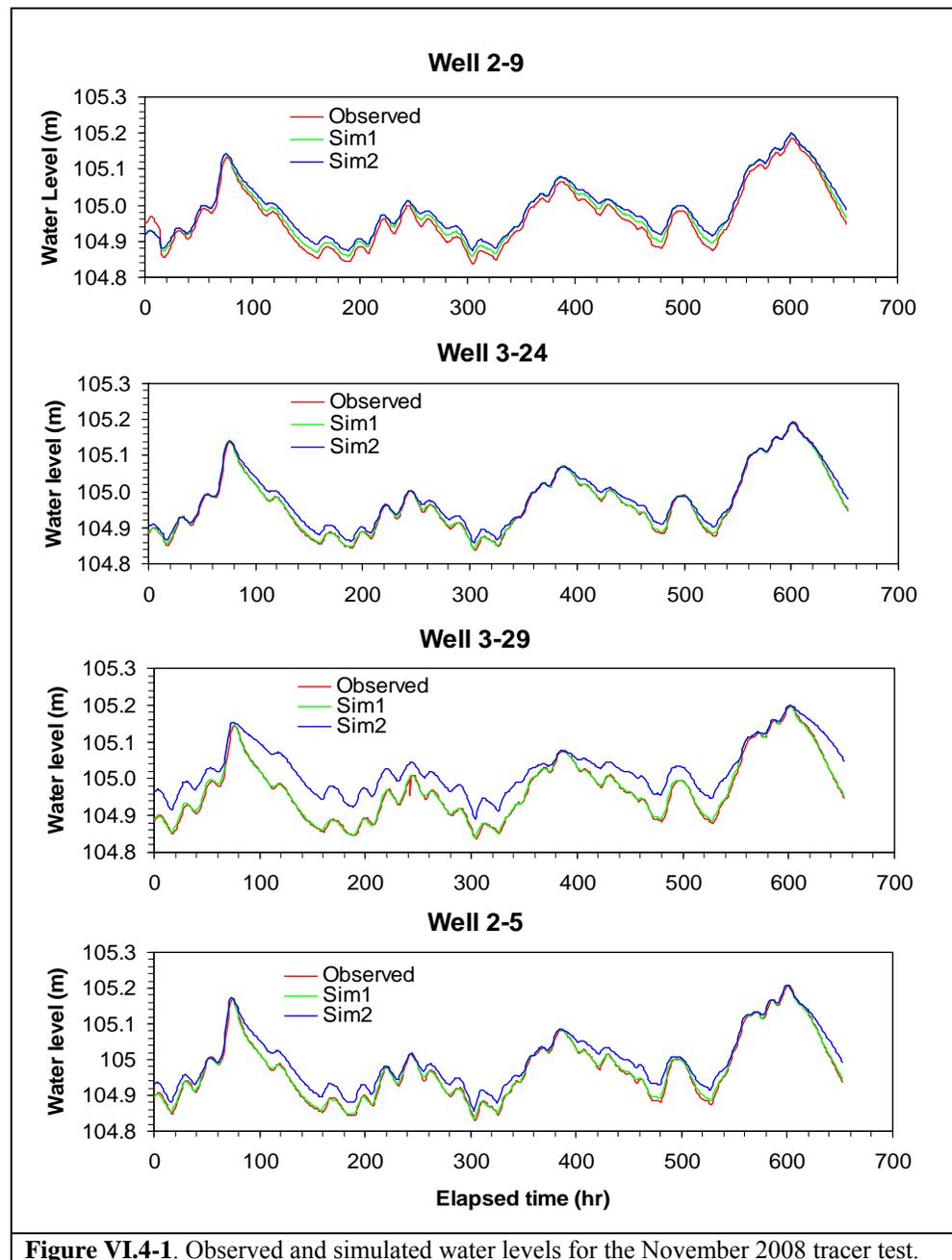
November 2008

*Modeling Approach*.  Numerical simulations of the Nov08 tracer test have been performed using both the STOMP (White and Oostrom, 2006) and MODFLOW-MT3D (Zheng and Wang, 1999) simulators.  Only the STOMP results are discussed here. Several STOMP models have been developed, representing domains that are either 91x91 m or 121x121 m in lateral extent, and 10 m in vertical extent. The smaller of these two STOMP models uses uniform 1-m grid spacing in the horizontal plane (x-y) and uniform 0.5-m grid spacing in the vertical (z) direction. In the vertical direction the domain extends from an elevation of 97 to 107 m. The lower part of the modeled domain extends down into a region representing a low-permeability, fine-grained subunit of the Ringold Fm.  The 107-m elevation extends into the lower vadose zone, above the average seasonal high-water level.

Lateral boundary conditions for the flow equation in STOMP are defined as linked lists of seepage faces with corner-point reference pressures defined by either extrapolating the equations of planes fit to water level data from within the IFRC well field, or interpolating (triangulating) water levels from a combination of far-field wells and wells from within the IFRC well field. The seepage face boundary is equivalent to a hydraulic head (Dirichlet) boundary below the water table and to a (Neumann) zero-flux boundary above the water table when the aqueous pressure is less than atmospheric. The upper and lower boundaries are specified as (Neumann) zero-flux boundaries. For solute transport, the lateral boundaries are specified as inflow-outflow boundaries.

*Results.*  Figure VI.4-1 shows comparisons of observed and simulated water levels for four wells within the IFRC well field for two simulation cases. The base case, Sim1, represents early modeling efforts using simple kriging with an assumed anisotropic covariance structure for spatial interpolation of hydraulic conductivity. Excellent matches between observed and simulated water levels were obtained for this case, with root-mean-squared-errors of less than 1 cm, except for well 2-9 during the injection period. Sim2 represents a more recent modeling effort in which PPEST (Doherty, 2004) was used in an attempt to find global optimum variogram parameters (correlation lengths, angle of anisotropy in horizontal plane), and

K values for a low-K region in the middle of the profile in which the screened intervals are located for the intermediate-depth screen wells (2-28, 3-32, and 2-31). Ordinary kriging was used in the Sim2 case. Although the correspondence between observed and simulated Br concentrations is generally better for the Sim2 case, the correspondence between observed and simulated water levels is worse. Both cases use the linear correlation to estimate porosity from site gamma log data.

Figure VI.4-2 and Figure VI.4-3 show comparisons of observed and simulated Br concentrations for the Sim1 and Sim2 cases for 30 observation wells, including two of the three sets of cluster wells that are screened at different depth intervals. Both simulations capture the general behavior of the plume that was observed during the Nov08 tracer test, but the Sim2 results generally match the observed concentrations better than the Sim1 results. However, as noted earlier, the Sim2 results do not match the observed water levels as well as the Sim1 results. Equal (unit) weighting was applied to both the head and concentration data for the PPEST optimization run.
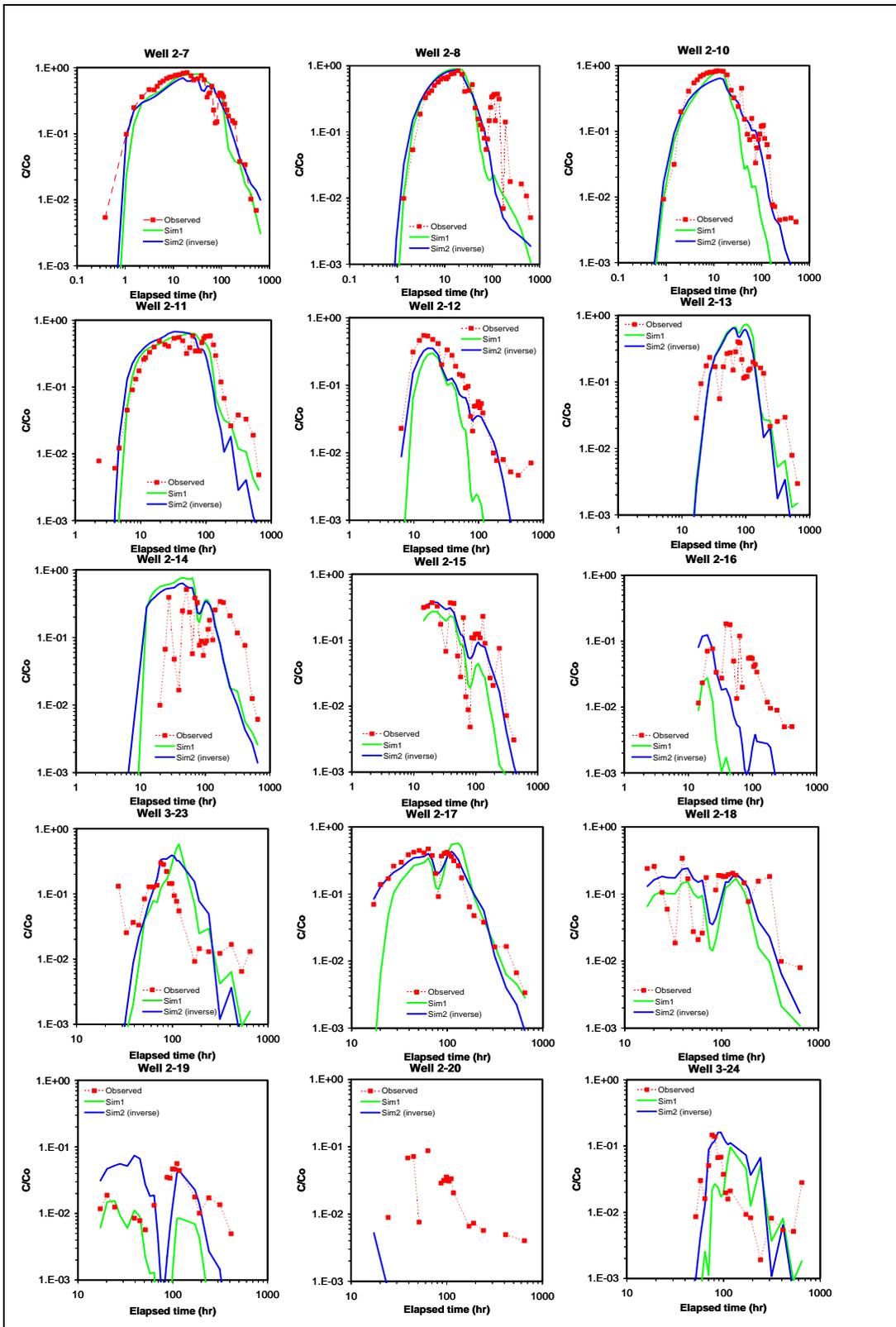


**Figure VI.4-1**. Observed and simulated water levels for the November 2008 tracer test.

**Figure VI.4-2**. Observed and simulated Br breakthrough curves for selected wells closer to the injection well (2-9) for the November 2008 tracer test at the 300 Area IFRC site.
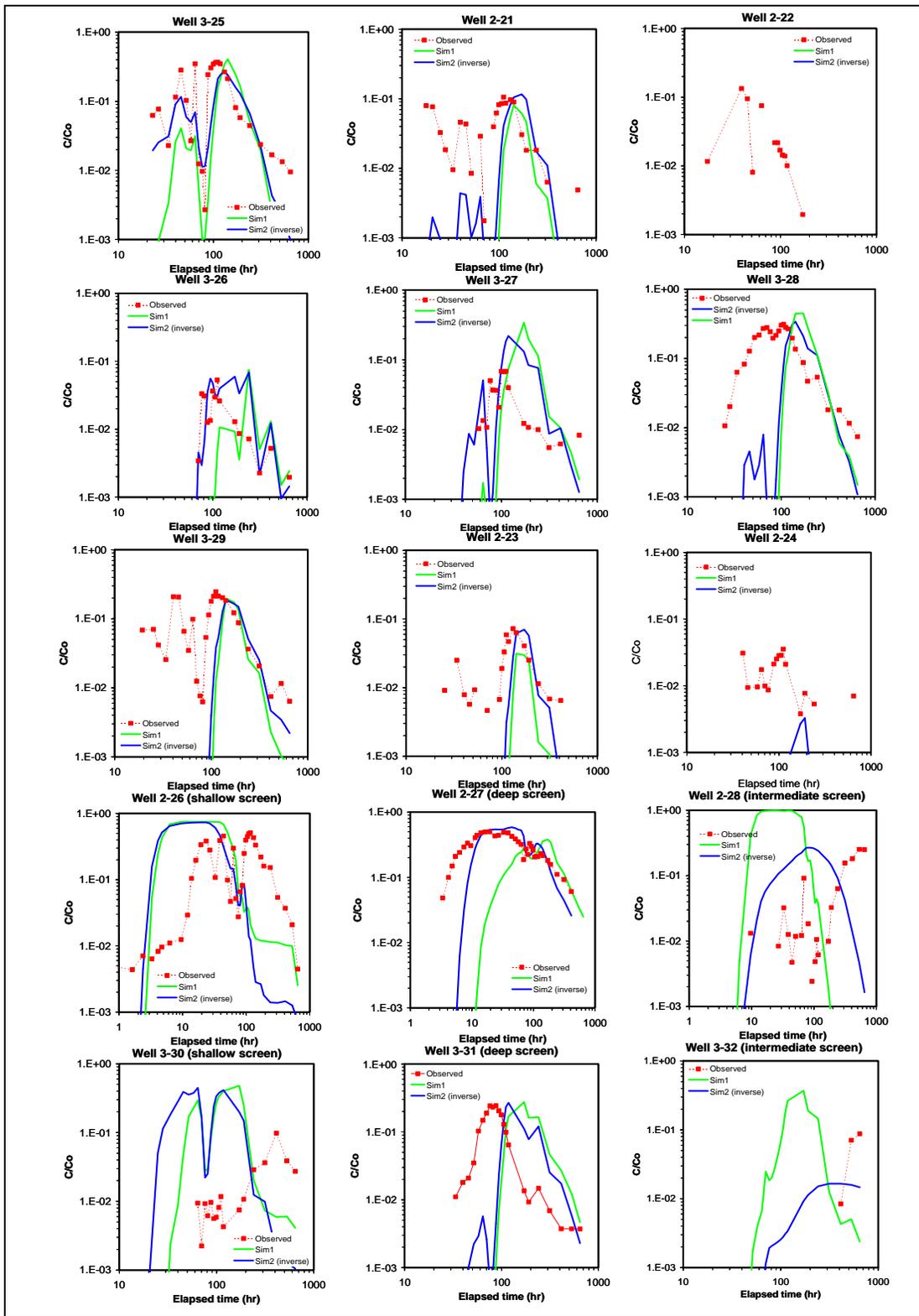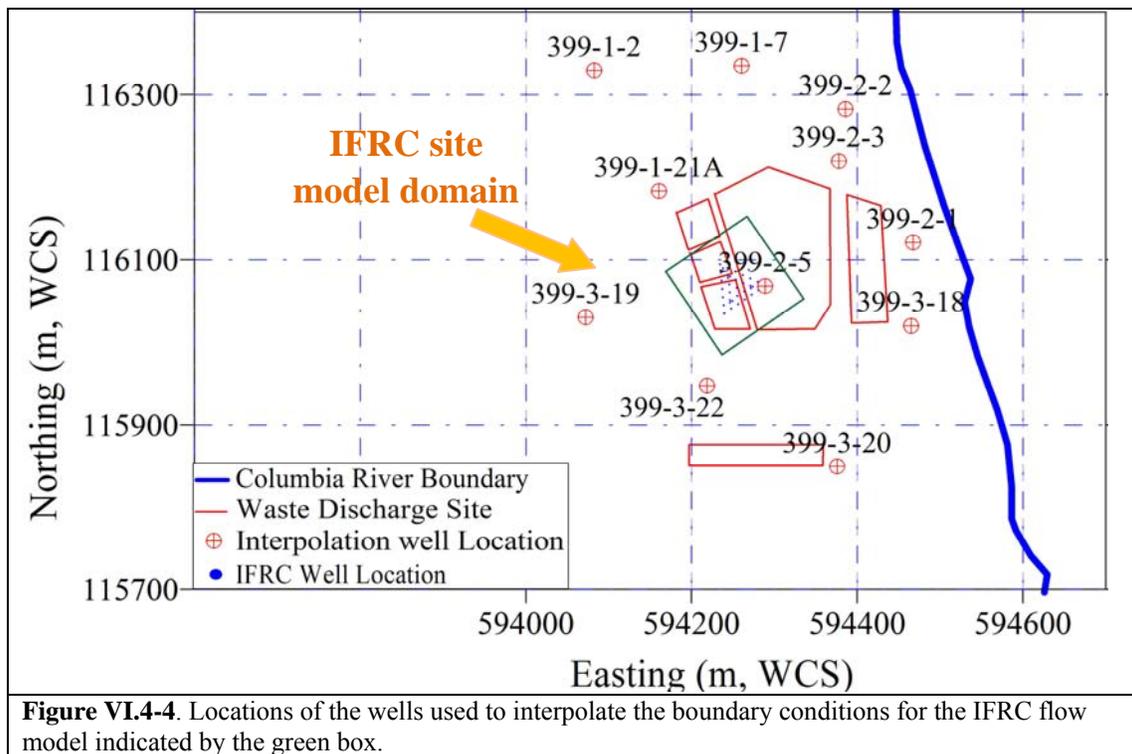
**Figure VI.4-3**. Observed and simulate Br breakthrough curves for selected wells farther from the injection well (2-9) for the November 2008 tracer test at the 300 Area IFRC site.

March 2009

*Modeling Approach.* This modeling analysis built upon above simulations of the Nov08experiment, but were performed by a different IFRC participant (Zheng) utilizing a different suite of codes with somewhat different capabilities. Hydrologic boundary conditions were calculated using different assumptions. These two modeling contributions represent a Hanford IFRC philosophy to utilize and evaluate multiple state-of-the-art simulators and modeling strategies for coupled process parameterization and complex experiment interpretation. The specific aims of these calculations were to: i.) examine the intra-borehole vertical flow phenomenon induced by the highly dynamic groundwater flow field and its effect on the representativeness of pumped water samples for average solute concentrations in long-screened wells; ii.) simulate conservative Br tracer behavior in the March 2009 experiment to further elucidate physical heterogeneities in the aquifer; and iii.) evaluate the utility of temperature data in comparison with Br tracer data to quantify the three-dimensional hydraulic conductivity distribution.

*Groundwater Flow Model.* A saturated, 3D groundwater flow model was developed to simulate the tracer test. The flow simulations were carried out with MODFLOW (Harbaugh et al., 2000). The model domain was discretised by 60 columns (x-direction), 61 rows (y-direction) and 27 layers (z-direction), covering a horizontal distance from west to east of 120 m, from north to south 122m and a vertical thickness of 22.5 m. The vertical grid spacing ranges from 0.2 m to 1 m throughout the model domain. The finer vertical spacing (0.2 m) is at the contact between Ringold and Hanford formations while the coarser vertical spacing (1 m) is for the top layer to prevent the cells from drying due to dynamic water level fluctuations. The horizontal spacing was selected to be 2 m uniformly. The western, eastern, northern and southern sides of the mesh are defined as time-varying specified-head boundaries with the MODFLOW Time-Varying Constant-Head (CHD) package. The bottom of the grid is represented as a no-flow boundary, and the uppermost layer is also treated as no flow since recharge through the vadose zone is very small.



**Figure VI.4-4**. Locations of the wells used to interpolate the boundary conditions for the IFRC flow model indicated by the green box.

78

The rapid fluctuations in the Columbia River stage require at least a hourly time discretization for an adequate definition of the lateral boundary conditions. Measured hourly water level data from existing wells near the IFRC plot (both inside and outside the IFRC site) were utilized to interpolate the time-varying specified head values at the four boundaries. The wells used to interpolate boundary conditions are 399-1-7, 399-1-21, 399-3-19, 399-3-22, 399-3-20, 399-3-18, 399-2-1, 399-2-3, and 399-2-5 (shown in Figure VI.4-4). The wells used for interpolation are fairly evenly distributed near the IFRC site and have a high precision for the monitored water level (~0.00001 m). The monitoring wells within the IFRC site allow for a comparison of calculated and observed water level data inside the model domain. For consideration of the intra-borehole vertical flow in the long-screened observation wells, we implemented the Multi-node Well) (MNW) package for flow and transport (Halford and Hanson, 2002; Zheng, 2006).

*Br Tracer Model.* The Br transport was simulated with the MT3DMS code (Zheng and Wang, 1999; Zheng, 2006). The transport solution technique employed in the simulation was the third-order total-variation-diminishing (TVD) algorithm which is highly accurate and minimizes numerical dispersion while conserving mass (Zheng and Bennett, 2002). For the initial setup, the effective porosity was assumed to be 0.18 in the Hanford Formation and 0.15 in the Ringold Formations (William et al., 2008). The porosity value was slightly adjusted later during model calibration. A longitudinal dispersivity ($\alpha_L$) of 1 m was used for the Hanford Formation; and both Ringold units were assigned a longitudinal dispersivity of 0.5 m. The horizontal and vertical dispersivities were assumed to be 10% and 1% of the longitudinal dispersivity in all formations, respectively. The dispersivity value was also further calibrated later.

*Heat Tracer Model.* Based on the mathematical analogy between heat and solute transport, the multi-species transport model MT3DMS, originally developed for solute transport, was used in its present form to simulate heat transport by re-interpreting some variables for the solute transport (Langevin et al. 2009, Ma and Zheng, 2009; Hecht-Méndez et al. 2009). The background groundwater temperature at the IFRC site is about 16.8°C with very small variation. For simplicity, the initial condition of the temperature for the model is set to 16.8°C throughout the entire model
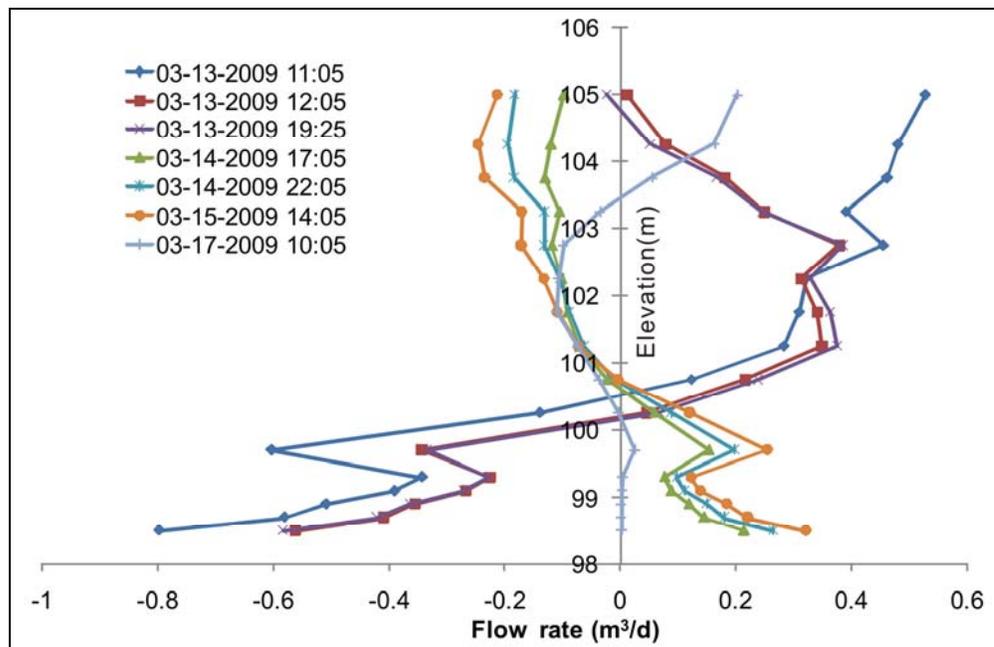


**Figure VI.4-5**. Horizontal flows between the aquifer and well bore inside well 399-2-7 calculated with the MODFLOW Multi-node-well Package (a positive flow rate indicates that water flows from well bore to aquifer; a negative value from aquifer to well bore).

domain. The four lateral boundaries were all treated as having a constant temperature of 16.8$^{o}$C since the tracer test didn't affect the boundary during the experiment period.

*Inverse Model for Parameter Estimation.* In order to calibrate the 3D aquifer heterogeneity, the inverse modeling software PEST (Doherty, 2002) was employed to calibrate the heterogeneous parameter distribution of the aquifer (mainly the hydraulic conductivity). We used the pilot point method as implemented in the PEST code to calibrate the model (Doherty, 2003). The pilot points were assigned at the same locations as the IFRC wells, and others were included at other locations where necessary. A total of 368 pilot points were assigned in the model domain. Although the model boundary was extended beyond the IFRC site in order to minimize the effect of boundary conditions on the model domain, we only aimed to calibrate the hydraulic conductivity distribution within the IFRC site. The measured head, tracer, and temperature data (e.g., Figure V.1-3) were used as the calibration targets for the flow and transport model. The objective of the PEST based model calibration is to minimize the difference between observed and calculated heads, concentrations, and temperatures.

*Intra-Borehole Vertical Flow.* Simulation results revealed that there was complex intra-borehole flow movement inside the long-screened observation wells. As an example, Figure VI.4-5 shows the variation in the flow rates between the aquifer and well bore at different depths in well 399-2-7. The positive value of the flow rate indicates that the groundwater flows from well bore to aquifer, while the negative value from aquifer to the well bore. If the flow rate is positive on the upper part of the well bore and negative in the lower part, then the intra-borehole flow is upward, and vice versa. The magnitude and direction of the intra-borehole flow in well 399-2-7 varies substantially with time, reflecting the complicated and highly dynamic nature of intra-borehole flow. When the river water intrudes and retreats, groundwater in some parts of the aquifer would be preferentially affected by the river stage change, which could cause the water level at different depths at the same location to behave differently (e.g., Figure IV.4-2). That, in turn, can lead to abrupt changes in the concentration of the sampled water from a long-screened observation well as the water sample may represent the concentration at a specific depth of the aquifer rather than well mixed from different depths.

Thus, there are two reasons that can explain the concentration fluctuations in the observed breakthrough curves: i.) frequent changes in the horizontal flow direction lead to corresponding changes in tracer plume movement that strongly affects the concentration distribution in an observation well; and ii.) intra-borehole vertical flow that alternates between upward and downward directions so that the sampled waters are not representative of the depth averaged concentrations.
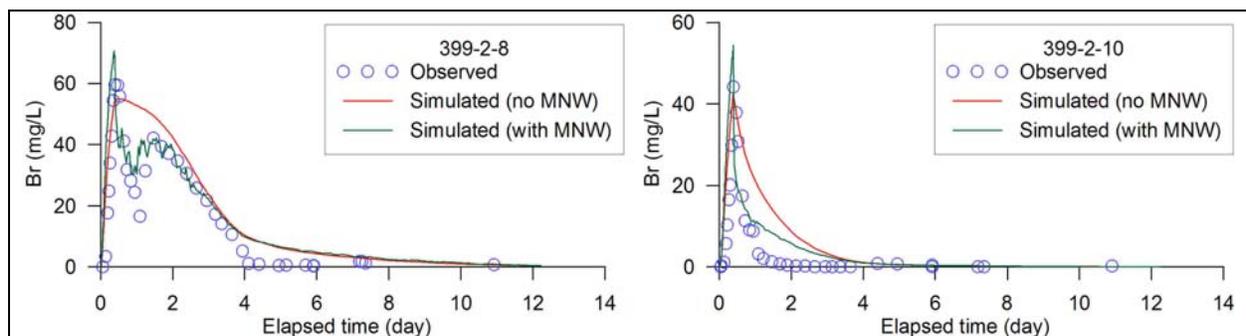


**Figure VI.4-6**. Comparison of observed concentrations with simulated concentrations with and without the Multi-node Well Package at two well locations.

We compared the simulated breakthrough curve obtained considering the intra-borehole flow (with the MNW Package of MODFLOW and MT3DMS) with that obtained without considering the intra-borehole flow (without the MNW Package). The comparison result shows that the consideration of intra-borehole flow can lead to an improved match between the observed and simulated concentrations (Figure VI.4-6). In particular, it is noteworthy that the simulated concentration breakthrough curve with the MNW Package (green line) for well 399-2-8 has ups and downs, similar to those observed in the field (cycles), while the simulated concentration breakthrough curve without the MNW Package (red line) has a smooth trend.

*Crucial Importance and Difficulties of Defining Boundary Conditions.* We applied the measured hydraulic conductivity values from the EBF tests as the initial input to simulate the groundwater flow and tracer transport. We applied both manual trial-and-error adjustment and automated optimization procedure based on the PEST code to calibrate the hydraulic conductivity distribution by matching the simulated hydraulic heads, solute concentrations, and fluid temperatures against the observed values. We experimented with different interpolation methods and selected different wells near the IFRC plot to obtain the specified-head boundary conditions for the IFRC site-scale flow model. We found that slightly different boundary conditions could lead to equally good matches between the observed and calculated head distributions but drastically different tracer plume movements. Thus, the transport model is much more sensitive to the boundary condition than the flow model. We concluded that the boundary condition is a crucial aspect of model calibration at the IFRC site and that use of head data alone is totally insufficient to constrain the model calibration.

*Comparison of Simulated and Observed Br Tracer Transport.* In addition to the head data, tracer data were used to further constrain the interpolation of boundary conditions and estimation of the hydraulic conductivity distribution, based on the comparison of observed and simulated Br tracer concentrations at different locations and different times. First, we fixed the hydraulic conductivity distribution in the model and tested the boundary condition until the general direction of plume movement was obtained. Then, we adjusted the hydraulic conductivity distribution to improve the match between the simulated and observed Br concentrations. The simulated Br concentrations from the long-screened observation wells can be either depth-averaged or corrected by the MNW Package as described above.

Figure VI.4-7 shows a comparison of simulated and observed Br concentrations at 20 observation wells for the March 2009 Br tracer experiment, while Figure VI.4-8 compares the simulated and observed concentration distributions spatially at six selected times. These results are based on our most up-to-date calibration runs, but do not include the geostatistical from **Section VI.3** that have on recently become available. From Figure VI.4-7, it can be see that there is an overall agreement between the observed and measured breakthrough curves in a majority of the observation wells, especially in terms of arrival times and general trends. The simulated concentrations have been corrected by the Multi-node Well Package to account for the intra-borehole vertical flows. Figure VI.4-8 further confirms that the simulated tracer plumes at different times agree with the observed plumes reasonably well.

Significant discrepancies still exist between the simulated and observed concentrations at some observation wells and around certain parts of the model domain. Efforts are continuing to improve the transport calibration through automated parameter estimation. The geostatistically constrained hydraulic conductivity field being developed in Section VI.3 will be implemented ready. The objective function,

which measures the weighted residual between the simulated and observed concentrations at all observation wells, has decreased from $3 \times 10^7$ to $2 \times 10^6$ after 10 iterations. The objective function is expected to continue to decrease until an optimal distribution of hydraulic conductivities is obtained.
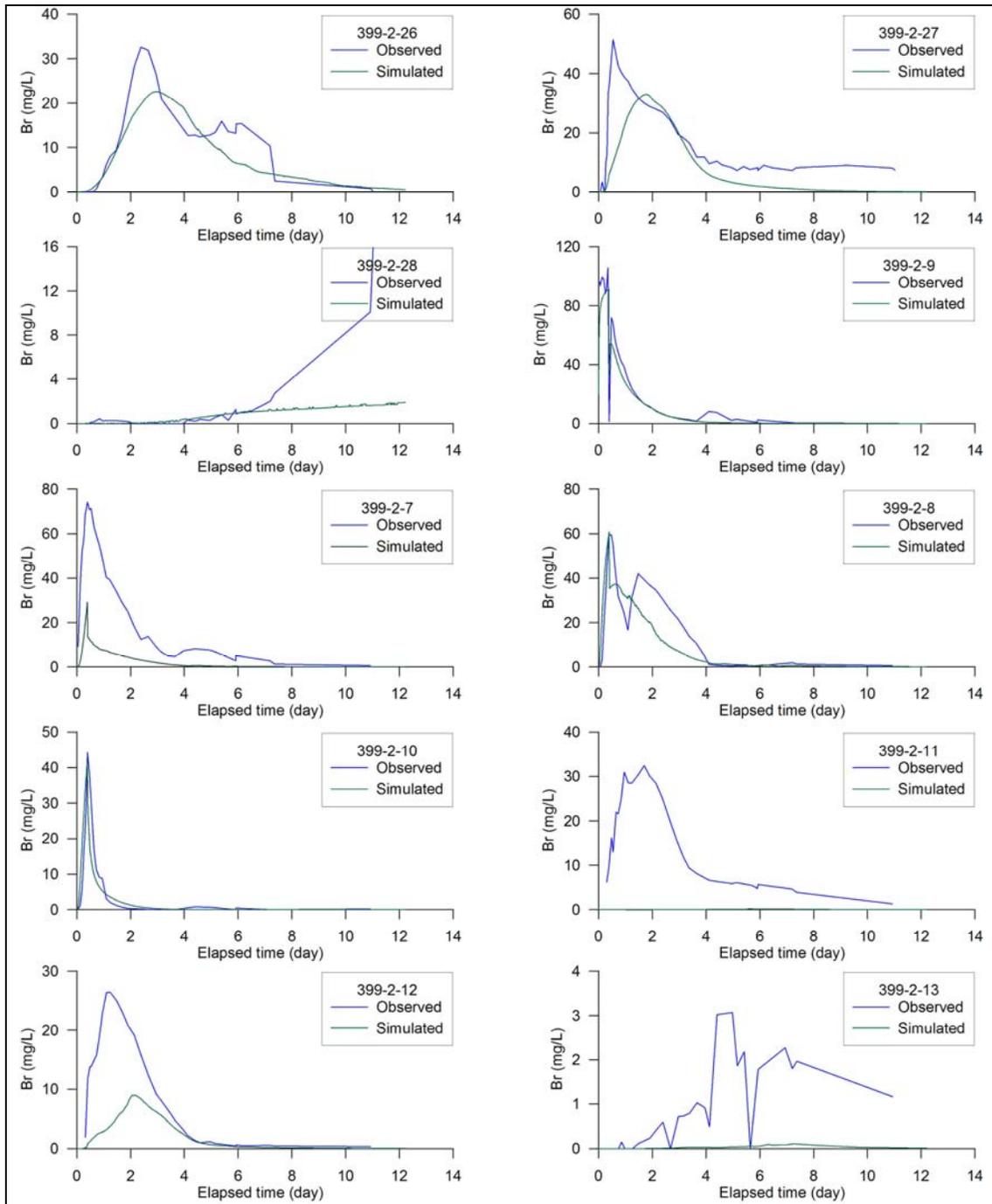


**Figure VI.4-7**. Comparison of simulated and observed Br concentrations at 20 observation wells for the March 2009 Br tracer experiment. (Continue to the next page).
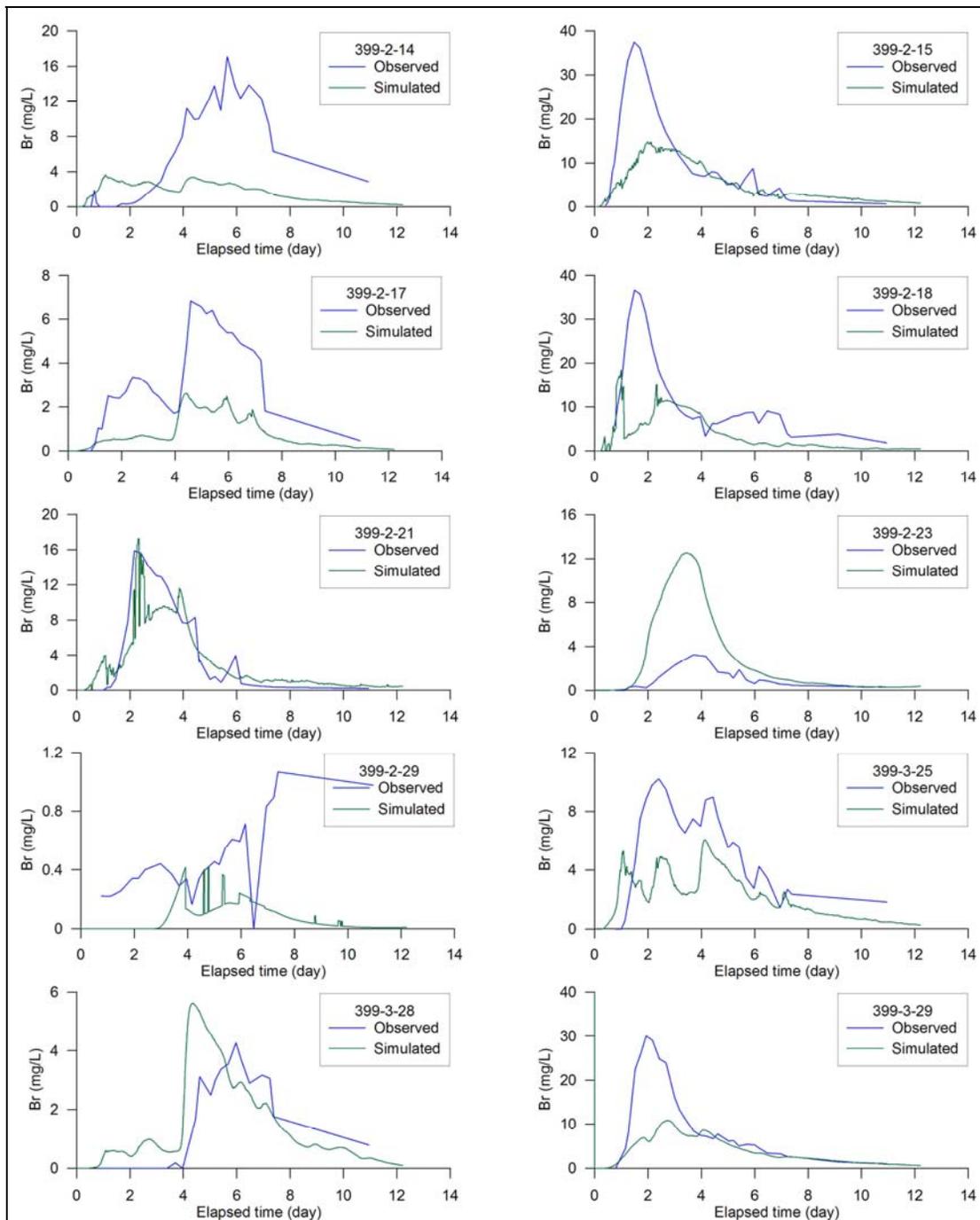
**Figure VI.4-7** (continued from the last page). Comparison of simulated and observed Br concentrations at 20 observation wells for the March 2009 Br tracer experiment.

*Use of 3D Temperature Data in Future Calibration.* While the Br tracer data are essential to model calibration, their usefulness is limited by the fact that most of these data are depth-averaged and thus lack of the sensitivity to characterize 3D hydraulic conductivity for most of the IFRC site. The results of the heat tracer transport model based on the hydraulic conductivity distribution calibrated from the Br transport model indicated that the general trends are similar between the observed and simulated

temperature changes at the observation wells. From the comparison between the observed and simulated temperature breakthrough curves at different depths in several wells, it can be seen that although the general trends are similar between the observed and simulated temperature changes, the temperature data at different depths of any observation well exhibit significant vertical variabilities that the current model could not capture particularly well. Thus, the 3D temperature data offer an additional avenue to further constrain the estimation and calibration of the hydraulic conductivity at the IFRC site, especially in the vertical direction.

Summary and Future Directions

Field-wide average K profiles determined using the bulk K and EBF data suggest that the shallow part of the aquifer is somewhat (a factor of ~1.25) more permeable than the deep part of the aquifer, and both the shallow and deep parts are more permeable (a factor of ~2 to 2.5) than the middle portion. In summary, Elev<101.5 m, Kavg ≈ 6900 m/d; Elev 101.5-102.5 m, Kavg ≈ 3400 m/d; Elev>102.5 m, Kavg ≈ 8600 m/d (or Kshallow > Kdeep > Kmiddle). Tracer breakthrough curves from both tracer tests suggest, however, that the lower part of the profile is significantly more permeable and/or has lower porosity than the upper part of the profile, and the middle part of the profile has much lower permeability and higher porosity than both the overlying and underlying sediments (Kdeep > Kshallow >> Kmiddle). Moreover, the analysis of tracer breakthrough curves for the Mar09 experiment suggests that the down-gradient end of the well field has somewhat higher permeabilities than the up-gradient end of the well field.

The apparent disparity between the direct measurements of hydraulic conductivity and the tracer behavior can be explained by one or more of the following factors: i.) there are significant differences in connected porosity for the shallow, middle, and deep portions of the aquifer, ii.) there are strongly preferential flow features within the domain, particularly in the deep part of the profile along the Hanford/Ringold Fm interface, that are not fully described by traditional two-point (variogram-based) geostatistical methods using the available data, iii.) the EBF profiles underestimate the true variability of the K field because of smoothing effects caused by the sand pack, and iv.) water and Br injected in well 2-9 were not evenly distributed over the entire screened interval and/or heterogeneity at that location and its connectivity with down-gradient wells is not well described by the available characterization data and interpolation methods that have been used, or v.) one or more of the intermediate depth screened wells (e.g. 2-28) is screened within a rip-up clast of lower permeability Ringold Fm sediments.

In addition to the work presented here, exploratory data analyses have been performed to evaluate anisotropy at the site. Analyses of resistivity data indicate that the principal directions of anisotropy change with elevation or depth (Greenwood et al., 2009). More recent variography performed using gamma log data grouped by elevation also reveals different anisotropy structures that are not evident when the gamma log data are pooled into a single data set representing the whole Hanford Fm. Incorporation of this type of information into future modeling efforts will likely lead to improved correspondence between observed and simulated tracer responses.

Several alternative parameterization methods are being employed by IFRC project participants and collaborators. These include Markov chain Monte Carlo and Bayesian methods (Murakami et al., 2009; Chen et al., 2009), and a pilot point method implemented in PEST. These methods offer the potential for improvement in the correspondence between observed and simulated results for both the Nov08 and Mar09 tracer tests, and for assimilating additional types of site characterization data (e.g. resistivity). We

recommend that both the Nov08 and Mar09 experiments be evaluated in these efforts, since different flow paths were accessed during the two experiments. If good correspondence can be obtained between observed and simulated water levels and concentrations for both experiments, using the same parameter distributions (K and porosity), then these parameter distributions could be considered to be a robust basis for subsequent reactive transport modeling.

There is a significant, temporally variable vertical head gradient in the aquifer that is caused by the highly dynamic fluctuations of the Columbia River. This, in turn, causes significant intra-borehole vertical flow with alternating upward and downward movements in the long screened observation wells. These flows impact the representativeness of the water samples from these wells. The intra-borehole vertical flow must be explicitly considered in sampling, and in subsequent modeling analysis of the data for the results to be more meaningful and scientifically impactful. The groundwater head data alone are insufficient to constrain the hydraulic conductivity distribution, especially with the hydraulic conductivity in the range of 7000 m/day as at the IFRC Hanford 300A site.

Drilling of additional wells is planned for spring 2010 to provide better control on boundary conditions for modeling of future IFRC field experiments, and to provide more depth-discrete monitoring within the well field (see **Section III**). Additional analyses of intact cores core samples and development of petrophysical relationships are also underway.  Use of these data and assimilation of other types of geophysical data using stochastic inversion and optimization methods is expected to lead to improved results.

Br tracer data are very important to constrain and improve the estimation of hydraulic conductivity and determination of the boundary condition. Through manual trial-and-error adjustment and automated parameter optimization procedure, we have obtained reasonable matches between the simulated and observed Br tracer concentrations for both non-reactive tracer experiments. However, additional calibration is needed and the work is on-going.  The temperature data can be a cost-effective proxy for conservative solute tracers, and are expected to help further calibration of 3D aquifer heterogeneity at the Hanford 300A site.  Additional temperature injection experiments are planned in the near future.
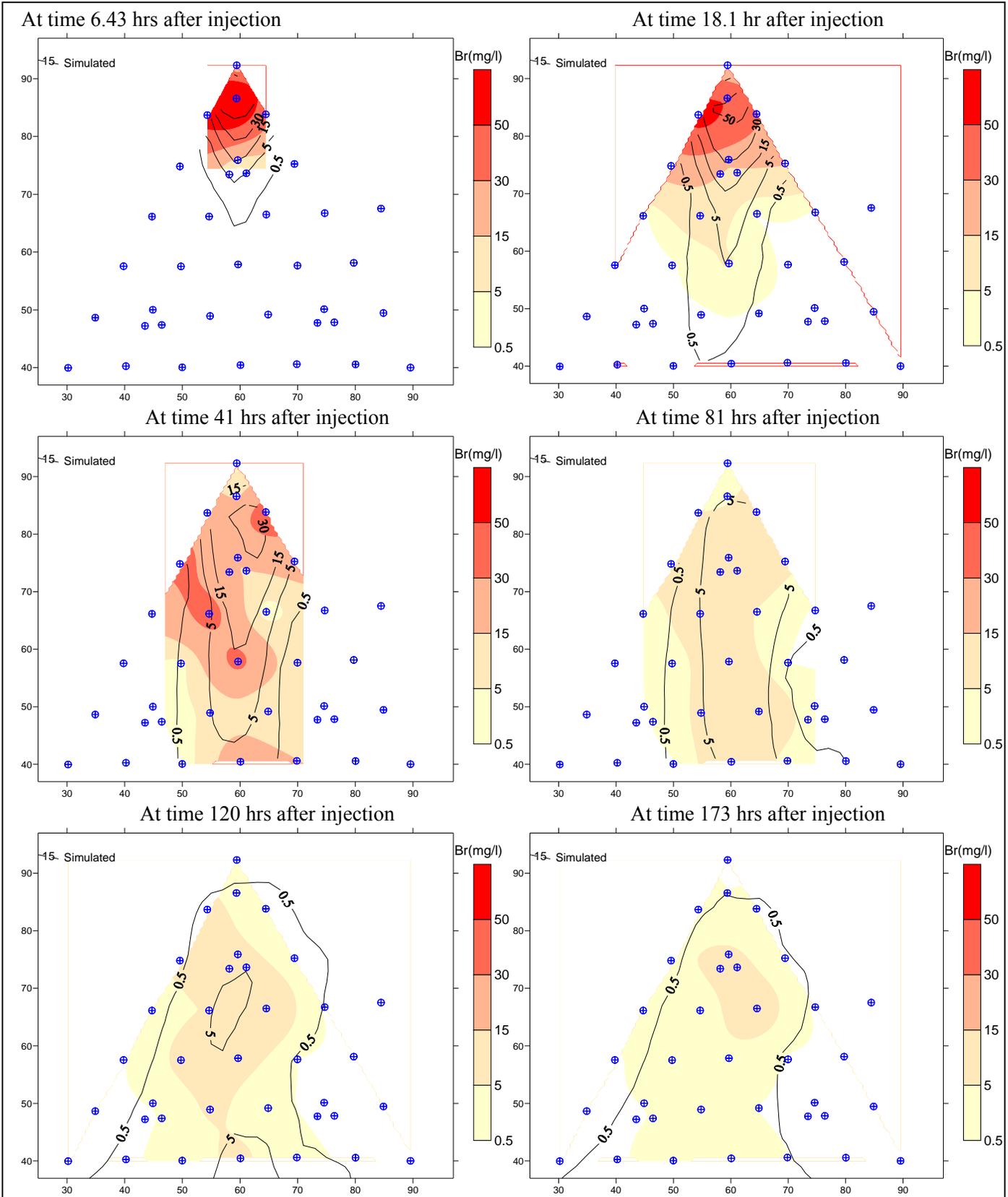
**Figure VI.4-8**. Comparison of simulated and observed concentration distributions at selected times.
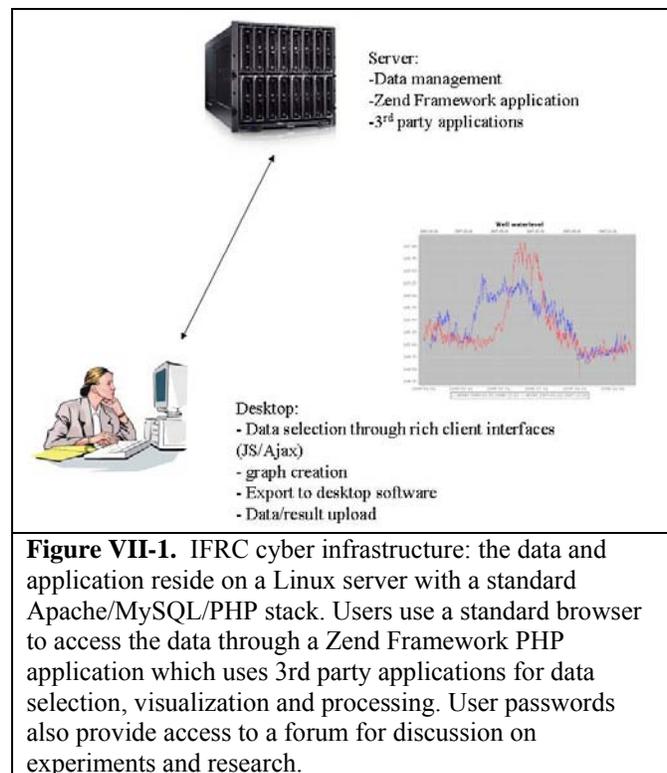
# VII. PROJECT DATA BASE

One of the requirements identified by DOE as part of the Hanford 300 Area IFRC effort is for all data associated with this IFRC (both historical data as well as data collected and generated as part of this and other ongoing projects) to be captured, documented and made available and accessible for both current project participants as well as future researchers. For the Hanford 300 area IFRC, such data includes both IFRC specific data as well as broader 300 Area site data (both regulatory related, research related and environmental data, e.g. weather and river-stages). The objective of the data management effort is to meet this requirement.

Approach

For single PI projects, where one scientist "owns" all the data and associated models, the computer environment in which data processing occurs is a standard desktop, on which both the data and software applications co-exist. Data organization is typically idiosyncratic with the result that datasets are virtually inaccessible by other scientists. Clearly, such an approach is not viable for a multi-disciplinary, multi-institutional effort, with PIs spread between different organizations and time zones, and where multiple PIs need easy and rapid access to the same datasets. The initial effort for the Hanford 300 Area IFRC was to formulate a sustainable approach, and to design and implement a software framework through which all data from this site would be available both for project scientists and future research in an integrated and sustainable manner. The design and implementation effort was completed in early 2009, and since then the underlying database has been populated with a range of different data. This is done in parallel with an expansion of the framework to provide additional functionality.

Software

IFRC data are stored in a relational MySQL database. Access to the data is provided through a web application which is implemented within Zend Framework (an open source, object oriented web application framework written in PHP). Graphing functionality is provided through JFreechart and OpenDX. Users interact with this web application through any compliant modern browser (Figure VII-1), where they can upload data, search for results, view and graph data and download selected datasets. In addition, users have access to a IFRC specific forum (which uses the PHP BB Forum software, an open source package). While access to some of the public data is open to the general public, access to project specific data requires a username and password.



**Figure VII-1.** IFRC cyber infrastructure: the data and application reside on a Linux server with a standard Apache/MySQL/PHP stack. Users use a standard browser to access the data through a Zend Framework PHP application which uses 3rd party applications for data selection, visualization and processing. User passwords also provide access to a forum for discussion on experiments and research.

The philosophy behind the web application is to make a maximum use of existing open source tools for data access and processing. This includes the use of existing data models for data storage as well as the use of e.g. Google Maps as a data selector (Figure VII-2).

Project Data

The pass-word protected database includes about thirty different data types, subdivided in eight major theme areas.

1. Geological data
   a. Borehole logs and data
   b. Sample data (including data on cores and grab-samples)
2. Hydrological data
   a. River-stage data from both a monitoring station located adjacent to the Hanford 300 Area and the USGS and COE gaging stations
   b. Well -level data from a monitoring array which includes both wells in the 300 Area and wells in the IFRC array
   c. Data from the HEIS regulatory effort
   d. Field hydrologic test results
3. Weather data from the PNNL weather station
4. Geophysical data



**Figure VII-2.** (left) Google Map interface to Hanford IFRC data. By clicking in the labels for each well users can directly access well-logs and borehole data (right) associated with that well.

   a. Electrical resistivity data (including a series of 100 realizations of a geostatistical inversion)
   b. EM31 surface data
   c. Geophysical borehole logs (spectal gamma, neutron moisture, crosshole GPR, EM induction)
5. Laboratory characterization measurements and model parameterization
   a. Geochemical characterization results (total U, extractable U, U-$K_d$, surface area, etc)
   b. Physical characterization results including grain size metrics
   c. Geochemical model parameterization studies (batch, stirred reactor, column, intact core)
   d. Geophysical and petrophysical measurements for transfer function
6. Field Experiment Results
   a. Conductivity measurements from multiple monitoring well
   b. Uranium concentrations in groundwater
   c. Non-reactive tracer experiment data packages
   d. Passive experiment data packages
   e. U transport experiment data packages
7. Temperature data
   a. Well and river temperature
   b. Data from the IFRC temperature array
8. Site wide data
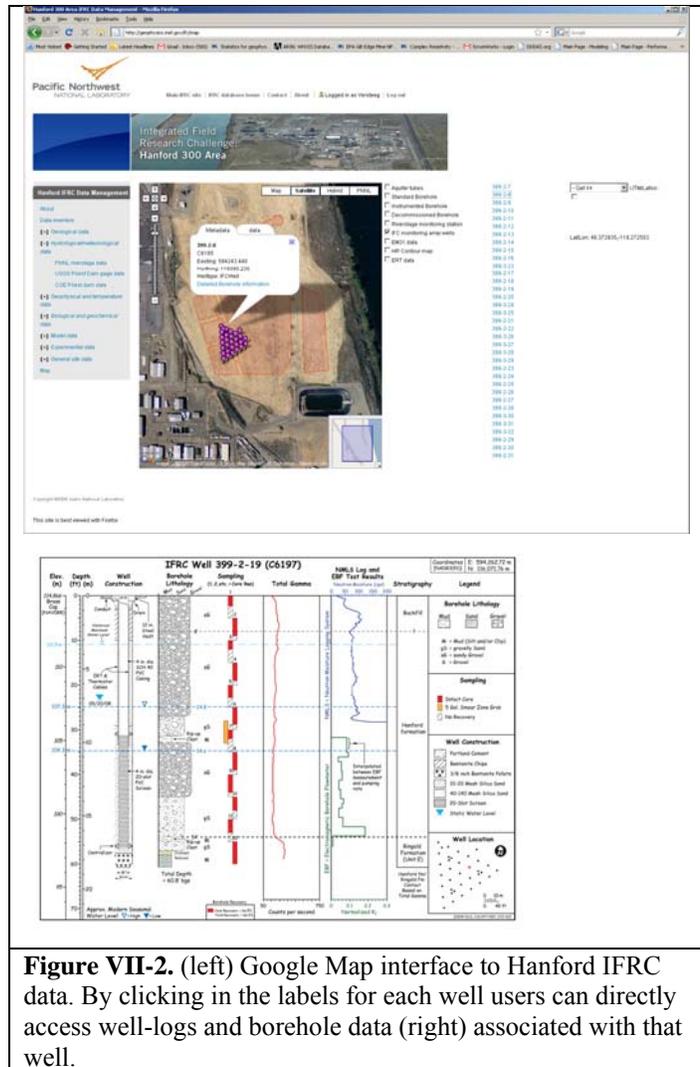
a. Topography
b. Columbia River bathymetry
c. Interface information

This data is accessible either as a direct download or a graphical interface which allows users to explore data before downloading selected subsets. Sometimes there is a lag between data completion and posting due to personnel limitations. Data bases in intermediate stages of completion are posted on PNNL's internal IFRC Share-Point site. These, in turn, are distributed to project participants when needed.
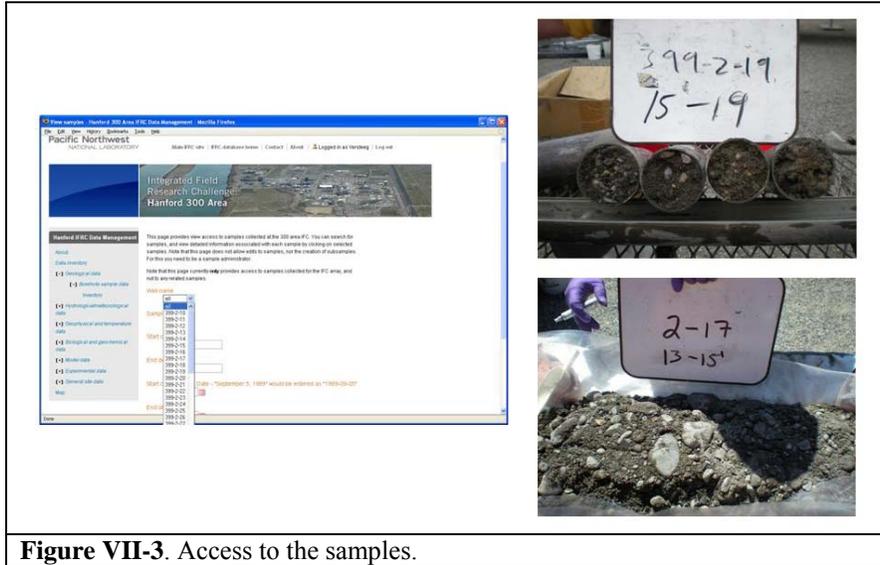


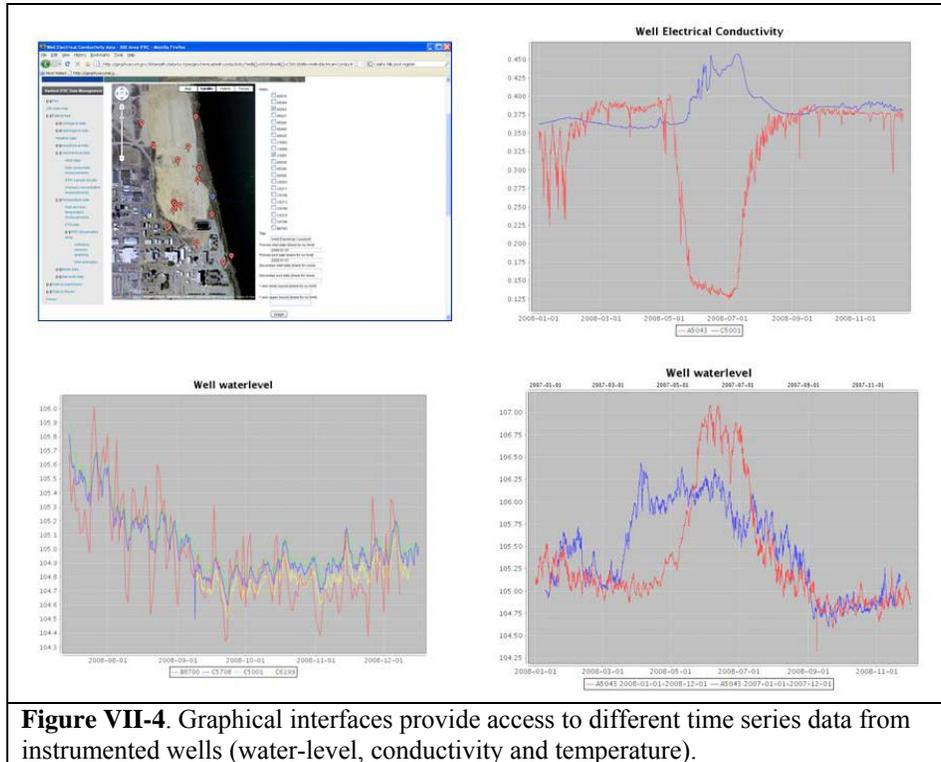**Figure VII-3**. Access to the samples.



**Figure VII-4**. Graphical interfaces provide access to different time series data from instrumented wells (water-level, conductivity and temperature).
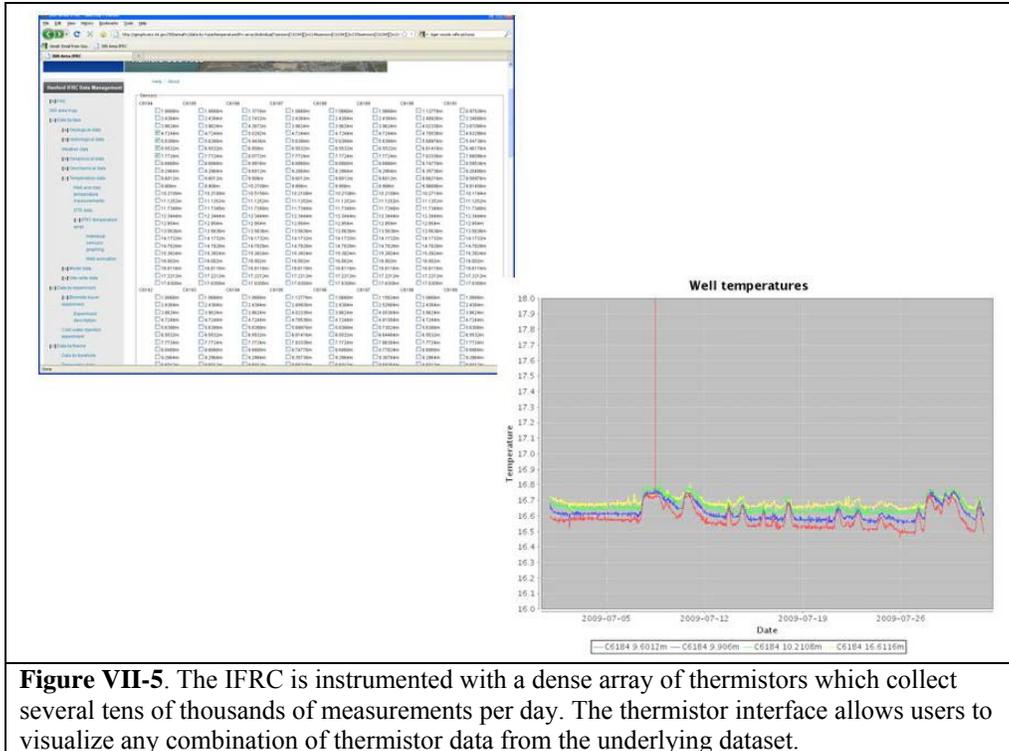
**Figure VII-5**. The IFRC is instrumented with a dense array of thermistors which collect several tens of thousands of measurements per day. The thermistor interface allows users to visualize any combination of thermistor data from the underlying dataset.

<u>Future Directions</u>

The current interface provides access to most of the data collected for the IFRC. In the near future the plans are to complete the database with a comprehensive description of all the experiments, as well as results of the recent modeling activities. In addition, a planned update of the server will result in a substantial increase in delivery of results (specifically for the temperature dataset, which currently contains about 15 million records).

# VIII.    PLACING THE IFRC SITE IN PERSPECTIVE: MULTIPLE REALIZATIONS AND PLUME SCALE MODELING

The 1600 $m^2$ IFRC field site allows the testing and evaluation of both conceptual and numeric models of U(VI) reactive transport developed in the laboratory, and provides a context for up-scaling studies of different type.  But perhaps more importantly, the field experiments described in **Section V.,** and their interpretation and modeling in **Section VI.,** allow identification of in-situ controlling processes and their rates and timescales at and above the decameter scale. This scale represents the "prediction scale" for some field systems.  The dominant processes interactions and their integrated impact on transport may be very different from those expected based on laboratory measurements and characterizations at the decimeter scale and below.  The IFRC is making significant progress in evaluating these scaling issues between the laboratory and field.

An important stated objective of the Hanford IFRC project is to provide field scale insights on the complex functioning and behavior of the 300 A U plume. The 300 A U plume is 2 $km^2$ in spatial extent and the IFRC site represents a mere 0.08 % of this region.  Are extrapolations of IFRC behaviors to the plume scale valid given inevitable variations in geology, heterogeneity, U inventory and geochemical controls, and local hydrologic conditions?  If the answer is yes, then what variables or diagnostic behaviors merit consideration at the plume scale; and how should extrapolations be performed?  Beyond these important rhetorical questions, knowledge or observation of key variables that may be crucial at the plume scale can inform field mechanistic hypotheses that may be resolved at the decameter or IFRC site scale.  Consequently there are important conceptual feedbacks between the different scales (decameter and kilometer) that may lead to more comprehensive system understanding if pursued.

In an effort to extend the implications of project findings to the plume scale and to facilitate up- and down-scale knowledge exchange, the IFRC has been collaborating with a SciDAC-2 project (Peter Lichtner, LANL P.I.) with funding provided by DOE BER and DOE ASCR.  The intent of this collaboration has been to cast the IFRC site, and it's contained processes and responses, in the broader context of the 300 A plume through high performance computing.  This activity is in its early stages, and results will become more realistic as improved conceptual and numeric models of processes and their interactions are developed at the IFRC site, and other plume-scale measurements are pursued to reduce key uncertainties identified through modeling. A summary of this collaborative effort is provided below.

Objective

Understanding complicated processes involving natural systems generally requires collecting large amounts of data to support modeling of these processes. Such data support is becoming more burdensome as models become more sophisticated with increasing data needs. However, often it is not apparent which data and processes are most important and essential to the system under consideration and hence much time and resources can be wasted collecting data that is not relevant. Thus an important role for modeling geochemical systems is assessing the importance of various processes on system behavior, thereby potentially reducing the amount of data that is necessary to collect. An important caveat, however, is that the model must be sufficiently accurate to capture the relevant processes taking place since otherwise false conclusions could be reached.

This contribution takes a large-scale view of the Hanford 300 uranium plume through the use of field-scale modeling to evaluate the importance of various processes that can influence uranium migration at the site. Processes that can affect the natural attenuation of uranium include adsorption and desorption, the role of the hyporheic zone and Hanford sediment heterogeneity on the flow velocity, and the high frequency fluctuations in the Columbia River stage. One potential system-scale mathematical metric that can be used to judge the importance of these processes is the cumulative flux of uranium into the Columbia River. This metric provides a time-averaged measure of the loss of uranium into the river that averages over the high frequency river stage fluctuations and results in an approximately linear increase in mass of uranium released to the river over time. Through conservation of mass, the cumulative flux at the river boundary is related to the time-averaged leach rate of uranium from the source regions of contaminated Hanford sediments. Cumulative flux is very important to the site regulator and steward as they both seek insights on how long the 300 A plume may persist with groundwater concentrations in excess of the regulatory limit.

It should be emphasized that at different scales, both spatially and temporally, different processes may dominate in describing the phenomena of interest. Thus to model the injection and passive experiments at the decameter-scale IFRC site, an accurate understanding of the instantaneous flow field and adsorption effects (rates and extent) are essential. However, by averaging over the high frequency fluctuations of the river stage, the cumulative system scale flux at the kilometer scale appears to be much simpler to predict in comparison to the highly transient behavior required for modeling the plume at the IFRC site. While the uranium flux at the river boundary and velocity field are highly transient quantities characterized by high frequency fluctuations, their time average exhibits a much simpler, quasi-linear behavior as a function of time.

Model simulations are performed using a realistic 3D model with relatively high spatial resolution. The source of uranium employed in the model includes both labile (bicarbonate extractable U, **Section VI.1**) and non-labile forms distributed in the vadose and saturated zones. Uranium in the vadose zone is released to groundwater as the water table rises and falls (**Section V.3**). Labile uranium is described through an equilibrium adsorption (surface complexation) isotherm and a multirate kinetic model based on laboratory column experiments derived from Liu et al. (2008) and as described in **Section VI.2**. Non-labile uranium is represented by the dissolution of metatorbernite as a surrogate source under far from equilibrium conditions. The calculations were carried out using the massively parallel code PFLOTRAN run on the Cray XT4/5 super computer Jaguar at ORNL with thousands of processor cores.

PFLOTRAN

PFLOTRAN is a subsurface multiphase, multicomponent reactive flow and transport code intended for use on a variety of computer architectures ranging from laptops to leadership-class supercomputers (Hammond et al., 2010b). It is founded upon established frameworks for high-performance computing [i.e. HDF5 (Hierarchical Data Format 5), MPI (Message Passing Interface), PETSc (Parallel Extensible Toolkit for Scientific computing), SAMRAI (Structured Adaptive Mesh Refinement Application Interface)], and supports seamless integration of Fortran9X, C and C++ programming languages. PFLOTRAN is written using a novel implementation of object oriented Fortran9X which distinguishes it from all other codes in its class. This allows modular development of the code resulting in seamless integration of additional processes. It is licensed under an open source license (LGPL) that allows others to use and contribute to the code.

PFLOTRAN is founded upon parallel data structures and solvers provided by PETSc. The code employs domain decomposition through PETSc DA (Distributed Array) or DM objects (The DM object is a generalization of the DA object for managing an abstract grid object.) to partition a physical gridded domain across processor cores, depending on whether structured or unstructured grids are employed (Note: Unstructured grids are currently in the development phase, yet to be completed). With this approach, each processor core possesses locally the data necessary to calculate its portion of the global problem being solved, regardless of the algorithm employed. With this decomposition in place, PETSc provides the necessary index sets or mappings for passing data between processors during the course of the simulation (e.g. updating ghost cells, checkpointing vectors, etc.), and performs the necessary vector gather/scatters when requested, masking the details of communication between processor cores.

Through SciDAC-2 funded development, PFLOTRAN has been run on problems composed of up to two-billion degrees of freedom and utilizing up to 131,072 ($2^{17}$) processor cores on ORNL's Jaguar Cray XT5, currently the world's fastest supercomputer. These large-scale problems are based on real-world variably-saturated flow and geochemical transport modeling of uranium at the Hanford 300 Area in Washington State.

Multiple Realization Simulations

Perhaps one of the most unique and innovative features of PFLOTRAN is its ability to launch multiple simulations of different realizations simultaneously, each realization being executed across multiple processor cores (Hammond et al., 2010b). Although the embarrassingly parallel execution of multiple simultaneous realizations is common, launch of each in parallel through domain decomposition within a processor sub-communicator group is a novel feat within subsurface simulation. This feature should greatly enhance the ability to use Monte-Carlo style analyses to better quantify uncertainty in the subsurface (e.g., **Sections VI.1 and VI.3**).

For the user, the implementation of a stochastic multi-realization simulation is quite straightforward. For example, suppose multiple realizations of permeability are to be employed in a Monte-Carlo fashion. Assuming the correlated random fields have been generated beforehand, a simple script is utilized (e.g., a Python script using h5py and numpy libraries) to load these datasets into an HDF5 formatted file with a name describing the dataset and the realization *id* (e.g. Permeability1—permeability for realization #1). At the prompt or within the job script, the user enters command line arguments that specify that the simulation be run in stochastic mode with a specified number of realizations and processor groups (Note: the number of processor groups must be less than or equal to the number of processor cores). An example of the command line arguments follows:

```
mpirun -np 10000 pflotran \
  -stochastic \
  -num_realizations 1000 \
  -num_groups 100
```

Upon execution, the realizations and parallel job's processor cores are divided as evenly as possible among the processor groups. In this case, 1000 realizations will be run on 100 processor groups using 10,000 processor cores. Each processor group will utilize 100 processor cores (np/num_groups) and run

10 realizations (num_realizations/num_groups) apiece, one after another. Thus, only 100 realizations may be executed simultaneously as each processor group may only simulate a single realization on 100 processor cores at a time. Each processor group continues to run realizations until its allocation of 10 has completed.

An alternative approach would be a master-slave paradigm where the root processor core assigns realizations to sub-communicator groups on a one by one basis. This approach would prove beneficial should significant load imbalance exist between sub-communicator groups. Either way, the implementation of the algorithm is straightforward and embarrassingly parallel.

Output for the stochastic simulation is written to files labeled by the realization *id* and/or processor group *id*. The user then employs scripts or codes to post process the results, computing statistical averages, sampling data, etc. To date, this approach has been successfully demonstrated with PFLOTRAN on stochastic simulations composed of hundreds of thousands of realizations and utilizing thousands of processor cores. The multiple realization implementation is being used in collaboration with IFRC team member Rubin and his students to develop a more realistic representation of the heterogeneity in the Hanford sediment based on well data taken from the IFRC site (**Section VI.3**).

Hanford 300 Area Conceptual Model

Evidence exists for the presence of two generally distinct forms of U(VI) in contaminated Hanford sediment (McKinley et al., 2007; Stoliker et al., 2009; Um et al., 2010). One form is the more easily removed, exchangeable, labile fraction which consists primarily of sorbed U(VI) but may also include soluble salts in the vadose zone. The other less readily dissolved non-labile form occurs in mineralized and amorphous phases and may also be co-precipitated with calcite. Metatorbernite, for example, has been observed in small quantities in one vadose sediment depth interval beneath the North Process Pond (Catalano et al., 2006; Arai et al., 2007). However, the exact form of non-labile U(VI), and its spatial and depth distribution both within the IFRC site and the broader 300 A plume domain remains elusive to this day and is a major uncertainty. With present-day, dilute, oxidizing groundwater compositions it is reasonable to expect that bulk pore waters are undersaturated with respect to non-labile forms of U(VI), with the possible exception of the vadose zone where complete or partial dry out could lead to high U(VI) concentrations.

This study focuses on understanding mobilization and transport of U(VI) in the Hanford 300 Area based on a 3D representation of the site, and addresses the roles played by sorptive processes and the rapid fluctuations in the Columbia River stage on the rate of natural attenuation of the U(VI) plume. Specifically, this study attempts to address the question of what is the present-day rate of attenuation of U(VI) at the site. This question is far easier to answer than the more ambitious question of how long it will take to reduce U(VI) aqueous concentrations to acceptable levels, which would require knowing the present-day in-ground U(VI) inventory and its chemical form, both of which are currently unknown. A measure for the attenuation rate is provided by the cumulative flux of U(VI) into the river averaged over the river-aquifer boundary. A working hypothesis is that the persistence of U(VI) at the 300 Area can be explained by slow leaching of U(VI) from source regions located both above and below the water table in the Hanford sediment which feed the plume (e.g., **Sections V.3 and VI.1**), combined with the fluctuating Columbia River stage which causes continually changing directions for flow and transport of U(VI) both towards and away from the river (see Figure VIII-1). The source regions consist of both adsorbed

(surface complexed) and non-sorbed U(VI), the latter in the form of precipitated solids in the vadose and saturated zones. After complete removal of all sources of U(VI), adsorptive processes together with river stage fluctuations are expected to control the final stages of U(VI) removal from the site.

To set up a model to describe migration of the U(VI) at the Hanford site it is necessary to specify the initial conditions corresponding to $t$=0 that are to be imposed on the model. This includes concentrations of both aqueous and solid phases. The most obvious and easily implemented initial condition is simply to assume uncontaminated conditions before U(VI) and other waste products were first deposited at the site in 1943 as done by Yabusaki et al. (2008) and more recently



**Figure VIII-1**. The Columbia River stage over a one-year period. The red diamond at approximately 3500 hours indicates the position of the insert. The symbols in the insert represent 1 hour intervals. The time interval of the river stage data ranges from 8 pm December 25, 1992 to 8 pm December 25, 1993.

by Ma et al. (2009). This, however, is problematic because the composition and variability of the waste stream over time and its rate of deposition is largely unknown and would be impossible to accurately reconstruct from historical records. In addition, it would seem difficult to develop models that could account for the inter-granular deposition of U(VI) on mineral surfaces from concentrated waste streams that presumably occurred during disposal. Finally, significant perturbations in hydrology occurred due to water mounding below the process ponds and trenches causing wide dispersal of U(VI). As a consequence of these considerations it is apparent that a first-principles approach beginning with waste deposition is presently not, and may never be, feasible. Thus a more pragmatic approach must be implemented.
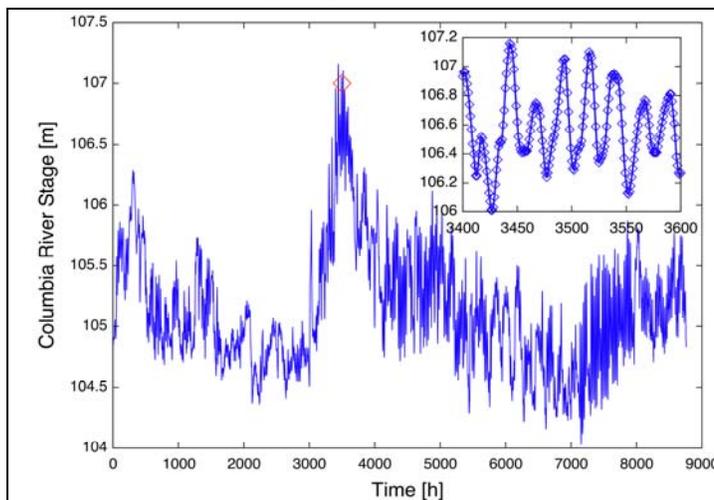
An alternative formulation might be to begin the calculation with a localized source region with a continuous release of U(VI) and follow the advance of the U(VI) plume through uncontaminated sediment to the river. However, this approach would require long simulation times due to the relatively high retardation of U(VI) by the Hanford sediment, especially in 3D, and would not lead to any additional insight, since it does not conform to actual conditions of waste emplacement.

To avoid these difficulties this work is distinguished from other attempts to model U(VI) migration at the Hanford 300 Area by the introduction of a new formulation for the initial conditions imposed on the system and using a realistic plume-scale 3D domain. In this formulation, the time evolution of the system is divided into three phases corresponding to: (I) initial waste emplacement; (II) present-day conditions of slow leaching of U(VI) from source regions and its discharge into the Columbia River; and (III) final removal of all sources of U(VI), both in the saturated and vadose zones. This work focuses on the second phase in which the Hanford sediments are equilibrated initially with U(VI) over a region extending from the source region where waste was originally deposited to the Columbia River, representative of present-day conditions. Therefore, instead of attempting to calculate the current in-ground U(VI) distribution starting from pristine sediment conditions, the initial time ($t$=0) is set to correspond to the time when the U(VI) plume already extends from the various source regions to the river as currently observed. Both

labile and non-labile forms of U(VI) are included in the model. Metatorbernite is used as a surrogate mineral for non-labile U(VI) in the source region; the identity of this phase is likely to change as more information becomes available. Adsorbed U(VI) in the vadose zone provides an additional source as the river stage rises and falls desorbing U(VI) and releasing it into the saturated zone **(Section V.3)**. Adsorption is described through both an equilibrium surface complexation model developed by Bond et al. (2008) and as further refined in **Section VI.2**, and a multirate model devised by Liu et al. (2008). Liu et al. (2008) fit the multirate model to observations of U(VI) breakthrough curves obtained from column experiments containing contaminated North Process Pond sediment. An improved data set is now available for intact cores of IFRC saturated zone sediments that will be included in the model shortly. In the approach taken by Yabusaki et al. (2008) and Ma et al. (2009), these authors only considered adsorption and treated non-labile U(VI) as completely inert.

Numerical Modeling Results of Hanford 300 Area Uranium Plume

*Approach.* Numerical simulations are based on the Richards equation mode in PFLOTRAN sequentially coupled to the reactive transport mode using fully implicit time stepping. Fully implicit methods have the advantage over operator splitting in that larger time steps are possible. To avoid operator splitting errors very small time steps would be required due to the high flow velocities encountered at the Hanford 300 Area. Disadvantages of the fully implicit approach are the much larger memory required to store the Jacobian matrix [this is mitigated though the use of parallel computing as well as Jacobian-Free Newton-Raphson methods which, however, still require a preconditioning matrix (Hammond et al., 2005)], and time truncation errors if too large a time step is taken. PFLOTRAN is founded on the PETSc parallel libraries for its parallel framework



**Figure VIII-2.** Three dimensional isosurfaces for the U(VI) concentration, saturation (side panels) and pressure (painted on contact between the Hanford and Ringold formations). The domain size measures 900 m x 1300 m x 20 m.

using domain decomposition (Balay et al., 2009). PFLOTRAN is written in object-oriented Fortran9X.
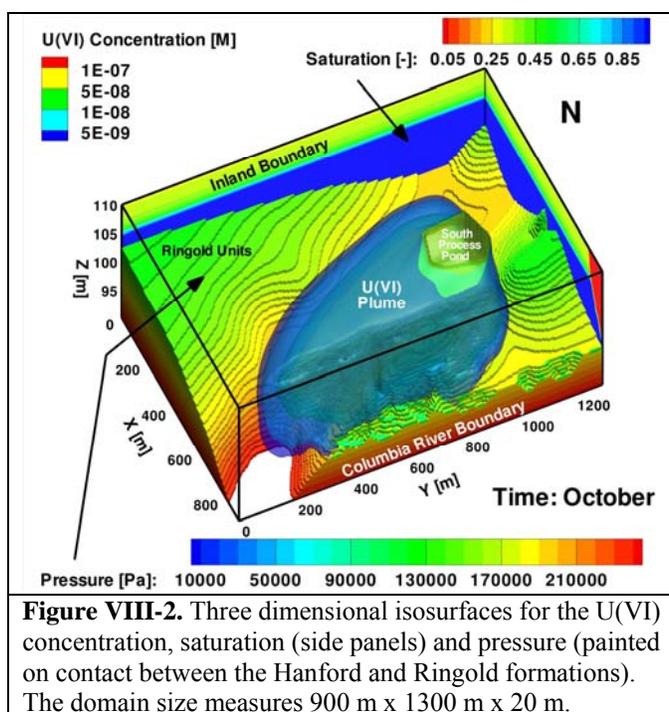
Three-dimensional simulations were carried out on a field-scale computational domain measuring 900 m x 1300 m x 20 m using a grid spacing of 5 m in the *x*-and *y*-directions and 0.5 m in the *z*-direction (see Figure VIII- 2). Fifteen components or primary species were used to represent the chemical interactions in the system including aqueous speciation, surface complexation, and precipitation/dissolution reactions. Both calcite and metatorbernite are included in the model with effective rate constants of $10^{-12}$ and $2 \times 10^{-17}$ mol/cm$^3$/s, respectively. The surface complexation model is combined with the multi-rate model and involves 100 primary sorbed concentrations. A sorption site concentration of 15 mol/m$^3$ corresponding to bulk sediment is used in the simulations. The implicit time stepping algorithm used in the simulations enables incorporation of the multirate model with little additional computational effort. In particular, the Jacobian matrix block size involves only the 15 aqueous primary species concentrations and not the sorbed concentrations which otherwise would have greatly complicated the numerical solution.

Calculations involving over 28,000,000 degrees of freedom were performed on ORNL's Jaguar Cray XT4/5 supercomputer using 4096 processor cores. The runs were carried to one-year simulation time requiring approximately 6 hours of cpu time. A detailed description of the calculations and their results were submitted for publication (Hammond and Lichtner, 2010; Hammond et al., 2010a).

Boundary conditions imposed on the model domain consist of no-flow conditions at the north and south boundaries, and prescribed transient piezometric heads at the river and inland boundaries. The transient inland boundary condition is constructed by triangulating and projecting piezometric head data obtained from wells 399-8-1, 399-6-1 and 399-4-1 onto the western face of the domain. Thus the three wells define a transient planar piezometric surface that is interpolated and/or extrapolated to the boundary face. In a similar manner, river stage and gradient are projected onto the eastern boundary. Representation of the interaction of groundwater and the river through the hyporheic zone is accomplished by introducing a conductance coefficient as a fit parameter (see Hammond and Lichtner, 2010).

*Results.* The flow rate and U(VI) flux into the Columbia River predicted by the model are highly sensitive to aquifer permeability and the value used for the conductance coefficient in the boundary condition at the river-sediment interface. Shown in Figure VIII-3 is a comparison of the piezometric head at well 399-2-1 for different conductance coefficients including a seepage boundary condition with no conductance. A conductance coefficient of $10^{-12}$ m gives a reasonable fit to the observations and significantly reduces the flow rate compared to the seepage boundary condition.
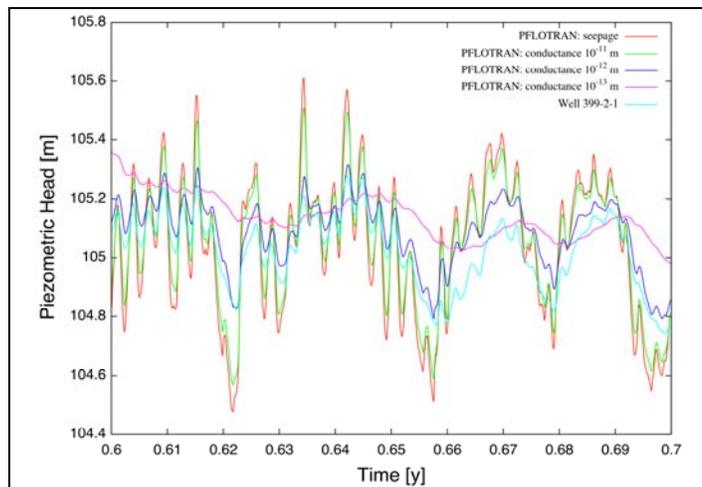


**Figure VII-3.** Piezometric head comparisons at well 399-2-1 with and without a conductance boundary condition at the river-aquifer interface. A conductance coefficient of $10^{-12}$ m gives the best fit to the head. A seepage boundary condition greatly over and under predicts the observed head.

Using a conductance coefficient of $10^{-12}$ m, the predicted velocity fields are shown in Figure VIII-4a and their time-integrated form in Figure VIII-4b. As can be seen from Figure VIII-4a, the velocity fields are highly fluctuating with time. The velocity component perpendicular to the river $q_x$ is the largest and $q_z$ is the smallest. The component parallel to the river $q_y$ is negative in the direction of the river flow. Integrating the velocities over time gives the results shown in Figure VIII-4b. A much simpler behavior emerges compared to the instantaneous velocities. By averaging out the high frequency fluctuations an almost linear displacement is obtained along the *y*-direction. The *x*-direction exhibits piecewise linear displacements caused by the reversal in the flow direction to and from the river. To understand this behavior the flux of water at the river-sediment boundary is investigated next.

The cumulative and instantaneous flux for $H_2O$ with a conductance coefficient of $10^{-12}$ m is shown in Figure VIII-5. Also shown in the figure are fits to the cumulative flux with lines of constant slope between flow reversals. Surprising, is the emergence of lines of constant slope resulting from time averaging the instantaneous $H_2O$ flux. As can be seen from the figure, flow to the river generally occurs over longer periods of time compared to the reverse direction for this same time period. A mean flux of $10^9$ kg/y is obtained which is in good agreement with previous estimates (Williams et al., 2008).

Shown in the Figure VIII-6a is the instantaneous flux for the equilibrium and multirate sorption models and the case with no sorption based on the Bond et al. (2008) model, the Liu et al. (2008) multirate sorption model. Also shown is the cumulative flux for these cases. The calculations shown in the figures are based on a conductance coefficient of $10^{-12}$ m. The cumulative flux for all three cases gives similar results with an approximate linear increase with time in the mass of U(VI) discharged to the river with slope of 25 kg/y in reasonable agreement with measurements carried out at the site (Fritz and Arntzen, 2007; Peterson, 2009).[1]

The calculations demonstrate that U(VI) is released into the Columbia River at a highly fluctuating rate in a ratchet-like behavior with nonzero U(VI) flux occurring only during flow from contaminated sediment into the river (Figure VIII- 6b). Noteworthy, is that the rapid fluctuations in the U(VI) flux average out over time yielding a much simpler description through the cumulative flux with small seasonal deviations from a straight-line fit.  These deviations are more pronounced for the case without adsorption. It should be noted that at any given instant



**Figure VIII-4.** a)  Instantaneous velocities in *x*-, *y*-, and *z*-directions; b) Velocities in the *x*-, *y*-, *z*-directions integrated over time.

in time there is approximately 2,000 kg $^{238}$U present in the plume as adsorbed and aqueous U(VI).  This value is maintained through release of U(VI) from the source term provided by the surrogate mineral metatorbernite as well as adsorbed U(VI) in the vadose zone which is released slowly into the saturated zone.
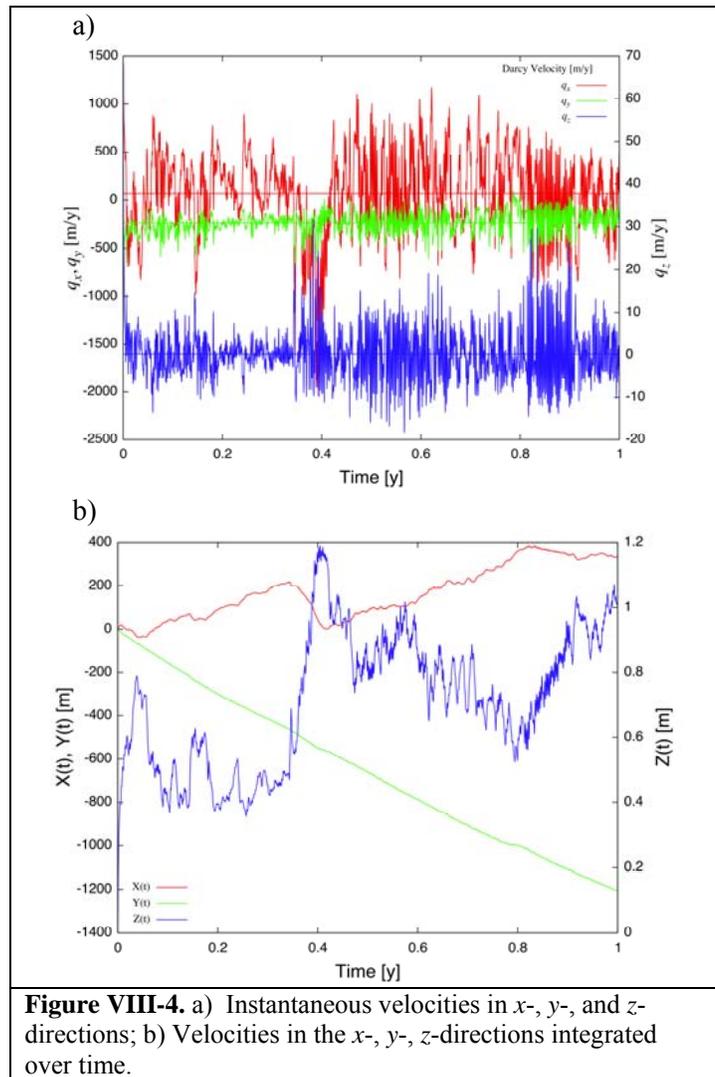
---

[1] Based on previous simulations at the site, the U(VI) flux for the case of no adsorption is found to be generally lower than the cases with adsorption. Although seemingly counterintuitive, this behavior is due to adsorption maintaining the U(VI) concentration higher near the river boundary during high river stage by desorbing U(VI) from the sediment retarding its movement, whereas without adsorption the concentration drops at the river boundary as the plume moves inland. This phenomenon was not apparent in the current simulations since the size of the non-adsorbing U(VI) plume increased slightly while the adsorbing plume did not. With the increased interfacial area at the river boundary, the non-adsorbing plume produced a larger cumulative flux than expected, masking the effect described above. Had a larger initial plume been used, it is likely that the flux with adsorption would be somewhat larger than without.

Somewhat surprising is that the equilibrium and multirate adsorption models give almost identical results compared to the case with no adsorption. The multirate model was originally developed to help explain the breakthrough curves obtained from column experiments (Liu et al., 2008) by leaching U(VI) from contaminated Hanford sediment taken from the 300 Area. Similar results are reported herein for IFRC lower vadose zone sediments (**Section VI.2**). The equilibrium adsorption model is not able to explain the column experiment results even approximately as shown in Figure VIII-7. In this
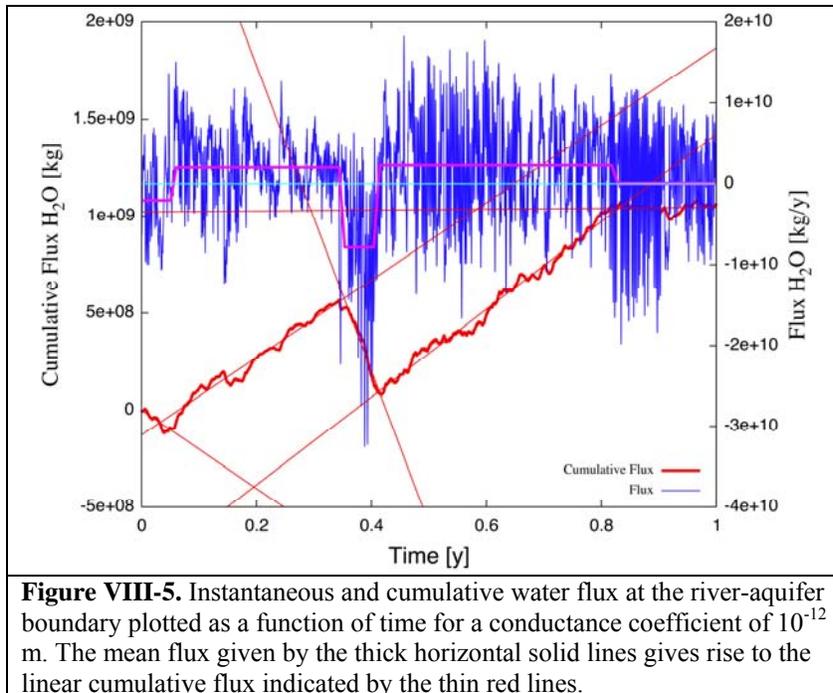


**Figure VIII-5.** Instantaneous and cumulative water flux at the river-aquifer boundary plotted as a function of time for a conductance coefficient of $10^{-12}$ m. The mean flux given by the thick horizontal solid lines gives rise to the linear cumulative flux indicated by the thin red lines.

figure is shown the multirate model fit to the experimental breakthrough curve compared to the equilibrium adsorption model and the case without sorption. As can be seen from the figure, the multirate breakthrough curve is bracketed (except for very long times when U(VI) becomes completely depleted in the column) by the equilibrium adsorption model and the case of no adsorption.

The question arises if the multirate and equilibrium adsorption models are so different in the column experiment, why are they not also different in the field simulation? This conundrum can be resolved by referring to Figure VIII-8 in which is shown the U(VI) concentration calculated from the 3D model plotted as a function of time near the river at the location of well 399-2-1. In the figure the three different cases of no adsorption and equilibrium and multirate adsorption are compared. The concentration without adsorption shows the greatest fluctuations approaching zero as river water infiltrates into the domain. For the cases with adsorption, the U(VI) concentration does not drop to near zero as river water infiltrates at the observation point because of desorption of U(VI) from the sediment. As a consequence, the variations in concentration are not as extreme in the presence of adsorption. Again in this case, the U(VI) concentration predicted by the multirate model lies between the cases of no adsorption and equilibrium adsorption. As a consequence, by changing the kinetic rate constants in the multirate model it is not possible to substantially alter the influence of the multirate model on the U(VI) discharge to the Columbia River.

*Heterogeneity Effects.* To assess the sensitivity of the cumulative U(VI) flux to heterogeneous permeability at the site, stochastic correlated random fields of permeability were generated based on extrapolated geostatistical data using a sequential Gaussian method (Hammond et al., 2010a). Stochastic permeability fields were generated based on field data obtained from the Hanford 300 Area IFRC site. Short-duration, constant-rate injection tests were made on 14 wells within the 300 Area IFRC well field to generate estimates of the spatial variability in transmissivity at the site. The calculated transmissivities were used in conjunction with the saturated thickness of the Hanford unit to estimate bulk hydraulic

conductivity (K) values. The saturated thicknesses were estimated as the difference between the average water table elevation at the time of each constant-rate injection test and the elevation of the Hanford-Ringold unit contact. Within the area of the IFRC well field, the elevations of the Hanford-Ringold unit contact were based primarily on the well picks (Bjornstad et al., 2009). Beyond the well field, the elevations of the Hanford-Ringold unit contact were based on an EarthVision model rendition of the interpretations described by Williams et al. (2008). The average saturated hydraulic conductivity based on the 14 constant-rate injection tests was 6945 meters per day. As part of the field IFRC characterization efforts, electromagnetic borehole flow meter (EBF) testing was also performed in 26 wells at 1- to 2-ft depth intervals. The EBF data were used to partition the bulk K values for the wells where constant-rate injection tests were performed into depth-discrete K values, assuming the bulk K value represents the arithmetic mean of the depth-discrete K values within each of the screened intervals.

Variogram analyses were used to estimate spatial autocorrelation lengths of saturated hydraulic conductivity from the depth-discrete K values. Insufficient EBF and pump test data were available to reliably estimate K anisotropy in the horizontal plane. However, initial simulation results obtained using STOMP (White et al., 2004), with K fields that were isotropic in the x-y plane suggested that there is an anisotropic structure to the K field. Horizontal correlation lengths and anisotropy were estimated based in part on the field K data, and in part on observed model performance relative to a field tracer test



**Figure VIII-6.** a) Instantaneous and cumulative U(VI) flux plotted as a function of time for equilibrium and multirate sorption and no sorption using a conductance coefficient of $10^{-12}$ m. The slope of the straight-line fit to the cumulative flux is 24.76 kg/y that compares favorably with Peterson's estimated value of 20-50 kg/y (Peterson et al., 2009)). The horizontal line gives a mean flux of 24.89 kg/y. Also shown is the case with no sorption giving a slope of 25.67 kg/y. The multirate and equilibrium sorption models give essentially identical results; b) Magnification of the time interval showing the instantaneous and cumulative U(VI) flux and the ratcheting effect of the release of U(VI) into the Columbia River for equilibrium sorption, multirate sorption, and no sorption shown in Figure 5a.

that was performed at the site in November 2008 (Rockhold et al., 2009). Preliminary interpretations suggest correlation lengths of approximately 30 meters and 10 meters in the horizontal plane, with an azimuth of approximately $9^{\circ}$ (clockwise from north) for the direction of maximum spatial continuity, and a vertical correlation length of 2 meters, for spherical variogram models. It should be emphasized that
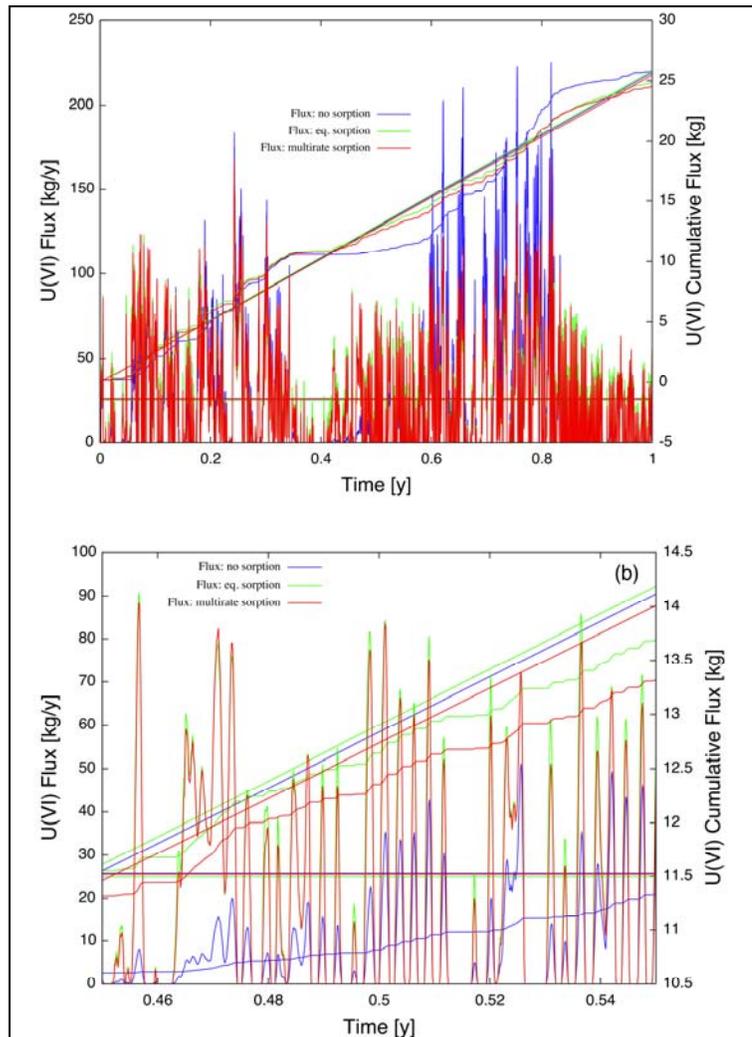
these interpretations are preliminary. Improved descriptions of the spatial variability and structure of the *K* field are expected following the completion of other characterization activities that are underway, and after additional inverse modeling of other more recent field tracer tests that have been performed at the site.

Using the pump and EBF testing and kriging data described above, SGSIM (Deutsch and Journel, 1997) was employed to generate 10 correlated random permeability fields within the modeled region at a 1 x 1 x 0.5 meter resolution, a factor of 5 finer than the modeled horizontal grid resolution of 5 meters. Thus, the geostatistically generated



**Figure VIII-7.** Comparison of breakthrough curves and internal U(VI) concentrations for the 1D column experiment with calcite present, for the cases without sorption, and for equilibrium and multirate sorption models over long time spans. As can be seen from the figure, the multirate breakthrough curve is bracketed by the no sorption and equilibrium sorption cases except at very long times. The symbols refer to the small column experiment discussed in Liu et al. (2008).

fields represent grids with 46.8 million cells that are upscaled to ~1.9 million cells. The purpose of the higher-resolution field was to enable the use of as many IFRC wells as possible, many of which would have been collocated within the grid cells of a 5 meter resolution grid. The fields were subsequently upscaled following methods described by Williams et al. (2008).

The cumulative U(VI) flux resulting from 10 realizations of random permeability and a single homogeneous realization are illustrated in Figure VIII-9 where the cumulative fluxes are tightly clustered within 7% of each other, suggesting that the cumulative U(VI) flux is rather insensitive to heterogeneity permeability field at the site. This sensitivity analysis, which involved far more than the 11 simulations discussed above and required millions of hours on ORNL's Jaguar supercomputer, illustrates the utility of high performance computing for better uncertainty quantification and analysis. Just these 10 simulations would have required 25 years wall clock time to run on a serial workstation, and that is assuming an extremely conservative parallel efficiency of 50% for PFLOTRAN.

Discussion

The flow field is sensitive to transient pressure boundary conditions imposed on the sides of the domain. Unfortunately it is difficult to obtain data for the inland boundaries that coincide with river stage data because of the lack of continuous monitoring at the inland wells. Generally, these boundary conditions must be set by extrapolation with nearby wells. Ultimately it would be desirable to remove the no-flow boundary conditions imposed on the north and south boundaries. To do this, however, would require better characterization of the transient pressure fields at these locations and at the west inland boundary. This may be difficult, however, because the water table undulates with time in the east-west direction, and thus a planar triangulation and projection of the piezometric head will likely fail to capture the many frequencies of oscillation in the water table. The model domain would need to be extended further north
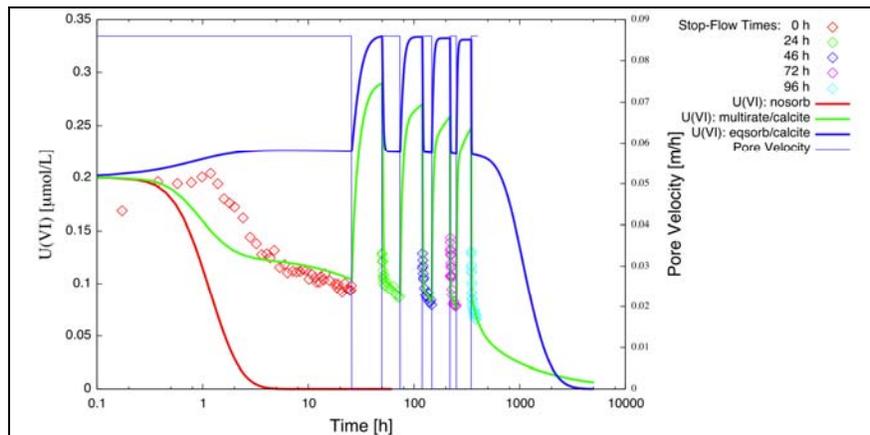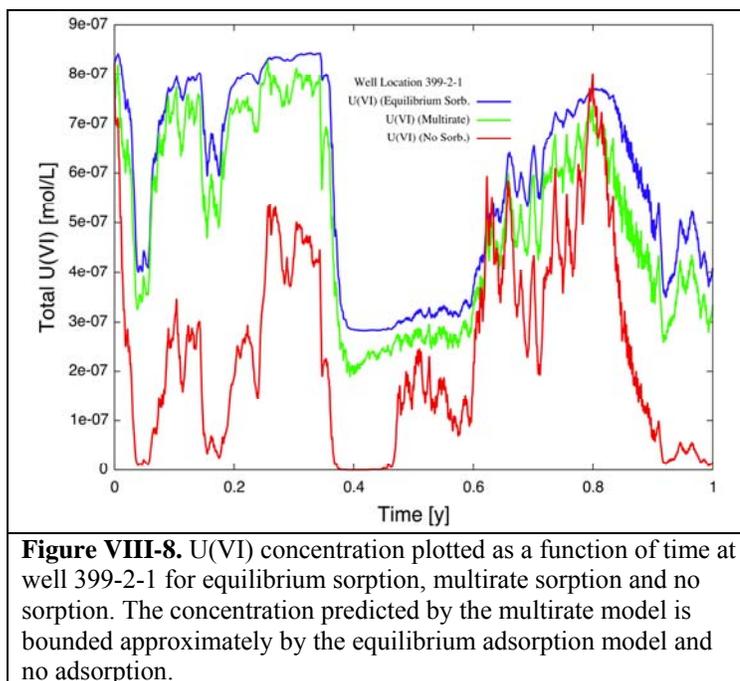
and south to lessen the impact of the linear triangulation approximation at the boundary on the inner portions of the domain.

It should be emphasized that the only adjustable parameters in the present model not determined by field observations are the river conductance which is fixed by approximately matching the observed piezometric head, and the effective U(VI) source-term rate for non-labile U(VI). If this latter parameter could be measured at the site, it could provide further confirmation of the model. This would require, however, carrying out the calculations further in time so that U(VI) released in the source region could impact the river boundary and affect the flux of U(VI) to the river. The source-term release rate, it should be noted, is constrained both by the U(VI) flux to the river and also by the maximum observed aqueous U(VI) concentration.



**Figure VIII-8.** U(VI) concentration plotted as a function of time at well 399-2-1 for equilibrium sorption, multirate sorption and no sorption. The concentration predicted by the multirate model is bounded approximately by the equilibrium adsorption model and no adsorption.

The estimate for the U(VI) flux of 25 kg/y does not include all the U(VI) source contributions: e.g. NPP, trenches, smear zone, etc., but only includes the SPP. Adding additional source regions to the model will increase the flux, and thus the present value provides a lower bound on the model prediction. Note that the model results are within the range estimated by Peterson et al. (2009) of 20–50 kg/y. Adding the NPP would expect to roughly double the present value obtained for the mean U(VI) flux to the river agreeing with the upper bound derived by Peterson et al. (2009). However, the current model may actually indirectly include some of the other sources to the extent that U(VI) pathways from these regions to the river overlap with the pathway from the SPP. This is because the initial distribution of U(VI) in the sediment is calculated by equilibrating with the aqueous U(VI) concentration obtained by transporting U(VI) unretarded from the SPP source to the river.

It should be noted that further work is needed to ascertain the utility of the multirate formulation as a predictive model. This is one of several IFRC objectives for field experiments. First, the model employed by Liu et al. (2008) uses equal site densities associated with each rate constant. This does not seem reasonable given that the multirate model should also account for distributed diffusive mass transfer pathways. However, to vary the site density would introduce numerous fit parameters and markedly increase computation time. Second, the rate constants are not species-dependent as is generally the case in kinetic rate laws. Finally, there is no clear methodology for upscaling the multirate model from laboratory to field scales. This is an active area of research for Hanford IFRC and PNNL collaborators. It remains an open question whether the multirate model is simply a fitting function, or whether it provides some fundamental insight into the processes taking place.

Finally, the impact of heterogeneous permeability at the site on the U(VI) flux to the river appears to be negligible.  This result is based on the extrapolation of geostatistical data from the smaller plot scale Hanford IFRC site to the larger plume scale, and thus may not capture the influence of larger scale geologic structure and heterogeneity at the site. Hammond, et al. (2009) investigated alternative coarse scale formulations for heterogeneity at the site (e.g. scaling of correlation lengths, etc.). However, the results suggested a similar insensitivity to random permeability.  It is likely that further studies will be necessary to further substantiate this result.

Summary and Future Directions



**Figure VIII-9.** Cumulative U(VI) flux plotted as a function of time for equilibrium surface complexation using a conductance coefficient of $10^{-12}$ m. The homogeneous realization of permeability, provided for comparison purposes, is anisotropic based on the average permeability in each principle direction for all 10 random fields.  The tight clustering of the cumulative U(VI) fluxes (within 7% of each other) demonstrates a relatively low sensitivity to random permeability fields generated based on extrapolated Hanford 300 Area IFRC data.

This work is the first application of a high-resolution, fully three-dimensional reactive flow and transport model to describe quantitatively natural attenuation of U(VI) at the Hanford 300 Area.  A new conceptual model was introduced to represent present-day conditions with U(VI) initially occupying sorption sites between the source region and the Columbia River, referred to as Phase II. In Phase II a continuous release of U(VI) from the source region, taken as the South Process Pond, was included in the calculations using metatorbernite as a surrogate mineral to represent non-labile forms of U(VI). The model calculations help resolve a long-standing puzzle as to why U(VI) persists over long time spans in the Hanford sediments at concentration levels that exceed EPA standards.

Rather than a picture of complexity of U(VI) depletion at the 300 Area, one of relative simplicity emerges given the nature of the performance metric (cumulative flux). This picture is characterized by an approximate linear increase in the mass of U(VI) discharged to the river with an average slope of 25 kg/y which agrees well with current estimates of the U(VI) flux based on field-based estimates of 20-50 kg/y (Peterson et al., 2009). Likewise, the flux of $H_2O$ of $10^9$ kg/y was also in good agreement with previous estimates (Williams et al., 2008). The longevity of the U(VI) plume can be explained by the rapid fluctuations in the Columbia River stage and source regions which feed the plume. The river stage fluctuations cause the plume to advance and recede thus slowing down the discharge of U(VI) into the river. Adsorption appears to play only a secondary role in retarding the movement of the plume, and would be expected to enhance the release of U(VI) into the river compared to the case of no adsorption. This is because adsorption acts to retain U(VI) near the river, unlike the case without adsorption where it is pushed farther inland. There also appears to be minimal uncertainty in the cumulative flux of U(VI) to the river due to heterogeneity in the Hanford permeability.  Finally, the model calculations were able to elucidate why in the column experiment with unidirectional flow the multirate sorption model gave very
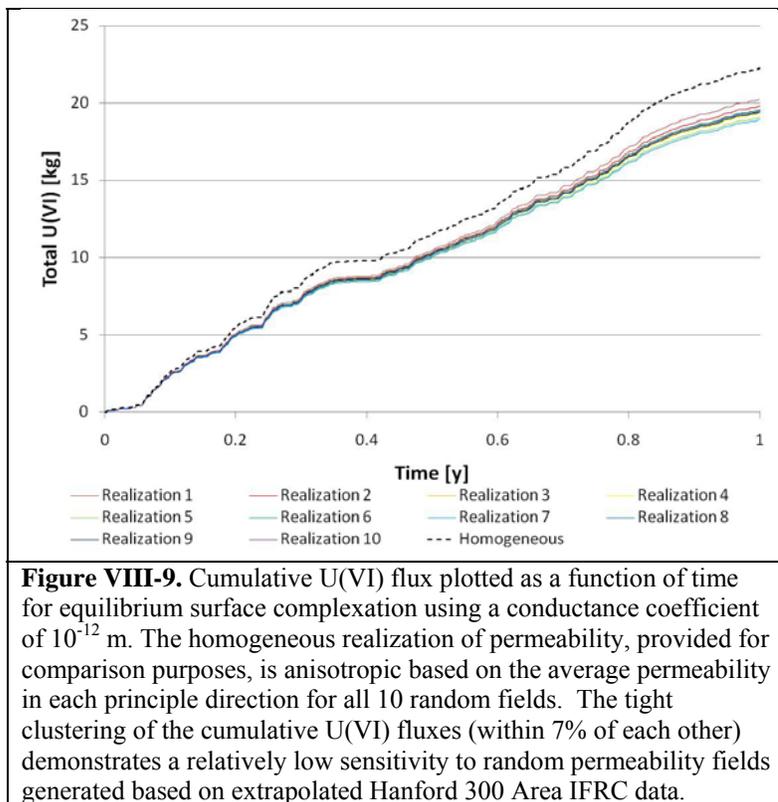
different results compared to equilibrium sorption and no sorption, whereas for the field with changing flow direction all three gave similar results. These results however, remain as a hypothesis for future evaluation.

The fluctuating flow field, and in particular the river-aquifer interface (hyporheic zone) modeled through a conductive boundary condition, was found to play an essential role in controlling the release rate of U(VI) into the Columbia River. The conductance coefficient was fit to match the hydraulic head at well 399-2-1 yielding a value of $10^{-12}$ m. This parameter was the only fit parameter used in the model simulations. For longer time spans than the one year used in the current simulations, the rate of release of U(VI) from the source regions would also contribute to the flux at the river boundary adding an additional adjustable parameter.

Central to this work was the use of high performance computing (HPC) carried out on the world's fastest open science supercomputer Jaguar, the Cray XT4/5 at ORNL. Use of HPC made possible the ability to capture the rapidly fluctuating Columbia River stage and multi-component U(VI) chemistry including aqueous speciation, adsorption through both an equilibrium and multirate model, and mineral dissolution at a sufficiently fine grid resolution to resolve more accurately fluctuations in groundwater velocities in a realistic 3D domain. The simulations involved approximately 28 million degrees of freedom for multi-component reactive transport, run on 4096 processor cores—runs that would have required years of computation time on a conventional single processor workstation.

# IX.    CHALLENGES AND CONCERNS

The following three concerns are articulated given our limited but growing site experience.

1.)  Lack of correlations between geochemical reactivity and properties

Close to two hundred sediment grab samples have now been characterized in the laboratory for physical and geochemical properties.  These measures were carefully selected based on literature review and extensive site experience. An important objective of these measurements has been the establishment of correlations between easily measured properties and reactive transport parameters such as adsorption strength (e.g., surface complexation log K) and kinetics (statistical distribution of rate constants).  These correlations are important as they would allow estimation of the spatial distribution of reactive transport properties based on surrogate geophysical or other measures.  At this time, however, we have been unable to establish strong, predictive correlations. For example, we expected, but did not observe strong correlation between surface area and silt plus clay or between surface area and U(VI)-$K_d$. Also not observed were correlations between U(VI)-$K_d$ and extractable Fe(III) forms.  The absence of clear correlation underscores the fact the mineral phases responsible for U(VI) adsorption at the very low U concentrations present are not well understood.  The unfortunate solution to this situation is simply the performance of more characterization measurements (primarily $K_d$ from which surface complexation parameters are derived) to better constrain a geostatistical model.

2.)  Well bore flows and depth specific monitoring

This issue has been well described in this report and the January 2010 Quarterly.  It is the most important project concern.  Our strategies to address the problem are four-fold. First, we will establish the capability to perform both injection and monitoring experiments in the upper high K zone through shallow and multi-level well installation in spring 2010, and the deployment of inflatable packers in the fully screened wells during the period of the experiments. This zone is a crucial source term to the U plume and its behaviors must be understood.  Second, a series of low cost, temperature injection experiments will be performed to better characterize the simultaneous distribution of well bore-flows across the well-field in response to river stage dynamics. These experiments will involve injection of temperature modified waters selectively into either the upper or lower high K zones, followed by high resolution (spatial/temporal) in-situ monitoring with our robust thermistor array. Results will provide comprehensive data sets for further calibration of the hydraulic conductivity field causing complex flow patterns. Third, efforts to model well bore flows will continue as described in **Section VI.4**, emphasizing the development and incorporation of a robust hydraulic model that integrates conductivity hydrologic testing data of different forms, non-reactive tracer experiments, and 3-D geophysical measurements.  Finally, all new wells installed within the IFRC site domain from this point forward will be completed in depth discrete intervals.  All future experiments will be designed with this issue in mind.

3.)  Hydrologic/time-scale constraints on field experiments

We have always had concerns about the hydrologic constraints of the 300 A site given the coarse-textured nature of the sediments, and hydrologic linkage with the Columbia River.  Initially we were concerned that the average linear groundwater velocities would be too high to for successful field experiments. CY09 experimentation has shown that this is not the case, and that injected plumes remain within the

well-field for desired periods. Average flow velocities vary dramatically by hydraulic conductivity zone affording ample ranges for experimentation.

However, our preliminary U injection experiment (**Section V.4**) was disappointing. U attenuation was limited, and groundwater concentrations rebounded more rapidly than expected based on our laboratory calibrated model. This model was based on results of reactive transport experiments with three intact sediment cores from the IFRC. Thus, there is an apparent difference in lab versus field scale behaviors. We are now beginning to model the results of the U desorption experiment to identify effective in-situ reaction parameters for the different hydraulic conductivity zones. A comparison of these effective parameters with the lab-derived ones will be a first step in assessing causes for the disparity. Beyond this, we expect that extensive pre-modeling will be required of all future U experiments to assure that the combination of injection volume, duration, and timing generate conditions in terms of time-scale and distance from equilibrium that allow evaluation of the in-situ kinetic processes controlling U groundwater concentration.

# X.    FUTURE RESEARCH PLANS

We now have approximately 16 months of research experience with the IFRC field site.  By all metrics, we are early on the learning curve in understanding its complex physical, hydrologic, geochemical, and microbiologic characteristics and behaviors.  Only recently has characterization data been integrated into site heterogeneity models to allow estimation of the spatial distribution of key properties and variables.  Our ability to model the site hydrological dynamics is good but preliminary, and increases with each new characterization measurement and inversion analysis of tracer and geophysical data.  The initial version of the IFRC site reactive transport simulator was completed in early February 2010 and is based on a conceptual geochemical reaction model and parameters resulting from laboratory experiments.  This model has seen limited application to site data for conceptual model validation and process-parameter evaluation against the reality of field-scale behavior. The field experiments so far completed were all of generally exploratory character, as each was performed during a different season with different hydrologic constraints and dynamics.  Each experiment had new elements that tested different aspects of site infrastructure.  Thus the project is still in its early stages given the complexity of the site and sophistication of the monitoring system.

The project does have challenges and concerns as discussed in **Section IX**, and the plans below assume that the proposed mitigation activities will be followed.  The remaining project duration is 2.5 y, and research plans need be consistent with this period.

Hydrophysical Characterization

There are still significant uncertainties in the hydraulic conductivity field and the locations and behaviors of mass-transfer limited domains.  This field must be accurately characterized in order to predict transport through the site and well-bore responses to pressure gradients.   Part of the existing uncertainty in hydraulic conductivity results from the presence of vertical borehole flows and the partial reliance on EBF data for vertical hydraulic conductivity profiles that may be affected by the sand filter pack.

New temperature tracer and solute tracer experiments are planned to further refine the hydraulic conductivity field.  These will begin in Spring 2010 with emphasis on the upper high K zone during the period of water table rise and fall (April-June).  Multiple smaller scale experiments are planned for this time frame when the water table is at different elevations.  Different access wells will be used for tracer dispersal (low volume, high concentration) that are associated with observed vadose zone sources of U to groundwater.  The tracer experiments will be performed in association with comprehensive, multi-level, multi-component groundwater monitoring.

The central low K zone and disconnected regions of comparable physical properties function as mass-transfer limited zones within the IFRC site. These zones are hypothesized to function as both sources and sinks for dissolved U.  Scoping hydrologic calculations indicate that the low K zone associated with several of the multiple well clusters exhibits hydraulic properties that are conducive to push-pull experimentation (beginning first with the multi-well cluster 2-29, 2-30, 2-31).  Several small-scale push-pull experiments will be performed in these zones during summer 2010 to characterize their physical mass transfer behavior in support of U-geochemistry and microbiologic activity studies described below.

Microbial Ecology and In-Situ Activity

The PNNL SFA has active ongoing research on the microbial ecology of Hanford's unconfined river-corridor aquifer, and is using the IFRC site as its primary field site.  Their primary objectives have been to characterize the microbial biomass, phylogenetic diversity, and biogeochemically relevant activities of the in-situ community.  Given that little was known about the microbiology of the river corridor aquifer prior to IFRC site installation, these objectives were beyond the scope of the original IFRC proposal.  Analyses of both cores and groundwaters from the IFRC well field have shown that the highly transmissive Hanford formation is a region of substantial microbial abundance and potentially high metabolic activity.  The microbial community is highly diverse, with 1,233 unique bacterial operational taxonomic units (OUT's) and 99 archaeal OTUs determined at 97% sequence similarity of the 16S rRNA gene.  Ongoing research seeks to understand the extent of microbial heterogeneity in the system, the controlling environmental variables, and the extent of community change in response to seasonally dynamic hydrologic and geochemical conditions.

Further exploration of the microbiologic community and its biogeochemical function in the U plume was initiated in late CY09 and early CY10 with IFRC support, and the preliminary results from microcosm deployment to IFRC wells are promising as described in **Section V.5**.  Based on these findings, the microcosm string with multiple colonization substrates and water and gas samplers has been re-configured for more optimal sampling, and re-deployed to IFRC wells for an additional 4 month period. The passive biogeochemical sampling systems will be further complemented with flux meters to quantify biogeochemical reaction rates, and identify hydrochemical controls on in-situ biogeochemical function.  Future studies will build on new results as they are received given the small existing knowledge base on this system.

The results of continued SFA research in CY 10 and the ongoing IFRC microcosm experiments are expected to provide sufficient information to plan a series of push-pull experiments for late CY 11 in the intermediate low K zone to assess the in-situ microbiologic activity of specific functional groups. The experiment will involve injection of as yet undefined substrates (e.g., stable isotope-labeled) to track the metabolism of target microorganisms. This planning will be aided by collection of a new series of sediment samples from the low K domain during our spring 2010 well installation of a new multiple depth well cluster in the central domain of the well field (see **Figure III-1**).  These new samples will enable more targeted characterization of the in-situ community, given the experience and results from the first characterization phase.  Additionally, sediments will be available to evaluate the effectiveness of candidate activity-tracing substrates in the laboratory under representative field conditions of water flux and composition.

Uranium (Bio)Geochemistry

Our experimental program with U has only just begun.  However field sampling and experimentation in CY 09 that revealed oscillating vertical borehole flows and vertical stratification in groundwater U concentrations provide important constraints that must be considered.  Our next experimental campaigns for U will focus on the following targets.  i.) The upper high K zone during the spring 2010 water table oscillation by passive monitoring and low-volume tracer addition. The addition of new wells in March 2010 will increase the number of monitoring points and allow the leading edge of the water table to be followed over the complete trajectory of rise and fall.  ii.) In-situ desorption and adsorption rates and

extent in the upper high K zone evaluated by injection experiment (to this zone only) during fall 2010 after passage of the spring U recharge event.  iii.) Mass transfer limited adsorption/desorption in the intermediate low K evaluated by depth discrete push-pull injection of high-U site groundwater in early spring 2011.

In association with field experiments described above, we will work toward a 3-D reactive transport model of the lower vadose zone, the upper high K aquifer zone, and the middle low K aquifer zone.  We currently suspect that interactions within and between these zones have the greatest impact on U concentrations and distributions within the plume.  The transport model will explicitly include measured and estimated spatial distributions of geochemical, physical, and hydrologic transport properties as well as various process specific model parameters derived from both laboratory and field experimentation. Additional laboratory reactive transport experiments with intact cores from these zones will begin in CY 10.  The up-scaling of kinetic parameters and models is an important focus of both the experimental and modeling program. The transport model will used to simulate results of passive monitoring and injection experiments, and to pre-model follow-on experiments for hypothesis evaluation.  The model will be calibrated to field observations if necessary.  We seek a flexible, transparent model to simulate IFRC behavior with realistic processes and parameters, and one to evaluate representative injection and/or transport scenarios for learning and planning purposes.

Research in CY 11 will work toward a culminating injection experiment where we will investigate the in-situ lability of adsorbed U(VI) in the saturated zone by isotopic exchange using groundwaters from the north-end of the 300A that display different isotopic composition (see **Section IV.3**).  This experiment will require careful planning as it will be severely constrained by the number of samples that can feasibly analyzed for isotopic composition.  The experiment will be performed in push-pull format in the low K intermediate zone, if possible, to reduce sample numbers for time-consuming isotopic analyses.

Relationships to the Plume Scale

We will continue collaborative modeling activities with the SciDAC 300 A modeling project to place our decameter-scale results in broader perspective, to obtain insights on key scientific questions at the plume-scale that the IFRC might address, and to assure that the plume-scale model embodies the most accurate and defensible process representations possible. We feel that continued dialog along these lines will allow the IFRC project to have maximum scientific and site impact, and to develop the most comprehensive understanding of overall system behavior. During CY 10 we will devise a research approach combining both laboratory column and field monitoring experiments to better understand the coupled adsorption-desorption process that occurs with river stage fluctuation, and to quantify the overall flux of U from the site. The flux question will require the deployment of new measurement devices to IFRC well field, and initial discussions have been had with K. Hatfield of the University of Florida on this subject. This information will address an important uncertainty in the plume scale model, and will provide a data set to which the plume-scale model can be compared. We will also transfer our most current conceptual and parameterized-process level models for the IFRC site to the SciDAC team to update PFLOTRAN in late CY10.  Critical to this are conceptual improvements to the vadose zone release model,  an improved description of the non-labile U fraction, and more representative surface complexation and mass-transfer rate parameters derived from field experimentation.  Collaborative iterations between laboratory experiments, field measurements, and plume scale modeling will continue through CY 11 to the mutual benefit of both projects, and those seeking a holistic understanding of plume behavior.

# XI. OUTREACH ACTIVITIES

Over the past year, a number of outreach efforts occurred with the outside community. These interactions included the Hanford Site DOE contractor community as well as regulator and stakeholder groups who are keenly interested in results from the project. One such interaction was at a Hanford Science and Technology Workshop at Washington State University, Tri Cities, where the project was described in the plenary session by David Lesmes (DOE-BER) and in a session focused on soil and groundwater issues. Another was before the Hanford Advisory Board (HAB) and DOE staff from the Richland Operations Office and the Office of River Protection where a seminar was given on the IFRC as an example of impactful Office of Science research being performed at the Hanford site. IFRC team members provided a Hanford Site open seminar on the results of the spring 2009 vadose zone U(VI) mobilization experiment which provided the first direct experimental measurements of a long-hypothesized U recharge mechanism to the persistent plume. Our recent documentation of vertical flows in fully screened IFRC monitoring wells and their cause and effects, has huge implications for groundwater monitoring along the river corridor at the Hanford Site where such wells are ubiquitous. Our findings and their implications have been proactively communicated to Hanford Site contractors and DOE. Team members interact regularly with Hanford Site contractor staff responsible for 300 A site remediation to provide updates on progress that may impact remedy testing and evaluation.

A number of visitors toured the IFRC site during CY09. The site hosted group of scientists from Migration 09 (an international conference on radionuclide migration that occurred in Kennewick, WA in September, 2009) that discussed field experiments of radionuclide transport. Dr. William Brinkman, head of the Office of Science, visited the IFRC site in November. Earlier in August, DOE Secretary Chu toured the Hanford Site along with Ines Triay, head of the DOE Office of Environmental Management, and Washington State Senators Patty Murray and Maria Cantwell. Although the tour did not include a stop at the 300 Area, scientific findings from the IFRC were described by John Zachara. The management team for the EM-30 modeling activity (ASCEM) visited the site in November, 2009 for discussions over its suitability for model validation activities. Tom Nichols of the Nuclear Regulatory Commission has also inquired about the use of IFRC site data for similar purpose. EM-30 management (Collazo and Chamberlain) visited the site while our vertical flow mitigation experiment with packers was underway in early February, 2010.

The IFRC site has proactively sought other collaborators from the ERSP (SESP) program, and two new projects have been funded in FY10 (Day-Lewis, Burgos) that will utilize IFRC site infrastructure and/or site sediments.

# REFERENCES

Alhagrey, S. A. 1994. Electric study of fracture anisotropy at Falkenberg, Germany. *Geophysics* **59**, 881-888.

Arai, Y., M. A. Marcus, N. Tamura, J. A. Davis, and, J. M. Zachara. 2007. Spectroscopic evidence for uranium bearing precipitates in vadose zone sediments at the Hanford 300-Area Site. *Environ. Sci.& Technol.* **41**, 4633-4639.

Balay, S., K. Buschelman, V. Eijkhout, W. D. Gropp, D. Kaushik, M. G. Knepley, L. C. McInnes, B. F. Smith, and, H. Zhang. 2009. *PETSc Users Manual*, Tech. Rep. ANL-95/11 - Revision 3.0.0, Argonne National Laboratory.

Bjornstad, B. N., A. Horner, V. R. Vermeul, D. Lanigan, and, P. D. Thorne. 2009. Borehole Completion and Conceptual Hydrogeologic Model for the IFRC Well Field, 300 Area, Hanford Site - Integrated Field Research Challenge Project. *PNNL-18340*, Pacific Northwest National Laboratory, Richland, Washington.

Bond, D. L., J. A. Davis, and, J. M. Zachara. 2008. Uranium(VI) release from contaminated vadose zone sediments: estimation of potential contributions from dissolution and desorption. In *Adsorption of Metals by Geomedia II: Variables, Mechanisms, and Model Applications*, Eds. Barnett, M. O. and, Kent, D. B., Elsevier: Amsterdam, p. 375-416.

Catalano, J. G., J. P. McKinley, J. M. Zachara, S. Heald, S. C. Smith and, G. Brown Jr. 2006. Changes in uranium speciation through a depth sequence of contaminated Hanford sediments. *Environ. Sci. & Technol.* **40**, 2517-2524.

Chen, X., H. Murakami, M. S. Hahn, M. L. Rockhold, V. Vermeul and, Y. Rubin. 2009. Integrating tracer test data into geostatistical aquifer characterization at the Hanford 300 Area, Eos Trans. AGU, **90**(52), Fall Meet. Suppl. Abstract H43F-1095.

Deutsch, C. V., and, A. G. Journel. 1997. *GSLIB: Geostatistical Software Library and User's Guide*, 2nd Edition. Oxford University Press, New York.

Doherty, J. 2002. *Manual for PEST,* 5th Edition. Watermark Numerical Computing. Brisbane, Australia, www.sspa.com/pest.

Doherty, J. 2003. Ground water model calibration using pilot points and regularization. *Ground Water* **41** (2), 170-177.

Doherty, J. 2004. *PEST - Model-Independent Parameter Estimation, User's Manual*, 5th Edition, Watermark Numerical Computing, Australia.

Draper, K., L. Ward, S. Yabusaki, C. J. Murray and, J. Greenwood. 2009. Abundances of natural radionuclides (40K, 238U, 232Th) in Hanford and Rifle Integrated Field Research Challenge Site

sediments and the application to the estimation of grain size distributions, AGU, **90**(52), Fall Meet. Suppl. Abstract, H33B-0872.

Ezzedine, S., Y. Rubin and, J. Chen. 1999. Bayesian method for hydrogeological site characterization using borehole and geophysical survey data: Theory and application to the Lawrence Livermore National Laboratory Superfund site. *Water Resour. Res*. **35**(9), 2671-2683.

Furness, P. 1999. Mise-a-la-masse interpretation using a perfect conductor in a piecewise uniform earth. *Geophys. Prospecting* **47**, 393-409.

Fritz, B. G. and, E. V. Arntzen. 2007. Effect of rapidly changing river stage on uranium flux through the hyporheic zone, *Ground Water* **45**(6), 753–760.

Greenwood, W. J., A. L. Ward, R. J. Versteeg, T. C. Johnson, and, K. Draper. 2009. Azimuthal resistivity investigation of an unconfined aquifer at the Hanford Integrated Field Research Challenge Site. AGU, **90**(52), Fall Meet. Suppl. Abstract, NS23A-1120.

Halford, K. J. and, R. T. Hanson. 2002. User guide for the drawdown- limited, multi-node well (MNW) package for the U.S. Geological Survey's modular three-dimensional finite-difference ground-water flow model, versions MODFLOW-96 and MODFLOW-2000: *U.S. Geological Survey Open-File Report 02-293*, p. 33.

Haggerty, D. R. and, P. Reeves. 2002. STAMMT-L 1.0 user"s manual. *ERMS #520308*, p. 76 Sandia National Laboratories, Albuquerque, New Mexico.

Hammond, G. E., A. J. Valocchi, P. C. Lichtner. 2005. Application of Jacobian-free Newton-Krylov with physics-based preconditioning to biogeochemical transport. *Adv. Water Resour.* **28**(4), 359-376.

Hammond, G. E. and, P. C. Lichtner. 2010. Field-scale model for the natural attenuation of uranium at the Hanford 300 Area using high performance computing. *Water Resources Research* (Submitted).

Hammond, G. E., P. C. Lichtner, and, M. L. Rockhold. 2010. Stochastic simulation of uranium migration at the Hanford 300 Area. *Journal of Contaminant Hydrology* (Submitted).

Hammond, G. E., P. C. Lichtner, C. Lu and, R. T. Mills. 2010. PFLOTRAN: reactive flow & transport code for use on laptops to leadership-class supercomputers, Bentham E-Book (Submitted).

Harbaugh, A.W., E. R. Banta, M. C. Hill and, M. G. McDonald. 2000. MODFLOW-2000, the U.S. Geological Survey modular ground-water model — User guide to modularization concepts and the ground-water flow process: *U.S. Geological Survey Open-File Report 00-92*. p.121.

Johnson, T. C., R. J. Versteeg, A. L. Ward, C. E. Strickland and, J. Greenwood. 2009. Electrical geophysical characterization of the Hanford 300 Area Integrated Field Research Challenge using high performance DC resistivity inversion geostatistically constrained by borehole conductivity logs: AGU, **90**(52), Fall Meet. Suppl. Abstract NS41A-08.

Johnson, T., R. Versteeg, H. Huang and, P. Routh. 2010. A data domain correlation approach for joint inversion of time-lapse head, concentration, and electrical resistivity data. *Geophysics* **74**, F127 - doi:10.1190/1.3237087.

Johnson, T., R. Versteeg, A. Ward, F. Day-Lewis and, A. Revil. 2010. Improved hydrogeophysical characterization and monitoring through parallel modeling and inversion of time-domain resistivity and induced polarization data. *Geophysics* (In press).

Johnson, T., R. Versteeg, A. Ward, J. Greenwood and, C. Strickland. 2010. Electrical geophysical characterization of the Hanford 300 Area Integrated Field Research Challenge wellfield using high performance DC resistivity inversion geostatistically constrained by borehole conductivity logs. *Water Resources Research* (Submitted).

Langevin, C. D., A. M. Dausman and, M. C. Sukop. 2009. Solute and heat transport model of the Henry and Hilleke laboratory experiment. *Ground Water* DOI: 10.1111/j.1745-6584.2009.00596.x (Published online 6/29/2009).

Li, P. and, F. Stagnitti. 2004. Direct current electric potential in an anisotropic half-space with vertical contact containing a conductive 3D body. *Math. Prob. Engineer.*, 63-77.

Lindberg, J. W. and, R. E. Peterson. 2004. 300-FF-5 operable unit. In: M. J. Hartman, L. F. Morasch, and W. D. Webber (Eds), Hanford Site Groundwater Monitoring for Fiscal Year 2004. *PNNL-15070*, pp. 2.12-1–2.12-31. Pacific Northwest National Laboratory, Richland, Washington.

Liu, C., J. M. Zachara, O. Qafoku, J. P. McKinley, S. M. Heald, and, Z. Wang. 2004. Dissolution of uranyl microprecipitates from subsurface sediments at Hanford site, USA. *Geochim. Cosmochim. Acta*. **68**(22), 4519-4537.

Liu, C., J. M. Zachara, N. P. Qafoku, and, Z. Wang. 2008. Scale-dependent desorption of uranium from contaminated subsurface sediments, *Water Resour. Res*. **44**, W08413, doi: 10.1029/2007WR006478.

Liu, C., Z. Shi, and, J. M. Zachara. 2009. Kinetics of uranium(VI) desorption from contaminated sediments: effect of geochemical conditions and model evaluation. *Environ. Sci. & Technol*. **43**(17), 6560-6566.

Ma, R., C. Zheng, H. Prommer, J. Greskowiak, C. Liu, J. M. Zachara, and, M. L. Rockhold. 2010. A field-scale reactive transport model for U(VI) migration influenced by coupled multi-rate mass transfer and surface complexation reactions, *Water Resour. Res*. doi:10.1029/2009WR008168 (In press).

Ma, R., and, C. Zheng. 200**9.** Effects of density and viscosity in modeling heat as a groundwater tracer. *Ground Water*. DOI: 10.1111/j.1745-6584.2009.00660.x.

McKinley, J. P., J. M. Zachara, C. Liu, and, S. M. Heald. 2006. Microscale controls on the fate of contaminant uranium in the vadose zone, Hanford Site, Washington. *Geochim. Cosmochim. Acta*, **70**, 1873-1887.

McKinley, J. P., J. M. Zachara, J. Wan, D. E. McCready, and, S. M. Heald. 2007. Geochemical controls on contaminant uranium in vadose Hanford formation sediments at the 200 Area and 300 Area, Hanford Site, Washington. *Vadose Zone J.* **6**, 1004-1017.

Mitrofan, H., I. Povara, and, M. Mafteiu. 2008. Geoelectrical investigations by means of resistivity methods in karst areas in Romania. *Environ. Geol.* **55**, 405-413.

Mullick, M. and, R. K. Majumdar. 2002. A Fortran program for computing the mise-a-la-masse response over a dyke-like body. *Computers & Geosci.* **28**, 1119-1126.

Murakami, H., X. Chen, M. S. Hahn, Y. Liu, M. L. Rockhold, V. Vermeul and, Y. Rubin. 2009. Three-dimensional characterization of a high-K aquifer at the Hanford 300 Area and retrospective analysis of experimental designs, Eos Trans. AGU, **90**(52), Fall Meet. Suppl. Abstract  H43F-1082.

Osiensky, J. L. 1995. Time-series electrical potential-field measurements for early detection of groundwater contamination. *J. of Environ. Sci. and Health Part a-Environ. Sci. and Engineer. & Toxic and Hazardous Substance Control* **30**, 1601-1626.

Osiensky, J. L. 1997. Ground water modeling of mise-a-la-masse delineation of contaminated ground water plumes. *J. Hydrology* **197**, 146-165.

Osiensky, J. L. and, P. R. Donaldson. 1994. A modified mise-a-la-masse method for contaminant plume delineation. *Ground Water* **32**, 448-457.

Osiensky, J. L. and, P. R. Donaldson. 1995. Electrical flow through an aquifer for contaminant source leak detection and delineation of plume evolution. *J. Hydrology* **169**, 243-263.

Osiensky, J. L. and, R. E. Williams. 1996. A two-dimensional MODFLOW numerical approximation of mise-a-la-masse electrical flow through porous media. *Ground Water* **34**, 727-733.

Pant, S. R. 2004. Tracing groundwater flow by mise-a-la-masse measurement of injected saltwater. *J. Environ. Eng. Geophys.* **9**, 155-165.

Peterson, R. E., C. F. Brown, and, R. J. Serne. 2009. Mass Balance Aspects of Persistent Uranium Contamination in the Subsurface at the Hanford Site, Washington.  *PNNL-SA-67979*, Pacific Northwest National Laboratory, Richland, Washington.

Prommer, H., D. A. Barry, and, C. Zheng. 2003. MODFLOW/MT3DMS based reactive multicomponent transport modeling. *Ground Water* **41**(2), 247-257.

Rockhold, M. L., V. R. Vermeul, R. Mackley, B. Fritz, D. Mendoza, E. Newcomer, D. Newcomer, C. J. Murray and, J. M. Zachara. 2010. Hydrogeologic characterization of the Hanford 300 Area Integrated Field Research Challenge Site and numerical modeling of the first aquifer tracer test. *Ground Water* (In preparation).

Rockhold, M. L., V. R. Vermeul, C. J. Murray, and, J. M. Zachara. 2009. Hydrologic characterization and results for the first tracer experiment at the Hanford 300 Area IFRC site. Presented at 4th Annual DOE-ERSP PI Meeting, Lansdowne, Virginia. April 20-23.

Stoliker, D. L., J. A. Davis, and, J.M. Zachara. 2009. Characterization of metal-contaminated sediments: Distinguishing between samples with adsorbed and precipitated metal ions. *Environmental Science and Technology* (Submitted).

Wang, T., J. A. Stodt, D. J. Stierman, and, L. C. Murdoch. 1991. Mapping hydraulic fractures using a borehole-to-surface electrical resistivity method. *Geoexploration* **28**, 349-369.

Ward, A. L., R. J. Versteeg, C. E. Strickland, F. Tao, and, V. Vermeul. 2009. Evaluation of heat as a tracer to quantify variations in groundwater velocities at Hanford's Integrated Field Research Challenge (IFRC) Site: AGU, **90**(52), Fall Meet. Suppl. Abstract H31F-04.

White, P. A. 1994. Electrode arrays for measuring groundwater-flow direction and velocity. *Geophysics* **59**, 192-201.

White, M. D., and, M. Oostrom. 2004. STOMP, Subsurface Transport Over Multiple Phases, Version 3.1, User's Guide. *PNNL-14478*, Pacific Northwest National Laboratory, Richland, Washington.

Williams, M. D., M. L. Rockhold, P. D. Thorne and, Y. Chen. 2008. Three-Dimensional Groundwater Models of the 300 Area at the Hanford Site, Washington State. *PNNL-17708*, Pacific Northwest National Laboratory, Richland, Washington.

Wood, W., and, D. Palmer. 2000. The application of mise-a-la-masse and resistivity surveys to the detection of pollution from leaking sewers. *Exploration Geophysics* **31**, 515-519.

Yabusaki, S. B., Y. Fang, and, S. R. Waichler. 2008. Building conceptual models of field-scale uranium reactive transport in a dynamic vadose zone-aquifer-river system, *Water Resour. Res.***44**, W12403, doi:10.1029/2007WR006617.

Yin, J., D. R. Haggerty, J. D. Istok, D. B. Kent and, C. Liu. 2010. Effects of transient flow and water chemistry on U(VI) transport. *Water Resources Research* (In preparation).

Zachara, J. M., J. A. Davis, C. Liu, J. P. McKinley, N. P. Qafoku, D. M. Wellman, and, S. B. Yabusaki. 2005. Uranium Geochemistry in Vadoze Zone and Aquifer Sediments from the 300 Area Uranium Plume. *PNNL-15121*, Pacific Northwest National Laboratory, Richland, Washington.

Zheng, C. 2006. MT3DMS v5.2 supplemental user's guide. Department of Geological Sciences, University of Alabama, Tuscaloosa, AL.

Zheng, C., and, P. P. Wang. 1999. MT3DMS: A modular three-dimensional multi-species transport model for simulation of advection, dispersion and chemical reactions of contaminants in groundwater systems; documentation and user's guide. *U.S. Army Engineer Research and Development Center Contract Report SERDP-99-1*, pp. 202. Vicksburg, MS. http://hydro.geo.ua.edu/mt3d/

Zheng, C., R. Ma, H. Prommer, J. Greskowiak, C. Liu, J. M. Zachara and, M. L Rockhold. 2009. Modeling field-scale uranium reactive transport in physically and chemically heterogeneous media *(Invited)*: AGU, **90**(52), Fall Meet. Suppl. Abstract H32C-02.

# PRESENTATIONS

<u>**2010**</u>

Ma, R., C. Zheng, C. Liu, J. Zachara, H. Prommer, and J. Greskowiak. 2010. "A Multi-Rate Mass Transfer Model for Field-Scale Uranium Transport in a Physically and Chemically Heterogeneous Aquifer." Presentation at Ground Water Summit, Denver, CO.

Greskowiak, J., M.B. Hay, H. Prommer, C. Liu, V. Post, and J.A. Davis. 2010. "Comparison of Chemical and Physical Non-Equilibrium Models to Simulate Multi-Scale Kinetic Mass-Transfer and Surface Complexation of U(VI) in Porous Media." Presentation at Ground Water Summit, Denver, CO.

<u>**2009**</u>

Bjornstad, B.N., J.A. Horner, V.R. Vermeul, D.C., Lanigan and P.D. Thorne. 2009. "The IFRC Well Field: Drilling, Sampling, Well Construction, and Preliminary Hydrogeologic Interpretations." Presented by Bruce Bjornstad at ERSP 4th Annual PI Meeting, Lansdowne, VA on April 22, 2009. PNNL-SA-66151.

Greskowiak, J., H. Prommer, C. Liu, V.E.A. Post, R. Ma, C. Zheng, and J. Zachara. 2009. "Scaling Effects on Parameter Sensitivities in a Dual-Domain, Multi-Rate Reactive Transport System." Presented at the ModelCARE 2009 International Conference, Wuhan, China.

Hammond, G.E., P.C. Lichtner and M.L. Rockhold. 2009. "Stochastic Simulation of Uranium Migration at the Hanford 300 Area." Presented at Migration '09, Sept. 20-25, 2009, Kennewick, WA.

Konopka A., X. Lin, D.W. Kennedy, and R. Knight. 2009. "Hanford 300A Subsurface Microbial Ecology." Presented by Allan Konopka (Invited Speaker) at Science Focus Area Project Meeting at W.R. Wiley, Environmental Molecular Sciences Laboratory at PNNL on February 26, 2009, Richland, WA. PNNL-SA-65207.

Konopka A., X. Lin, D.W. Kennedy, J.K. Fredrickson, M.S. Lipton, and R. Knight. 2009. "Microbial Ecology in Subsurface Sediments from Hanford 300A Area." Presented by Allan Konopka (Invited Speaker) at ERSP 4th Annual PI Meeting on April 20, 2009 Lansdowne, VA. PNNL-SA-65923.

Lichtner, P.C. 2009. "Modeling Multiscale-Multiphase-Multicomponent Subsurface Reactive Flows using Advanced Computing: Application to the Hanford 300 Area." ERSP PI Meeting, April 20-24, Lansdowne, VA.

Lin X., D.W. Kennedy, J.K. Fredrickson, and A. Konopka. 2009. "Distribution of Microbial Biomass and the Potential for Anaerobic Respiration in Hanford Site Subsurface Sediments." Presented at American Society for Microbiology on May 19, 2009, Philadelphia, PA. PNNL-SA-66505.

Ma, R, C. Zheng, J.M. Zachara, M. Rockhold, and A. Ward. 2009. "Modeling Heat Transport as a Groundwater Tracer." Presented at GSA Annual Meeting, Portland, OR.

Ma, R., C. Zheng, H. Prommer, J. Greskowiak, C. Liu, J. Zachara, and M. Rockhold. 2009. "Modeling Field-Scale Multi-Rate Surface Complexation Reactions to Quantify Their Impact on Uranium Mobility at the Hanford Site." Presented at the ModelCARE 2009 International Conference, Wuhan, China.

Mills, R.T., G.E. Hammond, P.C. Lichtner, V. Sripathi, G.K. Mahinthakumar, and B.F. Smith. 2009. "Modeling Subsurface Reactive Flows Using Leadership-Class Computing." SciDAC 2009, San Diego, CA.

Rockhold M., V. Vermeul, C. Murray, and J. M. Zachara. 2009. "Hydrologic Characterization and Results from the First Tracer Experiment at the Hanford 300 Area IFRC Site." PNNL-SA-65958, Pacific Northwest National Laboratory, Richland, Washington.

Rubin, Y. 2009. "The MAD Concept and its Applications in Hydrogeology." Invited seminar, Chevron Research Center, San Ramon, CA.

Rubin, Y. 2009. "Bayesian Geostatistical Design: Optimal Site Investigation When the Geostatistical Model is Uncertain." Presented at the European Geophysical Union General Assembly meeting.

Rubin, Y. 2009. "The Method of Anchored Distributions (MAD) for Integration and Inversion of IFRC Hydro Geological Data and for Establishing a Geostatistical Site Model." Presented at the 4th ERSP Annual PI Meeting." April 20-23, 2009.

Rubin, Y. 2009. "Inverse Modeling of Random Fields Using the Method of Anchored Distribution." Invited talk, Chevron Corp., January 2009, San Ramon, CA.

Rubin, Y. 2009. "Inverse Modeling in Hydrogeology. Invited lecture at Interagency Federal Cooperation Project on Multimedia Environmental Modeling." June 18, 2009, Washington, DC.

Rubin Y. 2009. "Integrating Scale-Dependent Hydro Geological Data Using a Bayesian Geostatistical Framework." DOE-ERSP 4th Annual PI Meeting, April 20-23, 2009, Lansdowne, Virginia.

Rubin Y. 2009. "A Bayesian Geostatistical Inversion Method for Hydro Geological Data Integration in Probabilistic Risk Assessments." Waste Management Symposium 2009, Phoenix, Arizona.

Yin, J., R. Haggerty, J.D. Istok, D.B. Kent, and M. Rockhold. 2009. "Experimental Investigation of the Effect of Transient Groundwater Glow on U(VI) Transport in the Hanford 300 Area." DOE ERSP annual PI meeting, April 20-23, 2009, Lansdowne, VA.

Yin, J., R. Haggerty, J.D. Istok, D.B. Kent, and M. Rockhold. 2009. "Experimental Investigation of the Effect of Transient Groundwater Flow on U(VI) Transport in the Hanford 300 Area." Isotope Hydrology and Biogeochemistry Workshop, Jun. 9, 2009, Corvallis, OR.

Zachara, J.M., M.D. Freshley, V.R. Vermeul, B.G. Fritz, R.D. Mackley, J.P. McKinley, M.L. Rockhold, and A. L. Ward. 2009. "Testing at the Hanford Site 300 Area Integrated Field Challenge, Washington." Presented at the 7th Washington Hydrogeology Symposium, April 28-30, 2009 Tacoma, Washington.

Zachara, J.M and the IFRC Research Team. 2009. "New Results from the Hanford Integrated Field Research Challenge (IFRC)." Hanford Site-Wide Seminar, on February 24, 2009, Richland, WA.

Zachara, J.M., B.N. Bjornstad, J.N. Christensen, M.S. Conrad, J.K. Fredrickson, M.D. Freshley, R. Haggerty, G.E. Hammond, D.B. Kent, A. Konopka, P.C Lichtner, C. Liu, J.P. McKinley, M.L.

Rockhold, Y. Rubin, V.R. Vermeul, R.J. Versteeg, A.L. Ward, and C. Zheng. 2009. "New Results from the Hanford Integrated Field Research Challenge (IFRC)." Presented by Allan Konopka (Invited Speaker) at DOE-ERSP 4th Annual PI Meeting on April 20, 2009, Lansdowne, VA. PNNL-SA-65032.

Zheng, C., R. Ma, H. Prommer, J. Greskowiak, C. Liu, J. Zachara, and M. Rockhold. 2009. "Modeling Field-Scale Multi-Rate Surface Complexation reactions at the Hanford IFRC site." Presented at the ERSP PI Meeting, Lansdowne, VA.

Zheng, C., R. Ma, H. Prommer, J. Greskowiak, C. Liu, J. Zachara, and M. Rockhold. 2009. "Reactive Transport Modeling at the Hanford IFRC Site." Presented at the Ground Water Summit, Phoenix, AZ.

Zheng, C., R. Ma., H. Prommer, J. Greskowiak, C. Liu, J. Zachara, M. Rockhold. 2009. "Modeling Field-Scale Uranium Reactive Transport in Physically and Chemically Heterogeneous Media." Invited presentation at AGU Fall Meeting, San Francisco, CA.

Zheng, C., R. Ma, H. Prommer, C. Liu, J. Greskowiak, J. Zachara, and M. Rockhold. 2009. "Accounting for Physical and Chemical Heterogeneities in Contaminant Transport Modeling." Presented at the Ground Water Summit, Tucson, AZ.

**2008**
Bjornstad, B.N., J.P. McKinley. 2008. "Well-Field Installation, Sampling Plan, and Monitoring System Update." PNNL-SA-60429, Pacific Northwest National Laboratory, Richland, Washington.

Hammond, G. and P. Lichtner. 2008. "Massively Parallel Ultrascale Subsurface Simulation." Computational Methods in Water Resources XVII, July 6-10, 2008.*(Partial IFRC support).*

Hammond, G.E., P.C. Lichtner, R.T. Mills, and C. Liu. 2008. "Toward Petascale Computing in Geosciences: Application to the Hanford 300 A." *Journal of Physics Conference Series.* 125, Art No. 012021. doi:10.1088/1742-6596/125/1/012051.

Liu, C., D.B. Kent, R. Haggerty. 2008. "Conceptual Model of Mass Transfer at 300 A." PNNL-SA-60523, Pacific Northwest National Laboratory, Richland, Washington.

Ma, R., C. Zheng, H. Prommer, J. Greskowiak, C. Liu, J. Zachara, and M. Rockhold. 2008. "A Preliminary Assessment of the Effects of River Water Dynamics and Chemistry on Uranium Fate and Transport at the Hanford 300A site." Presented at AGU Fall Meeting, San Francisco, CA.

Ma, R., C. Zheng, H. Prommer, J. Zachara, C. Liu, and M. Rockhold. 2008. "Modeling Uranium Fate and Transport at the Hanford Integrated Field Challenge Site," Presented at the "MODFLOW and More 2008" International Conference, Golden, CO.

Zheng, C. and M. Rui. 2008. "Modeling Uranium Fate and Transport at the Hanford site: An Integrated Field Challenge." Invited keynote presentation at the International Groundwater Forum 2008, Changchun, China.

Rockhold, M. 2008. "Hanford 300 Area IFC Flow and Transport Modeling Integration and Coordination." PNNL-SA-60272, Pacific Northwest National Laboratory, Richland, Washington.

Stoliker, D. 2008. "Geochemical Studies with Hanford 300 Area Sediments." PNNL-SA-60570, Pacific Northwest National Laboratory, Richland, Washington.

Vermeul, V., J.S. Fruchter, B.G. Fritz, R.D. Mackley, D.M. Wellman, and M.D. Williams. 2008. "In-Situ Uranium Stabilization through Polyphosphate Injection: Pilot-Scale Treatability Test at the 300 Area, Hanford Site." PNNL-SA-58147, Pacific Northwest National Laboratory, Richland, Washington.

Versteeg, R. 2008. "Web centric data management for the Hanford 300 Area IFC." *Eos Trans. AGU*, 89(53), Fall Meet. Suppl, Abstract IN23B-1083.

Versteeg, R. 2008. "300 Area IFC Data Management." PNNL-SA-60571, Pacific Northwest National Laboratory, Richland, Washington.

Ward, A., and V.R. Versteeg. 2008. "Geophysical Characterization: Discussion Points." PNNL-SA-60533, Pacific Northwest National Laboratory, Richland, Washington.

Yabusaki, S., Y. Fang, and S. Waichler. 2008. "Reactive Transport Modeling of Uranium Surface Complexation and Mass Transfer in the 300 Area Hydrologic System." PNNL-SA-60382, Pacific Northwest National Laboratory, Richland, Washington.

Yin, J., R. Haggerty and J. D. Istok. 2008. "Experimental Investigation of the Effect of Transient Groundwater Flow on Dispersion." *Eos Trans. AGU, 89*(52), Fall Meet. Suppl., Abstract H41C-0888.

Zachara, J.M., J. Davis, J. P. McKinley, D. Singer, J. Stubbs, G.E. Brown, and Z. Wang, and J.–F. Boily. 2008. "Frontiers in Environment Remediation Research." Presented at the Synchrotron Environmental Science IV Conference, December 12, 2008, San Francisco, CA.

Zachara, J.M., M. Rockhold, J. Fredrickson, V. Vermeul, A. Ward, C. Liu, J.M. McKinley, B. Bjornstad, M. Freshley, R. Haggerty, D. Kent, P. Lichtner, Y. Rubin, R. Versteeg, and C. Zheng. 2008. "Hanford's 300 Area Integrated Field Research Challenge Site." *Eos Trans. AGU 89*(53), Fall Meet. Suppl. Abstract H33G-1102.

Zachara, J.M., and IFC Team. 2008. "Multi-Scale Mass Transfer Processes Controlling Natural Attenuation and Engineered Remediation: An IFC Focused on Hanford's 300 Area Uranium Plume." PNNL-SA-65733, Pacific Northwest National Laboratory, Richland, Washington.

Zhang, Z., and Y. Rubin. 2008. "Gaussian Random Field Inverse Modeling with the Method of "Anchored Distributions" (MAD) in Statistical Issues in Monitoring the Environment." A Workshop on Environmetrics, NCAR, Boulder, CO.

Zhang, Z., and Y. Rubin. 2008. "MAD: A New Method for Inverse Modeling of Spatial Random Fields with Applications in Hydrogeology." Presented at the AGU Fall Meeting, December 2008, San Francisco, CA.

Zheng, C. and M. Rui. 2008. "Modeling Uranium Fate and Transport at the Hanford site: An Integrated Field Challenge." Invited keynote talk at the International Groundwater Forum 2008, Changchun, China.

# PUBLICATIONS

**2010**
Greskowiak, J., H. Prommer, C. Liu, V.E.A. Post, R. Ma, C. Zheng, and J.M. Zachara. 2010. Comparison of parameter sensitivities between a laboratory and field scale model of uranium transport in a dual domain, distributed-rate reactive system. *Water Resources Research* (Accepted).

Hammond, G.E., P.C. Lichtner, and M.L. Rockhold. 2010. Stochastic simulation of uranium migration at the Hanford 300 Area. *Journal of Contaminant Hydrology* (Submitted).

Hammond, G.E. and P.C. Lichtner. 2010. Field-scale model for the natural attenuation of uranium at the Hanford 300 area using high performance computing. *Water Resources Research* (Accepted).

Harrington, S.J., B.D. Wood, and R. Haggerty. 2010. Effects of equilibrium pH and inorganic carbon on uranium transport in Hanford sediment. *Environmental Science and Technology* (Submitted).

Johnson, T., R. Versteeg, A. Ward, F. Day-Lewis, and A. Revil. 2010. Improved hydrogeophysical characterization and monitoring through parallel modeling and inversion of time-domain resistivity and induced polarization data. *Geophysics Journal* (Submitted).

Johnson, T.C., R. J. Versteeg, A. Ward, J. Greenwood, and C. Strickland. 2010. Electrical geophysical characterization of the Hanford 300 Area Integrated Field Research Challenge wellfield using high performance DC resistivity inversion geostatistically constrained by borehole conductivity logs. *Geostatistics* (Submitted).

Ma, R., C. Zheng, H. Prommer, J. Greskowiak, C. Liu, J. Zachara, and M. Rockhold. 2010. A Field-scale reactive transport model for U(VI) migration influenced by coupled multi-rate mass transfer and surface complexation reactions. *Water Resources Research* (In press).

Ma, R., and C. Zheng. 2010. Effects of density and viscosity in modeling heat as a groundwater tracer. *Ground Water.* doi:10.1111/j.1745-6584.2009.00660.x.

Ma, R.J. Greskowiak, H. Prommer, C. Liu, C. Zheng and J. Zachara. 2010. Model-based quantification of the influence of calcite on uranium mobility at the groundwater/surface water interface. *Environmental Science and Technology* (Submitted).

McKinley, J.P., J.M. Zachara, C.T. Resch, D.L. Girvin, M.D. Miller, J.L. Phillips, V.R. Vermeul, and T.A. Beck. 2010. Vadose zone contributions to groundwater U plume driven by water table fluctuations in a riparian aquifer at the Columbia River, Washington. *Environmental Science and Technology* (Submitted).

Murakami, H., X. Chen, M.L. Rockhold, V.R. Vermeul, and Y. Rubin. 2010. Bayesian geostatistical inversion of constant injection test data for a high-K aquifer characterization at the Hanford 300 Area. *Water Resources Research* (Submitted).

Newcomer, D.R., B.N. Bjornstad, and V.R. Vermeul. 2010. Vertical wellbore flow monitoring for assessing spatial and temporal flow relationships with a dynamic river boundary. *Groundwater Monitoring and Remediation* (To be submitted in March).

Nowak, W., F. De Barros, and Y. Rubin. 2010. Bayesian geostatistical design: Optimal site investigation when the geostatistical model is uncertain. *Water Resources Research* (Submitted).

Rockhold, M.L., V.R. Vermeul, R. Mackley, B. Fritz, D. Mendoza, E. Newcomer, D. Newcomer, C.J. Murray, and J.M. Zachara. 2010. Hydrogeologic characterization of the Hanford 300 Area Integrated Field Research Challenge Site and numerical modeling of the first aquifer tracer test. *Groundwater* (In preparation).

Rubin, Y., X. Chen, H. Murakami, and M. Hahn. 2010. A Bayesian approach for inverse modeling, data assimilation, and conditional simulation of spatial random fields. *Water Resources Research* (Submitted).

Spane, F.A. and R.D. Mackley. 2010. Removal of river-stage fluctuations from unconfined aquifer well response using a multiple-regression deconvolution approach. *Groundwater* (To be submitted in March)

Stoliker, D.L., J.A. Davis and J.M. Zachara. 2010. Characterization of metal-contaminated sediments: Distinguishing between samples with sorbed and precipitated metal ions. *Environmental Science and Technology* (Submitted).

Um, W., J.M. Zachara, C. Liu, D. Moore and K. A. Rod. 2010. Resupply mechanism to a contaminated aquifer: A laboratory study of U(VI) desorption from capillary fringe sediments. *Geochimica et Cosmochimica Acta* (Accepted).

Vermeul, V.R., J.P. McKinley, D.R. Newcomer, R.D. Mackley, and J.M. Zachara. 2010. River induced wellbore flow dynamics in long-screen wells and their impact on aqueous sampling results. *Groundwater* (To be submitted in March).

Yin, J., D.R. Haggerty, J.D. Istok, D.B. Kent and C. Liu. 2010. Effects of transient flow and water chemistry on U(VI) transport. *Water Resources Research* (In review).

Zachara, J.M., J.P. McKinley, C. Murray, Y. Bott, and D. Moore. 2010. A geochemical heterogeneity model for a contaminated vadose zone - aquifer system with dynamic water table fluctuation. *Contaminant Hydrology* (In preparation).

Zachara, J.M., M. Oostrom, C. Liu, J.P. McKinley, T. Wietsma, and C.T. Resch. 2010. Mass transfer limited adsorption and desorption of U in intact sediment cores retrieved from a contaminated aquifer. *Environmental Science and Technology* (In preparation)

Zang, Z. and Y. Rubin. 2010. Inverse modeling of spatial random fields using anchors. *Water Resources Research* (Submitted).

## 2009

De Barros, F. P. J., Y. Rubin, and R.M. Maxwell. 2009. The concept of comparative information yield curves and its application to risk-based site characterization. *Water Resour. Res.*, 45, W06401. doi:10.1029/2008WR007324.

Liu, C., S. Shi, and J.M. Zachara. 2009. Kinetics of uranium (VI) desorption from contaminated sediments: Effect of geochemical conditions and model evaluation. *Environ. Sci. Technol.,* 43(17):6560-6566.

Mills, R.T., G.E. Hammond, P.C. Lichtner, V. Sripathi, G.K. Mahinthakumar, B.F. Smith. 2009. Modeling subsurface reactive flows using leadership-class computing. *Journal of Physics Conference Series.* 180, Art. No. 012062. doi:10.1088/1742-6596/180/1/012062.

Singer, D.M., J.M. Zachara and G. E. Brown. 2009. Uranium speciation as a function of depth in contaminated Hanford Site sediments - A micro-XRF, micro-XAFS, and micro-XRD study. *Environ. Sci. Technol.* 43(3):630-636.

Stubbs, J.E., L.A. Veblen, D.C. Elbert, J.M. Zachara, J.A. Davis and D.R. Veblen. 2009. Newly recognized hosts for uranium in the Hanford site vadose zone. *Geochim. Cosmochim. Acta.* 73(6):1563-1576.

## 2008

Liu, C., J.M. Zachara, N. Qafoku and Z. Wang. 2008. Scale-dependent desorption of uranium from contaminated subsurface sediments. *Water Resour. Res.* 44, W08413. doi:10.1029/2007WR006478.

McKinley, J.P., J.M. Zachara, J. Wan, D.E. McCready and S.M. Heald. 2008. Geochemical Controls on Contaminant Uranium in Vadose Hanford Formation Sediments at the 200 Area and 300 Area, Hanford Site, Washington. *Vadose Zone,* 6:1004-1017.

Versteeg, R., and T. Johnson. 2008. Using time lapse geophysics to monitor subsurface processes. *The Leading Edge*, 27(11):1488-1497.